
ZINC OXIDE IN FORMULATION
FOR RESPIRATORY VACCINATION

Dissertation

zur Erlangung des Doktorgrades
der Mathematisch-Naturwissenschaftlichen Fakultät
der Christian-Albrechts-Universität zu Kiel

vorgelegt von

Marie Gerda Hellfritsch

Kiel 2021

Erster Gutachterin

Prof. Dr. Regina Scherließ

Zweiter Gutachter

Prof. Dr. Dr. Thomas Rades

Tag der mündlichen Prüfung

21.06.2021

Für meine Familie

"Fight for the things that you care about, but do it in a way that will lead others to join you."

Ruth Bader Ginsberg

Lack of a specific mark or a reference to trademark or a patent does not imply that this work or part of it can be used or copied without copyright permission.

Table of contents

1	Introduction	1
2	Objectives	4
3	Mucosal vaccination via the respiratory tract.....	5
3.1	Introduction.....	5
3.2	The immune system of the respiratory tract.....	7
3.2.1	Immune system in the nose.....	8
3.2.2	Immune system in the lung.....	9
3.3	Advantages of mucosal immunisation	9
3.4	Prerequisites for mucosal vaccination	10
3.4.1	Particle uptake in immune cells.....	10
3.4.2	Particle size	10
3.4.3	Particle shape.....	11
3.4.4	Charge and functionalisation.....	12
3.5	History of respiratory vaccination.....	12
3.6	Formulations for respiratory vaccination: general considerations	13
3.7	Adjuvants for respiratory vaccines	15
3.8	Therapeutic vaccination.....	17
3.9	Respiratory vaccine formulations.....	18
3.9.1	Nasal vaccine formulations	18
3.9.2	Pulmonary vaccine formulations.....	19
3.9.3	Respiratory vaccines in research and development	21
3.10	Pulmonary and nasal administration devices.....	24
3.10.1	Nasal administration	24
3.10.1.1	Liquid preparations	25
3.10.1.2	Dry powder devices.....	26
3.10.2	Pulmonary administration.....	27

3.10.2.1	Liquid preparations	27
3.10.2.2	Dry powder inhaler	28
3.11	Conclusion	29
4	Materials	30
4.1	Zinc oxide tetrapods	30
4.2	Zinc oxide	31
4.3	Aluminium hydroxide and aluminium phosphate.....	32
4.4	Mannitol.....	33
4.5	Hyaluronic acid.....	33
4.6	Proteins	34
4.6.1	Bovine serum albumin.....	34
4.6.2	Ovalbumin.....	35
4.6.3	Alpha-lactalbumin.....	35
4.6.4	Avidin	35
4.6.5	Lysozyme	36
4.7	Cells for in-vitro experiments	36
4.7.1	Calu-3.....	36
4.7.2	RPMI2650	37
4.7.3	Murine bone marrow-derived dendritic cells.....	37
4.8	Devices	37
4.8.1	Unit dose system powder device	37
4.8.2	Cyclohaler.....	38
5	Methods	39
5.1	Spray drying	39
5.2	Characterisation	42
5.2.1	Morphology and elementary analysis.....	42
5.2.2	Particle size distribution.....	43
5.2.2.1	Particle size distribution with the RODOS module	44

5.2.2.2	Particle size distribution with the SPRAYER module	45
5.2.2.3	Particle size distribution with the INHALER module	45
5.2.3	Protein quantification	46
5.2.3.1	Loading.....	46
5.2.3.2	SDS-PAGE.....	47
5.2.3.3	Size exclusion chromatography.....	48
5.2.4	Adsorption	49
5.2.5	Aerodynamic assessment.....	50
5.2.5.1	Next Generation Pharmaceutical Impactor.....	50
5.2.5.2	Precise Inhale	53
5.2.6	pH and solubility.....	54
5.2.7	Release study	57
5.2.8	Osmolality	58
5.2.9	Hygroscopicity.....	58
5.2.10	Crystallinity.....	58
5.2.10.1	X-ray powder diffraction	58
5.2.10.2	Differential scanning calorimetry.....	59
5.2.11	Density and surface area	59
5.2.11.1	Density.....	59
5.2.11.2	Surface area.....	60
5.2.12	Size exclusion	60
5.2.12.1	Wet sieving	61
5.2.12.2	Air jet sieving	61
5.2.13	Rheology.....	61
5.3	In-vitro cell experiments.....	62
5.3.1	Calu-3 and RPMI2650.....	62
5.3.1.1	Cytotoxicity by MTT assay	63
5.3.1.2	pH and transepithelial electrical resistance	64

5.3.2	Murine bone marrow-derived dendritic cells.....	65
5.3.2.1	Isolation and cultivation of murine bone marrow-derived dendritic cells.....	66
5.3.2.2	Cell activation experiment.....	66
5.4	Statistics.....	67
6	Results and discussion.....	69
6.1	Adsorption of proteins to different zinc oxides.....	69
6.1.1	Morphology and particle size distribution.....	69
6.1.2	Adsorption.....	75
6.1.3	Summary and conclusion.....	86
6.2	Spray dried zinc oxide formulations.....	88
6.2.1	Spray dried zinc oxide for nasal application.....	88
6.2.1.1	Morphology and particle size distribution.....	88
6.2.1.2	Aerodynamic assessment using the NGI.....	95
6.2.1.3	pH and solubility.....	97
6.2.1.4	Mucus rheology.....	104
6.2.1.5	Cytotoxicity.....	106
6.2.1.6	Loading.....	108
6.2.1.7	Summary and conclusion.....	113
6.2.2	Spray dried zinc oxide for pulmonary application.....	115
6.2.2.1	Morphology and particle size distribution.....	115
6.2.2.2	Aerodynamic assessment using the NGI.....	120
6.2.2.3	pH and solubility.....	124
6.2.2.4	Release study.....	128
6.2.2.5	Cytotoxicity.....	136
6.2.2.6	pH – cell culture.....	138
6.2.2.7	Loading.....	143
6.2.2.8	Aerodynamic assessment using the Precise Inhale.....	147
6.2.2.9	Cell activation experiment.....	149

6.2.2.10	Summary and conclusion.....	152
7	Conclusion and outlook.....	155
8	Abstract.....	157
9	Zusammenfassung	159
10	References	161
11	Appendix	181
11.1	Tables	181
11.2	Abbreviations	189
11.3	Reagents.....	193
11.4	Cells.....	196
11.5	Materials.....	196
11.6	Instruments	197

1 Introduction

In late 2019, the first cases of an unknown lung disease appeared in the Chinese city of Wuhan. On 31st December 2019, the WHO Country Office on the People's Republic of China officially reported the cases to the World Health Organisation, following an official media statement from the Wuhan Municipal Health Commission. In January 2020, the previously unnamed virus continued to spread outside of China, leading the WHO Director-General to declare the outbreak of the novel coronavirus a public health emergency of international concern with the highest level of alarm on 30th January 2020. On 11th February 2020, the virus was given the name SARS-CoV-2 (severe acute respiratory syndrome coronavirus type 2) and the corresponding disease COVID-19. Since then, the virus has been spreading rapidly all over the world, with partly more than 600,000 new infections per day worldwide [1]. One year later, on 12th February 2021, there are 106,991,090 confirmed cases and 2,347,015 deaths associated with COVID-19 worldwide [2]. An unprecedented situation for our generation is bringing the entire society to a standstill. While life is being shut down, the research for effective treatment and prevention is in full swing.

COVID-19 is mainly transmitted via droplets and aerosols and has an average incubation period of five to six days. Since COVID-19 causes substantially the same unspecific symptoms like the usual cold or flu (cough, fever, fatigue) a clear distinction is hard to make. This, as well as asymptomatic, but infectious patients promote further spreading and hence the danger of the virus. A disturbance of the sense of smell and/or taste that persists also after the infection is a common symptom of the lung disease. COVID-19 can manifest itself in many ways and not only in the respiratory tract, but also in other organ systems [3]. The high contagiousness in combination with the severity of the related disease substantiates the importance to minimise the chances of getting the disease and to develop vaccines to prevent COVID-19.

SARS-CoV-2 is a new beta coronavirus. Coronaviruses are enveloped RNA viruses and possess, among other things, spike proteins in their membrane, which are responsible for the entry into the host cell. This spike protein induces protective antibodies and is therefore of great interest for vaccine development. Since the beginning of the circulation of COVID-19 in humans, the viruses have acquired an increasing number of mutations. Virus variations with, e.g., different spike mutations were still rare at the beginning of the pandemic, but are now prevalent worldwide [4]. That is why it is important to broadly diversify the research for an appropriate vaccine.

Currently, a total of four different approaches to vaccine development are being pursued by various companies: gene-based vaccines, protein-based vaccines and virus-like particles, vector vaccines and inactivated whole-virus vaccines [5–8].

So far, three vaccines have received conditional approval from the European Medicine Agency (EMA): two m-RNA vaccines and one vector vaccine [9].

The two m-RNA vaccines from BioNTech and Pfizer as well as from Moderna are administered intramuscularly in two doses at an interval of three to four weeks and showed an efficacy of approximately 95 % [10]. As the name suggests, m-RNA vaccines contain m-RNA, which is produced during transcription where a section of DNA is transcribed into an RNA single strand and is subsequently translated into the corresponding amino acid sequence of a protein. The m-RNA has to be delivered into the cytoplasm of the cell in order to initiate the formation of proteins on ribosomes. To facilitate the uptake into the cells, the m-RNA can be packed in liposomes or lipid nanoparticles. Another possibility of gene-based vaccines are DNA vaccines. Here, an antigen-coding gene is inserted into a non-replicable expression plasmid. In the cell nucleus of the vaccinated person, the DNA is then transcribed into RNA followed by the formation of the proteins/antigens [5].

The vector vaccine from AstraZeneca is also administered intramuscularly in two doses and has shown an efficacy of approximately 82 % for doses separated by 12 weeks [10]. In vector vaccines, the genetic material for an antigen is inserted into an infectious, well known carrier virus. The additional gene in the vector virus is then read and translated into a viral protein. Vector vaccines are divided into replicating and non-replicating viral vectors. In the case of AstraZeneca's vaccine, it is a non-replicating viral vector platform, i.e., a modified chimpanzee adenovirus without the ability to replicate in the host's body [6].

Whole virus vaccines are the traditional vaccines. In this case, the pathogens are cultivated in eggs, animal or human cell lines and administered in an attenuated form that will not lead to the outbreak of the disease. Whole virus vaccines can be distinguished in attenuated and inactivated viruses. The attenuated viruses are mutants of the actual virus, in which the pathomechanisms are no longer functional. This means that it can still replicate and multiply, but would not trigger any relevant disease symptoms. The inactivated virus vaccine does not contain any replication-capable viruses, but has been completely inactivated chemically or physically [7].

Protein-based vaccines and virus-like particles contain purified viral proteins as antigens. Since the spike protein is already identified as antigen, this approach to vaccine development is very obvious in the case of COVID-19. Suitable cells are genetically equipped with the corresponding gene to produce the spike proteins. In culture, these cells can produce the vaccine antigen in large quantities, which then has to be isolated and purified. Since the purified protein is usually not sufficiently immunogenic, the vaccines are often equipped with an adjuvant. Virus-like particles are a further development of protein-based vaccines, as they consist of viral structural proteins that, at least partly, have an inherent property of self-organisation and spontaneously assemble into small vesicles that mimic the morphology of the pathogen [8]. Most protein-based vaccines currently in phase-2 or phase-3 clinical trials are administered

intramuscularly, but three nasal vaccines are also being studied in phase-1 trials [10]. Phase-1 studies are human pharmacology studies. In these studies, the pharmacokinetics, tolerability and safety of the vaccine are first tested on a small number of healthy volunteers [11]. Since COVID-19 is transmitted via droplet infection and aerosols [3], the point of entry of the viruses into humans is, as for many other pathogens, the respiratory tract. In this context, mucosal immunisation via the respiratory tract is an obvious route of administration that has been little used to date, but which has numerous advantages and should also be considered in the prevention of COVID-19 [8].

2 Objectives

Mucosal immunisation via the respiratory tract is one non-invasive chance to prevent infectious diseases. As already mentioned, an adjuvant has to be added to a vaccine if the antigen used is not sufficiently immunogenic. Since aluminium hydroxide or aluminium phosphate, the most commonly used adjuvants for intramuscular administration, are not effective on the mucosa, the aim of this work is to investigate zinc oxide in formulation for respiratory vaccination. The focus of the thesis is on the use of zinc oxide in formulation for respiratory vaccination as an alternative to aluminium hydroxide and aluminium phosphate. Following the thesis, zinc oxide as adjuvant will be investigated in in-vivo studies.

In the first part of the thesis, the adsorption properties of different zinc oxides are investigated in relation to different proteins. The question to be answered is: what is the influence of the production method, the shape and the particle size of the different zinc oxides on the adsorption of proteins with varying molecular weights and isoelectric points.

The second part of the thesis starts with the production and characterisation of nasal formulations followed by the production and characterisation of corresponding pulmonary formulations. Both the nasal and the pulmonary formulations already contain the model antigen and different concentrations of zinc oxide. Finally, the question to be answered is: which formulation has the most promising properties with regard to mucosal vaccination via the respiratory tract. In addition to the question of whether it is a nasal formulation or a pulmonary formulation, the question of the "right" zinc oxide concentration will also be considered.

3 Mucosal vaccination via the respiratory tract

Chapter 3 with the title "Mucosal vaccination via the respiratory tract" was published as a review in 2019 in Pharmaceutics 11 (8) by Marie Hellfritzsch and Regina Scherließ [12].

3.1 Introduction

Active immunisation, which can achieve a lifelong immunity, is one chance to prevent infectious diseases. It has proven to be one of the most cost-effective public health interventions through the years and the number of immunised children is continuously increasing. Thus, the World Health Organisation (WHO) specifies that approximately two to three million lives could be saved every year because of immunisation and the highest number of vaccinated children was reported in 2017: 116.2 million [13].

One of the most recent examples of how vaccinations are important to prevent diseases is the measles vaccination. Measles are a viral illness and one of the most infectious diseases, especially in young children. Since the 1960s, where the first measles vaccine was used, the number of cases worldwide decreased from almost 4.5 million in 1980 to 90,000 in 2016 because of different types of measles vaccines, regardless of whether mono or combination preparations were used [13,14]. But in 2018, almost 83,000 cases were reported just in Europe again and, according to WHO, that is three times higher than in 2017 and 15 times higher than in 2016 [15]. Increasing outbreaks show that hard-won gains are easily lost. Even in countries with well-established health and national immunisation systems, political and economic changes can have an influence on vaccination status without constant attention [13]. Two of the main goals of the Global Vaccine Action Plan of the WHO [13] are increasing vaccination rates again and treating other infectious diseases with vaccines. The focus is on the research and development of vaccines against diseases that are widespread worldwide, such as malaria and HIV as well as new technologies. While Mosquirix®, a vaccine against malaria, has received positive scientific feedback from the European Medicines Agency and is now being tested in studies in three African countries, the vaccine development for HIV is more challenging in a technological view, because of great variability and mutability. However, regarding HIV vaccines, multiple candidate vaccines are in clinical and preclinical evaluation.

As already mentioned, vaccines can be divided into mono vaccines and combination vaccines. Another possibility of subdivision is the division into the following four groups: live attenuated (e.g., measles, oral polio virus), inactivated (e.g., whole-cell pertussis, inactivated polio virus), subunit (e.g., hepatitis B, pneumococcal) and toxoid (e.g., tetanus toxoid, diphtheria toxoid). Live attenuated vaccines are produced from disease-causing pathogens and weakened under laboratory conditions. They can grow and cause no or very mild infection in vaccinated individuals. The immune response is almost as good as that of the original pathogen as all pathogen components are present. However, it is conceivable that

this may go hand in hand with negative effects. Live attenuated vaccines have the rare potential to revert to the pathogenic form and cause diseases or adverse effects, immunosuppressed individuals may not be able to react to the antigen and they should also not be administered during pregnancy. In connection with pregnancy and childbirth, another problem may arise during vaccination: maternal antibodies [16]. Early in life, infants have an immature immune system and maternal antibodies are transferred from mother to child. These antibodies inhibit vaccination of the newborn and provide inadequate protection despite vaccination with different mechanism. In order to avoid inactivation and inadequate vaccination protection, different strategies are discussed, including maternal immunisation. It has the advantage that the maternal immune system will react well to vaccination and, thus, provides high levels of antibodies for the infant [16]. In addition, the vaccination of the mother would be possible through various methods of administration.

Because of a reliable systemic immune response and exact dosing possibilities, intramuscular administration is the most used method. Due to the fact that it is an invasive procedure, usage of a needle is always necessary. Hence, trained personnel for administration and a sterile dosage form are indispensable and undesired effects can occur as a result, e.g., accidental needle sticks. By far the biggest problem associated with injury to an infected needle is the transmission of infectious diseases, e.g., HIV, hepatitis, and the risk of sepsis [17].

In his review on needle-free immunisation, Mitragotri [17] shows various alternatives to intramuscular application (Table 3.1). Cutaneous and mucosal immunisations are possibilities of non-invasive administration. Particular emphasis should be placed on the mucosal immunisation via the respiratory tract, because pathogens mostly have their first contact with nasal and pulmonary mucosa when entering the human body.

Table 3.1. Various alternatives to intramuscular application [17].

Cutaneous immunisation	Mucosal immunisation
Epidermal powder immunisation	Ocular immunisation
	Nasal immunisation
Liquid-jet immunisation	Pulmonary immunisation
	Oral immunisation
Topical application	Vaginal immunisation
	Rectal immunisation

This review takes a closer look at mucosal immunisation via the respiratory tract as an alternative to intramuscular application. Different aspects will be investigated, starting with the immune system of the respiratory tract and particle uptake through formulations to therapeutic vaccination.

3.2 The immune system of the respiratory tract

To understand the function of the mucosal immune system, it is important to look at the structures of the upper (from the nasal and oral cavities to the throat) and lower (trachea and lung) respiratory tract. It should be noted that there are large differences between species and age groups. The immune system in the upper and lower respiratory tract can be structured in three parts (Table 3.2). As mentioned before the first parts are epithelial compartments with immunocompetent cells with four different cell types: alveolar macrophages, dendritic cells, M cells and intraepithelial lymphocytes. The second parts are the lymphoid structures of the nose and the bronchus: nose-associated lymphoid tissue (NALT), larynx-associated lymphoid tissue (LALT) and bronchus-associated lymphoid tissue (BALT). The third parts are lymph nodes that drain the respiratory system [18].

Pavot and coworkers [19] divide the mucosal immune system into inductive and effector sites. At the lamina propria, which is the effector site level, effector cells control foreign material and secretory antibodies are produced, especially IgA. The secretory IgA is very important in preventing infections, because it inhibits the adhesion of bacteria, viruses and other pathogens to epithelial cells. Immunoglobulin G is also produced and plays a role in neonatal immunity, because there is a passive delivery of IgG from mother to child. Intraepithelial T lymphocytes are concentrated in the surface epithelium; NK-like cells, macrophages and B and T cells are located in the sub-epithelial compartment; antigen presenting cells and dendritic cells are present in the mucosal lymphoid tissue. At the inductive site, which is the mucosa-associated lymphoid tissue (MALT), an immune response is initiated. The MALT is the biggest lymphoid tissue in the human body with 4/5 of all immune cells [20] and has three main functions:

1. Protect the mucosal surface against invasion by microbial pathogens;
2. Prevent internalisation of commensal bacteria or antigens as non-degraded proteins;
3. Induct tolerance against innocuous soluble substances.

Table 3.2. Location of immune cells within the respiratory tract [18,20–25].

Parts of the immune system	Location	Cells/structures
Epithelial compartments with immunocompetent cells	Nose/lung	Macrophages
		Dendritic cells (DCs)
		M cells
		T and B lymphocytes
Lymphoid structures of the nose and the bronchus	Nose: nasopharynx and tonsils	Nose-associated lymphoid tissue (NALT)
	Larynx	Larynx-associated lymphoid tissue (LALT)
	Lung: upper and lower airways (branching site)	Bronchus-associated lymphoid tissue (BALT)
Lymph nodes		T and B cells

3.2.1 Immune system in the nose

As the respiratory tract and especially the nose as part of the upper respiratory tract is one of the main entry ports for pathogens, it is well equipped with immunocompetent cells. The lymphoid tissue of the nose (nose-associated lymphoid tissue, NALT) is located in the nasopharynx and the tonsils as part of the Waldeyer's ring [18,21]. It is part of the common mucosal immune system, being characterised by circulation and homing of mature immune cells to the different mucosal sites [22], and can induce a local immune response in the respiratory tract as well as systemic immune reactions [23,25]. The NALT is characterised by a reduced number of ciliated and goblet cells compared to the normal respiratory epithelium present in the nose, numerous intraepithelial T and B lymphocytes and some macrophages [21]. It is known that in these areas, specialised epithelial cells allow intimate contact with lymphoid cells and antigens are taken up following this route to be presented to underlying dendritic cells [25]. Whereas NALT is located in confined structures, dendritic cells (DCs) as antigen presenting cells are also present throughout the complete epithelium. They might congregate immediately under epithelia, migrate into the epithelial layer and even extend dendrites into the lumen to capture antigens. Dendritic cells will then travel to the nearest draining lymph nodes, the cervical lymph nodes, to present the captured antigen to T cells [24]. Upon uptake the antigen is processed by a DC, which then will stimulate CD4-positive T cells to induce IgA-committed B cell development in the lymphoid follicle. After maturation, these B cells migrate from NALT to the regional cervical lymph nodes. Finally, antigen-specific CD4-

positive T cells and IgA-positive B cells migrate to effector sites (such as the nasal passage) through the thoracic duct and blood circulation [26].

3.2.2 Immune system in the lung

In the lung, MALT structures (here named bronchial-associated lymphoid tissue, BALT) can be found along the upper and lower airways, where they are mostly stretched out at the branching sites, where turbulent flow occurs which enhances the likelihood of antigenic particles impacting on these structures [21]. Within this lymphoid tissue the number of ciliated cells is reduced compared to normal respiratory epithelium, whereas numerous lymphocytes and macrophages are present. The frequency of immunocompetent cells varies between the upper bronchial airways, where a dense network of those cells can be found, and the lower respiratory tract with an increased number of alveolar macrophages compared to dendritic cells. Whereas macrophages play an important role in the first line defence of the innate immune system, dendritic cells are key players in adaptive immune responses [27]. Dendritic cells are found in the epithelial linings of the conducting airways, in the submucosa, within alveolar septal walls as well as on the surface of the alveoli [28]. From the cells in the conducting airways, about 2 % of the total cell population are airway mucosa dendritic cells, whereas only 1 % of the cell population in the lung parenchyma are dendritic cells. Nonetheless, there are indications that these cells are more efficient in antigen uptake than the DCs of the upper airways [27]. Due to the differences in distribution of the different immune cells throughout the lung, a targeted delivery to certain cells may be possible, which in turn can induce the desired immune response.

3.3 Advantages of mucosal immunisation

Inhalable pathogens enter the body or directly infect the host via the mucosal surface. For this purpose, it would be interesting to achieve an immune response at the mucosal surface. The problem is that intramuscular vaccination often creates a poor mucosal immune response [29]. Nasal and pulmonary delivery are the most effective routes to reach a local immune response besides a systemic immune response. That means mucosal immunisation produces antigen-specific IgA antibodies at the infection site as well as IgG for an additional systemic response and defence mechanism against the microorganism [18]. Furthermore cell-mediated responses can be stimulated, e.g., helper CD4-positive T cells and CD8-positive cytotoxic T lymphocytes [30].

The nasal mucosa is a very interesting route of drug delivery [31]. Partidos [32] mentioned in his review different reasons why the nose is an attractive route for immunisation:

- Easily accessible;
- Highly vascularised;
- After intranasal immunisation, both mucosal and systemic immune responses are induced;

- Immune response can be induced at distant mucosal sites owing to the dissemination of effector immune cells in the common mucosal immune system;
- Can be used for the immunisation of large population groups;
- Does not require needles and syringes, which are potential sources of infection.

Lu and Hickey [28] confirmed the reasons for nasal immunisation also for pulmonary immunisation and complement the arguments of Partidos:

- Rapidly immunisation of the population;
- Avoid the risk of transmitting hepatitis B, HIV and other blood-borne diseases;
- Highly responsive immune system.

Mucosal immunisation is a promising application technique, because of a rapid onset of action, activation of all the different arms of the immune system, fewer side effects and all the practical advantages [18,30,33,34].

3.4 Prerequisites for mucosal vaccination

For mucosal vaccination, there are some specific requirements, which differ from parenteral vaccination. Most importantly, the antigen needs to be presented in a particulate form in order to provoke local and systemic immune response. Further, an adjuvant with mucosal effectivity is needed. Finally, the formulation needs to be capable for respiratory delivery via a suitable device, deposition at the target site and interaction with the immune cells.

3.4.1 Particle uptake in immune cells

To induce an immune response in the respiratory tract, the antigen has to be taken up by antigen-presenting cells (APCs) in a particulate form [35]. This is easy if the antigen itself is a particle similar to an attenuated or inactivated pathogen, but it is more complicated for subunit vaccines, where the antigen needs to be formulated with a particulate vaccine carrier. Dendritic cells are efficient stimulators for B and T cells [36]. DCs are able to take up microbes and particles by phagocytosis, further they are able to form large pinocytotic vesicles incorporating extracellular fluid and solutes with this taking up soluble antigens by macropinocytosis. They are also equipped for targeted uptake following receptor-mediated endocytosis via C-type lectin receptors or mannose receptors [35]. Upon uptake, DCs are able to form large amounts of peptide-MHC II complexes which are then shown on the cellular surface instead of degrading protein antigens in lysosomes.

3.4.2 Particle size

De Temmerman and coworkers [35] describe the targeting of particulate antigens to dendritic cells, which are the most potent and versatile antigen presenting cells. The corresponding particle size ranges from nanometres to the lower micrometre range. For particulate uptake in DCs, it can be shown that

there is a certain size-dependent efficacy in terms of immune response, as smaller particles of about 200 nm provoke a higher immune response than larger particles of 700 nm [37]. Own studies found a particle size of 200 nm to 300 nm to be optimal for dendritic cell uptake [38]. Smaller particles in a virus-like size (20 nm to 200 nm) are taken up by endocytosis and rather provoke a cellular immune response, whereas very small nanoparticles are not processed locally, but are directly drained to the lymph nodes similar to soluble antigens [35]. This results in local tolerance and a predominantly systemic immune response, if at all [39]. Larger particle ($> 0.5 \mu\text{m}$) are absorbed by phagocytosis or micropinocytosis and lead to a bacteria-like humoral response [40].

Nonetheless, nanoparticles, as discussed in more detail in Section 3.9.3, may only carry a small antigen load. This can be increased largely with microparticulate carriers, which are not very well taken up by DCs, but can be taken up by M cells in the MALT. Tafaghodi and coworkers [41] report on the size analysis of microspheres and how size influences the uptake by M cells. Particles up to $10 \mu\text{m}$ are taken up. Furthermore, the sizes are subdivided with regard to their immune response. While particles smaller than $5 \mu\text{m}$ stimulate the mucosal and systemic immune responses, particles in the range of $5 \mu\text{m}$ to $10 \mu\text{m}$ stimulate only the mucosal immune system. Some studies implicate, that particles larger than $5 \mu\text{m}$ can be taken up by M cells, but will remain in these cells rather than being transferred to underlying APCs [42].

Furthermore, Fifis and coworkers [43] and Singh and coworkers [44] published papers on size-dependent immunogenicity and opportunities and challenges of pulmonary route for vaccination. They report on size restrictions for uptake in macrophages of particles in the micrometre range starting from $0.5 \mu\text{m}$. Alveolar macrophages are reported to be especially efficient in the uptake of particles between $3 \mu\text{m}$ and $6 \mu\text{m}$ [45]. Therefore, for DC-targeted uptake in the respiratory tract the particle size should be lower than $3 \mu\text{m}$, best lower than $0.5 \mu\text{m}$.

3.4.3 Particle shape

Apart from size, the shape of the particles also plays a role for cellular uptake [46]. When particles of different aspect ratios are compared, it was shown that elongated particles are taken up better than spherical particles or cylindrical particles and that disc-shaped particles are taken up to the least extent [47]. Aspect ratio will not only determine the ratio of volume to surface, but can also determine particle orientation and recognition [48]. For macrophages it could be shown that the particle extension at the point of cell attachment is more important for uptake than the total size [47]. Shape could also play an important role in intracellular particle transport. Here, a shape not correlating with intracellular actin- or microtubule-dependent transporting could prevent further particle processing. In a study from Liquidia, the immunological response on antigens being formulated in differently shaped PRINT particles was

looked at and they found, that the antibody titre was highest from earthworm-like particles compared to cylindrical, hexnut formed or cubic particles [49].

3.4.4 Charge and functionalisation

Further characteristics such as charge and functionalisation of the particles also play a role in the efficacy of uptake [50]. Generally, positively charged particles can better interact with negatively charged cell membranes than negatively charged particles, with this increasing contact time and mediating uptake [51]. This effect can also result in a higher immune response of cationic particles in-vivo [52]. Whether cationic particles exceed uncharged particles is discussed controversially and may also depend on hydrophobicity of the particle [53]. Particle functionalisation comprises PEGylation which may increase stability of the particulate system and minimise aggregation [54], and also comprises attachment of receptor ligands for targeted cell interaction and uptake [55] such as lectins, toll-like receptor (TLR) ligands and other pathogen-associated molecular patterns (PAMPs) [56], which may also serve as adjuvants because of their immunostimulatory effects.

In areas where both DCs and macrophages are present such as the epithelium of the respiratory tract, uptake into macrophages should be avoided as these cells are not presenting antigen to subsequent immune cells [27], but predominantly clear the respiratory tract from particulate waste. It is reported that the phagocytic activity of macrophages is generally higher than of DCs, but uptake in DCs can be enhanced if the particle carries a positive charge [57].

3.5 History of respiratory vaccination

First reports on respiratory vaccination (called "variolation") reach back to ancient China and India as early as 100 BC, where a treatment with powdered scabs from patients infected with smallpox for the protection of other people is reported [58]. The scabs of patients smallpox lesions of the skin were collected and dried with this attenuating the virus and ground to a powder. The powder was then administered to the nose of non-infected patients by a small blow pipe or it was air-dispersed for inhalation. This treatment was not harmless and bore a risk for a deadly smallpox infection of 0.5 % to 2 %, but compared to a mortality of 20 % to 30 %, when the disease was obtained through natural infection, this was a great success. For long, this application remained the only reported respiratory vaccination and it was in use in India until the 1970s.

In the last century, major trials were performed in the former Soviet Union where several thousand humans were successfully aerosol vaccinated over a period of many years with live-attenuated strains such as dry anthrax spores [28,59]. The first major clinical trial was probably performed by Albert Sabin and colleagues in Mexico in the 1980s when around 4 million children were vaccinated by a nebulised attenuated Edmonston Zagreb measles vaccine. This trial and the following trials showed that the immune response in children following the aerosol route of delivery was superior to injection [60]. They

used a custom-made device for aerosolisation, which made use of the commonly available product for injection, which was reconstituted and had to be kept on ice during nebulisation in order to keep it stable.

These examples prove the respiratory tract to be highly interesting as route of vaccine administration and many more preclinical and clinical trials are currently being undertaken to strengthen the scientific basis for respiratory vaccination as well as to develop vaccine products for respiratory vaccination for disease prevention and in the therapeutic field.

3.6 Formulations for respiratory vaccination: general considerations

Unlike parenteral vaccine formulations, which have to be injectable liquids, formulations for the respiratory tract comprise solutions or suspensions administered by nasal sprays, pressurised nasal sprays/pressurised metered dose inhalers or nebulisers as well as dry powder formulations which can be administered by passive or active dry powder dispensers. However, for all formulations, whether liquid or solid, it is important that the antigens are presented in a particulate form to induce a local and systemic immune response. Various factors influencing particle properties are discussed in Section 3.4.

Liquid preparations face a high risk of instability over storage due to the high molecular mobility and with this, increased likelihood of chemical reactions and physical instability [61]. This is the reason why many liquid vaccine preparations need to be stored and transported under refrigeration. For a liquid antigen preparation, stability can be enhanced by a selection of pH buffering salts and often amino acids are also used for stabilisation [62,63]. The aim is to ensure and maintain optimal antigen hydration without physical instability or chemical degradation. Hence, osmolarity may play a critical role. For the respiratory mucosa, the osmolarity and pH of the administered liquid (solution or suspension) are also important parameters, as preparations, which deviate largely from physiological conditions, may cause irritancy. In addition, it has been shown that buffer ionic strength may influence the uptake of nanoparticles into M cells [64].

Stability, especially thermal stability, can be increased largely if the antigen can be stabilised and dried. Liquid preparations are often freeze dried to enhance storage stability, with this minimising molecular mobility and, hence, risk of intermolecular reactions. If they shall be administered in liquid form, they need to be re-dispersed in buffer directly prior to administration. With this, the antigen needs to be stable in liquid and has to be stabilised during freezing (cryoprotection) and the subsequent drying step (lyoprotection) [65]. During freezing the molecule needs to be protected from harmful effects of the forming ice crystals and a shift in pH, which may easily occur due to the formation of saturated solutions differing in salt composition from the original buffer during freezing [66]. Afterwards, the molecule needs to be stabilised from dehydration during the removal of water. This can be achieved by an exchange of water with other hydrophilic molecules which may replace it as hydrogen bond forming partner. Another

possibility is the formation of a sugar glass matrix, which has been shown to stabilise vaccine preparations [67]. This principle can also be used in other drying techniques such as spray-freeze drying or spray drying. Formulations, which shall be administered as dry powder, face the same problem as intermediate formulations in the dried state: the antigen and its carrier system need to be stabilised during drying. Amorij and coworkers [66] describe different possibilities to stabilise vaccines. As protein formulations are more stable in a solid state than in a liquid state, they discuss different sugars, which can stabilise proteins during spray and freeze drying (Table 3.3).

The described mechanisms and stabilisers are not only used in influenza vaccines, but also in numerous other formulations in literature [68,69]. Furthermore, the dried formulation needs to have a particle size allowing deposition in the targeted area of the respiratory tract, should have good dispersion characteristics and low agglomeration and adhesive tendencies to allow powder handling, packaging and efficient release from the device. Particle size can be controlled by the parameters of the drying procedure. Here, processes resulting in a dispersible dry powder in one step (such as spray drying) are favoured to freeze drying, where the freeze dried cake might need to undergo a milling step to obtain the desired particle size [70,71]. Cohesive and adhesive behaviour are, in part, determined by particle size: the larger the particles, the better their flow characteristics and the lower their agglomeration. Powder characteristics can further be controlled by the use of dispersion modifiers, which either cover the surface of the microparticles resulting in reduced hygroscopicity and surface energy [72–74] or which form separate particles in the dry powder [75] increasing the dispersion capability.

Its particulate carrier may also achieve stability of the antigen. Drying nanoparticles without further bulking excipients normally leads to highly aggregated particles of undefined size, which are difficult to re-disperse and have a very low yield. Therefore, further excipients can be added which serve as a matrix, embedding and stabilising the individual nanoparticles in a Nano-in-Microparticle (NiM) formulation and increasing re-dispersibility upon matrix dissolution [76]. The matrix component should consist of a material which is capable of quickly releasing the particulate vaccine carrier upon dispersion in media or deposition on the respiratory mucosa. Normally, this is secured by the use of water-soluble carbohydrate matrices, which dissolve in the aqueous mucus.

Table 3.3. Stabilisers used in vaccine during the drying process [66,68,69].

Vaccine	Method	Stabiliser
Influenza	Spray drying	DPPC/HES (dipalmitoyl phosphatidylcholine/hydroxyethyl starch)
		Inulin [59]
	Spray-freeze drying	Arginine
		Dextran
		Lactose
		Mannitol
		Trehalose
	Freeze drying	Dextran
		HYAFF (esterified hyaluronic acid) microspheres
		Inulin
		Sorbitol
		Trehalose
	Air drying	D-xylose
	Smallpox	Freeze drying
Measles, mumps and rubella	Freeze drying	Sorbitol
		Sucrose
Hepatitis B	Spray-freeze drying	Inulin
		Dextran
		Trehalose

3.7 Adjuvants for respiratory vaccines

Antigens for mucosal vaccination often require an adjuvant to achieve both systemic and local immune response. Adjuvants are substances that have to be administered together with the antigen in the

formulation to obtain the desired immune response [77]. This is of special need when the antigen does not bear a strong immunogenicity such as for subunit vaccines and purified antigens, especially for mucosal delivery routes. Here, the targeted epithelium, which naturally is in contact with many potential antigens, need a strong immunostimulating signal in order not to induce tolerance [38,78].

Table 3.4. Mucosal adjuvant in the respiratory tract [79,80].

Mucosal adjuvant	Mechanism	Immune response in the respiratory tract
Lipopolysaccharide (LPS)–protein complexes (endotoxins): Cholera enterotoxin (CT) Heat-labile enterotoxin (LT) from <i>E. coli</i>	Enhance antigen-specific mucosal IgA and systemic IgG responses to administered proteins [81]	Yes [28]
Monophosphoryl lipid A (MPL)	Activate cells via Toll-like Receptor 4 (TLR4) [82]	Yes [83]
Muramyl dipeptide (MDP)	Enhance the cell-mediated immune response [84]	Yes [85]
Oligonucleotids (CpG)	Stimulate B cells to proliferate and secrete immunoglobulins, activate APCs and stimulate cytokine production [86]	Yes [87]
Saponins like QuilA (e.g., ISCOMS)	Improve T cell responses and antigen uptake by APC [88,89]	Yes [89]
Non-ionic block polymers (Poloxamers)	Enhance antigen presentation by binding protein antigens to the surface of the oil droplets [90]	Yes [86]
Dehydroepiandrosterone (DHEA)	Increase cell-mediated immunity [90]	Yes [91]
Cytokines II-1 II-12	Enhance B cell growth (II-12) and influence the differentiation of Th cells (II-1) [92]	Yes [92]

Further, adjuvants can be used to guide the immune response as they may determine whether a predominant Th1- or Th2-mediated immune response or an immune response based on cytotoxic T

lymphocytes (CTL) is developed [39]. This is of special interest when a CD8-positive CTL-specific immune reaction is needed such as it is the case for therapeutic vaccines [93,94].

Chadwick and coworkers [79] present various mucosal adjuvants in their review of nanotechnologies, whereas only those listed in Table 3.4 can be used in the respiratory tract, and Lu and coworkers [28] talk about different mechanisms of action.

To be feasible as mucosal adjuvant, the substance should enhance immunogenicity of the co-administered antigen but should not have intrinsic immunoactivity or toxicity. It has to be noted, that enterotoxins such as the heat-labile toxin from *E. coli* or the cholera toxin, which have proven to be effective mucosal adjuvants, may not be used in the nose due to the possible neurotoxic effects [95]. Non-toxic mutants or derivatives such as MPL are a feasible alternative, but the efficiency for subunit vaccine preparations may be questionable [96].

3.8 Therapeutic vaccination

Active immunisation utilises vaccination to prevent infectious diseases. Therapeutic vaccination provides a new tool for the treatment of cancer, autoimmune diseases or persistent infections, but it is much more challenging [97]. Several mechanisms are described for developing or influencing these diseases, e.g., genetic factors, exogenous factors and a dysregulated function of the immune system [98]. Cancer cells are characterised by the fact that they are genetically altered and have lost normal cellular regulatory processes. As a result, they tend to express different surface markers which could be recognised by immune cells followed by a presentation on MHC I complexes. These complexes can be recognised by CD8-positive T cells. In cancer patients, the immune system does not react in the right way. DCs and T cells may treat cancer antigens more as body's own components than as foreign antigens. This leads to a T regulatory cell response rather than an effector response, T cells cannot infiltrate the tumour and factors in the microenvironment of the tumour suppress effector cells [99]. Here, therapeutic vaccines may help teach the immune system to regain its full function by (repeated) administration of a tumour-specific antigen along with immune-stimulating adjuvants and typically a tumour-suppressive chemotherapy [100]. As mentioned before, the therapy is usually not successful with a single administration, but typically is needed as a routine therapy. Further, a monotherapy by therapeutic vaccination is often not possible, because of the tumour-induced immunosuppression in the surrounding tissue and comedication by chemotherapy has to be administered [101].

Currently, there are many different approaches to therapeutic vaccination against cancer. Basically, a distinction must be made between three different approaches: cell vaccines (tumour or immune cell), protein/peptide vaccines and genetic (DNA, RNA, viral-based vectors) vaccines [100].

Tumour cell vaccines use, as the name suggests, tumour cells for vaccination. A differentiation has to be made between the use of the patient's own tumour cells, which are removed, specially treated and re-

applied (autologous tumour cell vaccines) and a whole tumour cell vaccine, which typically contains two to three typical cell lines (allogeneic tumour cell vaccines). In addition to tumour cell vaccines, there are also immune cell vaccines. Autologous DCs of the patients are loaded with tumour-associated antigens and the mature DCs are re-administered to the patients together with an adjuvant. Individualised tumour therapy sounds like a promising approach, but the availability of patient samples and the complex manufacturing process greatly limit its use [100].

Protein/peptide vaccines are recombinant vaccines containing peptides from defined tumour-associated antigens. They are then administered together with an adjuvant. Even if they are cheaper than individualised vaccines, they have a decisive disadvantage as they only target one or a few epitopes of the tumour-associated antigen and the one tumour type does not always have to be the same. An exception is the Stimuvax®, which contains CD4-related and CD8-related epitopes [100].

Genetic vaccines are another strategy to deliver antigen or fragments of antigens. After the administration of genetic vaccines, DCs that infiltrate the tissue during an inflammatory reaction are transfected, which leads to a direct antigen production and subsequent presentation. A distinction is made between DNA, RNA and viral-based vector vaccines. A big advantage is the easy administration of DNA or RNA encoding for different antigens and a complex activation of the immune system [100].

What all approaches have in common is that a rational vaccine design is needed to achieve a concentrated antigen delivery to DCs and effective DC activation leading to the induction of CD4-positive and CD8-positive T cell responses [97]. For this reason, a mucosal vaccination is to be preferred, since here a high cytotoxic effect and a good cellular immune response can be achieved.

3.9 Respiratory vaccine formulations

3.9.1 Nasal vaccine formulations

Primary antigen carriers are usually too small to be delivered directly to the nasal cavity, they would mostly get inhaled to the lung, hence, they need to be processed further to a formulation which can be deposited securely in the nose. Nanoparticles in suspension would be delivered within larger spray droplets. Spray droplet size will mainly be defined by the spray nozzle of the device as well as by further parameters like viscosity and surface tension of the dispersion medium. For nasal spray products, FDA guidelines require most of the spray droplets to be larger than 10 μm to ensure nasal deposition without a major postnasal fraction which would get inhaled to the lung [102]. For nasal dry powders, Hickey and coworkers [58] propose to use particles larger than 50 μm to ensure predominant nasal deposition. Dry nanoparticles tend to form uncontrolled agglomerates due to the large surface area, hence, they would be formulated in NiM particles. If dry powder Nano-in-Microparticle formulation, where the vaccine carrier is immobilised in a larger matrix particle, is directly administered to the nose, particles may cause physical irritancy depending on their size and concentration. Furthermore, all water-soluble components

start dissolving in the nasal mucus. This may result in a concentrated solution of high osmolarity, which can also cause irritancy and increased ingress of water to dilute the substance causing a running nose. Finally, the nose is a highly sensitive organ for olfaction. Therefore, formulation smell is an important factor for patient compliance as well as taste, because all formulations will be cleared to the pharynx and will also be tasteable on the tongue. In order to increase nasal retention time and with this the time for interaction between the formulation and the nasal mucosa to allow uptake of particulate antigen preparations, mucoadhesive substances (hydrophilic polymers such as chitosan, hydroxypropyl methylcellulose or carbomer) can be used. Apart from the variability in formulations, another advantage of nasal administration is the difference in microbiological requirements as a nasal formulation does not need to be sterile. Further additives may comprise preservatives, which are mandatory for liquid multidose devices to ensure microbiological stability, and adjuvanting substances. Preservatives in nasal formulations are under controversial discussion especially in chronic use, as they may have an effect on ciliary function [103,104]. The choice of an effective and non-toxic adjuvant for nasal vaccination is a challenging task. Especially, it must be tested whether vaccine components can enter the central nervous system (CNS) and cause safety problems. It has been shown by molecular imaging for a botulism vaccine in monkeys that the antigen did not enter the CNS upon nasal administration [105]. The reports on Bell's palsy following a nasal administration of an influenza vaccine adjuvanted with the heat labile *E. coli* enterotoxin (LT) are allocated to translocation of the adjuvant component to the CNS, which led to withdrawal of the vaccine from the market [106].

Fluenz Tetra™ [107] is the first marketed respiratory vaccine. It is licensed in the EU for children (2 years to 18 years) and FluMist Quadrivalent® in the USA and Canada for children and adolescents (2 years to 49 years) for the active immunisation against influenza disease. They are tetravalent vaccines with four influenza virus strains, which are cold-adapted, temperature-sensitive and attenuated. The selection of the virus strains is based on the annual recommendations of the World Health Organisation (WHO). These live virus particles are suspended in a buffered solution containing sucrose, gelatine and amino acids to increase stability. For application, a nasal spray syringe with 0.2 mL of the formulation is used, wherein 0.1 mL is administered into each nostril. Live attenuated influenza vaccines have to mildly infect and replicate in mucosal cells in order to protect. Because of presenting viral proteins in their native form, the immune response is similar to those by natural influenza infection. This results in a higher efficacy compared to inactivated vaccines in children [108] and also comparable protection for adults.

3.9.2 Pulmonary vaccine formulations

Similar to nasal formulations, the primary antigen carrier formulation needs to be processed further to obtain a product which is capable for efficient delivery to the lungs. This can be performed either as a liquid, which can be nebulised or delivered by a pressurised metered dose inhaler (pMDI) or as a dry powder formulation. Comparable to nasal formulations, aerodynamic behaviour and particle size of the

administered formulation play an important role for the location of deposition. In general, an aerodynamic particle size between 0.5 μm and 5 μm is believed to be optimal for pulmonary delivery. Larger particles will already be deposited in the oropharynx, whereas smaller particles might get exhaled [109]. Aerodynamic particle size does not only depend on particle diameter, but also on particle shape and density, which determine how the particle will behave when moving with the air flow. Aerodynamic particle size is the diameter of a sphere with unit density having the same aerodynamic behaviour (terminal settling velocity in still air) as the observed particle and is given by the mass median aerodynamic diameter (MMAD). The MMAD is a cut-off particle size in which 50 % of the mass of the aerosol is smaller and the other 50 % is larger than the referred parameter [110]. As aerodynamic particle size is a result of particle dispersion in the air stream, dispersion characteristics of the formulation and the device used for dispersion are important influencing factors for the resulting MMAD. For pulmonary formulations, the number of fine particles in the inhalable range can be calculated from aerodynamic characterisations (e.g., in an impactor) and serves as an important parameter. It is given as the fine particle fraction (FPF) of either the loaded dose or the dose being emitted from the respective device. With respect to the therapeutic target of the vaccine, different regions in the lung may be interesting for delivery. Larger particles $> 5 \mu\text{m}$ could be used for diseases where the pathogen colonises of the upper part of the bronchi such as *Bordetella pertussis* and *Chlamydia pneumonia*. Small particles $< 3 \mu\text{m}$ are able to diffuse into the deep lung and may be used in the prevention of infections from *Streptococcus pneumonia* and *Bacillus anthracis* [28]. Depending on the dispersion characteristics of the formulation it may needed to be modified to the Nano-in-Micro formulation in order to increase the dose delivered to the lung. To increase the FPF of a microparticulate powder, interactive mixtures can be used, where the fine vaccine formulation adheres to a larger carrier, with this minimising agglomeration and adhesion and easing bulk handling, and is separated during inhalation [111,112]. This leaves the large carrier in the oropharynx, whereas the smaller particles are entrained in the inhalation flow to reach the deep lung. Other approaches make use of a fine particulate excipient to increase dispersion [113]. More advanced modifications could take into account in which region the vaccine formulation should deposit and could make use of broader or smaller particle size distributions of the formulation or even monodisperse particles in order to reach the targeted area.

A vaccine formulation for the lung will be quite restricted in the choice of excipients, as the list of substances already approved for use in pulmonary dosage forms is limited. Apart from lactose, which is used as carrier in many dry powder formulations in the treatment of asthma or COPD, mannitol, glucose and sorbitol as well as some surfactants, some solvents and a limited number of polymers could be used without the need for registration of a novel excipient including all toxicity and safety tests [114,115]. Similar to a nasal vaccine NiM formulation, the matrix excipient needs to be capable for rapid dissolution in the lung mucus or the surfactant fluid in order to release the vaccine carrier [115]. If the formulation

has a sufficient FPF for efficient lung delivery, it should not cause irritancy as this effect is normally caused by larger particles impacting in the oropharynx. In the delivery of high-dose antibiotics, single doses of as much as 4×28 mg (from the Tobi Podhaler, Novartis Pharmaceuticals) have been reported to be delivered without adverse reactions [116]. Similar to nasal formulations, pulmonary formulations do not need to be sterile, but are usually required to have a very low level of microbial contamination, which practically results in aqueous nebuliser preparations to be provided sterile.

3.9.3 Respiratory vaccines in research and development

In the last centuries a lot of work and research has been done on respiratory vaccine delivery. The particulate vaccine delivery system is a growing technology and is increasingly used strategically in vaccine design. Packaging antigens in particles changes its capturing and processing by antigen presenting cells. In principle, we differentiate between four particle effects [117], which are influenced by different properties of the particle systems. First, modulation of the innate immune system, e.g., using polystyrene, PLGA or alum particle. Second, modulation of quality and quantity of antigen presentation, e.g., depot effect controlled through particle dissolution rate. Third, targeting dendritic cells, e.g., with amphiphilic polymers, or targeting cell compartments, e.g., with usage of surface charge. Fourth, enhancing uptake of antigen, e.g., with positive surface charges, in antigen presenting cells, or particle entrapment in dendritic cells [117].

Polymeric particles are the most stable particle vehicles. Different polymers are described in the literature comprising polylactide (PLA), polyglutamic acid (PGA), polylactide-co-glycolic acid (PLGA), polymethyl methacrylate (PMMA), polycaprolactone (PCL), cationic polymers, e.g., polyethyleneimine (PEI) and biopolymers, e.g., chitosan and alginate.

Various examples of polymers in mucosal vaccination as well as advantages and disadvantages of the polymeric nanoparticles [79,118,119] are described in literature. Rice-Ficht and coworkers discuss different vaccine technologies with controlled release and adjuvant effects that occur during encapsulation [117]. They speak of a single dose pulsed release using a mixture of PLA and PLGA and sufficient immunisation through a single dose by encapsulating, e.g., subunit vaccines with PLA and PLGA.

There are also numerous examples of nasal immunisation in the field of polymers. Jaganathan and Vyas developed surface-modified PLGA microspheres with chitosan [120]. A recombinant hepatitis B surface protein was used as an antigen. As a result, they observed a lower mucociliary clearance of the modified PLGA in comparison to unmodified PLGA and they could measure a humoral and a cellular immune response after nasal administration. Pawar and coworkers used a similar approach [121]. They also encapsulated the hepatitis surface antigen in PLGA and coated this particle with chitosan. Additionally, glycol-chitosan-coated PLGA nanoparticles were prepared. Because of the nanoparticle size and a higher

mucoadhesive effect of glycol chitosan, glycol-chitosan-coated PLGA nanoparticles seemed to induce a higher systemic and mucosal immune response.

Chitosan has been used as polymer for micro- and nanoparticulate preparations in many studies, as it shows numerous beneficial characteristics for mucosal administration such as mucoadhesivity and penetration-modulating properties. Ilum and coworkers explain in their paper the mechanism of mucoadhesive properties of chitosan. As a cationic polymer, it can bind to negatively charged materials. The mucus at the surface of the respiratory tract contains mucin. Sialic acid, which is a significant component of mucin, has a negative charge at physiological pH. As a result, chitosan can electrostatically interact with mucin [122].

Heidland describes in a study the particle formation method of ionic gelation [123]. Chitosan as mucoadhesive biopolymer with adjuvant activity [124] was dissolved in diluted acetic acid and carboxymethyl cellulose (CMC) or sodium deoxycholate (DOC) as a counter ion, respectively, in water. Negatively charged dissolved CMC or DOC was dripped to positively charged dissolved chitosan. Particles were formed by ionic interaction and size could be tuned both by the chitosan quality and by the ratio of chitosan and counter ion [125]. Ovalbumin was added as a model antigen to the solution with chitosan and got incorporated into the nanoparticles upon particle formation. The prepared nanoparticle suspension was then spray dried with mannitol to form Nano-in-Microparticles to allow dry powder inhalation or dry powder nasal administration, respectively [126]. As an alternative to the method of spray drying, freeze drying can also be used to immobilise the nanoparticles, as described in the dissertation by Buske [127].

Similar particles being loaded with ovalbumin as model antigen have been tested with respect to their in-vitro and in-vivo activity with the aim to use them as therapeutic vaccine. It was shown that antigen being incorporated in chitosan-CMC nanoparticles is 10 times more effective in creating immunogenic cytokine levels and that particle uptake, antigen processing and cross-presentation can be induced in-vitro in mouse and human cells [128]. In an in-vivo study [129], a mild humoral and good cytotoxic immune response can be achieved after pulmonary instillation in combination with cAMP as mucosal adjuvant.

In her dissertation, Trows describes the preparation of chitosan microparticles as antigen carriers by spray drying [130]. For comparison, agarose nanoparticles were produced by nanoprecipitation. Both particulate vaccine systems have been assessed in a mouse model after nasal dry powder administration and without the use of further adjuvants created higher local cellular immune responses than ovalbumin alone [131].

Different antigens were tested in various preclinical studies of pulmonary vaccine in mice, rats, macaques or guinea pigs. The following diseases are the focus of preclinical development: influenza, measles,

hepatitis B, diphtheria [132], anthrax, *Yersinia pestis*, *Bordetella pertussis* [28], tuberculosis and *Bacillus Calmette–Guerin* (BCG) [133]. Several vaccines with different target groups were already tested in clinical trials: measles (\pm rubella, \pm mumps), human papilloma virus, *Streptococcus pneumoniae* [132].

To increase the stability of the measles vaccine, Sievers and coworkers developed a dry powder measles vaccine which is administered by oral inhalation or nasal–orally via a face mask [134–136]. The first phase I clinical trial was performed successfully (NCT01557699, 2013). As mentioned in Section 3.5, an aerosolised measles vaccine was developed in the 1980s. Since then, numerous children have been treated with it. As the study situation had been very inconsistent, Low and coworkers conducted a randomised, controlled trial of an aerosolised vaccine against measles involving children from 9.0 months to 11.9 months of age in 2015 [137]. The data showed that the aerosolised vaccine against measles was immunogenic, but in terms of the seropositivity rate, inferior to the subcutaneous vaccine.

More recently, two nasal vaccines against seasonal influenza were approved by the authorities: Flumist/Fluenz (MedImmune/Astra Zeneca) for the US and Europe, respectively, and Nasovac (Serum Institute of India Ltd.) in India. Both vaccines make use of an attenuated influenza virus formulated in a liquid, which must be stored cold and is administered by a nasal sprayer. The vaccines have been administered to several million patients so far without any reports of severe adverse events or vaccine failure [138] and it was shown to produce a long-lasting, humoral and cellular immune response which closely resembles natural immunity. Further, nasal vaccination against influenza provides increased protection against virus drift variants and, especially, infants and children are better protected than with the inactivated, injectable influenza vaccine [108].

Audouy and coworkers used the process of spray-freeze drying to produce a dry powder influenza vaccine for pulmonary vaccination [86,139]. Inulin as a cryoprotector and different types of inactive viruses of influenza were suspended in HEPES buffered saline. This dispersion was further spray-freeze dried in liquid nitrogen with a two-fluid nozzle. In in-vivo mouse experiments for pulmonary immunisation with this dry powder obtained comparable protection to one single intramuscular immunisation with an injection of a subunit vaccine.

Pulmonary immunisation is of particular interest in developing countries, where the use of intramuscular vaccines is often associated with problems. Tuberculosis and hepatitis B are two of the world's leading infectious diseases and the treatment and prevention of these diseases are currently important subjects of research.

Formulation of tuberculosis vaccines as dry powder with nasal or pulmonary administration may provide attractive options. Källenius and coworkers [140] discuss in their paper if new tuberculosis vaccines should be administered intranasally. They consider protection against different types of mycobacteria while using live BCG, killed BCG with adjuvant subcomponent or recombinant adenovirus-based vaccines

for intranasal vaccination. However, they also mentioned some disadvantages for nasal application, e.g., the potential access to the central nervous system and in connection therewith, the composition of the formulation. This point is also an aspect in the paper of Fourie and coworkers [141]. They developed a nasal dosage form for pulmonary administration as a preferential route for deep-lung deposition of dry powder tuberculosis vaccines and talking about spray dried formulations with leucine, PLGA, sucrose and trehalose. Garcia-Contreras and coworkers [142] also used a relatively high amount of leucine (95 %) for the spray drying process with the mycobacteria (5 %). After nine months in a refrigerator (4 °C) almost no negative effects of biological activity and other characteristics in comparison to day 1 were detectable. In in-vivo experiments with guinea pigs, pulmonary application had a higher reduction of viable bacteria per millilitre of tissue homogenate than parenteral immunisation, compared with untreated controls.

Dry powder formulations of hepatitis B could also be candidates for pulmonary administration. For this purpose, Muttill and coworkers [143] created nanoparticle-aggregate formulations, made of PLGA (core) and PEG (shell) with recombinant hepatitis B surface antigen by the double emulsion method. The aqueous nanosuspension (10 %) was then spray dried with leucine (90 %). In in-vivo experiments with guinea pigs, the formulation showed a protective antibody level and high local IgA antibody titres after pulmonary administration, which was higher compared to intramuscular administration.

These examples show that pulmonary immunisation with dry-powder formulations is possible and would be particularly useful for pulmonary diseases.

3.10 Pulmonary and nasal administration devices

3.10.1 Nasal administration

For nasal administration and deposition of vaccine formulations, properties of the devices, in addition to the formulation properties, have a great effect, especially with respect to dispersion capacity and spray velocity. Usually, nasal application requires a droplet/particle size above 10 µm. Devices that can be used for nasal administration can be found in Table 3.5.

Table 3.5. Examples of devices for nasal administration.

Devices for liquid preparations		Dry powder devices	
Device	Company	Device	Company
Nasal pressurised metered dose inhaler	3M, USA	Unit dose powder device	Aptar, France
Unitdose System	Aptar, France	Turbohaler	Astra Zeneca, Sweden
Unidose Xtra	Bespak, UK	OptiNose	Optinose UK Ltd.
Nebuliser, e.g., ViaNase	Kurve Technology, USA	Fit-lizer	SNBL Pharma, Japan
OptiNose	Optinose UK Ltd.		
Single dose spray devices Syringe with conical nosepiece with a spray tip, e.g., MAD Nasal	Teleflex, USA		
Metered dose spray pumps			

3.10.1.1 Liquid preparations

Liquid nasal formulations are mainly aqueous solutions. Drops delivered with a pipette are the oldest forms of nasal delivery and often used in infants. Liquid has to be sucked into a glass pipette and then dropped into the nostrils. The handling of nose drops for a perfect distribution in the nose is complicated, which leads to the fact that the popularity and also the compliance are rather low.

Squeeze bottles, where a bottle need to be squeezed for atomising the drug through a jet outlet, metered dose spray pumps and single dose spray devices are possibilities for mechanical spray pumps. Metered dose spray pumps are the most used ones at the market. They offer high reproducibility of the emitted dose and it is possible to avoid preservatives because of special mechanisms or constructions, e.g., aseptic air filters. Most over-the-counter (OTC) drugs, like decongestants are available in this device. For drugs with a narrow therapeutic window, expensive drugs or vaccines, single dose spray devices are preferred. For this purpose, a conical nosepiece with a spray tip can be connected to a normal syringe. This device is, for example, used to deliver FluMist®, the influenza vaccine.

For single dose or bi-dose applications, simple systems are available, in which a liquid container is pierced and emptied upon actuation (e.g., the Unitdose System from Aptar, France, or the Unidose Xtra from Bespak, UK).

Propellant driven spray systems, e.g., nasal pressurised metered dose inhalers, produce, like spray pumps, a localised deposition, but because of the quick evaporation of hydrofluoroalkanes (HFA) a noticeable "drip-out" could be less problematic.

Electrically powered nebulisers break up solutions or suspensions into small droplets with pulsation of a membrane or a vibrating mesh. They can be directly inhaled into the mouth or the nose. Because of the special mechanism characteristics and in connection therewith the deposition can be modified and used in a more targeted manner. Usually, nebulisers are bigger, not handheld devices [144].

3.10.1.2 Dry powder devices

Among other things, particle size as a result of the formulation and the dispersion capacity of the device has an effect on nasal deposition and absorption. The function of a nasal powder device is based on one of three principles: a compressible compartment to provide a pressure and create a plume, breath-actuated inhalers and nasal insufflators, where a mouthpiece is connected with a nosepiece and the patient blows the powder into its own nose while exhaling into the mouthpiece.

Different nasal powder inhalers already exist and have to be actuated by breathing. Astra Zeneca designed a modified Turbohaler for nasal administration (Rhinocort Turbohaler®, Astra Zeneca, Södertälje, Sweden). This multi dose inhaler device is marketed for nasal rhinitis.

Nasal powder sprayers have the advantage in comparison to nasal powder inhalers that the patient does not have to apply the powder with his own inspiration. Fit-lizer™ (SNBL Pharma, Japan) is a capsule based, single dose powder device. The top and the bottom of a capsule are cut off by sharp blades and the compressed plastic chamber passes the air through the device and the powder is emitted.

The unit dose powder device (UDS powder, Aptar, France) is a single dose, single use device in which an air filled compartment is compressed, a pin ruptures a membrane and the released pressure emits the plume of powder [144].

Nasal powder insufflators are breath powered technologies. OptiNose (Optinose UK Ltd., Swindon, UK) developed this breath powered, bi-directional nasal delivery technology. The patient utilises the exhaled breath to deliver the drug to the nose. Because of a special mechanism within the administration process drug deposition, clearance patterns and clinical device performance are unique and promising. OptiNose can be used for both liquid and dry powder formulation and vaccines have already been tested with the device [144].

3.10.2 Pulmonary administration

For pulmonary administration of vaccine formulations, device dispersion must result in an inhalable fine aerosol with aerodynamic characteristics suitable for lung delivery, which normally requires an aerodynamic particle size below 5 μm . Devices that can be used for pulmonary administration can be found in Table 3.6.

Table 3.6. Examples of devices for pulmonary administration [28,140,145–148].

Devices for liquid preparations		Dry powder inhalers	
Device	Company	Device	Company
Pressurised metered dose inhaler	Aptar, France 3M, USA Bespak, UK	ResQhaler	Aespira, Israel
Nebuliser		Twister	Aptar, France
Mesh nebuliser, e.g., I-neb Adaptive Aerosol Delivery System	Philips N.V., The Netherlands	TwinCaps	Hovione, Portugal
		Twincer	Stichting Groningen Centre for Drug Research, The Netherlands
Ultrasonic nebuliser, e.g., aerosonic	Flores Medical GmbH, Germany	Cyclohaler	
		PuffHalder	
Air jet nebuliser, e.g., PariLC	Pari GmbH Germany	Unihaler	

3.10.2.1 Liquid preparations

For liquid preparations, nebulisation is a feasible approach. Here, devices like mesh nebulisers, ultrasonic nebulisers or air jet nebulisers such as the Mexican device, may be utilised. Pulmonary nebulisers are normally designed to produce a fine aerosol which can penetrate deep into the lung. Unfortunately, they sometimes have been reported to adversely affect macromolecules such as antigenic proteins due to the energy stress of the nebulisation procedure. This can result in a loss of potency of the vaccine formulation [28]. Similar to nasal administration, liquid solution or suspension preparations can also be administered by a pMDI, but the pharmaceutically available propellants are generally not considered as suitable dispersants for biologicals such as vaccine preparations [28].

3.10.2.2 Dry powder inhaler

The most promising pulmonary vaccine delivery devices are dry powder inhalers. Sievers and coworkers used two types of dry powder inhalers, which actively disperse the measles vaccine powder and are meant for either oral inhalation or inhalation with a face mask from a reservoir, where the dispersed powder cloud is captured. Actuation is performed by actively generating an air puff either by a squeeze bulb or by an air filled syringe [136]. The air puff entrains the powder, which is dispersed in a powder reservoir, from where it is subsequently inhaled. During storage, the vaccine powder is either stored in single dose blisters in the case of PuffHaler or in special "capsules" having thin plastic films on either side, which rupture upon actuation [145]. Another possibility is to store the single vaccine dose in gelatine or HPMC capsules, which can then be used in the commercially available Cyclohaler device or other capsule based dry powder inhalers such as the Unihaler [146] or the Twister (Aptar Pharma, France). The principle of operation is the same for all of these passive dry powder inhalers. The capsule is placed in the device, it is pierced or cut open and upon patient inhalation, the powder is entrained in the inhalation air flow and gets inhaled to the lung. The powder is dispersed passively by the patient's inhalation. Hence, efficiency depends on the patient's inhalation capabilities and manoeuvre. For vaccination applications, single or dual use systems might be of advantage as vaccination should best be carried out as a single shot, perhaps with one or two boosts after certain time intervals. Here, a dual dose system such as the TwinCaps Inhaler (Hovione, Portugal) could be used. Two doses are prefilled in capsules within the device and can be inhaled subsequently. The inhaler itself is disposable after use. Other single dose devices made for disposal after use are, among others, the Twincer (Stichting Groningen Center for Drug Research, The Netherlands) and the DryPod (now resQhaler, Aespira, Israel) [147]. Both inhalers have originally been developed for dry powder inhalation of high dose drug products, but they could also be used for vaccination. In the resQhaler, the powder dose is prefilled in a mesh-like reservoir, which starts beating upon patient inhalation through the device and with this release, the powder (ActiveMesh technology). In the Twincer device [148], the powder is sealed in a blister, which is opened directly prior to inhalation. The powder is dispersed with the help of two classifier chambers and is entrained in the patient's airflow upon inhalation.

For all types of inhalers, it is important that the vaccine formulation is compatible with the material it directly comes into contact with. This might be an issue for formulations of protein antigens being filled in gelatine capsules, but also for inhaler materials, which could adsorb formulation components by electrostatic interactions with this minimising the emitted dose or could lead to forced degradation of the antigen. In general, the device plays an important role for the dispersion and, hence, delivery of the formulation. Therefore, a vaccine formulation for pulmonary delivery must always be developed and characterised together with the respective inhalation device.

3.11 Conclusion

Vaccination via the respiratory tract is an attractive strategy for a number of applications in preventive and therapeutic immunisation. The mucosa-associated lymphoid tissue is an excellent induction site as both systemic and local immune response along with a high cytotoxic effect and a cellular immune response can be used. The multitude of formulation possibilities and the comparatively simple handling of the devices leave room for the development of new ideas. Precisely for these reasons, the respiratory tract is an application route that will be increasingly used for vaccination in the future.

4 Materials

Numerous materials are used in this work. In the following, the most important ones will be discussed in more detail. All used reagents, cells, materials and instruments are listed in the appendix.

4.1 Zinc oxide tetrapods

Zinc oxide tetrapods in the form of bulk are a white to slightly yellowish white loose powder with a cotton wool-like consistence. Zinc oxide tetrapods as single particles have a three-dimensional tetrapodial structure with arm diameters of 200 nm to 1 μm and an arm length of 5 μm to 30 μm , whereby the angle between the arms is approximately 109.5° [149,150].

Zinc oxide tetrapods can be produced by flame transport synthesis (FTS), which is shown in Figure 4.1. [151]. A mixture of polyvinyl butyral (PVB), zinc powder (Zn) and ethanol is burned in a ceramic crucible at 900°C in a muffle furnace. The flame generated during the combustion of PVB transports the Zn microparticles upwards, where they are subsequently converted to the vapour state, in the form of individual Zn atoms, Zn dimers, Zn trimer, etc. These highly unstable variants of zinc in the vapour state immediately participate in nucleation and growth processes with the help of oxygen molecules in the environment. Initially, Zn and oxygen form a stable core. Further available Zn and oxygen atoms lead to the growth of a 1D structure, which develops into a 3D-tetrapod-like structure through homogeneous nucleation. This highly efficient and cost-effective process leads to a yield of 99.9 %, whereby the structure of the zinc oxide tetrapods is highly dependent on the position of the material to be harvested.

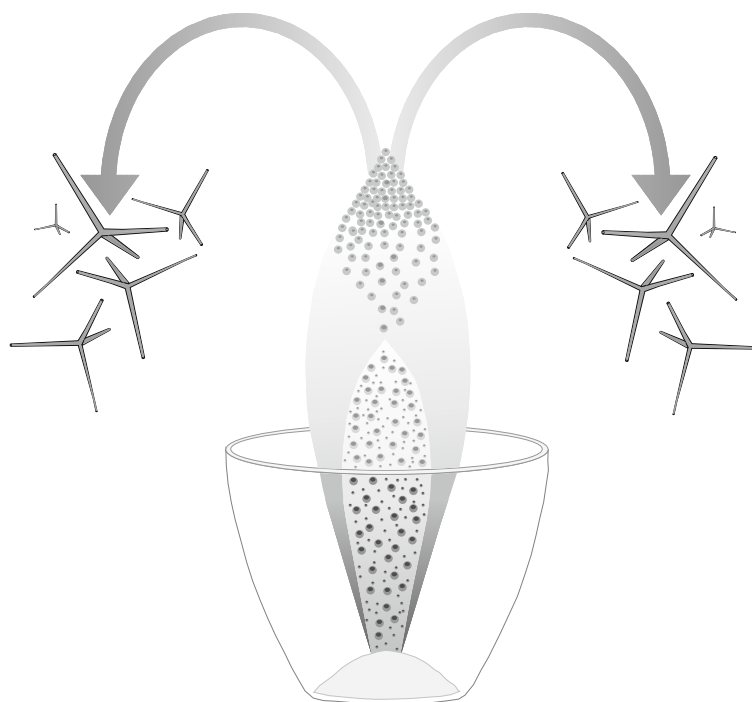


Figure 4.1. Schematic picture of the flame transport synthesis.

The potential uses of zinc oxide tetrapods are manifold due to its properties. They are summarised in an article by Yogendra Kumar Mishra and Rainer Adelung [152]. Particularly worth mentioning is the application area in biomedical technology. Zinc oxide tetrapods were used, among other things, for nanoimmunotherapy in in-vivo mice experiments with promising results. Zinc oxide tetrapods had a strong virus trapping ability, when used as a microbicide, and significantly reduced the clinical signs of the disease and effectively decreased the mortality of the animals. In addition, viruses bound to zinc oxide tetrapods could be absorbed by antigen-presenting cells in the mucosa and then presented to activate the immune system. Furthermore, the administration of the viruses in combination with the zinc oxide tetrapods led to an increase in T cell proliferation and in the CD4-positive and CD8-positive cell population. These results suggested that zinc oxide tetrapods might be useful as a prophylactic, preventive and/or adjuvant formulation for viral infections [149,151].

The zinc oxide tetrapods used were provided by the working group "Functional Nanomaterials" headed by Prof. Rainer Adelung (Institute of Materials Science, Faculty of Engineering, Kiel University, Germany).

4.2 Zinc oxide

Zinc oxide is a white to pale yellowish white powder, which is practically insoluble in water and ethanol 96 %, but soluble in dilute mineral acids [153]. Zinc oxide particles are mostly rod and needle-shaped crystalline particles in a size range from 20 nm to 400 nm [154].

Zinc oxide can be produced by three different methods: the French indirect method, the American direct method or a wet chemical method [155]. In the French method, zinc metal is melted and evaporated by boiling. Afterwards it is oxidised with the oxygen in the air to produce zinc oxide. In the American method, the zinc-containing raw material, e.g., zinc ore, has to be first reduced by carbon. The resulting zinc vapour is then oxidised by air combustion and zinc oxide is formed. In the wet chemical process, zinc scraps are first dissolved in sulphuric acid. Afterwards, the resulting zinc sulphate is purified, converted into zinc hydroxide by the addition of sodium hydroxide and separated. To produce zinc oxide, the precipitate has to be dried.

Zinc oxide has many different uses and is, e.g., used as a semiconductor in electronic components, as a catalyst in the chemical industry and as a white pigment in the production of various colours. Zinc oxide also plays an important role in the manufacture of cosmetic products, e.g., in sunscreens, as it is transparent in the visible part of the light spectrum but acts as a physical filter against UV-B and UV-A sunlight. Furthermore, zinc oxide is used in the pharmaceutical industry for the production of zinc creams, pastes, patches and bandages due to its antibacterial and astringent effect [154].

As an essential trace element, zinc is found as a divalent cation in almost all tissues of the human body and is a cofactor of numerous enzymes. Zinc is involved in cell growth, insulin storage, wound healing

and an intact immune system, whereby the latter is probably due to improved maturation of the T lymphocytes and an increased number of T lymphocytes [156,157].

The zinc oxide used was purchased as "zinc oxide (for external use)" from Caesar & Loretz GmbH, Germany.

4.3 Aluminium hydroxide and aluminium phosphate

The aluminium hydroxide used is a white to almost white translucent, viscous colloidal pseudo-boehmite gel. It is an aluminium compound consisting of fine crystalline boehmite [158]. Boehmite is a long $\text{AlO}(\text{OH})$ chain with terminal water molecules. As the chains are considerably shorter in pseudo-boehmite, the water content increases accordingly at the same concentration [159]. The gel has an aluminium concentration of 10.69 mg/mL and an isoelectric point at pH 10.2, which means that at the pH value of the gel of pH 7.6, the $\text{AlO}(\text{OH})$ chains are positively charged, enabling the adsorption of negatively charged antigens [160].

The aluminium phosphate used is a wet gel suspension of aluminium hydroxyphosphate ($\text{Al}(\text{OH})_x(\text{PO}_4)_y$). It is an amorphous material with both hydroxyl and phosphate groups on the particle surfaces [161]. The suspension has an aluminium concentration of 0.5 % (w/w) and an isoelectric point at pH 5 [162]. As a result, at the pH value of the wet gel suspension of pH 6.4, $\text{Al}(\text{OH})_x(\text{PO}_4)_y$ is negatively charged and thus enables the adsorption of positively charged antigens [163].

The binding of the antigens to aluminium hydroxide and aluminium phosphate can be achieved by two different interactions: on the one hand, the recently described electrostatic forces and on the other hand, a ligand exchange related adsorption, which is stronger in comparison to the non-covalent electrostatic interaction, as phosphate groups of an antigen can displace a hydroxyl group on the adjuvant surface. This covalent interaction ensures a prolonged antigen release [160,164].

The associated formation of a depot and the increased production of antibodies describes the first of three possible adjuvant mechanisms of alum enhancing humoral immunity. The second mechanism comprises the development of an inflammation and the associated activation of antigen-presenting cells. The conversion of a soluble antigen into a non-soluble particulate form, resulting in phagocytosis by the antigen-presenting cells with subsequent presentation of the antigens, explains the third theory [164]. Due to the good adjuvant effect with different antigens and the favourable production method, aluminium hydroxide and aluminium phosphate are the most commonly used adjuvants in human and veterinary adsorbed vaccines [165].

As early as 1926 Alexander Glenny discovered the adjuvant effect of vaccines containing aluminium salts [164]. Since then, there have been repeated discussions about numerous side effects of these formulations, such as neurotoxic effects and accumulation in the human body. A maximum dose of

aluminium of 1.25 mg per dose is specified in the monograph Ph. Eur.: "Vaccines for humans" as the limit value, with all approved vaccines being well below this value [153]. The Paul-Ehrlich-Institute has not found any evidence of aluminium-related toxicity nor any risk to children or adults from aluminium-containing vaccines [166].

As aluminium hydroxide and aluminium phosphate show a very good adjuvant effect in a humoral, but not in a cellular immune response, it was only used in this work as a reference in the adsorption experiments, analogous to the monograph Ph. Eur.: "Hydrated aluminium hydroxide for adsorption" [153]. The method for determining the adsorption capacity was performed in a modified way as described in chapter 5.2.4.

The aluminium hydroxide used as reference substance for adsorption was obtained as "VAC20" from SPI Pharma, USA and the aluminium phosphate as "Adju-Phos" from Brenntag Biosector, Denmark.

4.4 Mannitol

Mannitol is a white to almost white crystalline powder which is easily soluble in water (216 mg/mL) and practically insoluble in ethanol 96 %.

Mannitol is a non-reducing sugar alcohol that can be obtained from plants, algae or fungi. It is industrially synthesised by hydrogenation from hexoses, e.g., fructose or mannose. Mannitol is characterised by polymorphism and can occur in three modifications, α , β and δ . The β -modification is the most thermodynamically stable one. The used mannitol is Pearlitol 200 SD and was produced by spray drying a previously hydrogenated mannose solution. The result is an anhygroscopic powder with a molecular mass of 182.2 g/mol, an average particle size of 170 μm and a high stability [167]. Along with lactose and glucose, mannitol is one of the sugars approved by the FDA as an excipient in inhalation. Mannitol can be used in particle engineering for inhalation, as an active pharmaceutical ingredient for inhaled products to treat patients with cystic fibrosis and as a protective excipient for stabilising proteins [168]. The main use of mannitol, however, is its use as excipient for direct tableting and, in a mixture with 0.5 % highly dispersed silica, as a filler for capsule manufacture due to its good properties.

The mannitol used was obtained as Pearlitol 200 SD from Roquette Frères, France.

4.5 Hyaluronic acid

Hyaluronic acid is a white to almost white, very hygroscopic powder, which is slightly soluble to soluble in water (5 mg/mL), but practically insoluble in acetone and anhydrous ethanol.

Sodium hyaluronate, which is the sodium salt of hyaluronic acid, can be produced using two different methods. First, sodium hyaluronate can be extracted from rooster combs, whereby the animals must comply with food law requirements for human consumption and second, by fermentation with

streptococci. It should also be noted that the manufacturing process must ensure that pyrogenic and inflammation promoting components are reduced to a minimum [153].

Hyaluronic acid is a glycosaminoglycan and is often present as a long-chain, linear polysaccharide. It is a key component of connective tissue and involved in numerous processes in the human body, e.g., as a pseudoplastic lubricant for all joint movements. Sodium hyaluronate also shows advantages in the field of formulation development, e.g., it can be used as an adhesive between individual nanoparticles to produce a microparticle as well as a mucoadhesive and penetration enhancing additive [169,170].

The hyaluronic acid used for the pulmonary and nasal formulations was purchased as sodium salt from Caesar & Loretz GmbH, Germany.

4.6 Proteins

Various proteins are used in the experiments as model antigens. Antigens are substances that can be recognised by the immune system and induce an immune reaction. In experimental immunology, proteins are often used as antigens. A particularly high immunogenicity can be expected if the proteins are as large and complex as possible and not closely related to the body's own proteins [171]. The proteins used are explained in more detail below.

4.6.1 Bovine serum albumin

Bovine serum albumin (BSA), a protein of the blood plasma of the domestic cattle, consists of 583 amino acids and has a molecular mass of approximately 66 kDa. The isoelectric point is at pH 4.9.

BSA is the most abundant protein in the blood plasma of cattles, where it is responsible for colloid osmotic pressure and thus for maintaining plasma volume. It has a high binding capacity for both polar and non-polar substances and acts as a transport protein [172].

Serum albumins can be obtained by various methods, e.g., cold ethanol fractionation (Cohn-fractionation), modified ethanol fractionation methods, heat shock or preparative chromatography. The BSA used is produced using cold ethanol fractionation. This gentle fractionation is performed at low temperatures (0 °C to 10 °C). Several fractions are separated by different ethanol concentrations, targeted selection of pH value, ionic strength and temperature. Since the fraction five contains albumin, BSA is also named Cohn fraction V. With the help of crystallisation or activated carbon filtration the albumin solutions are further purified. Finally, the albumin is freeze dried to ensure a stable, storable form [173].

The freeze dried beige "powder" (Bovine serum albumin, Merck KGaA, Germany) used for the adsorption experiments has a purity higher than 96 % and is used as a reference substance in numerous biochemical experiments due to its inexpensive production [174]. BSA was used as protein for the adsorption experiments.

4.6.2 Ovalbumin

Ovalbumin (OVA), the main component of chicken egg white, is a glycoprophosphoprotein consisting of 385 amino acids. With a molecular mass of about 44 kDa, it is sufficiently large and complex to be immunogenic. For this reason, it is often used as an antigen for immunological research. Ovalbumin denatures at a temperature of 84.5 °C and has an isoelectric point at pH 4.5.

Ovalbumin is produced by crystallisation. It is precipitated from chicken egg white by ammonium sulphate and then crystallised. The resulting crystalline ovalbumin is then freeze dried for better storage and stability [175].

The freeze dried beige "powder" used (Albumin from chicken egg white, Merck KGaA, Germany) has a minimum purity of 98 % [176]. It was used as model antigen for all in-vitro experiments.

4.6.3 Alpha-lactalbumin

Alpha-lactalbumin, a small, globular whey protein, consists of 123 amino acids and has a molecular mass of approximately 14 kDa. The isoelectric point is at pH 4.4.

Together with β -1,4-galactosyltransferase, alpha-lactalbumin forms the lactose synthetase and catalyses lactose production in the mammary gland [177].

Alpha-lactalbumin is a component of whey proteins, the second highest number of proteins in mammalian milk. With the help of acid precipitation and ion exchange membranes, the different components of the whey proteins are separated. Finally, alpha-lactalbumin has to be freeze dried to ensure stability and storage [178].

The freeze dried white to beige powder used (Alpha-lactalbumin from bovine milk, Merck KGaA, Germany) has a purity of at least 85 % and was used for adsorption experiments.

4.6.4 Avidin

Avidin, a component of chicken egg white, is a glycoprotein containing four identical subunits. The monomer consists of 128 amino acids. This results in a total molecular mass of approximately 66 kDa and an isoelectric point at pH 10.5.

Avidin has the ability to bind biotin and can therefore cause a biotin deficiency. A property which can lead to numerous disorders and negative effects in the human body, is used in the biotechnological field to breed special maize varieties. The transgenic maize is able to produce avidin and thus bind high amounts of biotin. This makes it toxic to and prevents development of insects.

Avidin can be obtained by various methods, e.g., ion exchange chromatography or affinity chromatography. As it is often contaminated with lysozyme after an ion exchange chromatography a special ion exchange chromatography procedure with defined pH value, ionic strength and salts can be

used for purification purposes. A subsequent chromatography is increasing the purity of avidin. Because of the high affinity to biotin, avidin can also be purified using affinity chromatography with a very high purity and recovery [179]. The used avidin is purified using affinity chromatography, dialysed and finally freeze dried for a better stability and storage.

The freeze dried white to beige powder used (Avidin from egg white, Merck KGaA, Germany) has a purity higher than 98 %. It was used for the adsorption experiments.

4.6.5 Lysozyme

Lysozyme, obtained from chicken eggs, consists of 129 amino acids and has a molecular mass of approximately 14 kDa. The isoelectric point is at pH 11.

Lysozyme is able to break glycosidic bonds and thus it has an important role in bacterial defence mechanism, e.g., in the human respiratory tract. Lysozyme cleaves a substance in the bacteria wall, peptidoglycan, by hydrolysing the 1,4- β -linkages between the N-acetyl-muramic acid and N-acetyl-D-glucosamine residues. Gram-negative bacteria are less sensitive to lysozymes than gram-positive bacteria due to comparably low amounts of peptidoglycan in their bacteria walls

Different methods can be used to obtain lysozyme, e.g., precipitation, aqueous two-phase system, ion exchange chromatography, affinity chromatography and ultrafiltration, whereby different purities are produced [180]. The lysozyme used is purified from chicken egg, crystallised three times, dialysed and supplied as freeze dried powder for a better stability and storage.

The lysozyme used for the adsorption experiments (Lysozyme, Merck KGaA, Germany) has a purity of at least 90 %.

4.7 Cells for in-vitro experiments

To classify the influence of the formulations in-vivo, various in-vitro cell experiments were carried out. The cell models used for these experiments are presented below.

4.7.1 Calu-3

Calu-3 cells are adherent, pulmonary epithelial cells. They originate from the adenocarcinoma of a 25-year-old male, Caucasian patient [181]. They are well differentiated, characterised and reflect sufficient the properties of the submucosal bronchial glands, i.e., the production of fluid, needed in the surface of the respiratory tract, as well as mucus and immunologically active substances. In addition, they can grow as a confluent air-liquid interface, which allows a better approach to the in-vivo situation [182].

Calu-3 cells were purchased from the American Type Culture Collection (ATCC, USA) and used for cytotoxicity tests (passage number 53) in a liquid culture and for pH studies (passage number 56) in an air-liquid interface.

4.7.2 RPMI2650

RPMI2650 cells are adherent, nasal epithelial cells. They were derived from squamous cell carcinoma of the septum of a 56-year-old male patient [183]. Like Calu-3 cells, they are able to form a confluent air-liquid interface. However, they tend to form clusters with free spaces between them. Nevertheless, their use in permeation studies is repeatedly described [184,185].

RPMI2650 cells (passage number 17) were used for cytotoxicity tests in a liquid culture in cooperation with the working group of Prof. Ben Forbes at Kings College London.

4.7.3 Murine bone marrow-derived dendritic cells

Murine bone marrow-derived dendritic cells (BMDC) were isolated and cultured from mouse bone marrow. Dendritic cells form a bridge between the innate and adaptive immune system. They are specialised in taking up a broad spectrum of pathogens and presenting their antigens on the cell surface [171].

Due to the small number of dendritic cells that can be isolated, ex-vivo studies are often a challenge [186]. For this reason, the experiments were conducted with the Vaccine Design and Delivery group of Prof. Camilla Foged at University of Copenhagen. Murine BMDC were obtained from 10 weeks to 12 weeks old female CF57BL/6N mice as described in the methods section in chapter 5.3.2.1. They were subsequently used for immunological cell experiments.

4.8 Devices

Various inhalers are used for the in-vitro experiments. In the following, the Unit dose system powder device (UDS powder, Aptar Pharma, France) for nasal administration and the Cyclohaler (Jenapharm GmbH & Co. KG, Germany) for pulmonary administration are presented.

4.8.1 Unit dose system powder device

The UDS powder is designed for single dose nasal therapies where a small, precise amount of powder formulation is needed. One possible use would be immunisation, as usually only one dose per interval is necessary. The UDS powder is a device that is ready to use and also protecting the drug, e.g., from light prior to administration. It is independent of the patient's performance and can be used with one hand in any position [187]. In Figure 4.2 the schematic structure of the UDS powder is shown.

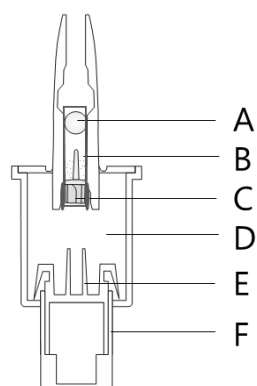


Figure 4.2. Schematic picture of the unit dose system powder device. A) Plastic ball, B) Sample container + sample, C) Plastic thorn, D) Air, E) Bar, F) Lower part.

The corresponding amount of the formulation is weighed into the sample container, which is already closed on one side with a plastic thorn. The container is then closed with a plastic ball and the UDS powder is assembled accordingly to the instruction. The UDS powder is activated by pressing the lower part of the device. The thorn, pushed up by the bar, can push the ball upwards and an open system is created. The compressed air resulting from the activation expands and a cloud of powder is created.

4.8.2 Cyclohaler

The Cyclohaler is a passive, capsule based powder inhaler for pulmonary administration of single doses. Figure 4.3 shows the schematic of the Cyclohaler.

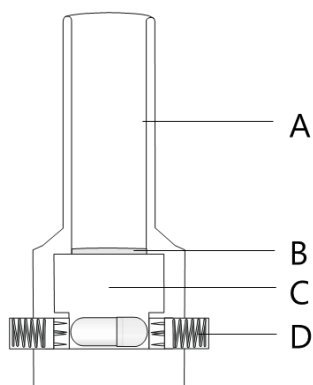


Figure 4.3. Schematic picture of the Cyclohaler. A) Mouthpiece, B) Mesh, C) Rotation chamber, D) Capsule reservoir + capsule + perforation mechanism.

The appropriate amount of the formulation is weighed into a capsule and placed in the Cyclohaler in advance to the inhalation. By pressing the two buttons while the inhaler is held vertically, the capsule is pierced evenly on both sides with four needles and thus opened. This enables the formulation to leave the capsule during the inhalation process. The capsule is lifted by the breath of the patient, leaves the capsule reservoir, rotates and therefore disperses the powder. A mesh prevents inhalation of the capsule and capsule fragments.

5 Methods

5.1 Spray drying

Spray drying was used to produce both pulmonary and nasal microparticles.

Dry powders can be produced from liquids in a continuous and rapid process which usually results in particles with a low density [188], while the morphology of the dried particles can vary considerably. Besides the classical spherical hollow spheres, there is also the possibility to produce solid, shell-only or wrinkled particles. This depends, like the particle size, on the drying parameters and the used materials [189,190]. Spray drying is suitable for the targeted production of dry powder formulations and for the preparation of powders for further processing. Thus, it is used in various areas in the pharmaceutical industry like powders for inhalation and tableting as well as in the food industry, where it for instance can be used for the production of milk powder.

The formulations produced within the project consisted of different concentrations of zinc oxide and/or mannitol. The model antigen ovalbumin and hyaluronic acid were constant in concentration. Six nasal formulations (Table 5.1) and six pulmonary formulations (Table 5.2) with different concentrations of zinc oxide and mannitol were spray dried. The different compositions of the suspensions for spray drying are listed in the following tables.

Table 5.1. Composition of the suspensions for the preparation of the nasal formulations.

	Zinc oxide, g	Mannitol, g	Acetic acid 2 %, g	Hyaluronic acid, g	Ovalbumin, g
Formulation 1	5	-	95	0.05	0.5
Formulation 2	4	1			
Formulation 3	3	2			
Formulation 4	2	3			
Formulation 5	1	4			
Formulation 6	-	5			

Table 5.2. Composition of the suspensions for the preparation of the pulmonary formulations.

	Zinc oxide, g	Mannitol, g	Water, g	Hyaluronic acid, g	Ovalbumin, g
Formulation 1	1	-	99	0.01	0.1
Formulation 2	0.8	0.2			
Formulation 3	0.6	0.4			
Formulation 4	0.4	0.6			
Formulation 5	0.2	0.8			
Formulation 6	-	1			

Zinc oxide as alternative adjuvant and mannitol as matrix-forming excipient were added to acetic acid 2 % (nasal formulations) or water (pulmonary formulations). This mixture was sonicated (Bandelin SONOREX SUPER RK 514 BH, BANDELIN electronic GmbH & Co. KG, Germany) for 30 min at room temperature. Hyaluronic acid as adhesive between the single zinc oxide particles was added while mixing the suspensions on a magnetic stirrer (IKA IKAMAG RET-GS, IKA-Werke GmbH & Co. KG, Germany) for 5 min and finally ovalbumin was added. After the suspension had been homogenised on the magnetic stirrer for another 10 min, the spray drying process was started.

Figure 5.1 shows the Mini Spray Dryer B-290 (Büchi Labortechnik AG, Switzerland) being used for the project.

The prepared suspension was continuously stirred during the spray drying process by the help of a magnetic stirrer in order to prevent sedimentation of the zinc oxide particles and thus to ensure a homogeneous distribution.

The spray drying process can be divided into three main subprocesses: atomisation, drying and separation [191]. The liquid is transported by a pump to the spray nozzle, where it is atomised into fine droplets and finely distributed in the gas stream (atomisation). Different nozzles can be used to atomise the liquid. In the case of the rotary disc atomiser [192], the liquid is dispensed on a rapidly rotating disc. The centrifugal force transports the liquid to the edge and breaks it into fine droplets. The ultrasonic nozzle [190,191] generates droplets by high frequency vibration at an atomising surface, which allows generating particle sizes between 10 µm and 60 µm. In a single-fluid nozzle [192], the liquid is forced through the nozzle at high pressure and set in a rotating motion in a swirl chamber. The two-fluid nozzle [192] (Figure 5.2) consists of two tubes, whereby the outer tube is transporting the gas and the inner

tube is transporting the liquid. Particles in the range of 2 μm to 25 μm are producible. The three-fluid [190,191] nozzle has a total of three channels, whereby it can consist of gas/liquid/gas or liquid/gas/liquid. The last three nozzles have in common that the liquid is broken up into small droplets when leaving the nozzle.

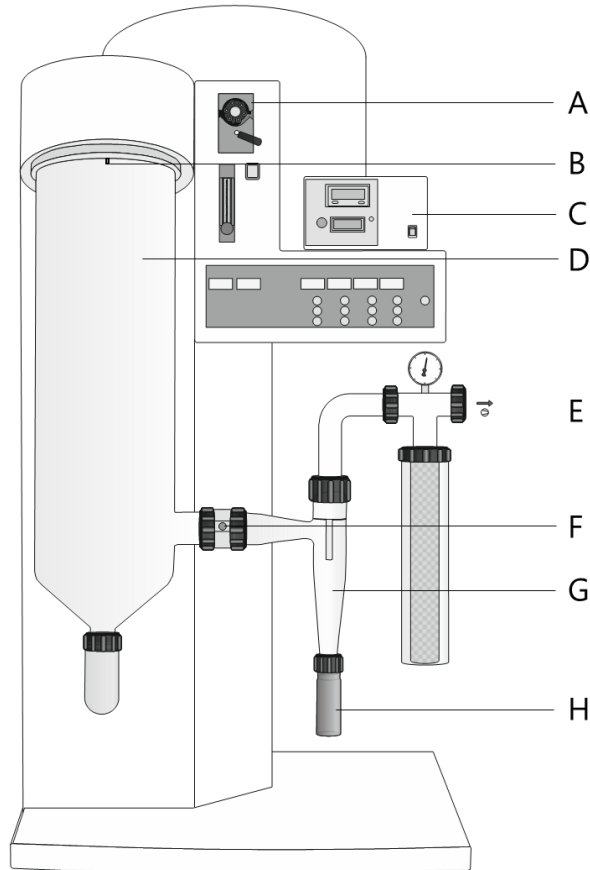


Figure 5.1. Schematic picture of the used Mini Spray Dryer B-290. A) Pump, B) Two-fluid nozzle, C) Magnetic stirrer, D) Drying chamber, E) Drying gas, F) Temperature sensor (outlet temperature), G) Cyclone, H) Dried powder.

A two-fluid nozzle was used for the project. Both the particle range for nasal application ($> 10 \mu\text{m}$) and the pulmonary application ($< 5 \mu\text{m}$) could be covered with this nozzle.

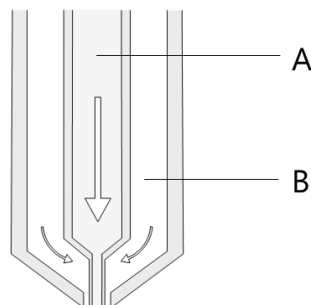


Figure 5.2. Schematic picture of a two-fluid nozzle. A) Liquid, B) Spray gas.

In the drying chamber, finely atomised droplets get in contact with hot drying air (drying). The advantage of the so called co-current flow is that the liquid droplet meets the hot air when they are the moistest, i.e., the initially high quantities of water are removed and due to the evaporative cooling, the

temperature at the droplet surface remains relatively low despite the high inlet temperature. The maximum temperature a particle comes into contact with is the outlet temperature, which can be set by the spray rate of the liquid. In the cyclone, the dried particles are finally separated from the drying gas (separation).

As already mentioned, the particle size can be controlled by adjusting the process parameters. The particles become smaller the lower the concentration of the liquid used and the higher the spray flow rate is. Reducing the pump rate and replacing the water with solvents can also have a corresponding influence on the particle size, but this effect is less noticeable [189].

With these considerations in mind, appropriate modifications were made for the production of the nasal and pulmonary formulations. In addition to the concentration, the process parameters were also adjusted. At an inlet temperature of 110 °C the suspension was atomised with a two-fluid nozzle and a spray gas flow rate of 536 L/min (nasal formulations) or 601 L/min (pulmonary formulations). The nozzle used consisted of a 0.7 mm nozzle tip and a 1.5 mm nozzle cap. This geometry led to a mixing of the gas and the fluid. The aspirator was set to 100 % (corresponds to approximately 35 m³/h) and the nozzle cleaner to 4 to prevent the nozzle from being clogged by the zinc oxide particles. The spray dryer was operated in a co-current drying gas and the outlet temperature was set to 55 °C ± 2 °C. Dried particles were finally separated from the drying gas in the cyclone, collected and analysed with different methods.

5.2 Characterisation

Various methods were used to characterise the materials and formulations.

5.2.1 Morphology and elementary analysis

The materials were visualised using the method of scanning electron microscopy.

Finely bundled electron beams are guided over the sample in a specific pattern and the backscattered electrons are detected. The interaction of the electrons with the material creates an image of the sample. To avoid interactions with air molecules, the entire process takes place in vacuum [193]. Non-conductive materials have to be coated with a thin gold layer.

For this purpose, the samples were first attached to an aluminium stub with double-sided carbon tapes and then coated for 40 s using the BAL-Tec SCP 050 Sputter Coater (Leica Microsystems, UK). The samples were measured with the Phenom World XL (Thermo Fisher Scientific Inc., USA) scanning electron microscope at an acceleration voltage of 5 kV to 15 kV, a vacuum of 10 Pa and a spot size of 3.3 nm. After the visualisation, the particle size of the material could be measured, e.g., with the help of the Feret diameter (Figure 5.3). In contrast to the volume-based distribution of laser diffraction, only a number-based particle size distribution would be generated.

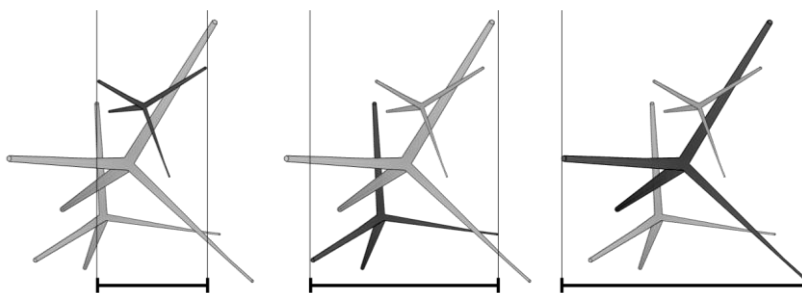


Figure 5.3. Schematic picture showing the possibility to measure samples with the Feret diameter. Vertical tangents are placed at the left and right end of the particle and the distance between the two lines is the diameter of the particle.

Energy dispersive X-ray spectroscopy (EDS) was used for elementary analysis using the scanning electron microscope.

An electron beam is used to stimulate the samples to emit X-rays. This enables the detection of substance quantities of less than 0.1 pg [194]. For this method, the materials should not have to be coated with a conductive gold layer.

The samples attached to an aluminium stub with double-sided carbon tapes, were directly measured with the Phenom World XL scanning electron microscope at a voltage of 15 kV, a vacuum of 1 Pa and a spot size of 5.1 nm.

5.2.2 Particle size distribution

Laser diffraction was used to determine the particle size distribution.

Spherical particles exposed to a beam of monochromatic light are evaluated with the help of the resulting diffraction pattern. Fraunhofer diffraction, a theory often used in the pharmaceutical field, assumes that the light waves initially spread in a linear and parallel manner. Strictly speaking, Fraunhofer theory can only be used if the particles are larger than the wavelength of the light used. With the Mie theory it is possible to measure even smaller particles, whereby additional information on the optical material properties, such as the refractive index or the absorption, are required [195].

If there is a particle in the beam path, the light beam is diffracted and detected by a multielement photodetector. Larger particles cause small diffraction rings with high intensity in comparison to smaller ones which in turn will lead to greater diffraction rings with less intensity. Numerical values representing the diffraction pattern are used to evaluate the measurements and transformed using optical models and mathematical algorithms. The optical models are based on spherical particles, which means even for non-spherical particles a particle size distribution equivalent to the spherical one is obtained. The result is a volume-based particle size distribution, since the ratio of the volume of a particle size class to the total particle size range is calculated [153,195]. This type of distribution is symbolised by the index 3, e.g., distribution density q_3 and distribution sum Q_3 . The distribution density provides information about the volume fraction of a certain particle size class. The distribution sum, on the other hand, indicates the

quantity of all particles with an equivalent diameter less than or equal to a certain particle size. Since the laser diffraction method cannot distinguish between agglomerates and single particles, the agglomerates have to be dispersed to single particles before the measurement. The possibilities used are explained in more detail below.

5.2.2.1 Particle size distribution with the RODOS module

Particle size distribution of zinc oxide and all spray dried formulation was measured using a HELOS laser diffractometer (Sympatec GmbH, Germany) with a RODOS module.

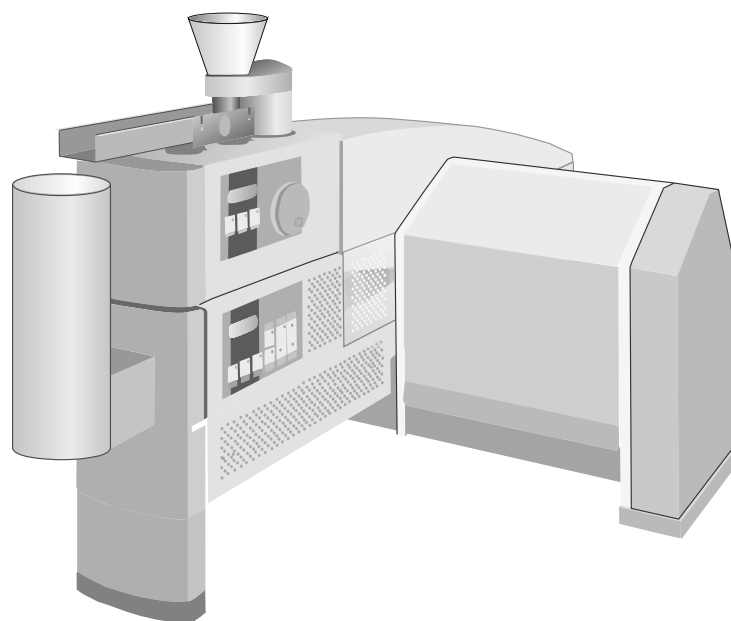


Figure 5.4. Schematic picture of the RODOS module.

With the RODOS module the powders were manually fed into the system and dispersed with pressurised air of 3 bar. The optimum pressure was selected using the span value (Equation 5.1), which gives an indication of the width of the distribution. It is important that the pressure is high enough to disperse agglomerates but not as high that it could lead to fragmentation of the primary particles. X_{10} , X_{50} and X_{90} are characteristic values of a particle size distribution. X_{10} means that 10 % of the particles have a smaller diameter than the value x . The span gives an indication of how far the 10 %-value and the 90 %-values are apart, normalised with the 50 %-value, i.e., the smaller the span value, the narrower the distribution. The pressure that resulted in the smallest span value leads to the narrowest particle size distribution and was chosen for the measurements. The particle size distribution was measured above an optical concentration of 0.5 %.

Equation 5.1. for calculating the span value.

$$span = \frac{x_{90} - x_{10}}{x_{50}}$$

5.2.2.2 Particle size distribution with the SPRAYER module

Particle size distribution of the nasal formulations was measured using a HELOS laser diffractometer with a RODOS module or with a SPRAYER module in combination with a Unit-Dose-System (UDS) powder device.

With the SPRAYER module 20 mg of the formulations were dispersed using the UDS powder device as dispersing unit. The distance to the measuring zone was set to 10 cm, the spray angle to 45° [196] and the actuator force to 60 N. The particle size distribution was measured for both modules with an R2 lens (particle sizes < 87.5 µm) and above an optical concentration of 0.5 %.

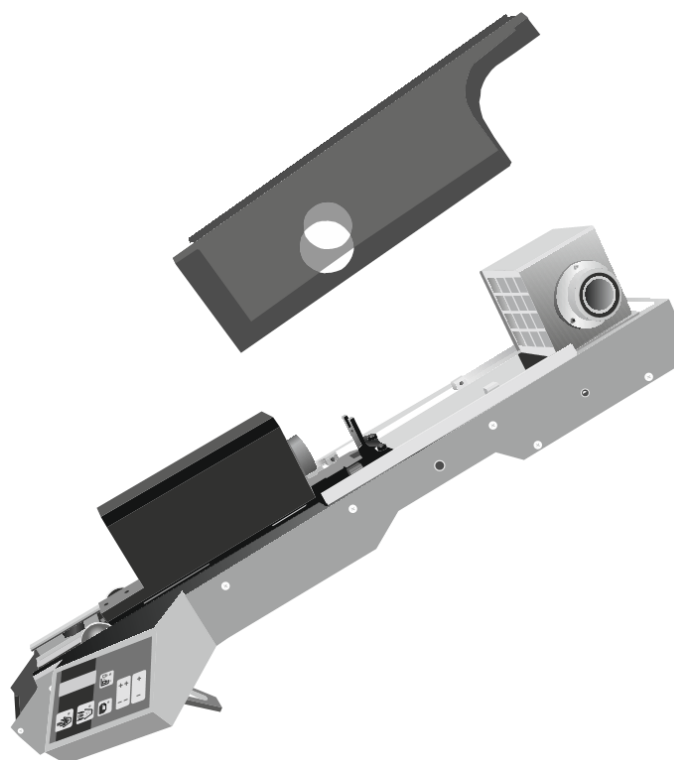


Figure 5.5. Schematic picture of the SPRAYER module.

5.2.2.3 Particle size distribution with the INHALER module

Particle size distribution of the pulmonary formulations was measured using a HELOS laser diffractometer with a RODOS module or with an INHALER module in combination with a Cyclohaler.

For measurements with the INHALER module 10 mg of the formulations were weighed into a capsule. With the aid of a software-controlled vacuum system, which ensured precise volume flow control, it was possible to measure formulations in dry powder inhalers that are dispersed by forces comparable to respiration. At a maximum adjustable pressure of 138 mbar, a breath of 82.7 L/min (DFM 2000 flow meter, Copley Scientific, UK) was simulated. A 90° glass angle imitated the throat and a preseparator ensured the separation of large particles. The particle size distribution was measured for both modules with an R1 lens (particle sizes < 35.0 µm) and above an optical concentration of 0.5 %.

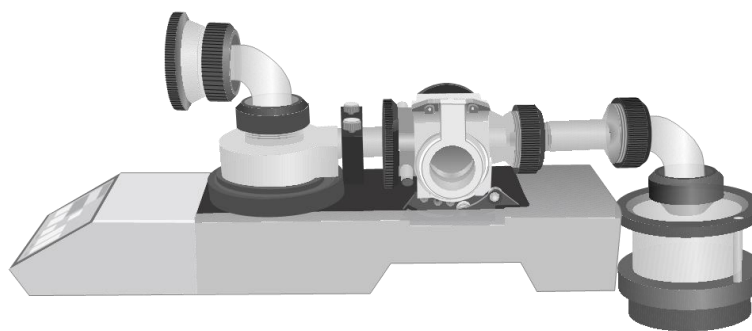


Figure 5.6. Schematic picture of the INHALER module.

5.2.3 Protein quantification

Proteins can be quantified in different ways. UV/Vis spectroscopy is a very simple method for the detection of proteins. Aromatic amino acids (tyrosine, tryptophane, phenylalanine) in the protein allow to measure the UV absorption at an absorption maximum of 280 nm, although other chromophores can easily interfere. Another possibility is to measure an absorption maximum at a wavelength of 190 nm for the detection of peptide bonds. Despite of the strong absorption of peptide bonds, oxygen can disturb the measurements and therefore lead to falsified results. Moreover, conventional spectrometers just show reduced performance at lower wavelengths. Peptide bonds can also absorb at higher wavelengths up to approximately 230 nm, whereby the intensity of the absorption decreases with increasing wavelength [197].

As a compromise the protein concentrations were determined at a wavelength of 205 nm in a semi micro quartz cuvette (Hellma GmbH & Co. KG, Germany) with a Shimadzu UV-1280 (Shimadzu Corporation, Japan) or at a wavelength of 220 nm in a 96-well plate (lumox 96 multiwell, Sarstedt AG & Co. KG, Germany) using the FluoStar Omega spectrometer (BMG Labtech GmbH, Germany). Different wavelengths were chosen because the lower limit of the adjustable wavelengths in the FluoStar Omega spectrometer was 220 nm. Nevertheless, the same results were obtained for 205 nm in the Shimadzu UV-1280 and for 220 nm in the FluoStar Omega spectrometer using a calibration curve.

5.2.3.1 Loading

Protein content of the spray dried formulations was determined by quantifying ovalbumin at a wavelength of 205 nm with a semi micro quartz cuvette. A sample of 2 mg of the nasal formulations was suspended in 2 mL phosphate buffer (6.8 mg/mL KH_2PO_4 in demineralised water) and a sample of 2 mg of the pulmonary formulations was suspended in 2 mL water. After the sample was vortexed at 3,000 rpm for 30 sec (IKA Vortex 4 basic, IKA-Werke GmbH & Co. KG, Germany), it was centrifuged at 10,000 rpm and 25 °C for 10 min (Centrifuge 5430 R, Eppendorf AG, Germany) to remove insoluble components, e.g., zinc oxide. Finally, the ovalbumin content in the supernatant was determined. The loading efficiency was calculated from the difference between the used ovalbumin amount and the measured concentration in the supernatant.

5.2.3.2 SDS-PAGE

SDS-PAGE, sodium dodecyl sulphonate polyacrylamide gel electrophoresis, can be used to determine the molecular weight of proteins and thus also provide information on fractionation of proteins contained in the particles. Polyacrylamide gels are stable and chemically inert. They are formed during polymerisation of an acrylamide/bisacrylamide stock solution (60 g acrylamide 2 x, 1.6 g bisacrylamide ad 200 mL aqua bidest) by adding ammonium persulphate (500 mg ad 5 mL aqua bidest) and tetramethyl ethylenediamine. A clear, transparent gel is obtained. Pore size can be controlled by the amount of polyacrylate and crosslinker.

A combined gel composed of a stacking gel with a concentration of 6 % polyacrylamide and a pH of 6.8 and a resolving gel with a concentration of 12.5 % polyacrylamide and a pH of 8.8 was prepared. 2 mg (nasal formulations) or 1 mg (pulmonary formulations) of the sample were suspended in 1 mL of incubation mix and centrifuged for 3 min at 13,000 rpm (Heraeus Biofuge pico, Thermo Fisher Scientific, USA). The incubation mix and all buffers contained SDS (Table 5.4), which masked the intrinsic charge of the protein and provided a constant negative charge. Thus, after application to the gel, the protein migrated in the electric field towards the anode. 3 µL incubation mix and 8 µL sample were loaded per well in the stacking gel following Table 5.3. After 8 min and a voltage of 120 V all samples were stacked on the interface of stacking gel and resolving gel. At a voltage of 200 V ovalbumin was separated. Ovalbumin as raw material and a peqGOLD Protein Marker III (VWR International GmbH, Germany) were used as references. After 45 min, the voltage was turned off and the resolving gel was rinsed with demineralised water. To stain the protein bands of the proteins the gel was first stained with 0.2 % coomassie blue (1 g coomassie brilliant blue, 50 mL glacial acetic acid, 125 mL isopropanol ad 500 mL aqua bidest) and finally silver staining (25 mL silver nitrate solution 2.5 %, 10 µL formaldehyde ad 250 mL aqua bidest) followed.

Table 5.3. Filling scheme of the wells of the SDS-PAGE gel with formulations 1 to 6 (F1 to F6), incubation mix (I), ovalbumin (OVA) and marker.

1	2	3	4	5	6	7	8	9	10	11	12	13	14	15
F1	I	F2	I	F3	I	OVA	I	marker	I	F4	I	F5	I	F6

Table 5.4. Composition of the buffers and incubation mix used.

Buffer for the electrophoresis chamber	25 mmol/L tris-base	15.14 g
	192 mmol/L glycine	72.07 g
	0.1 % SDS	5.0 g
	Aqua bidest	ad 5.0 L
	pH	8.3
Stacking gel buffer	250 mmol/L tris-base	15.14 g
	0.4 % SDS	2.0 g
	Aqua bidest	ad 500 mL
	pH	6.8
Resolving gel buffer	750 mmol/L tris-base	45.43 g
	0.4 % SDS	2.0 g
	Aqua bidest	ad 500 mL
	pH	8.8
Incubation mix	Resolving gel buffer	2.5 mL
	SDS	0.2 g
	Glycerine	1.0 mL
	β -Mercaptoethanol	0.5 mL
	Bromophenol blue	0.2 mL
	Aqua bidest	ad 10 mL

5.2.3.3 Size exclusion chromatography

SEC, size exclusion chromatography, is routinely used for analysis of proteins, often to evaluate the aggregation profile of proteins as well as for the separation and quantification of protein mixtures. The separation technique [198] of the SEC is based on the molecular size of the components. Very large molecules are excluded from the packed column material and elute first. Smaller molecules, depending

on their size, can diffuse into the pores to varying degrees, with the smallest penetrating furthest and therefore eluting last [199].

To determine aggregates, molecular weight of ovalbumin in the formulations was measured by size exclusion chromatography using Äkta Pure 25 (GE Healthcare, Germany) in combination with multi angle light scattering (MALS, DAWN 8⁺, Wyatt Technology Corporation, Germany). The complete SEC-MALS system comprised the UV detector at a wavelength of 280 nm, the SEC column (Superose™ 6 Increase 10/300 GL, GE Healthcare Bio-Sciences AB, Sweden), MALS and the refraction index detector (RI, Optilab T-rex, Wyatt Technology Corporation, Germany). The buffer was a solution of 0.15 mol/L NaCl, 0.025 mol/L NaH₂PO₄ monohydrate and 0.025 mol/L Na₂HPO₄ dihydrate (pH 6.85) in demineralised water, which was degassed using an ultrasonic water bath for 30 min (Bandelin SONOREX SUPER RK 514 BH, BANDELIN electronic GmbH & Co. KG, Germany). 40 mg (nasal formulations) or 20 mg (pulmonary formulations) of the sample were suspended in 1 mL buffer and filtered to separate undissolved zinc oxide particles using Chromafil Xtra PET 45/25 (Macherey-Nagel GmbH & Co. KG, Germany). The final ovalbumin concentration was 2 mg/mL. 100 µL of the sample were eluted at a flow rate of 0.7 mL/min. The data were analysed with ASTRA version 7.1.2.5 (Wyatt Technology Corporation, Germany) with a dn/dc of 0.185 mL/g [200].

5.2.4 Adsorption

Zinc oxide tetrapods and zinc oxide should be capable for being loaded with a protein. The adsorption capacity of zinc oxide tetrapods and zinc oxide was tested according to the monograph Ph. Eur.: "Hydrated aluminium hydroxide for adsorption" [153] with some modifications. Aluminium hydroxide and aluminium phosphate were used as references to ensure that the experimental set-up was valid. The substances were weighed or pipetted according to the target concentration of 1 mg/mL, i.e., 2 mg zinc oxide tetrapods and zinc oxide, 0.187 mL aluminium hydroxide (10.69 mg aluminium/mL) and 400 mg aluminium phosphate (0.5 % (w/w) aluminium). Different proteins were tested in the experiment: bovine serum albumin, avidin, ovalbumin, alpha-lactalbumin and lysozyme. After the protein solution had been added to the samples with a target concentration of 200 µg/mL, they were exposed to a 360° rotation at room temperature for 1 h. During this process the substances were in permanent contact with the dissolved protein. To perform the rotation, the adsorption wheel used was rotated at a speed of 20 rpm using a friabilator (ERWEKA GmbH, Germany). Finally, the suspensions were centrifuged at 10,000 g for 5 min at 25 °C with the Centrifuge 5430 R. The protein content of the supernatant was analysed at 205 nm with a calibration curve using a semi micro quartz cuvette. The protein content adsorbed at the surface of the samples could be calculated as the difference between the used amount of the protein and the measured protein concentration of the supernatant.

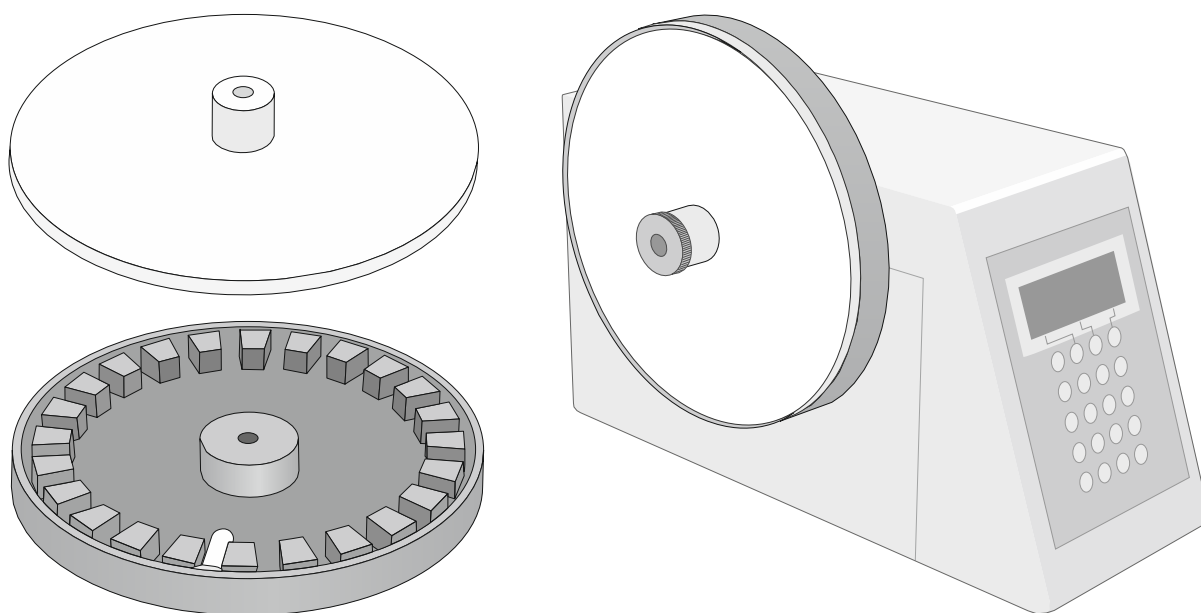


Figure 5.7. Schematic picture of the adsorption wheel (left) in combination with the friabilator (right).

5.2.5 Aerodynamic assessment

5.2.5.1 Next Generation Pharmaceutical Impactor

The aerodynamic characterisation of aerosols can be carried out using cascade impactors. Impaction analysis are methods for analysing in-vitro aerodynamic performances, i.e., aerodynamic diameters, but they cannot be seen as a lung model because of a lack of physiological conditions in the human lungs [201]. The principle is based on inertia-driven deposition of particles in the airstream. Inertial forces are dependent on the particle mass, which leads to heavier particles deposit earlier than comparatively lighter ones.

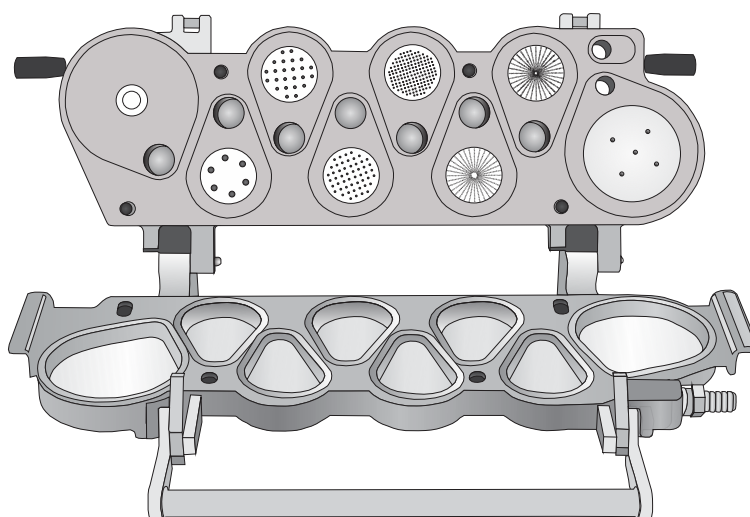


Figure 5.8. Schematic picture showing an open NGI.

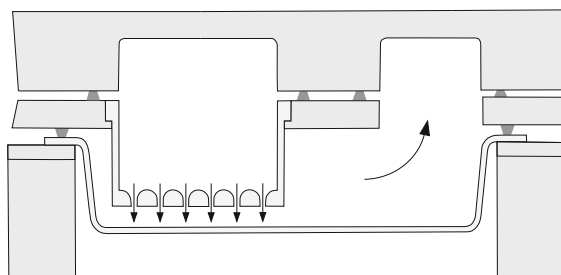


Figure 5.9. Schematic picture showing the principle of the NGI.

In the Next Generation Pharmaceutical Impactor (NGI, Copley Scientific, UK), a number of seven nozzles with decreasing orifice diameters and a terminal micro-orifice collector (MOC) are connected in series. In addition, the distance between the orifices and the impact plates is becoming increasingly narrow. As a result, the speed of the air increases from stage to stage. The larger the particle, the more likely it is to be impacted. Smaller particles, on the other hand, can follow the path further and are separated only at higher air speeds [195]. Depending on the flow rate and the nozzle diameter, the cut-off diameter, which is an aerodynamic diameter, of each stage is calculated according to Ph. Eur. 2.9.18: "Preparation for inhalation: aerodynamic assessment of fine particles" [153] using Table 5.5 and Equation 5.2, whereas y and x are factors from the table and Q is the flow rate in L/min [153].

Table 5.5. Parameters for calculating the cut-off diameter of each stage.

Cut-off diameter	y	x
7 (stage 8 = MOC)	0.34	0.67
6 (stage 7)	0.55	0.60
5 (stage 6)	0.94	0.53
4 (stage 5)	1.66	0.47
3 (stage 4)	2.82	0.50
2 (stage 3)	4.46	0.52
1 (stage 2)	8.02	0.54

Equation 5.2. for calculating the cut-off diameter.

$$d = y * \left(\frac{60}{Q}\right)^x$$

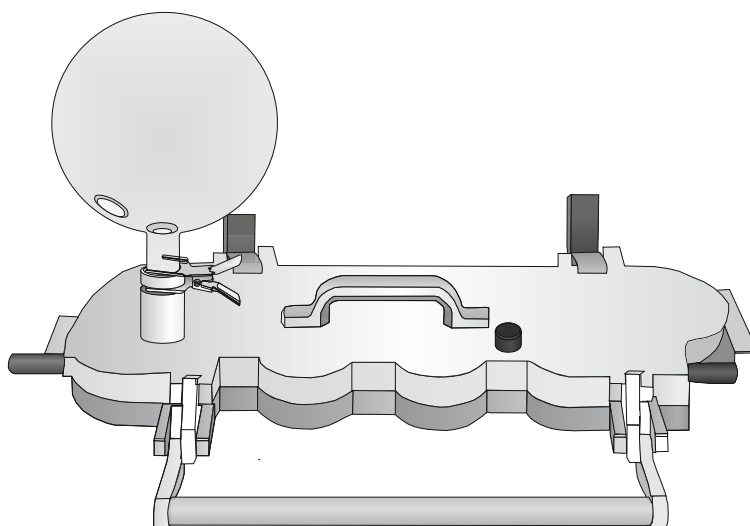


Figure 5.10. Schematic picture of the NGI with the nasal expansion chamber.

Aerodynamic assessment of the nasal formulations was performed according to Ph. Eur. 2.9.18: "Preparation for inhalation: aerodynamic assessment of fine particles" [153] with the NGI equipped with a 2 L nasal expansion chamber (NEC). All stages and the NEC were coated with a stage coating (isopropanol + 1,2-propanediol, 1 + 1). 20 mg of the formulations were weighed into a UDS powder device and the flow rate was set to 15 L/min using a DFM 2000 flow meter. The deposited amount of the formulations was calculated by dissolving the powder deposited at each stage in phosphate buffer (6.8 mg/mL potassium dihydrogen phosphate; NEC: 15 mL, stage 1 and MOC: 10 mL, stage 2 to 7: 5 mL) and analysing the content of ovalbumin using UV spectroscopy (205 nm). Deposition in the NEC and fine particle fraction (FPF), i.e., particles with an aerodynamic diameter smaller than 5 μm , were calculated using Excel.

Aerodynamic assessment of the pulmonary formulations was performed according to Ph. Eur. 2.9.18: "Preparation for inhalation: aerodynamic assessment of fine particles" [153] with the NGI equipped with a preseparator, a throat and a mouthpiece. All stages were coated with a stage coating (isopropanol + 1,2-propanediol, 1 + 1) and 15 mL of water were filled in the preseparator. 10 mg of the formulations were weighed into a capsule and the flow rate was set to 100 L/min using a DFM 2000 flow meter. Two capsules and a Cyclohaler were used per run. The deposited amount of the formulation was determined by dissolving the powder deposited at each stage, in the throat, the mouthpiece, the device and the capsules in water (device and capsules as combination as well as mouthpiece and throat as combination: 15 mL, stage 1 and MOC: 10 mL, stage 2 to 7: 5 mL) and analysing the content of ovalbumin of all samples, including the preseparator, using UV spectroscopy (205 nm). Fine particle fraction was calculated using Excel.

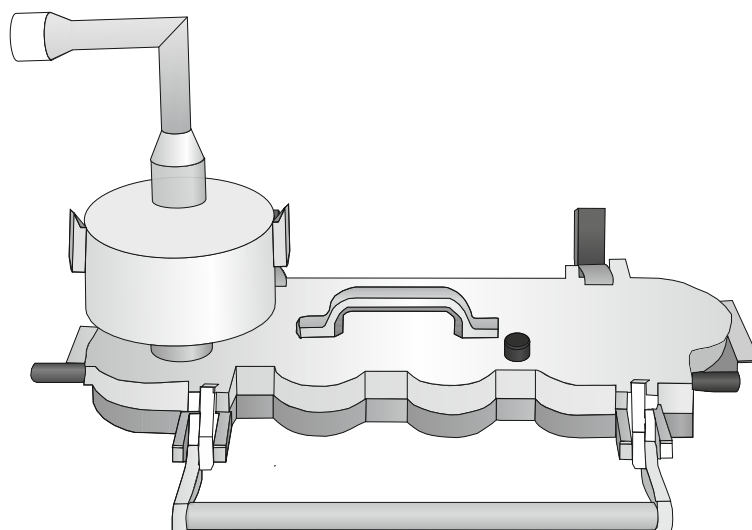


Figure 5.11. Schematic picture of the NGI with the mouthpiece, the throat and the preseparator.

Particle sizes as aerodynamic diameter of the particles were calculated using the equation described above according to Ph. Eur. 2.9.18: "Preparation for inhalation: aerodynamic assessment of fine particles" [153]. The aerodynamic diameter is an equivalent diameter, i.e., the measured diameter corresponds to the diameter of a sphere with a density of 1 g/cm^3 having the same settling velocity as the investigated particle.

5.2.5.2 Precise Inhale

The Precise Inhale system from Inhalation Sciences, Sweden was used to identify the best formulation out of the six spray dried formulations for pulmonary application for the finally planned in-vivo studies in terms of their aerodynamic performance.

The Precise Inhale system is an aerosol generating system for in-vitro, in-vivo and ex-vivo experiments. Most aerodynamic characterisation methods, such as the NGI, are used to analyse the in-vitro aerodynamic performance, but they cannot be seen as a lung model. By using different exposure modules, the Precise Inhale can generate data for the same aerosol in in-vitro, in-vivo and ex-vivo experiments. Even small amounts of a sample are sufficient to generate aerosols in precise, repeatable and controlled doses [202].

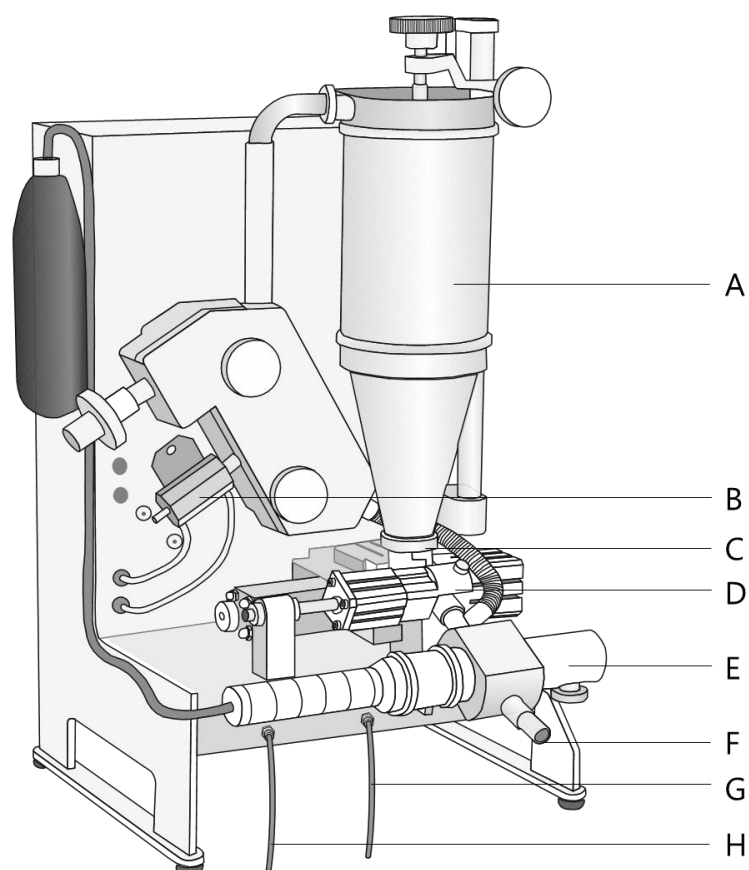


Figure 5.12. Schematic picture of the Precise Inhale. A) Aerosol holding chamber, B) Air humidifier, C) Powder chamber with impactor nozzle, D) V1 valve, E) Aerosol monitor, F) In-vitro exposure block, G) Vacuum, H) Exposure pressure.

For the tests with the Precise Inhale, 1 mg of each sample was weighed into the powder chamber. A high-pressure air jet of 130 bar was used to generate an aerosol from the powder in the 300 mL aerosol holding chamber with the aid of the impactor nozzle. This high pressure causes rapid deagglomeration of the powder agglomerates. The V1 valve was closed during the aerosol generating step. The resulting aerosol cloud rose upwards and was then drawn onto the in-vitro exposure block with the help of a vacuum flow with an exposure airflow of 400 mL/min and an exposure time of 90 sec. The V1 valve was open for the dispensing step. During the exposure, all data, e.g., particle size distribution and maximum aerosol concentration were recorded with the aid of the aerosol monitor. The yield, the maximum aerosol concentration and the inhaled aerosol dose were evaluated using the Precise Inhale and calculated using Excel.

The Precise Inhale measurements were assessed in cooperation with the Vaccine Design and Delivery group of Prof. Camilla Foged at University of Copenhagen.

5.2.6 pH and solubility

In physiology, pH values play an essential role in the activity of enzymes, the permeability of membranes, the structure of cells and during the immune reaction.

Solubility and pH changes of the formulations were tested in 24-h-solubility studies in various media, including phosphate buffers, sodium chloride solutions and simulated biological media for the nose and lungs.

Buffer systems are almost resistant to pH changes and change their pH value only minimally when acids or bases are added. Physiological buffer systems, including phosphate buffers, stabilise the pH value in the organism and thus serve to balance mainly temporary and minor pH value fluctuations [203].

Table 5.6. Composition of buffers and solutions [153].

Phosphate buffer	Potassium dihydrogen phosphate (KH_2PO_4)	6.80 mg/mL
	pH	1.2 – 7.4
Sodium chloride solution	Sodium chloride (NaCl)	2.923 mg/mL
	pH	1.2 – 7.4
Simulated nasal fluid, SNF [204,205]	Sodium chloride (NaCl)	7.45 mg/mL
	Potassium chloride (KCl)	1.29 mg/mL
	Calcium chloride dihydrate ($\text{CaCl}_2 \cdot 2 \text{H}_2\text{O}$)	0.32 mg/mL
	pH	6.4
Simulated lung fluid, SLF [206] Gamble's solution	Magnesium chloride (MgCl_2)	0.095 mg/mL
	Sodium chloride (NaCl)	6.019 mg/mL
	Potassium chloride (KCl)	0.298 mg/mL
	Di sodium hydrogen phosphate (Na_2HPO_4)	0.126 mg/mL
	Sodium sulphate (Na_2SO_4)	0.063 mg/mL
	Calcium chloride dihydrate ($\text{CaCl}_2 \cdot 2 \text{H}_2\text{O}$)	0.368 mg/mL
	Sodium acetate ($\text{NaC}_2\text{H}_3\text{CO}_2$)	0.574 mg/mL
	Sodium hydrogen carbonate (NaHCO_3)	2.605 mg/mL
	Sodium citrate dihydrate ($\text{Na}_3\text{C}_6\text{H}_5\text{O}_7 \cdot 2 \text{H}_2\text{O}$)	0.097 mg/mL
pH	7.4	

In order to simulate the physiological conditions, six phosphate buffers and six sodium chloride solutions with different physiological pH values were prepared: pH 1.2 and pH 2.5 (stomach), pH 4.0 (vaginal mucosa), pH 5.5 (endosomes), pH 6.4 (nose), pH 7.4 (blood, lungs). Since not all physiological aspects could be addressed with a phosphate buffer and hence correlation with in-vivo data was difficult to achieve, simulated biological media were used for the nose and lungs [206]. The compositions of all media are given in Table 5.6. The pH values were adjusted using a 0.2 mol/L sodium hydroxide solution and a 0.2 mol/L hydrochloric acid solution [153].

A 24-h-solubility study was performed to investigate saturation solubility and pH change of the formulations.

50 mg of the nasal formulations were suspended in 5 mL of the solutions. The samples were placed in an orbital shaker (Universalschüttler SM, Edmund Bühler GmbH, Germany) for 24 h. Before adding the formulations and after the experiment pH values (WTW Inolab pH 730 in combination with pH-electrode SentTix 81, Xylem Analytics Germany Sales GmbH & Co. KG, Germany) were monitored.

50 mg (pH 1.2) or 5 mg (pH > 1.2) of the pulmonary formulations were suspended in 5 mL of the solutions. The samples were placed in an orbital shaker for 24 h. Before adding the formulations and after the experiment pH values (Mettler Toledo SevenCompact Benchtop Meter with pH-electrode InLab Ultra-Micro-ISM, Mettler Toledo GmbH, Germany) were monitored.

After 24 h undissolved zinc oxide was separated via centrifugation and the zinc concentration in the supernatant was quantified with a zincon assay.

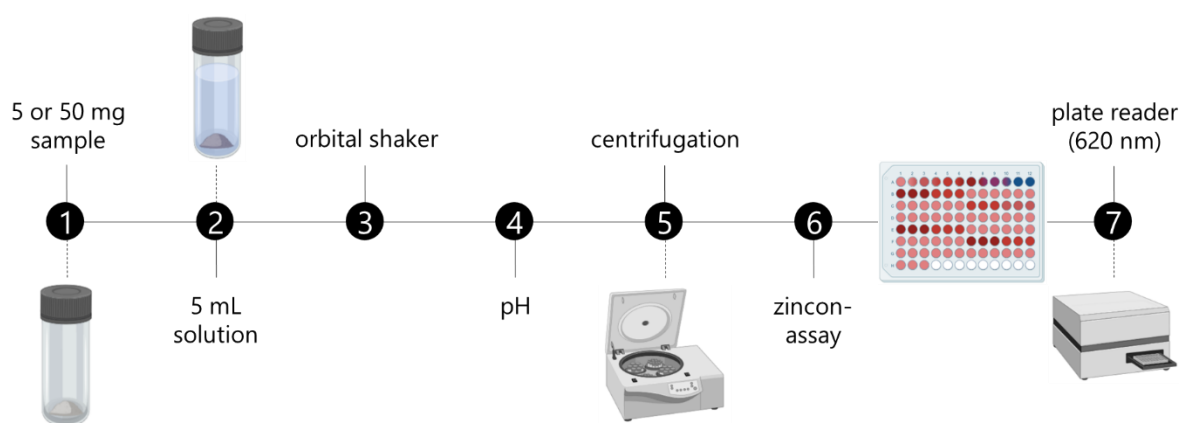


Figure 5.13. Schematic overview of the work flow of the 24-h-solubility study created with BioRender.

The determination of dissolved zinc ions can be done photometrically using a zincon assay. Zinc ions (Zn^{2+}) form a blue coloured complex with zincon in an alkaline environment, which can be measured at 620 nm. Since heavy metals can also form a coloured complex with zincon, they have to be complexed with cyanide before analysis. The addition of cyclohexane ensures the selective release of zinc ions (Zn^{2+}) [207]. Since all formulations only contained zinc oxide as a substance detectable by the zincon assay and demineralised water was used during the whole experiment the risk of interference factors was

negligible. 3.6 mL of demineralised water, 1 mL of sodium tetraborate buffer pH 9 (4.76 g $\text{Na}_2\text{B}_4\text{O}_7 \cdot 10 \text{H}_2\text{O}$ in 500 mL of water) and 0.1 mL of the sample were mixed with 0.3 mL of zincon solution (0.013 g zincon and 0.2 mL of 0.1 mol/L NaOH in 10 mL of water). 200 μL of the mixtures were analysed in a 96-well plate (microplate 96 well F, Sarstedt AG & Co. KG, Germany) using the FLUOstar Omega spectrometer at 620 nm [208,209].

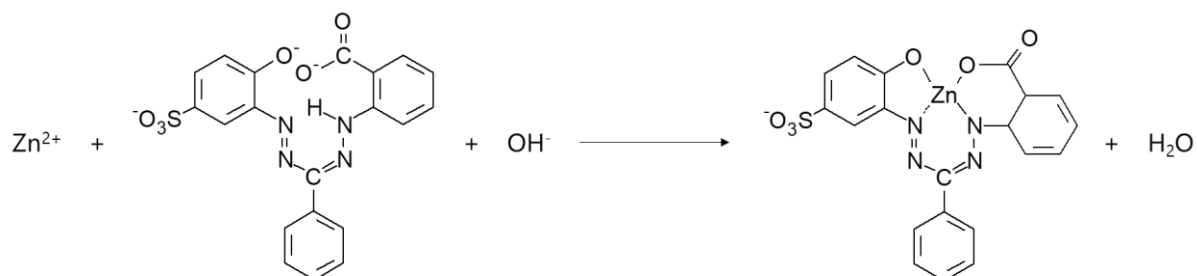


Figure 5.14. Reaction equation for the zincon assay. Red zincon (left) reacts with Zn^{2+} in an alkaline environment to a blue colour complex (right).

5.2.7 Release study

The release of ovalbumin from the pulmonary formulations was assessed using ThinCerts (Greiner Bio One International GmbH, Austria). ThinCerts are cell culture inserts for 12-well plates with a transparent membrane of polyethylene terephthalate (PET) and a pore diameter of 1 μm . 10 mg of the dry sample were placed on a ThinCert. 1 mg Ovalbumin was used as reference. After 1 mL water was added to the well below the ThinCert, the 12-well plate was gently moved at 15 rpm for 6 h at room temperature. 100 μL were drawn as sample directly at the beginning (0 min) and after 2 min, 5 min, 10 min, 15 min, 20 min, 45 min, 1 h, 2 h, 4 h and 6 h and replaced by fresh water. After 6 h, the filter was rinsed with the water below the ThinCert to determine the total protein content. The ovalbumin concentration was determined photometrically at 220 nm in a 96-well plate.

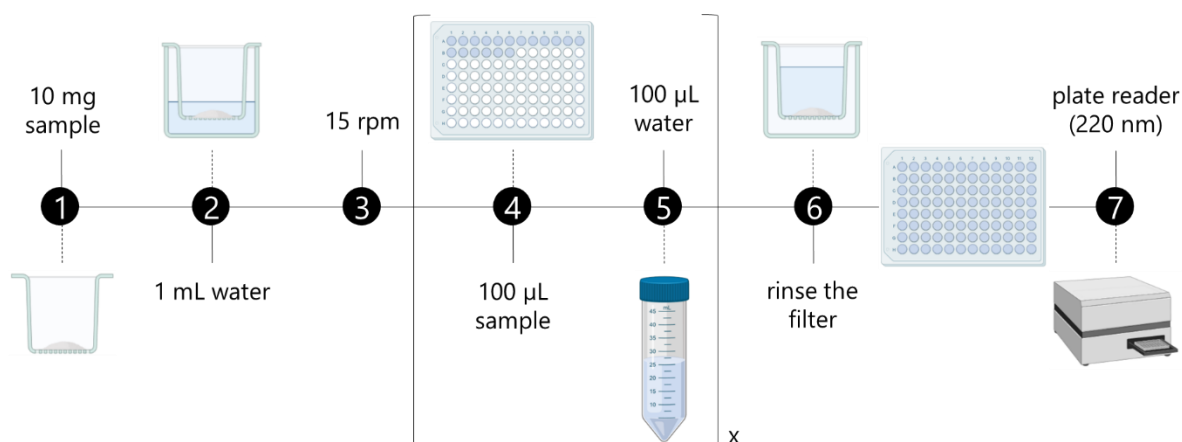


Figure 5.15. Schematic overview of the work flow of the release study created with BioRender.

5.2.8 Osmolality

To compare the osmotic activity of the pulmonary formulations the osmolality was measured with the Osmomat 030 (Gonotec GmbH, Germany).

Since both, osmotic pressure and freezing point depression of a solution are colligative properties, influenced only by the number of dissolved particles, the freezing point depression of the solution was used as measurement principle.

For this purpose, 1 mg of the sample was dissolved or suspended in 1 mL water and the osmotic activity was measured using the Osmomat 030.

5.2.9 Hygroscopicity

Hygroscopicity of the pulmonary formulations was measured using dynamic vapour sorption (DVS).

DVS is a gravimetric technique which measures the mass of a sample as it changes in response to alterations in humidity under isothermal conditions at 25 °C.

The double tree method with two cycles of 0 % - 90 % - 0 % relative humidity was chosen for the measurements. 11 mg of the formulations were weighed into the metal basket of the DVS 1 from SMS (Surface Measurement System Ltd., UK). After reaching a gravimetric equilibrium at a relative humidity of 0 %, where no significant change in mass (< 0.005 %/min for 10 min, but maximum 360 min) was noticed, relative humidity was increased or decreased by 10 % to the next stage. When gravimetric equilibrium was reached again, the relative humidity was increased or decreased by another 10 % and the measurement continued accordingly.

5.2.10 Crystallinity

5.2.10.1 X-ray powder diffraction

Crystallinity of the spray dried formulations was measured with X-ray powder diffraction using a STOE STADI P diffractometer built-up with a transmission geometry and equipped with a Cu K α anode in combination with a DECTRIS MYTHEN 1K strip detector (STOE & Cie GmbH, Germany) in the range of 5° to 50° 2 Theta.

The principle of X-ray powder diffraction is based on the diffraction of X-rays by electron clouds of individual atoms in the sample. The atoms in a crystal are arranged in different lattice planes. They are excited to oscillate by the X-ray beam and emit wave fronts of the same wavelength. During the measurement, different measuring angles are used. If the lattice planes of a crystal are at a certain angle to the direction of the X-ray beam, the path lengths of the emitted wave fronts of the different lattice planes can differ by an integer multiple. The diffracted beams, which thus oscillate in phase, intensify each other. At intermediate angles, phase-shifted oscillations occur, which weaken or level each other

out. This interference condition of the integer multiple can be described with the help of Bragg's equation. In a powder sample, crystalline particles are presented in a disordered manner, hence diffractions can occur at a multitude of different lattice planes. When the beam hits a powder sample, a large number of concentric diffraction cones of different angles are generated, which would produce an image of numerous concentric circles with the beam as centre point. The angle position can be determined by the intensity maxima of the circles. This makes it possible to differentiate between crystalline (sharp diffraction pattern) and amorphous (no sharp diffraction pattern) materials. Due to its crystal structure, every crystalline substance has a characteristic diffraction pattern [153,192].

5.2.10.2 Differential scanning calorimetry

Differential scanning calorimetry (DSC) enables the quantitative determination of changes in enthalpy and specific heat during heating and cooling of a substance. During a constant heating rate, the temperature difference can be analysed. The evaluation is carried out graphically by plotting the energy change over the temperature, which, in addition to the quantitative recording of the change, also enables the determination of the respective onset temperature of heat-flow related events. This method enables the quantitative and qualitative characterisation of a variety of thermal processes, e.g., melting, evaporation and recrystallisation. Based on the characteristic thermal processes of a substance, the determination or at least an indication of the presence of a substance is also possible with the help of a reference substance [195].

To get an idea about the components of the nasal formulations after spray drying, the Diamond DSC (PerkinElmer Inc., USA) was used with a heating rate of 20 °C/min in the range of 60 – 350 °C. Data were analysed using the Pyris software (PerkinElmer Inc., USA). Zinc oxide and zinc acetate were used as references.

5.2.11 Density and surface area

5.2.11.1 Density

When determining the density of solids, different densities can be distinguished in principle. Bulk density and particle density were measured within this work. While particle density determined by gas pycnometry already considers parts of the volume of the pores inside the individual particles, the bulk density also measures the volume of the voids formed in the powder bed. The bulk density is always lower than the particle density.

The bulk density was determined using a 10 mL cylinder. 10 mL of the zinc oxide tetrapods or the zinc oxide were filled into the cylinder. The quotient of the difference between the measured mass and the empty mass and the volume resulted in the bulk density.

The particle density was determined with the helium gas pycnometer AkkuPyk (POROTEC GmbH, Germany). The volume of inert gas displaced by the sample is measured. It does measure the volume of open pores, as the gas can penetrate into the open pores, but it does not measure the volume of closed pores, as they are not accessible to the gas [153].

Helium was used as inert gas because it has a high penetration capacity for small, open pores. The sample was filled in the measuring vessel and analysed in 10 cycles (zinc oxide) or 20 cycles (zinc oxide tetrapods). The mean value of these measurements was used as one measurement, i.e., these measurements were repeated two times to obtain a number of three repetitions for statistical evaluation.

5.2.11.2 Surface area

The specific surface area of a material can be determined by gas adsorption. A suitable method is the equation of Brunauer, Emmett and Teller (BET) with the assumption that the amount of adsorbed gas is proportional to the surface area of the sample. The BET theory was developed for the adsorption of N₂ molecules but can also be used for other inert gases. An alternative method for determining the surface area is inverse gas chromatography (iGC) which can easily measure BET isotherms at room temperature using organic probe molecules. The iGC is a chromatographic characterisation method which analyses the surface properties of solid materials. In contrast to gas chromatography, the stationary phase in iGC is packed with the unknown solid sample to be characterised and the mobile phase with known gas probe molecules is injected. To measure the retention time of the gas, a flame ionisation detector is used, which is based on the detection of ions formed during the flame combustion of organic solutes [210].

The sample was filled into a 30 cm pre-silanised glass column to provide the stationary phase. Depending on the expected surface area of the sample different diameters of the glass columns could be used. The column was pre-conditioned with helium carrier gas to remove any volatile contamination. The specific surface area of zinc oxide and the different zinc oxide tetrapods was determined with heptane using the iGC-SEA (inverse gas chromatography surface energy analyser, Surface Measurement System Ltd., UK). Heptane adsorption isotherms were measured at 303 K and 0 % relative humidity with a constant flow rate. The surface area (BET) was calculated from the corresponding heptane isotherms, within the partial pressure range of 5 % to 35 % P/P₀ using the SEA analysis software (Surface Measurement System Ltd., UK).

5.2.12 Size exclusion

Two different methods of sieving were used to separate the zinc oxide tetrapods into different particle sizes: wet sieving and air jet sieving.

5.2.12.1 Wet sieving

Two sieves (Retsch GmbH, Germany) with a diameter of 20 cm and different mesh sizes: 45 μm and 75 μm were used for the wet sieving method. The zinc oxide tetrapods were placed on the sieve, which was then placed in a container with an ethanol-water mixture. With the help of a magnetic stirrer on top of the sieve, zinc oxide tetrapods smaller than the mesh size of the sieve could be separated at medium speed. Both the zinc oxide tetrapods on top of the sieve and those passing through the sieve were filtered, washed twice with water and then dried at 60 $^{\circ}\text{C}$ in a drying oven.

5.2.12.2 Air jet sieving

The method of air jet sieving was performed with the help of the Alpine Air Jet Sieve e200 LS (Hosokawa Alpine AG, Germany). The zinc oxide tetrapods were placed on a sieve. A rotating nozzle with a very narrow gap below the sieve ensured that the velocity of the compressed air flows at high speed through the sieve and the particles are dispersed at the lid. The individual zinc oxide tetrapods, which are smaller than the mesh size of the sieve, can pass through the sieve and were transported into the sample vessel by the negative pressure created by a Hoover [211]. The three sieves used and the corresponding parameters can be seen in the following table (Table 5.7).

Table 5.7. Parameters of the air jet sieving.

Sieve	Time	Pressure
20 μm	5 min	4,000 Pa
32 μm	4 min	3,600 Pa
90 μm	3 min	3,400 Pa

5.2.13 Rheology

Rheology is the science that deals with the flow behaviour and deformability of materials. The flow of materials can only be achieved if the internal resistance, which is created by the interaction of the molecules, is overcome. The theory can be described with the help of Newton's law. F is a force acting on the liquid layers, A is the area of the liquid layer, η is the dynamic viscosity of the liquid, Δv is the difference of the velocity of the liquid layer and Δy is the distance between the liquid layer under consideration and the lowest, stationary layer. The viscosity can therefore be calculated from the shear stress $\tau = F/A$ and the shear rate $D = \Delta v/\Delta y$.

Equation 5.3. for calculating the viscosity with Newton's law.

$$\frac{F}{A} = \eta * \frac{\Delta v}{\Delta y} \rightarrow \eta = \frac{\tau}{D}$$

Mucus rheology without and with the nasal formulations was analysed using the Bohlin CVO 120 High Resolution rheometer (Bohlin Instruments, Germany) equipped with plate (40 mm diameter). Gap distance was fixed at 150 μm . Simulated nasal mucus [204,205] was prepared with simulated nasal fluid and 8 % mucin of porcine stomach type II. 20 mg of the sample were added to 500 μL of simulated nasal mucus and vortexed for 30 s. After letting the sample rest for 1 min 400 μL of the mixtures were added to the rheometer plate and the shear rate dependent viscosity was measured. Apparent viscosity measurement was carried out in the range of 1 s^{-1} to 100 s^{-1} at a temperature of 32 $^{\circ}\text{C}$, which is the temperature in the nasal cavity during inhalation [212]. Mucus without the nasal formulations was handled in the same way.

Rheology of water without and with the pulmonary formulations was analysed using the Bohlin CVO 120 High Resolution rheometer equipped with plate (40 mm diameter). Gap distance was fixed at 400 μm . 60 mg of the sample were added to 1,500 μL of water and vortexed for 30 s. After letting the sample rest for 1 min 750 μL of the mixtures were added to the rheometer plate and the shear rate dependent viscosity was measured. Apparent viscosity measurement was carried out in the range of 1 s^{-1} to 100 s^{-1} . Since these measurements were part of the release experiments, which were carried out at room temperature, the rheology of the pulmonary formulations was investigated at 25 $^{\circ}\text{C}$. Water as reference without the pulmonary formulations was handled in the same way.

Data were analysed with Excel using the resulted viscosity in a range of 60 s^{-1} to 100 s^{-1} .

5.3 In-vitro cell experiments

In order to be able to predict the influence of the formulations in-vivo, various in-vitro cell experiments with different cell models were used.

5.3.1 Calu-3 and RPMI2650

To investigate pH changes in in-vitro cell experiments and toxicity, nasal formulations were tested with RPMI2650, nasal epithelial tumour cells, and pulmonary formulations were tested with Calu-3, pulmonary epithelial tumour cells. They were cultivated in a 75 cm^2 cell culture flask containing 15 mL cell medium (10 % FBS). The media used for the in-vitro cell experiments with Calu-3 and RPMI2650 are shown in Table 5.8.

Table 5.8. Composition of all media used for the in-vitro cell experiments with Calu-3 and RPMI2650.

Medium	Composition
Medium (10 % FBS)	Dulbecco's Modified Eagle's Medium – high glucose, w 4.5 g/L glucose, w L-glutamine, w sodium carbonate, w/o sodium pyruvate (Merck KGaA, Germany) + 10 % fetal bovine serum (FBS) + 1 % sodium pyruvate + 1 % penicillin-streptomycin + 1 % non-essential amino acids
Medium (2 % FBS)	Dulbecco's Modified Eagle's Medium – high glucose + 2 % fetal bovine serum (FBS) + 1 % sodium pyruvate + 1 % penicillin-streptomycin + 1 % non-essential amino acids
Cell phosphate buffer (PBS)	Dulbecco's Phosphate Buffered Saline, w/o Ca ²⁺ , w/o Mg ²⁺ (Merck KGaA, Germany)
Salt solution	Hanks' salt solution – w 0.35 g/L NaHCO ₃ , w Ca ²⁺ , w Mg ²⁺ , w/o Phenol red (Merck KGaA, Germany)

5.3.1.1 Cytotoxicity by MTT assay

Cytotoxicity was determined using a MTT assay. Viability of cells was estimate after incubation with the formulations.

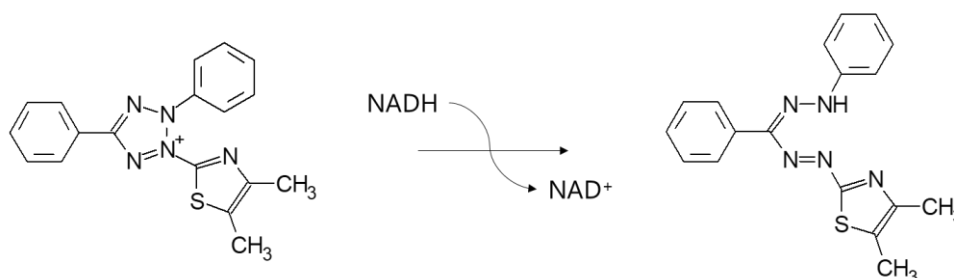


Figure 5.16. Reaction equation for the MTT assay. The yellow tetrazolium salt (left) is going to be reduced to a violet crystalline formazan (right).

This assay is based on the reduction of the yellow tetrazolium salt (3-(4,5-dimethylthiazol-2-yl)-2,5-diphenyltetrazolium bromide or MTT) to a violet crystalline formazan. This reduction is catalysed by the mitochondrial succinate dehydrogenase of the cells and can therefore only take place in metabolically

active cells. Depending on cell viability, the amount of dye formed varies and can be measured at a wavelength of 570 nm [213].

100 μL of RPMI2650 nasal epithelial cells (nasal formulations) or Calu-3 pulmonary epithelial cells (pulmonary formulations) were seeded in a 96-well plate (TC-plate 96 well, Standard, F, Sarstedt AG & Co. KG, Germany) at a density of 1×10^5 cells/mL. After 24 h incubation (HERAcell 150, Thermo Fisher Scientific Inc., USA) at 37 °C and 5 % CO_2 , the medium was removed and 100 μL fresh medium (2 % FBS) and 100 μL of different concentrations of the formulations in PBS were added to the cells. The used medium (10 % FBS) was replaced by fresh medium (2 % FBS), because the reduced amount of FBS guaranteed the survival of the cells but did not distort the experiment by an excessive nutrient content. The samples were used as suspensions at final concentrations of 0.005 mg/mL to 10 mg/mL. They were prior sonicated with a sonicator (SONOPLUS ultrasonic homogeniser HD 4100 in combination with the sonotrode TS 103, BANDELIN electronic GmbH & Co. KG, Germany) with an amplitude of 20 % for 30 s. 100 μL PBS and 100 μL medium (2 % FBS) were used as negative control, 50 μL Triton-X (1 % in PBS) and 100 μL medium as positive control. After 24 h the suspensions were removed and 100 μL fresh medium (2 % FBS) and 25 μL MTT (5 mg/mL in PBS) were added to the cells. After another 4 h in the incubator the MTT solution was removed gently and 100 μL SDS solution (10 % in dimethylformamide + water, 1 + 1, pH 4.7) were used as lysis solution. The plate was analysed after 12 h with UV/Vis spectroscopy at 570 nm (absorbance) and 650 nm (background) using a plate reader (FLUOstar Omega spectrometer). To calculate the data, first the difference between absorbance and background was calculated and then the corresponding viability could be determined using a two-point calibration over the positive and negative control.

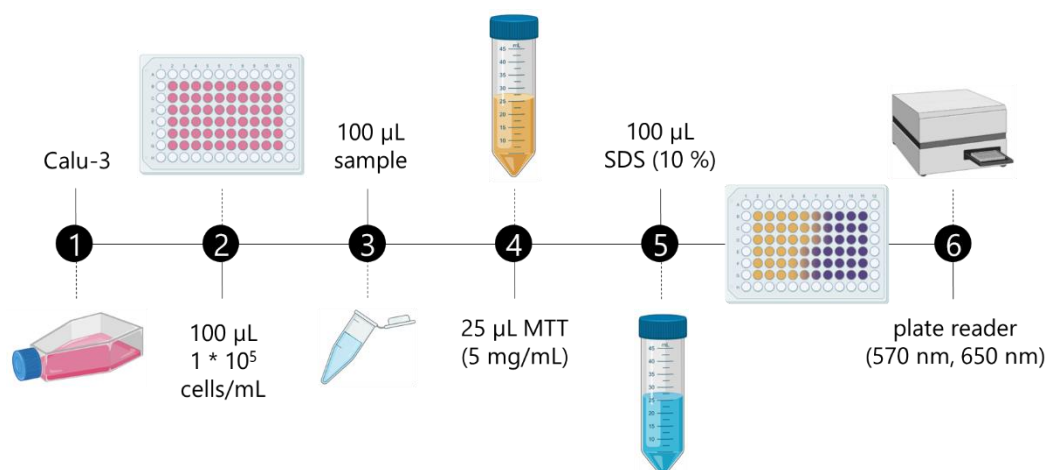


Figure 5.17. Schematic overview of the work flow of the MTT assay created with BioRender.

5.3.1.2 pH and transepithelial electrical resistance

In-vitro pH studies of the pulmonary formulations with Calu-3 cells were performed to get an idea of the behaviour of the cells after incubation with the formulations for 24 h in terms of pH changes.

200 μL of Calu-3 pulmonary epithelial cells were seeded at ThinCerts with 1 μm pore diameter at a density of 2.5×10^5 cell/mL. 1 mL medium (10 % FBS) was added to the 12-well plate and changed every 2 days. This ensured that the cells received sufficient nutrients from the medium below the ThinCert and could develop an air-liquid interface. After 10 days, the cells and the 12-well plate were cleaned with salt solution twice, 1 mL salt solution was added to the well and 500 μL of the formulations were added to the cells. The formulation concentrations in salt solution were related to the performed toxicity experiment. The concentrations used are displayed in Table 5.9.

Table 5.9. Used concentrations (= LD50) of zinc oxide and the pulmonary formulations.

	ZnO	F1	F2	F3	F4	F5	F6
Concentration, mg/mL	0.018	0.013	0.010	0.031	0.037	0.049	4.720

The pH levels were monitored after 0.5 h, 1 h, 2 h, 4 h, 8 h and 24 h using a pH meter (Mettler Toledo SevenCompact Benchtop Meter with pH-electrode InLab Ultra-Micro-ISM). Before and after the experiments, the cells were visually inspected and transepithelial electrical resistance (TEER) was determined using EVOM (World Precision Instruments, USA) to check whether the cells showed a significant change in their viability or functionality of their tight junctions.

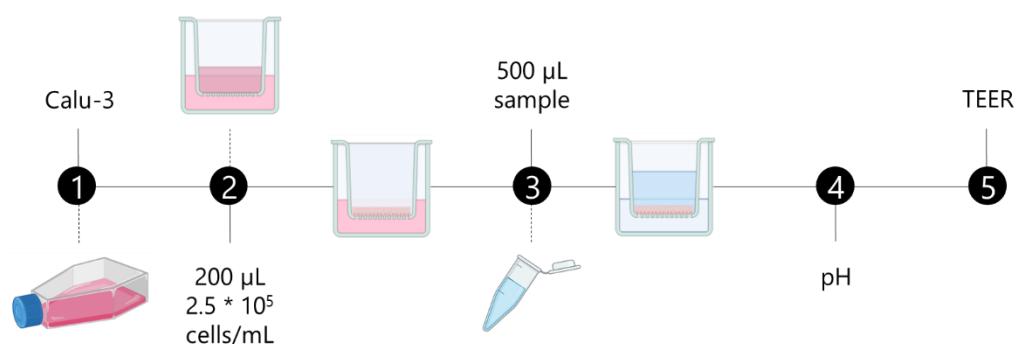


Figure 5.18. Schematic overview of the in-vitro pH studies of the pulmonary formulations created with BioRender.

5.3.2 Murine bone marrow-derived dendritic cells

As the isolation of sufficient numbers of dendritic cells for ex-vivo studies is challenging and requires expertise, the immunological cell experiments were performed with the Vaccine Design and Delivery group of Prof. Camilla Foged at the University of Copenhagen. Murine bone marrow-derived dendritic cells (BMDC) were isolated and cultured according to the following protocol. The media used for the in-vitro cell experiments with BMDC are shown in Table 5.10.

Table 5.10. Composition of all media used for the in-vitro cell experiments with BMDC.

Medium	Composition
Complete RPMI	Gibco RPMI 1640 Medium, GlutaMAX Supplement, w GlutaMAX, w/o sodium pyruvate (Thermo Fisher Scientific Inc., USA) + 10 % fetal bovine serum (FBS) + 1 % penicillin-streptomycin
Lysis Buffer	RBC Lysis Buffer (10 x) (BioLegend Inc., USA) diluted 1:10 with MilliQ water

5.3.2.1 Isolation and cultivation of murine bone marrow-derived dendritic cells

The legs of 10 weeks to 12 weeks old CF57BL/6N mice were largely freed from skin, muscle and fat using scissors and tweezers as well as ethanol (70 %). To obtain the bone marrow, the femur was separated from the tibia and opened on both sides using scissors. The bone marrow was rinsed out with 10 mL complete RPMI and collected in a petri dish. After destroying cell agglomerates by passing the cells repeatedly through a syringe with a needle, the cell suspension was filtered through a 40 µm filter. To lyse any red blood cells, 1 mL of lysis buffer was added to the cell pellet obtained after centrifugation for 5 min at 400 g. After 5 min, the lysis was stopped with complete RPMI and the suspension was centrifuged again with the same conditions. The resulting pellet was redispersed in complete RPMI and 4.25×10^5 cells were added to a 175 cm² tissue culture flask containing 30 mL complete RPMI and 20 ng/mL recombinant murine GM-CSF (PeproTech Inc., USA). The cells were incubated for a total of 10 days at 37 °C and 5 % CO₂. After 3 days and 8 days, 30 mL complete RPMI supplemented with 20 ng/mL recombinant murine GM-CSF were added, and the complete medium was changed once after day 6 by removing approximately 60 mL and adding 30 mL complete RPMI supplemented with 20 ng/mL recombinant murine GM-CSF. On day 10, the cells were harvested and 600 µL of a cell suspension were seeded in a 24-well plate (Cellstar 24-well plates, Greiner Bio One International GmbH, Austria) at a density of 1×10^6 cells/mL complete RPMI supplemented with 20 ng/mL recombinant murine GM-CSF.

5.3.2.2 Cell activation experiment

After incubating the cells for two hours at 37 °C and 5 % CO₂, the immunological in-vitro cell experiments were started. Complete RPMI was used as negative control, 10 ng lipopolysaccharide (LPS) as positive control and 5 µg ovalbumin as antigen. Pulmonary formulation 2 was applied in three different concentrations: 50 µg, 25 µg and 10 µg. After 16 h to 18 h incubation at 37 °C and 5 % CO₂, the samples were analysed using flow cytometry. Flow cytometry enables the counting and

characterisation of cells in a liquid flow. One of the main applications is fluorescence activated cell sorting (FACS), where fluorescent dyes are used to examine labelled cells. FACS is a method which allows sorting a heterogeneous sample of cells based on specific light scattering and fluorescence properties of each cell. The cell suspension is entrained in a liquid stream. A vibrating mechanism causes the cell stream to break up into individual droplets. Just before the stream breaks into droplets, the fluorescence properties of each cell are measured. An electric charge ring is placed at the exact point where the stream breaks into droplets. Based on the immediately preceding measurement of fluorescence intensity, a charge is placed on the ring and the opposite charge is trapped on the droplet as it breaks from the stream. The charged droplets fall into a container according to their charge due to the influence of an electrostatic deflection system [214].

Fluorescence staining is based on the antigen-antibody reaction, whereby antibodies labelled with fluorescent dye are used for the analysis. The suspended and partially labelled cells are passing a focused laser beam with a suitable wavelength. The electrons of the fluorescent dye are lifted to a higher energy level with exact excitation. When the electrons fall to the original level, the dye fluoresces and can be detected. The resulting emitted photon concentration is proportional to the amount of bound antibody. A significant advantage is that several fluorescent dyes can be detected in parallel, since the dyes used are excited at a common wavelength but show different characteristic emission spectra [215].

For analysing the immunological reaction and the expression of CD40, CD80, CD86 und MHC-II after 16 h to 18 h incubation cells were incubated for 15 min with 0.0125 µg FVS510 (fixable viability stain 510, BD Biosciences, Denmark) per well to discriminate viable from non-viable cells. After the treatment with Fc-block (BD Biosciences, Denmark) to ensure that solely antigen-specific binding can be observed the cells were stained with 1 µg anti-CD11c-BUV737 (HL3, BD Biosciences, Denmark), anti-CD40-PE (3.23, BD Biosciences, Denmark), anti-CD80-APC (16-10A1, BD Biosciences, Denmark), anti-CD86-FITC (GL1, BD Biosciences, Denmark) and anti-MHC-II-eF450 (M5/114.15.2, eBioscience, Thermo Fisher Scientific Inc., USA) per well. The fluorescent dye labelled samples were then measured using BD LSRFortessa (BD Corporation, USA) and FACSDiva software (BD Corporation, USA) and analysed using FlowJo software v 10 (Tree Star, USA).

5.4 Statistics

Various statistical methods were used to evaluate and present the data. Mean value and standard deviation were calculated according to Equation 5.4 and Equation 5.5, whereas \bar{x} is representing the mean value, s the standard deviation, n the sample size and x individual measured values. Results are expressed as mean value \pm standard deviation ($n > 2$), mean value \pm min/max ($n = 2$) or individual value ($n = 1$). In the diagrams, either the mean value and the standard deviation or min/max as positive and negative error bars are displayed or individual values without error bars.

Equation 5.4. for calculating the mean value.

$$\bar{x} = \frac{1}{n} * \sum_{i=1}^n x_i$$

Equation 5.5. for calculating the standard deviation.

$$s = \sqrt{\frac{\sum_{i=1}^n (x_i - \bar{x})^2}{n - 1}}$$

The results include a t-test to compare the means of two samples. Prerequisites for performing a t-test are the normal distribution of a population, no differences in the variances and a sample size that is not too small. If equality of variance is assumed although the variances are not equal, a serious error can occur. However, due to the robustness of the t-test, it can be performed appropriately without the assumption of equality of variances, i.e., it should be checked beforehand whether the variances are equal. Most results were based on a sample size of three samples. Even though the sample size was included in the calculations, this aspect should be taken into account when looking at the diagrams and evaluations. Since the sample size was the same for the mean values studied, the following equation can be applied (Equation 5.6). The variables correspond to the definitions of the previous equations.

Equation 5.6. for calculating the t-test value.

$$t = \sqrt{\frac{n_A * n_B}{n_A + n_B}} * \frac{\bar{x}_A - \bar{x}_B}{\bar{s}}$$

A t-test can be performed double- or one-sided. The t-test is performed in each case with a confidence interval of 95 % and a probability of error of 5 %. The t-value can be used to calculate the p-value, which is a statistical probability value. A p-value < 0.05 indicates a significant difference (*), a p-value < 0.01 indicates a very significant difference (**) and a p-value < 0.001 indicates a highly significant difference (***). Excel was used to calculate the equality of variances (F-test) and the corresponding p-values (t-test).

6 Results and discussion

6.1 Adsorption of proteins to different zinc oxides

In April 2016, Antoine and colleagues published the results of their study investigating zinc oxide tetrapods for their immunoprotective properties against genital herpes [151]. Herpes simplex virus 2 (HSV 2) can be transmitted not only through sexual contact, but also from mothers to newborns. The research group was able to show in in-vivo experiments with HSV 2-infected female mice that zinc oxide tetrapods could be used both to treat and prevent the infection.

During the treatment of HSV 2-infected female mice, zinc oxide tetrapods acted as a biocide when applied vaginally. They suppressed the infection and also intercepted the viruses due to their high affinity to the zinc oxide tetrapods. Trapping the virus significantly and effectively reduced animal mortality. Furthermore, zinc oxide tetrapods showed great promise regarding immunisation and thus prevention of HSV 2 infection. HSV 2 virions bound to zinc oxide tetrapods were presented more effectively by antigen-presenting cells, thereby enhancing the T cell and antibody responses and thus suppressing reinfection, than HSV 2 virions alone. In addition, zinc oxide tetrapods were found to have strong adjuvant properties comparable to alum.

Based on these positive results, the idea of using zinc oxide tetrapods as an alternative adjuvant for mucosal immunisation had emerged. In order to investigate whether the properties of zinc oxide tetrapods were related to the tetrapodial morphology or to zinc oxide itself, normal zinc oxide was also used for the experiments in addition to zinc oxide tetrapods.

6.1.1 Morphology and particle size distribution

Zinc oxide tetrapods were formed during flame transport synthesis in a muffle furnace as white to yellowish white powder. The zinc oxide tetrapods used were harvested at the top of the muffle furnace. In Figure 6.1 representative images of zinc oxide tetrapods derived from this process are shown. Image A shows the typical three-dimensional tetrapodial structure. All four arms of the tetrapods have the same length and the angles between the arms are almost identical. Image B shows the hexagonal shape of an individual arm of typical zinc oxide tetrapods. It can also be observed in these pictures that defects of the typical structure can occur during production and harvesting, e.g., different morphologies of an arm. These minimal differences and the production of completely different structures were possible during flame transport synthesis and post-processing.

As already mentioned above, the zinc oxide tetrapods used were harvested at the top of the muffle furnace. The morphology is strongly dependent on the position of the material to be harvested. Each scientist develops his own technique and the individual varieties of zinc oxide tetrapods change according to the position harvested. Thus, other forms were harvested in addition to the typical

tetrapodial morphology. In Figure 6.2 some structures are shown that were found during the project with the scanning electron microscope. The structural diversity ranges from narrow and thick arms, through various structures of the arms to the complete loss of the tetrapodial structure.

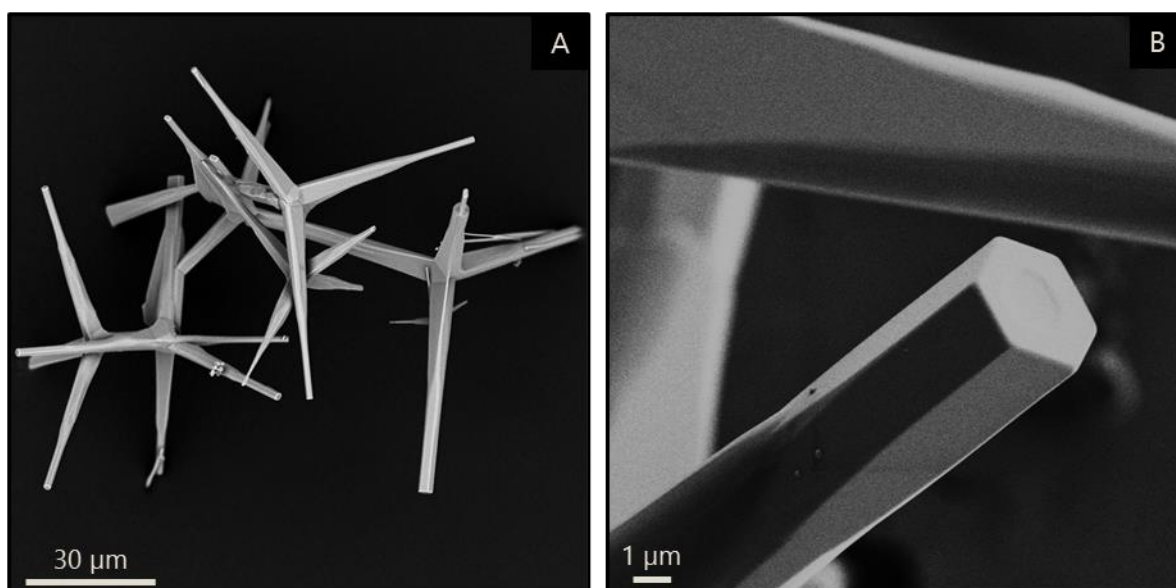


Figure 6.1. Representative scanning electron microscope images showing zinc oxide tetrapods with different magnifications.

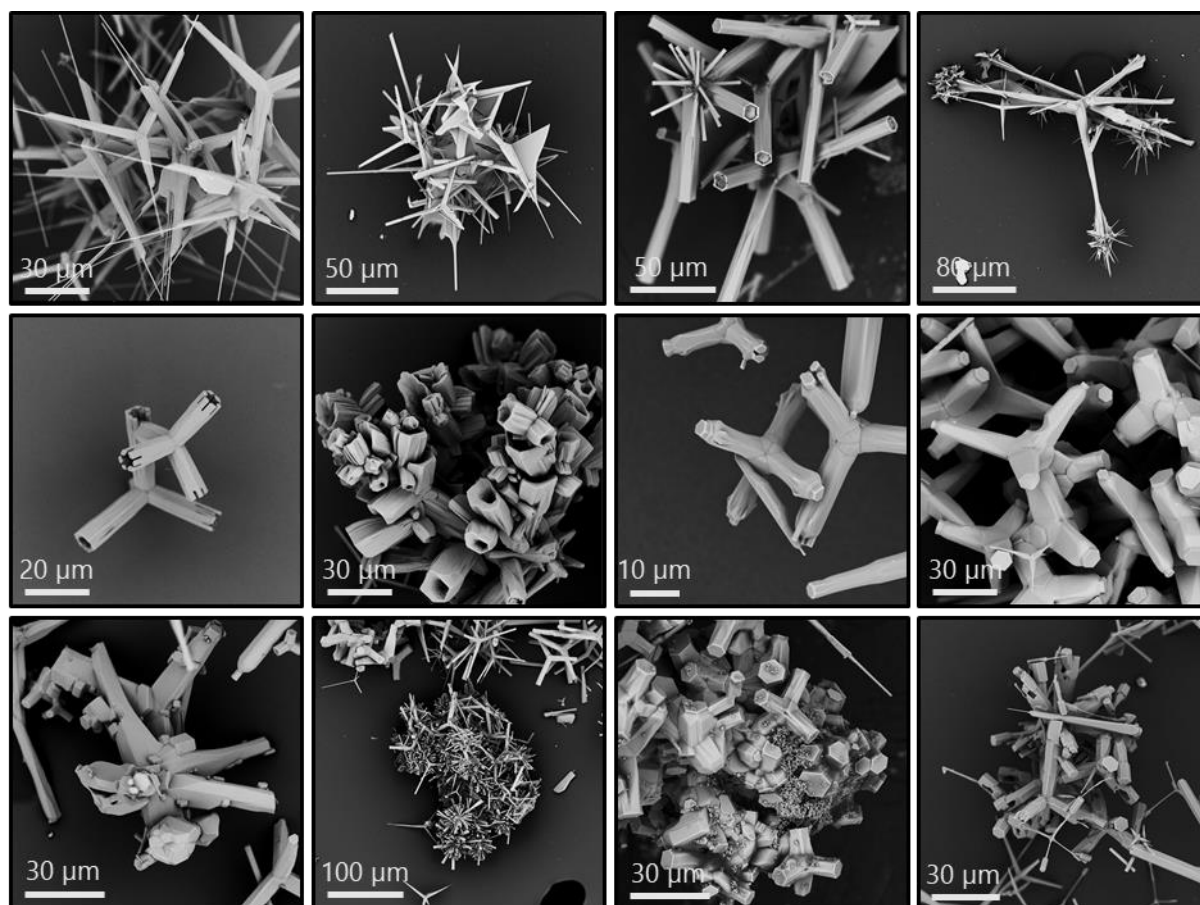


Figure 6.2. Representative scanning electron microscope images showing some different structures of zinc oxide tetrapods with different magnifications.

There are differences in morphology of the tetrapods and in particle size. The particle size of the zinc oxide tetrapods was measured by scanning electron microscopy based on the Feret diameter. With an average arm length of $47.0 \mu\text{m} \pm 21.5 \mu\text{m}$ and a diameter of $81.4 \mu\text{m} \pm 38.8 \mu\text{m}$, the particle size of the zinc oxide tetrapods is highly variable. While the particles could not be classified regarding morphology, they could probably be classified with regard to particle size, by sieving.

With the help of air jet sieving, the zinc oxide tetrapods were divided into different particle size classes through different sieves and different applied pressures. In Figure 6.3 representative images of zinc oxide tetrapods after air jet sieving are shown. Almost no tetrapodial structures are visible. The particle size was measured by scanning electron microscopy on the basis of the Feret diameter. On the sieve with a mesh size of $20 \mu\text{m}$ (A) the "zinc oxide tetrapods" have an average particle size of $31.2 \mu\text{m} \pm 9.9 \mu\text{m}$, on the sieve with a mesh size of $32 \mu\text{m}$ (B) they have an average particle size of $50.0 \mu\text{m} \pm 14.6 \mu\text{m}$ and on the sieve with a mesh size of $90 \mu\text{m}$ (C) they have an average particle size of $86.1 \mu\text{m} \pm 21.9 \mu\text{m}$.

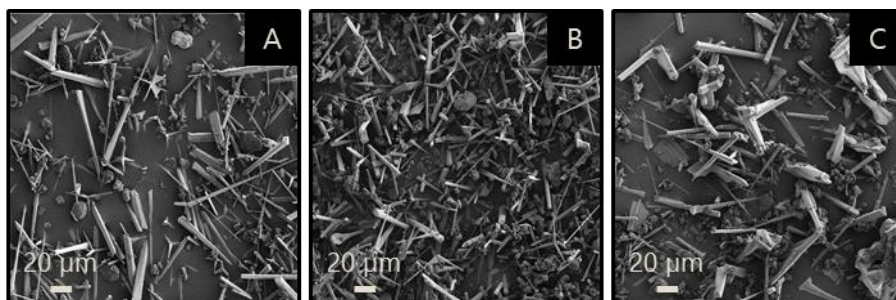


Figure 6.3. Representative scanning electron microscope images showing zinc oxide tetrapods after air jet sieving. A) sieve: $20 \mu\text{m}$, time: 5 min, pressure: 4,000 Pa; B) sieve: $32 \mu\text{m}$, time: 4 min, pressure: 3,600 Pa; C) sieve: $90 \mu\text{m}$, time: 3 min, pressure: 3,400 Pa.

Air jet sieving led to the destruction of the tetrapodial structures due to its functional principle. Because of the high pressure of the air passing through the sieve, agglomerates can be destroyed on the lid and thus a separation into different particle sizes should be possible. The high mechanical stress destroyed the zinc oxide tetrapods, i.e., individual arms broke off. These arms can pass the sieve lengthwise. Hence, it was neither possible to achieve sieve fractions according to the sieve size nor to maintain the tetrapodial structure. For this reason, another gentler method was tested to classify the zinc oxide tetrapods: wet sieving.

Wet sieving was performed in a liquid, in this case, in an ethanol-water mixture. In Figure 6.4 the sieve passage and the sieve residue are shown. After sieving, tetrapodial structures are visible. Nonetheless, a difference can be seen between the sieve passage containing less intact zinc oxide tetrapods, and sieve residue containing more intact zinc oxide tetrapods, and between the sieves with different mesh sizes. The particle size was measured by scanning electron microscopy on the basis of the Feret diameter. With a particle size of $68.9 \mu\text{m} \pm 28.2 \mu\text{m}$, the sieve residue of the sieve with the mesh size of $75 \mu\text{m}$ (B, right) shows the highest number of visible tetrapodial structures, followed by the sieve passage of the same

sieve (B, left) with a particle size of $55.8 \mu\text{m} \pm 25.4 \mu\text{m}$. The sieve residue of the sieve with the mesh size of $45 \mu\text{m}$ (A, right) shows less tetrapodial structures with a particle size of $60.9 \mu\text{m} \pm 35.4 \mu\text{m}$. Least tetrapodial structures are visible in the sieve passage of the same sieve (A, left) with $30.8 \mu\text{m} \pm 15.7 \mu\text{m}$.

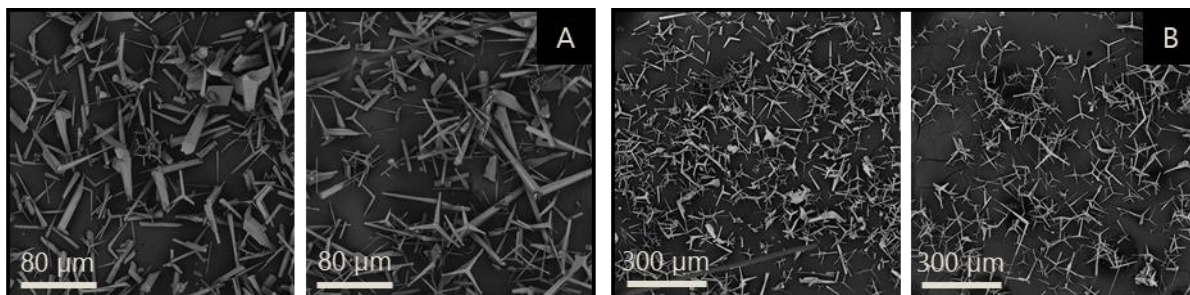


Figure 6.4. Representative scanning electron microscope images showing sieve passage (left) and sieve residue (right) of zinc oxide tetrapods after wet sieving. A) sieve: $45 \mu\text{m}$; B) sieve: $75 \mu\text{m}$.

The ethanol-water mixture had lower surface tension compared to water and thus ensured that the zinc oxide tetrapods formed less agglomerates. Thus, the tetrapodial structure was retained despite the use of a magnetic stirrer which supported the passage of the particles through the sieve. Both the sieve passage and the residue had to be washed with water afterwards to remove ethanol sufficiently from the surface of the zinc oxide tetrapods. This should ensure that the reactivity of the oxygen vacancies was not additionally influenced by ethanol. The presence of the oxygen vacancies, their influence on the reactivity of the zinc oxide and their generation have been investigated for years [216]. The generation and the influence of oxygen defects on the adsorption of proteins is discussed in more detail in chapter 6.1.2. Filtering, washing and drying of the zinc oxide tetrapods required a lot of work and time and resulted in a low yield.

Neither by air jet sieving nor by wet sieving it was possible to divide the zinc oxide tetrapods into particle size classes while maintaining both their tetrapodial structure and sufficient yield. For the adsorption experiments, the zinc oxide tetrapods were therefore crushed with defined parameters to ensure the extent to which the tetrapodial structure influences the adsorption of proteins. A total of three different zinc oxide tetrapod qualities were used: zinc oxide tetrapods with a tetrapodial structure, short milled and long milled zinc oxide tetrapods.

Zinc oxide can be produced by various methods as explained in chapter 4.2. It was not known which method was used to produce the zinc oxide used. The material used was a white to pale yellowish white powder. Figure 6.5 shows a representative image of zinc oxide. It can be seen that the used zinc oxide consists of needle-shaped particles in the nanometre range, whereby individual particles cannot be recognised. A closer look at the zinc oxide particles shows that miniature tetrapodial structures are sometimes also visible.

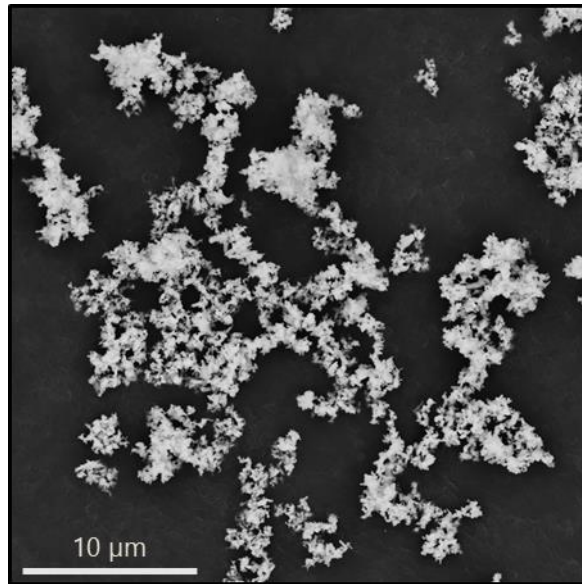


Figure 6.5. Representative scanning electron microscope image showing zinc oxide.

The particle size distribution of the zinc oxide particles was determined by laser diffraction and is shown in Figure 6.6 with a logarithmic x-axis. The zinc oxide particles show an almost monomodal distribution. On closer inspection, it is noticeable that also particles in both the smaller and the larger particle size ranges are present. With an x10 of $4.03 \mu\text{m} \pm 0.14 \mu\text{m}$, an x50 of $9.17 \mu\text{m} \pm 0.23 \mu\text{m}$ and an x90 of $24.16 \mu\text{m} \pm 4.67 \mu\text{m}$, a span value of 2.19 ± 0.45 results.

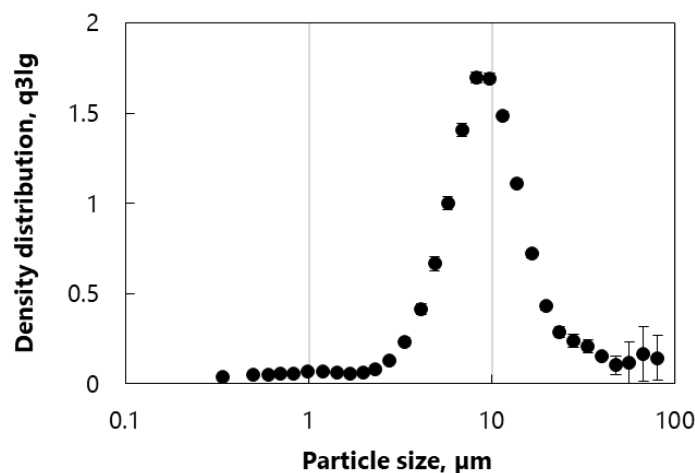


Figure 6.6. Particle size distribution using laser diffraction (HELOS) in combination with the RODOS module. $n = 3$, error bars = standard deviation.

Contrary to the expectations of measurements with the scanning electron microscope, the zinc oxide particles had a particle size in the lower micrometre range and not in the nanometre range. Due to the small particle size and the resulting large surface area, the zinc oxide particles tended to form agglomerates. This could already be seen in the scanning electron microscope image. Based on this, it could be assumed that the used pressure of 3 bar to determine the particle size distribution with the RODOS module was not sufficient to destroy these agglomerates. This can be seen in the diagram,

showing a peak at higher particle sizes as well as a high span value of 2.19. An increase in pressure, which would have led to further destruction of the agglomerates, was not possible with the available measuring instrument. As already described, small tetrapodial structures had been detected in addition to the needle-shaped structures. The optical models of laser diffraction are based on spherical particles. For non-spherical particles a particle size distribution equivalent to the spherical one is obtained. Due to the morphology of the zinc oxide particles the particle size distribution can be distorted. Based on the two findings above, too low dispersion pressure and non-spherical shape, the particle size distribution determined by laser diffraction appears to be too large in relation to the individual zinc oxide particles seen in scanning electron microscope images.

To ensure adsorption properties can be attributed to differences in tetrapodial morphology, XRPD had been carried out. The resulting diffraction pattern allows conclusions on the crystallinity of the sample, as well as on the identity, based on the unique diffraction pattern.

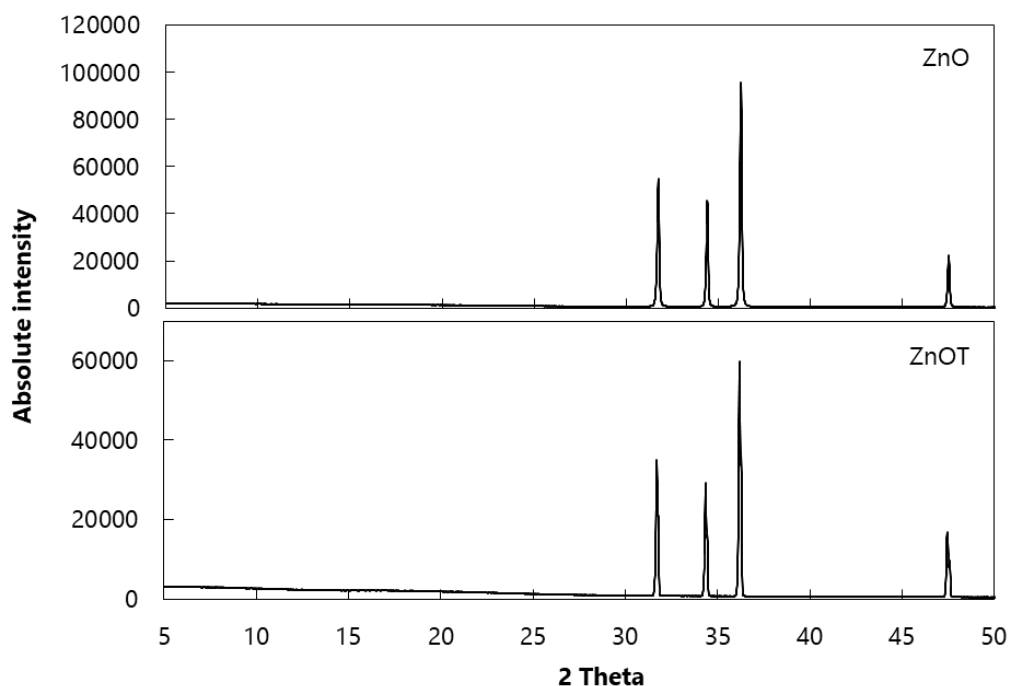


Figure 6.7. Representative diffractograms of X-ray powder diffraction showing the degree of crystallinity of zinc oxide (ZnO, top) and zinc oxide tetrapods (ZnOT, bottom). $n = 1$.

Figure 6.7 shows representative diffractograms of zinc oxide and the zinc oxide tetrapods. The sharp diffraction pattern shows that both zinc oxide tetrapods and zinc oxide are crystalline substances. When comparing the X-ray diffraction pattern of the zinc oxide tetrapods with the X-ray diffraction pattern of zinc oxide, it is noticed that they are identical. The different intensities merely indicate different sample weights and therefore different zinc oxide amounts. Measurements confirm that zinc oxide tetrapods consists of pure zinc oxide.

6.1.2 Adsorption

Four different materials were investigated in the adsorption tests: zinc oxide, zinc oxide tetrapods, short milled and long milled zinc oxide tetrapods. Zinc oxide and zinc oxide tetrapods were studied to investigate whether the tetrapodial structure influences the adsorption of proteins. Milled zinc oxide tetrapods were used to compare different particle sizes. As discussed above, it was not feasible to classify the tetrapods while maintaining their structure. Hence, to compare different particle sizes nevertheless, zinc oxide tetrapods were milled for either a shorter (5 min) or a longer period (60 min). For these experiments, a ball mill was used. Like the zinc oxide tetrapods themselves, the milled zinc oxide tetrapods were prepared by the working group "Functional Nanomaterials" headed by Prof. Rainer Adelung.

Figure 6.8 shows images of the zinc oxide (ZnO), zinc oxide tetrapods (ZnOT), short milled (ZnOT 5 min) and long milled (ZnOT 60 min) zinc oxide tetrapods as well as representative scanning electron microscope images of all materials. The same magnification was used for all materials to ensure comparability of the particle sizes. As it was not possible to determine particle size distribution with the same method for all materials, the particle size was not analysed.

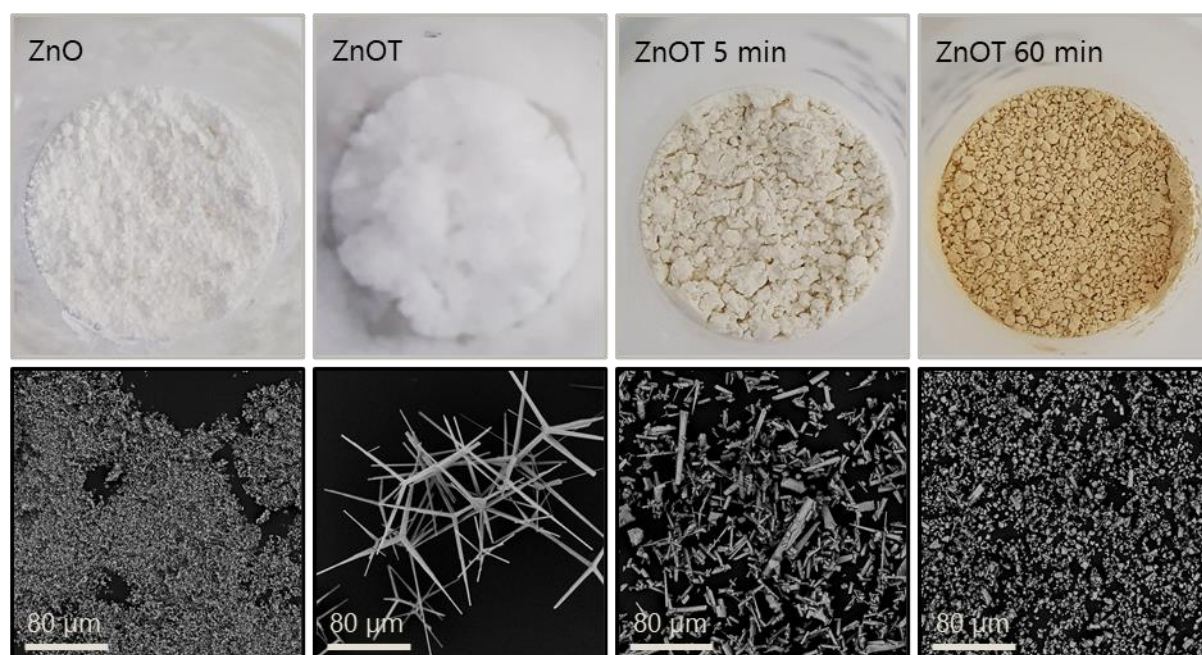


Figure 6.8. Representative scanning electron microscope images (bottom) and images of the dry powders (top) showing zinc oxide (ZnO), zinc oxide tetrapods (ZnOT), short milled (ZnOT 5 min) and long milled (ZnOT 60 min) zinc oxide tetrapods.

First, the images of the dry powders are studied. Zinc oxide is a white to pale yellowish white compact powder with agglomerates. The zinc oxide tetrapods form a white to yellowish white powder. As the bulk density is very low due to the tetrapodial structure, the powder is rather fluffy. Even though the bulk density of the two materials is highly significantly different ($\text{ZnO} = 0.596 \text{ g/cm}^3 \pm 0.007 \text{ g/cm}^3$, $\text{ZnOT} = 0.023 \text{ g/cm}^3 \pm 0.0002 \text{ g/cm}^3$, $p\text{-value} < 0.0001$), the particle density of the zinc oxide tetrapods

with $4.98 \text{ g/cm}^3 \pm 0.16 \text{ g/cm}^3$ and of zinc oxide with $5.52 \text{ g/cm}^3 \pm 0.04 \text{ g/cm}^3$ hardly differs, although this difference is very significantly different with a p-value of 0.0050. The short milled zinc oxide tetrapods are a slightly yellowish powder and the long milled zinc oxide tetrapods are an ochre yellow powder. Both materials form a rather compact powder with agglomerates.

The yellow colouring caused by the milling process can be explained by increasing oxygen vacancies during the milling process. Milling generated heat, which led to an increase in oxygen defects on the surface [217]. This phenomenon is not only observed with zinc oxide tetrapods, but also with zinc oxide. If zinc oxide gets in contact with a flame, its white colour turns into yellow. This yellow colour disappears after the zinc oxide is removed from the flame due to the saturation of the oxygen defects with oxygen from the environment. Oxygen defects are surface trapped holes which are caused by released oxygen. These defects narrow the band gap, which shifts the absorption into the visible violet area. The zinc oxide tetrapods or the zinc oxide therefore turn yellow. Oxygen vacancies could be measured with the help of Raman spectroscopy and X-ray photoelectron spectroscopy. As oxygen vacancies are charged defects, a change in material adsorption properties is possible [217]. Both a positive and a negative charge of the oxygen vacancies are described in literature [150,152].

In Figure 6.8 at the bottom, representative scanning electron microscope images of the materials are shown. Zinc oxide and zinc oxide tetrapods show the form described above. In the milled zinc oxide tetrapods almost no tetrapodial structure is visible. While in the short milled zinc oxide tetrapods individual arms of the zinc oxide trapods are still visible, in the long milled zinc oxide tetrapods no structures are visible reminding of the original morphology. The long milled zinc oxide tetrapods are slightly larger than zinc oxide and the short milled zinc oxide tetrapods are considerably larger. Due to their shape, zinc oxide tetrapods are many times larger than zinc oxide.

For the adsorption tests, zinc oxide, zinc oxide tetrapods, short milled and long milled zinc oxide tetrapods as well as aluminium hydroxide and aluminium phosphate as references were used. Aluminium hydroxide is positively charged and served as a reference for binding negatively charged proteins and aluminium phosphate is negatively charged and served as a reference for binding positively charged proteins. The adsorption properties of the afore-mentioned materials were tested with five different proteins. Electrostatic interaction is often described as the primary adsorption mechanism between antigen and adjuvant [165]. Hence, two different protein groups with varying isoelectric points (IEP) were used. BSA (IEP = pH 4.9), OVA (IEP = pH 4.5) and alpha-lactalbumin (IEP = pH 4.4) are characterised by an isoelectric point in the acidic pH range and were negatively charged in the almost neutral pH range of water. They should therefore tend to electrostatic interactions with aluminium hydroxide. Avidin (IEP = pH 10.5) and lysozyme (IEP = pH 11.0) have isoelectric points in the basic pH range and were positively charged in the pH range used. They should therefore be prone to electrostatic interaction with aluminium phosphate. Besides the isoelectric point other factors, such as molecular weight, the use of

phosphate buffer or the size of the aluminium particles could also have an influence on the adsorption [165]. To take this crucial factor into account, the choice of model proteins was also based on their molecular weight. BSA and avidin have a molecular mass of 66 kDa, OVA has a molecular mass of 44 kDa and alpha-lactalbumin and lysozyme have a molecular mass of 14 kDa.

In Figure 6.9 and Table 6.1 the results of the adsorption of proteins with an isoelectric point in the basic pH range on the above-mentioned zinc oxide, zinc oxide tetrapods, short milled and long milled zinc oxide tetrapods and the reference materials are shown. The adsorption studies on the materials with zinc oxide will be discussed in more detail below, the adsorption on the two reference substances aluminium hydroxide and aluminium phosphate is of particular interest in this diagram. In the adsorption studies, they were used to check whether the adsorption test has worked in principle. As already described, the proteins used in this experiment were positively charged and should therefore adsorb to aluminium phosphate due to the electrostatic interactions. With a binding of $103.34 \mu\text{g}/\text{mg} \pm 0.04 \mu\text{g}/\text{mg}$ (avidin) and $95.32 \mu\text{g}/\text{mg} \pm 1.08 \mu\text{g}/\text{mg}$ (lysozyme), approximately 100 % of the used proteins adsorb to aluminium phosphate. As these two proteins served as positive control, the experiment is valid and the results can be used for further evaluation.

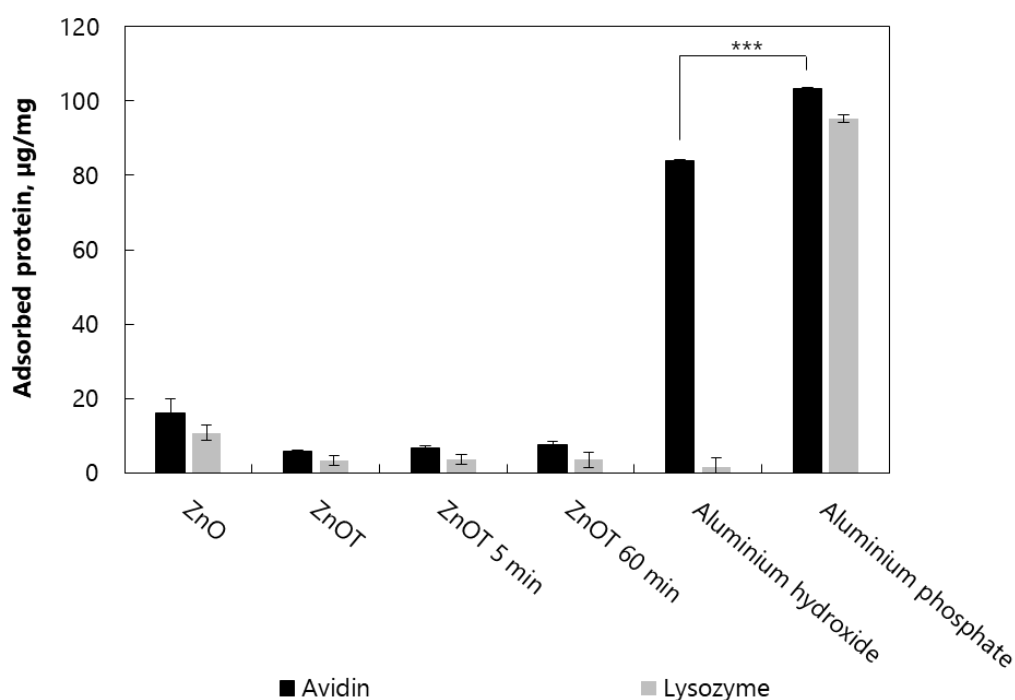


Figure 6.9. Adsorption studies of proteins with an isoelectric point in the basic pH range (IEP avidin = pH 10.5, IEP lysozyme = pH 11.0) and zinc oxide (ZnO), zinc oxide tetrapods (ZnOT), short milled (ZnOT 5 min) and long milled (ZnOT 60 min) zinc oxide tetrapods, aluminium hydroxide and aluminium phosphate. $n = 3$, error bars = standard deviation, p -value < 0.001 = highly significant difference (***).

If the adsorption is assumed to be based on electrostatic interactions, only a negligible part of the proteins should adsorb on aluminium hydroxide, which is positively charged like the proteins. With $1.52 \mu\text{g}/\text{mg} \pm 2.63 \mu\text{g}/\text{mg}$, almost no lysozyme binds to aluminium hydroxide. With

83.91 $\mu\text{g}/\text{mg} \pm 0.48 \mu\text{g}/\text{mg}$, however, a considerable part of the avidin adsorbs to aluminium hydroxide, even if the adsorbed amount is highly significantly different from the adsorbed amount of aluminium phosphate ($p\text{-value} = 0.0002$).

Another mechanism than electrostatic interaction had to be responsible for this high adsorption. This other mechanism might be ligand exchange, which is also an important mechanism of adsorption. Ligand exchange leads to strong protein adsorption, it can occur even in the presence of a repulsive electrostatic force between antigens and aluminium salts. It is assumed that the ligands present in the proteins, e.g., phosphoryl groups [165], interact with the hydroxyl group in aluminium hydroxide. Avidin is being investigated in numerous studies because of its high ligand binding activity [218]. For a more detailed study of the adsorption mechanism of the proteins on the aluminium hydroxide, e.g., the amount of phosphorus per mole of protein could be determined. However, this is not part of the work.

Adsorption to aluminium hydroxide is described as a stronger interaction than adsorption to aluminium phosphate and dependent on the molecular mass of the proteins. While aluminium phosphate has an amorphous structure, aluminium hydroxide is a crystal colloid gel. The resulting crystal form offers a uniform surface for the adsorption of proteins. In addition, it creates a kind of lattice structure, i.e., larger proteins are bound more strongly than proteins with a smaller molecular mass, comparable to a sieve. Particles smaller than the mesh size of the sieve could pass through the sieve and larger particles would be retained. Huang and Wang also described a linear relationship between molecular mass and adsorption. They investigated the adsorption of different proteins with different isoelectric points and molecular masses on aluminium hydroxide and aluminium phosphate [165]. In contrast to aluminium hydroxide, aluminium phosphate showed no correlation between the molecular mass of the proteins and the adsorption.

In Figure 6.10 and Table 6.1 the results of the adsorption of proteins with an isoelectric point in the acidic pH range on the above-mentioned zinc oxide, zinc oxide tetrapods, short milled and long milled zinc oxide tetrapods and the reference materials are shown. The adsorption studies on the materials with zinc oxide will be discussed in more detail below, the adsorption on the two reference substances aluminium hydroxide and aluminium phosphate is of particular interest in this diagram. With an adsorbed amount of 95.10 $\mu\text{g}/\text{mg} \pm 10.90 \mu\text{g}/\text{mg}$ (BSA), 99.14 $\mu\text{g}/\text{mg} \pm 0.56 \mu\text{g}/\text{mg}$ (OVA) and 96.50 $\mu\text{g}/\text{mg} \pm 0.56 \mu\text{g}/\text{mg}$ (alpha-lactalbumin), approximately 100 % of the used proteins bind on aluminium hydroxide. With 7.69 $\mu\text{g}/\text{mg} \pm 0.42 \mu\text{g}/\text{mg}$ (BSA), 3.46 $\mu\text{g}/\text{mg} \pm 0.88 \mu\text{g}/\text{mg}$ (OVA) and 5.20 $\mu\text{g}/\text{mg} \pm 11.25 \mu\text{g}/\text{mg}$ (alpha-lactalbumin), almost no protein adsorbs to aluminium phosphate.

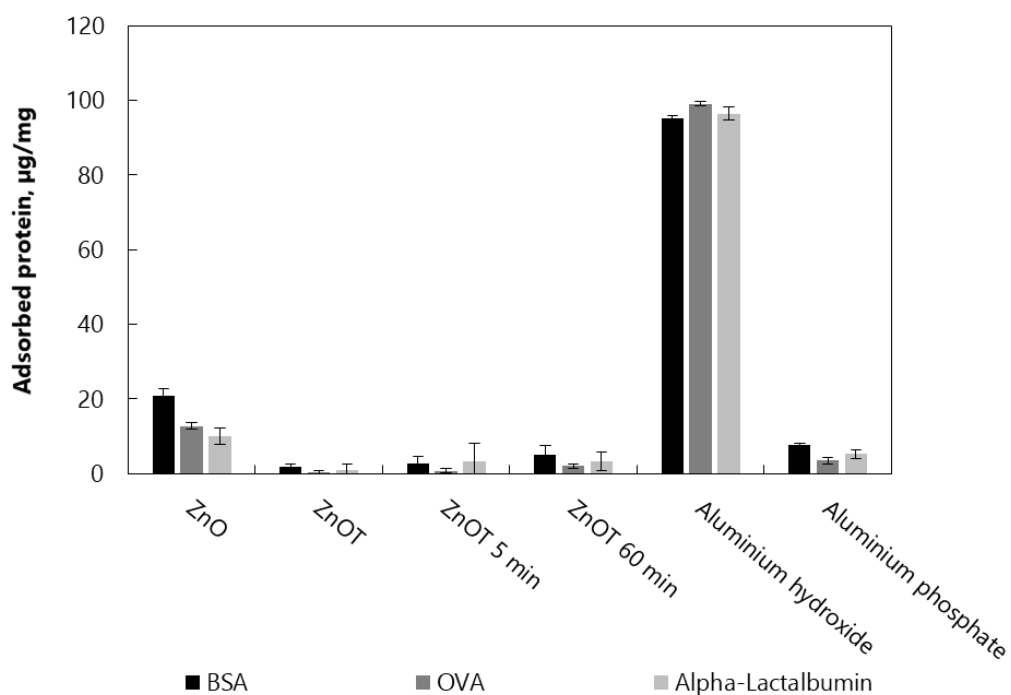


Figure 6.10. Adsorption studies of proteins with an isoelectric point in the acidic pH range (IEP BSA = pH 4.9, IEP OVA = pH 4.5, IEP alpha-lactalbumin = pH 4.4) and zinc oxide (ZnO), zinc oxide tetrapods (ZnOT), short milled (ZnOT 5 min) and long milled (ZnOT 60 min) zinc oxide tetrapods, aluminium hydroxide and aluminium phosphate. $n = 3$, error bars = standard deviation.

Table 6.1. Summary of amounts being adsorbed to the test materials (proteins with an isoelectric point in the basic pH range (IEP avidin = pH 10.5, IEP lysozyme = pH 11.0) and in the acidic pH range (IEP BSA = pH 4.9, IEP OVA = pH 4.5, IEP alpha-lactalbumin = pH 4.4) and zinc oxide (ZnO), zinc oxide tetrapods (ZnOT), short milled (ZnOT 5 min) and long milled (ZnOT 60 min) zinc oxide tetrapods, aluminium hydroxide and aluminium phosphate. $n = 3$, \pm = standard deviation.

	Avidin, µg/mg	Lysozyme, µg/mg	BSA, µg/mg	OVA, µg/mg	Alpha-Lactalbumin, µg/mg
ZnO	16.00 ± 3.48	10.84 ± 1.99	20.79 ± 2.05	12.73 ± 0.82	10.04 ± 2.19
ZnOT	5.99 ± 0.30	3.34 ± 1.38	1.66 ± 0.85	0.24 ± 0.41	0.88 ± 1.52
ZnOT 5 min	6.79 ± 0.42	3.67 ± 1.35	2.61 ± 1.94	0.66 ± 0.57	3.24 ± 4.72
ZnOT 60 min	7.65 ± 0.88	3.53 ± 1.98	4.94 ± 2.42	1.96 ± 0.54	3.22 ± 2.55
Aluminium hydroxide	83.91 ± 0.48	1.52 ± 2.63	95.10 ± 10.90	99.14 ± 0.56	96.50 ± 1.71
Aluminium phosphate	103.45 ± 0.04	95.32 ± 1.08	7.69 ± 0.42	3.46 ± 0.88	5.20 ± 11.25

The proteins used were negatively charged in the almost neutral pH range of water. Aluminium hydroxide was positively charged, so all proteins were able to build an electrostatic bond, and aluminium phosphate was negatively charged, so the negative charges repel each other and negligible adsorption can be observed. These results can be well explained by adsorption through electrostatic interactions.

In the following section, the results of the adsorption of the proteins on zinc oxide, zinc oxide tetrapods, short milled and long milled zinc oxide tetrapods are discussed.

Due to the different bulk density, shape and particle size of the materials, it was not easy to compare the adsorption of proteins, as the mass of the materials in this context was not a reliable reference value. To enable the comparison of all materials, the BET surface of the materials was determined by iGC. With a surface area of 0.3113 m²/g the short milled zinc oxide tetrapods show the lowest surface area, followed by the zinc oxide tetrapods with 0.3730 m²/g. This was contrary to the general expectation that the surface increases with milling. By analysing the milling process and the harvesting after the milling process of the material it became clear where this difference came from. While the zinc oxide tetrapods were not processed and all arms, however thin, were included in the surface measurement, the milled zinc oxide tetrapods had to be harvested from the ball mill at the end of the milling process. Due to the increased surface area of small fragments and the energy contribution, these components in particular could not be quantitatively removed from the ball mill. This led to a reduction of the surface, because the small fragments with the large surface area could not be detected in the measurement as they were remaining in the mill. The long milled zinc oxide tetrapods have a surface area of 1.0919 m²/g and zinc oxide has a surface area of 3.6609 m²/g.

The surface areas of zinc oxide, zinc oxide tetrapods, short milled and long milled zinc oxide tetrapods and the molecular weights of the proteins were included in the calculations. The amount of adsorbed protein was calculated in mmol per m² surface area.

In Figure 6.11 and Table 6.2 the adsorbed amounts in mmol of BSA and avidin on a m² surface area of zinc oxide and zinc oxide tetrapods are shown. The aim was to determine whether zinc oxide and the zinc oxide tetrapods were also able to adsorb proteins due to electrostatic interactions or whether there was no discernible trend with regard to the charge. BSA served as a negatively charged protein and avidin as a positively charged one. In the experiments with the aluminium hydroxide, avidin presumably also showed adsorption due to ligand exchange in addition to electrostatic interactions. Since the zinc oxide tetrapods and zinc oxide are only made of zinc oxide, avidin was nevertheless used as an example.

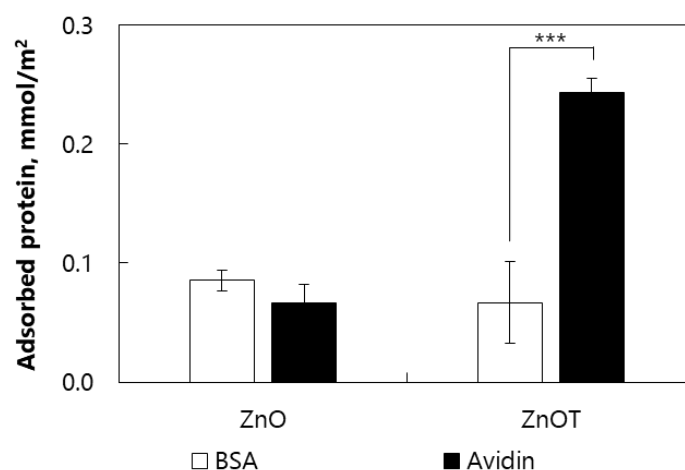


Figure 6.11. Adsorption studies of proteins with a molecular weight of 66 kDa and different isoelectric points (IEP BSA = pH 4.9, IEP avidin = pH 10.5) and zinc oxide (ZnO) and zinc oxide tetrapods (ZnOT). $n = 3$, error bars = standard deviation, p -value < 0.001 = highly significant difference (***).

0.08 mmol/m² ± 0.008 mmol/m² BSA and 0.07 mmol/m² ± 0.016 mmol/m² avidin adsorb to zinc oxide. There is no significant difference. 0.07 mmol/m² ± 0.034 mmol/m² BSA and 0.24 mmol/m² ± 0.012 mmol/m² avidin adsorb to the zinc oxide tetrapods. The binding of the positively charged avidin is therefore very significantly higher (p -value = 0.0005) than the binding of the negatively charged BSA.

Table 6.2. Adsorption studies of proteins with a molecular weight of 66 kDa and different isoelectric points (IEP BSA = pH 4.9, IEP avidin = pH 10.5) and zinc oxide (ZnO) and zinc oxide tetrapods (ZnOT). $n = 3$, ± = standard deviation.

	BSA, mmol/m ²	Avidin, mmol/m ²
ZnO	0.08 ± 0.008	0.07 ± 0.016
ZnOT	0.07 ± 0.034	0.24 ± 0.012

While there is no difference in the adsorption of negatively and positively charged proteins in zinc oxide, zinc oxide tetrapods tend to adsorb positively charged proteins. In other words, zinc oxide tetrapods appears to be negatively charged under experimental conditions. Theoretically, this negative charge could be confirmed, e.g., with the help of the zeta potential or atomic force microscopy. Due to the special morphology of the zinc oxide tetrapods, the measurement of the zeta potential did not seem to make any sense, as in theory the potential is measured on the surface of a sphere. The measurement with the help of atomic force microscopy was also not possible because the cantilever, which is used to measure the charge on the surface, could not measure the surface charge of an intact zinc oxide tetrapod due to its tetrapodial structure. But it was already published in 2012 by Antoine and colleagues that the surface of zinc oxide tetrapods could also exhibit a negative charge [150]. Their paper addressed the

virus trapping ability of zinc oxide tetrapods when investigating their prophylactic, therapeutic and neutralising effects against herpes viruses. The negatively charged surface of the zinc oxide tetrapods generated during the synthesis was able to adsorb the positively charged virus. They also investigated the change of the surface by UV radiation. Zinc oxide tetrapods treated with UV radiation could increase the number of oxygen vacancies and thus increased the negative charge of the surface. During the photoreaction, photogenerated holes and electrons were produced. Oxygen at an oxygen lattice position absorbed two of these photogenerated holes and was released. This creates an oxygen vacancy, which is negatively charged due to the electrons created in the photoreaction [219]. Analogous to these experiments mentioned before, long milled zinc oxide tetrapods should adsorb more protein due to the higher number of oxygen defects and therefore the higher negative charge of the surface. Furthermore, they had the largest surface area of the zinc oxide tetrapods which in turn should lead to a further increase in adsorption.

For zinc oxide, the adsorption capacity of all proteins and for the zinc oxide tetrapods, short milled and long milled zinc oxide tetrapods the adsorption capacity of proteins with an isoelectric point in the basic pH range was investigated.

In Figure 6.12 and Table 6.3 the results of the adsorption of proteins with an isoelectric point in the basic pH range and different molecular weights on zinc oxide tetrapods, short milled and long milled zinc oxide tetrapods are shown. For avidin, the short milled zinc oxide tetrapods with $0.33 \text{ mmol/m}^2 \pm 0.021 \text{ mmol/m}^2$ show the highest adsorption capacity and the long milled zinc oxide tetrapods with $0.11 \text{ mmol/m}^2 \pm 0.012 \text{ mmol/m}^2$ the lowest one. With $0.24 \text{ mmol/m}^2 \pm 0.012 \text{ mmol/m}^2$ the zinc oxide tetrapods are very significantly ($p\text{-value} = 0.0033$) different from the short milled zinc oxide tetrapods and highly significantly ($p\text{-value} = 0.0002$) different from the long milled zinc oxide tetrapods. The difference between the two milled zinc oxide tetrapods is also highly significant with a $p\text{-value} < 0.0001$.

A similar trend is observed for lysozyme. With $0.83 \text{ mmol/m}^2 \pm 0.303 \text{ mmol/m}^2$ the short milled zinc oxide tetrapods show the highest adsorption capacity, followed by the zinc oxide tetrapods with $0.63 \text{ mmol/m}^2 \pm 0.260 \text{ mmol/m}^2$ and the lowest adsorption capacity is shown by the long milled zinc oxide tetrapods with $0.23 \text{ mmol/m}^2 \pm 0.127 \text{ mmol/m}^2$. However, the differences are not significant.

The adsorption of the lysozyme with a molecular mass of 14 kDa is higher but not significantly higher than the adsorption of the avidin with a molecular mass of 66 kDa for all zinc oxide tetrapod variants. For simplification, explanation is just based on molecular weight. In this sense, more small lysozyme molecules can be placed on the same surface compared to avidin molecules, where one molecule occupies much more space due to its larger molecular weight.

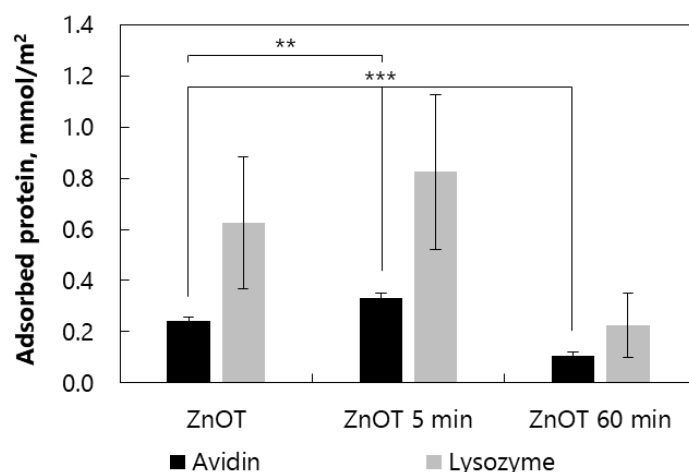


Figure 6.12. Adsorption studies of proteins with an isoelectric point in the basic pH range and different molecular weight (avidin: IEP = pH 10.5, 66 kDa; lysozyme: IEP = pH 11, 14 kDa) and zinc oxide tetrapods (ZnOT), short milled (ZnOT 5 min) and long milled (ZnOT 60 min) zinc oxide tetrapods. $n = 3$, error bars = standard deviation, p -value < 0.01 = very significant difference (**), p -value < 0.001 = highly significant difference (***).

Table 6.3. Adsorption studies of proteins with an isoelectric point in the basic pH range and different molecular weight (avidin: IEP = pH 10.5, 66 kDa; lysozyme: IEP = pH 11, 14 kDa) and zinc oxide tetrapods (ZnOT), short milled zinc oxides tetrapods (ZnOT 5 min) and long milled zinc oxide tetrapods (ZnOT 60 min). $n = 3$, \pm = standard deviation.

	Avidin, mmol/m ²	Lysozyme, mmol/m ²
ZnOT	0.24 ± 0.012	0.63 ± 0.260
ZnOT 5 min	0.33 ± 0.021	0.83 ± 0.303
ZnOT 60 min	0.11 ± 0.012	0.23 ± 0.127

Contrary to expectations, the short milled zinc oxide tetrapods with the smallest surface area and the medium number of oxygen defects showed the highest adsorption capacity and the long milled zinc oxide tetrapods with the largest surface area and the highest number of oxygen defects the lowest one. While the surface area had already been included in the calculations and therefore all materials should show the same adsorption, only the number of oxygen vacancies should show an influence on adsorption. If the zinc oxide tetrapods and the short milled zinc oxide tetrapods are considered, the increase in adsorption of the short milled zinc oxide tetrapods can be explained by the increase in the number of oxygen defects compared to the unmilled material. A further increase would be expected for the long milled zinc oxide tetrapods. However, the long milled zinc oxide tetrapods show the lowest adsorption.

A possible explanation could be the measured surface area, which was larger than for the short milled zinc oxide tetrapods and zinc oxide tetrapods. As a result, the nominator in the calculation of the

adsorbed amount was larger and thus the result in mmol/m^2 would be smaller. If it is assumed that adsorption and surface area increase proportionally, however, this should not make any difference compared to the short milled zinc oxide tetrapods and the zinc oxide tetrapods. If the long milled zinc oxide tetrapods were suspended in water, the individual smaller particles formed agglomerates due to the larger surface area and the entire surface area was not available for adsorption of the protein. The real surface available in the experiment was therefore smaller than the measured surface and the calculated value for the adsorbed protein amount was accordingly too low as the nominator, which was the surface area, was too high.

Another possible explanation for the lower-than-expected adsorption of the long milled zinc oxide tetrapods could be the nature of the surface. While the surfaces of the zinc oxide tetrapods and the short milled zinc oxide tetrapods were uniformly formed by the existing arms of the zinc oxide tetrapods, whether in the form of a tetrapod or individually, the long milled zinc oxide tetrapods formed an irregular surface due to the formation of agglomerates. As a result, an organised and uniform adsorption of the proteins was not possible resulting in a decrease of adsorbed proteins.

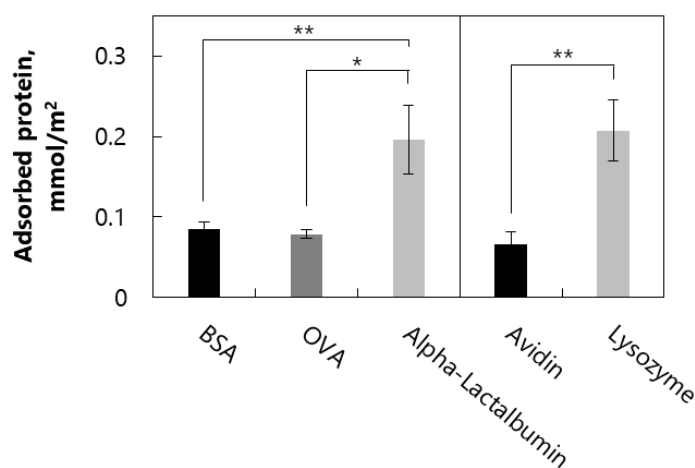


Figure 6.13. Adsorption studies of all proteins with different molecular weight and different isoelectric points (BSA: IEP = pH 4.9, 66 kDa; OVA: IEP = pH 4.5, 44 kDa; alpha-lactalbumin: IEP = pH 4.4, 14 kDa; avidin: IEP = pH 10.5, 66 kDa; lysozyme: IEP = pH 11, 14 kDa) and zinc oxide. $n = 3$, error bars = standard deviation, p -value < 0.05 = significant difference (*), p -value < 0.01 = very significant difference (**).

In Figure 6.13 and Table 6.4 the results of the adsorption of all proteins with different isoelectric points and different molecular weights on zinc oxide are shown. With $0.20 \text{ mmol}/\text{m}^2 \pm 0.043 \text{ mmol}/\text{m}^2$ the adsorption of alpha-lactalbumin is very significantly higher than the adsorption of BSA ($0.09 \text{ mmol}/\text{m}^2 \pm 0.008 \text{ mmol}/\text{m}^2$, p -value = 0.0059) and significantly higher than OVA ($0.07 \text{ mmol}/\text{m}^2 \pm 0.005 \text{ mmol}/\text{m}^2$, p -value = 0.0199). Lysozyme shows a very significantly higher adsorption with $0.21 \text{ mmol}/\text{m}^2 \pm 0.038 \text{ mmol}/\text{m}^2$ than avidin with $0.07 \text{ mmol}/\text{m}^2 \pm 0.016 \text{ mmol}/\text{m}^2$ (p -value = 0.0020).

Like zinc oxide tetrapods and milled zinc oxide tetrapods, the proteins with the low molecular weight of 14 kDa (alpha-lactalbumin and lysozyme) show higher adsorption than the proteins with higher molecular weights. OVA shows no significant difference to BSA in adsorption on zinc oxide. These results lead to the assumption that there is an upper limit to the loading of zinc oxide particles in terms of molecular weight similar to aluminium phosphate in the study of Huang and Wang, where aluminium phosphate showed no correlation between the molecular weight of the proteins and the adsorption [165]. In order to confirm this hypothesis, further experiments with other proteins with different molecular weights have to be performed but this is not part of this work.

Table 6.4. Adsorption studies of all proteins with different molecular weight and different isoelectric points (BSA: IEP = pH 4.9, 66 kDa; OVA: IEP = pH 4.5, 44 kDa; alpha-lactalbumin: IEP = pH 4.4, 14 kDa; avidin: IEP = pH 10.5, 66 kDa; lysozyme: IEP = pH 11, 14 kDa) and zinc oxide. n = 3, ± = standard deviation.

	BSA, mmol/m ²	OVA, mmol/m ²	Alpha-Lactalbumin, mmol/m ²	Avidin, mmol/m ²	Lysozyme, mmol/m ²
ZnO	0.09 ± 0.008	0.07 ± 0.005	0.20 ± 0.043	0.07 ± 0.016	0.21 ± 0.038

There was no clear difference between the proteins with varying isoelectric points, i.e., the adsorption of the proteins was not only due to electrostatic interactions. Like many other metal oxides, zinc oxide is hydrolysed in the presence of water and forms hydroxide layers on the surface. Water molecules are physically or chemically adsorbed on the surface of the dispersed zinc oxide. Due to their amphoteric character, the surface can be either positively charged by the reaction with H⁺ ions or negatively charged by the reaction with OH⁻ ions [220]. The adsorption of the proteins could be described by formation of hydrogen bonds or van der Waals forces [221]. The strengths of these two bonds are far below the strength of covalent bonds or electrostatic interactions. Hydrogen bonds are formed between a bound hydrogen atom and a free electron pair. The hydrogen atom is bound to small, very electronegative atoms. This hydrogen atom and a pair of electrons on the electronegative atom of another molecule attract each other and form a hydrogen bond [222]. They also occur, e.g., as weak bonds in proteins and thus lead to the formation of the secondary structure of proteins [223]. Van der Waals forces are intermolecular forces like the hydrogen bonds just described. The electron cloud of a molecule can be deformed at a certain point in time due to the movement of the electrons. As a result, one side of the molecule is temporarily more negatively charged than the other, but the orientation of the dipole will already be changed again the next moment. The dipole development takes place synchronously in neighbouring molecules, which ultimately leads to an attraction of the current dipoles [222].

6.1.3 Summary and conclusion

Zinc oxide tetrapods were produced using flame transport synthesis, resulting in a three-dimensional tetrapodial structure with the same arm length within a tetrapod and equal angles between these arms. The tetrapods showed large differences in particle size and the morphology was strongly dependent on the harvested position. The separation into defined particle sizes was neither successful with the help of air jet sieving nor with the help of wet sieving, because either almost no tetrapodial structure remained or a high work and time effort was necessary, which resulted in a low yield. Therefore, the zinc oxide tetrapods were crushed with defined parameters. Three different types of zinc oxide tetrapods could be used for adsorption: zinc oxide tetrapods, short milled and long milled zinc oxide tetrapods.

Zinc oxide can be produced using various processes and had been used in commercial quality. The zinc oxide used showed small needle-shaped particles with a resulting large surface area and a tendency to form agglomerates.

Both materials, i.e., the zinc oxide tetrapods and the zinc oxide, were crystalline substances consisting of zinc oxide. The adsorption experiments investigated to what extent the production method, shape and particle size had an influence on the adsorption of different proteins.

Five different proteins with varying isoelectric points and different molecular weights were tested for their adsorption on the materials consisting of zinc oxide: BSA, OVA, alpha-lactalbumin, avidin and lysozyme. Aluminium hydroxide was used as a reference for adsorption of negatively charged proteins, and aluminium phosphate as a reference for adsorption of positively charged proteins.

Zinc oxide and the zinc oxide tetrapods showed the structure just described. Almost no tetrapodial structure was visible in the milled zinc oxide tetrapods. Individual arms of the tetrapods were still visible in the short milled zinc oxide tetrapods. Long milled zinc oxide tetrapods showed no structure reminding of the original morphology. The BET surface determined by iGC increased in the following order: short milled zinc oxide tetrapods < zinc oxide tetrapods < long milled zinc oxide tetrapods < zinc oxide.

In a comparison of the adsorption of avidin and BSA on zinc oxide and the zinc oxide tetrapods, zinc oxide showed no difference in the adsorption of negatively and positively charged proteins. The zinc oxide tetrapods adsorbed very significantly higher amounts of positively charged proteins. Therefore, the following experiments investigated the adsorption capacity of all proteins on zinc oxide and the adsorption capacity of proteins with an isoelectric point in the basic pH range on the zinc oxide tetrapods and the milled zinc oxide tetrapods. The molecular weight of the proteins and the surface area of the zinc oxide, the zinc oxide tetrapods and the milled zinc oxide tetrapods were included in the calculation of the adsorption. This calculation resulted in the unit mmol/m² for the adsorption capacity.

For the zinc oxide tetrapods and the milled zinc oxide tetrapods, short milled zinc oxide tetrapods showed the highest adsorption capacity for avidin and lysozyme. The uniformly formed surface, as in the

case of the arms of the zinc oxide tetrapods, and the increase in the number of oxygen defects, as in the case of the long milled zinc oxide tetrapods, resulted in the optimum adsorption of positively charged proteins on short milled zinc oxide tetrapods. Lysozyme showed higher adsorption than avidin. As the calculation of the adsorption capacity included the molecular weight, it indicated a higher loading due to a smaller particle size.

Similar to the zinc oxide tetrapods and milled zinc oxide tetrapods, zinc oxide also showed a higher adsorption of smaller proteins due to numerically higher loading. However, as already mentioned, there was no difference between the proteins with varying isoelectric points.

A comparison of the zinc oxide tetrapods with the zinc oxide revealed a clear difference with regard to the adsorption of proteins. While the zinc oxide tetrapods were able to adsorb mainly positively charged proteins due to their negatively charged surface, there was no discernible difference in the case of zinc oxide. The assumption was that the difference in adsorption was related to the production method. Zinc oxide tetrapods and the milled zinc oxide tetrapods were then investigated only with the positively charged proteins and the adsorption capacity of zinc oxide with all the proteins used. A clear advantage of the short milled zinc oxide tetrapods and the small proteins was found in the investigations. Comparing the adsorption capacity of long milled zinc oxide tetrapods in relation to avidin and lysozymes with the adsorption capacity of zinc oxide in relation to avidin and lysozymes, almost no difference is recognisable. This weakened the assumption made at the beginning that the difference in adsorption was due to the production method and strengthens the idea that the tetrapodial structure in particular would be a decisive factor in increasing the adsorption capacity.

In conclusion, it was probably a combination of production method, shape and particle size that gave the best adsorption capacity results for the short milled zinc oxide tetrapods.

The adsorption capacities of the zinc oxide tetrapods, short milled and long milled zinc oxide tetrapods and zinc oxide were far below the adsorption capacity of the reference materials aluminium hydroxide and aluminium phosphate. Finally, the question would be whether the adsorbed amount of protein or, in the case of vaccination of an antigen, might even be sufficient to induce an immune reaction. However, since it was difficult to make a general prediction about the required adsorbed amount of protein or antigen, the adsorbed amount of protein of aluminium hydroxide and aluminium phosphate was considered as a reference value. For this reason, a method was sought for increasing the protein loading. In order to achieve maximum protein loading, the protein was spray dried in the following together with zinc oxide and other excipients in a formulation. Due to the varying morphology, particle size and properties of the zinc oxide tetrapods and the milled zinc oxide tetrapods, they were not considered in the further investigations.

6.2 Spray dried zinc oxide formulations

Spray drying is a very fast drying method where large amounts of solvents can be dried. It is widely used in the food and pharmaceutical industry, e.g., as production method for dry powders for inhalation. With different process parameters it was possible to spray dry large particles ($> 10\mu\text{m}$) for nasal application as well as small particles ($< 5\mu\text{m}$) for pulmonary application.

6.2.1 Spray dried zinc oxide for nasal application

Zinc oxide is already used in various areas. Due to its small particle size in the nanometre range and the associated larger surface area, zinc oxide particles tend to form undefined agglomerates. By spray drying, it is possible to produce particles with a defined particle size $> 10\mu\text{m}$ for nasal application. Since the aim of the work is to use zinc oxide as an alternative adjuvant in a formulation, it was spray dried together with hyaluronic acid, ovalbumin and mannitol. Acetic acid (2 %) was used as liquid medium.

The six spray dried formulations are all white dry powders independent of the different compositions. They were characterised in a pharmaceutical view and finally examined for their properties in in-vitro cell experiments. Besides the assessment of morphology, particle size distribution and aerodynamic behaviour, 24-h-solubility studies, mucus rheology and various protein characterisation methods were carried out.

6.2.1.1 Morphology and particle size distribution

Six different formulations with different concentrations of zinc oxide and mannitol as mentioned in Table 5.1 were spray dried. The amount of ovalbumin, as model antigen, and hyaluronic acid, as penetration enhancer and adhesive between the single zinc oxide particles, remained constant. The formulations were visualised with scanning electron microscopy.

Figure 6.14 shows representative images of the six different formulations in two different magnifications, whereby image A shows formulation 1 with the highest amount of zinc oxide (100 %) and image F shows formulation 6 without zinc oxide (0 %). From formulation 1 to formulation 6 the zinc oxide concentration decreases and the mannitol concentration increases. The images show wide particle size distributions, as both small and large particles are visible in the smaller magnification (right). Nevertheless, it is noticeable that all formulations seem to have a similar mean diameter, visible in the higher magnification (left). The cut-off diameter for nasal application is $10\mu\text{m}$. Particles larger than $10\mu\text{m}$ [102] (aerodynamic diameter) are deposited in the nose. Particles smaller than $10\mu\text{m}$ are separated in the throat. Particles smaller than $5\mu\text{m}$ [109] (aerodynamic diameter) can be inhaled into the lungs.

While almost no difference in particle size was visible, there is a difference in morphology. Formulation 6 (Figure 6.14, image F) and formulation 1 (Figure 6.14, image A) show the typical uniform spherical shape [191] of a spray dried powder. The surface of these formulations however is slightly different. While

particles of formulation 6 show a smooth surface, particles of formulation 1 are slightly indented. All the other formulations have clearly wrinkled particles (Figure 6.14, images B to E). The different morphology can be explained by the particle forming process.

The initially high amounts of solvent in the drop are removed at the beginning of the drying process. The drop becomes smaller and the concentration of dissolved or suspended components increases. As long as the surface of the drop is covered with solvent, both the drying speed and the temperature on the surface of the drop are constant. As drying progresses, the saturation solubility is exceeded. Shell formation occurs due to the concentrated solids on the surface. At the beginning of the shell forming process the solvent molecules inside the particle diffuse through the shell and evaporate. The drying speed becomes slower and slower. The diameter of the particle does not decrease further [191]. The temperature in the particle therefore continues to rise, as finally the solvent cannot evaporate further. As a result, the internal pressure also continues to rise. On the one hand, this leads to a stabilisation of the spherical form, on the other hand, the solvent vapour is pressed through small pores. As the process continues, the solvent inside the particle condenses, which leads to an enormous reduction in volume. The applied vacuum can cause the particles shell to collapse [224].

Mannitol was initially dissolved in the drop produced by the two-fluid nozzle. Due to the evaporation of the solvent on the surface, the particle initially became smaller and the mannitol concentration on the surface of the drop increased. When the saturation concentration was exceeded, mannitol precipitated and a shell was formed. The particle no longer changed its size. Due to the low glass transition point (approximately 10 °C) [225] and the low outlet temperature, a crystalline, uniform and smooth particle was formed. The solvent vapour inside the particles could not diffuse through the shell, which increased the pressure. However, as the lower outlet temperature caused the pressure inside the particle to increase only slightly and then decrease only slightly in the further process, the particle did not collapse. Small holes could be formed to release the solvent vapour.

Since acetic acid (2 %) was used as solvent, zinc oxide was initially partially dissolved and partially suspended in the drop produced by the two-fluid nozzle. By removing the solvent, an outer layer of the individual zinc oxide particles was formed. These were combined into a shell by the precipitation of the dissolved zinc oxide in acetic acid (2 %) as zinc acetate. A crystalline, uniform, almost spherical particle was formed whose matrix consisted of individual zinc oxide particles in combination with zinc acetate. This allowed the solvent vapour inside the particle to diffuse through the shell and they retained their shape.

When mannitol and zinc oxide were processed together as a matrix, mannitol and zinc oxide were partially dissolved and a part of zinc oxide was suspended. The drying of the solvent led to a higher concentration of a mixture of mannitol, zinc oxide and the dissolved zinc oxide on the surface of the

drop. Crystalline and spherical particles were formed. As this was a suspension, the shell was formed more quickly than in a solution. The solvent vapour inside the particles, which was now exposed to higher temperatures, created a higher pressure. When the solvent vapour condensed, decreasing volume created a vacuum and the shell collapsed.

The different compositions are clearly visible in the SEM images. The colour of the particles becomes darker and darker with the appropriate setting of contrast and brightness, starting with formulation 1 (Figure 6.14, image A). Small particles and areas in a lighter grey represent zinc oxide particles and areas in a darker grey represent mannitol.

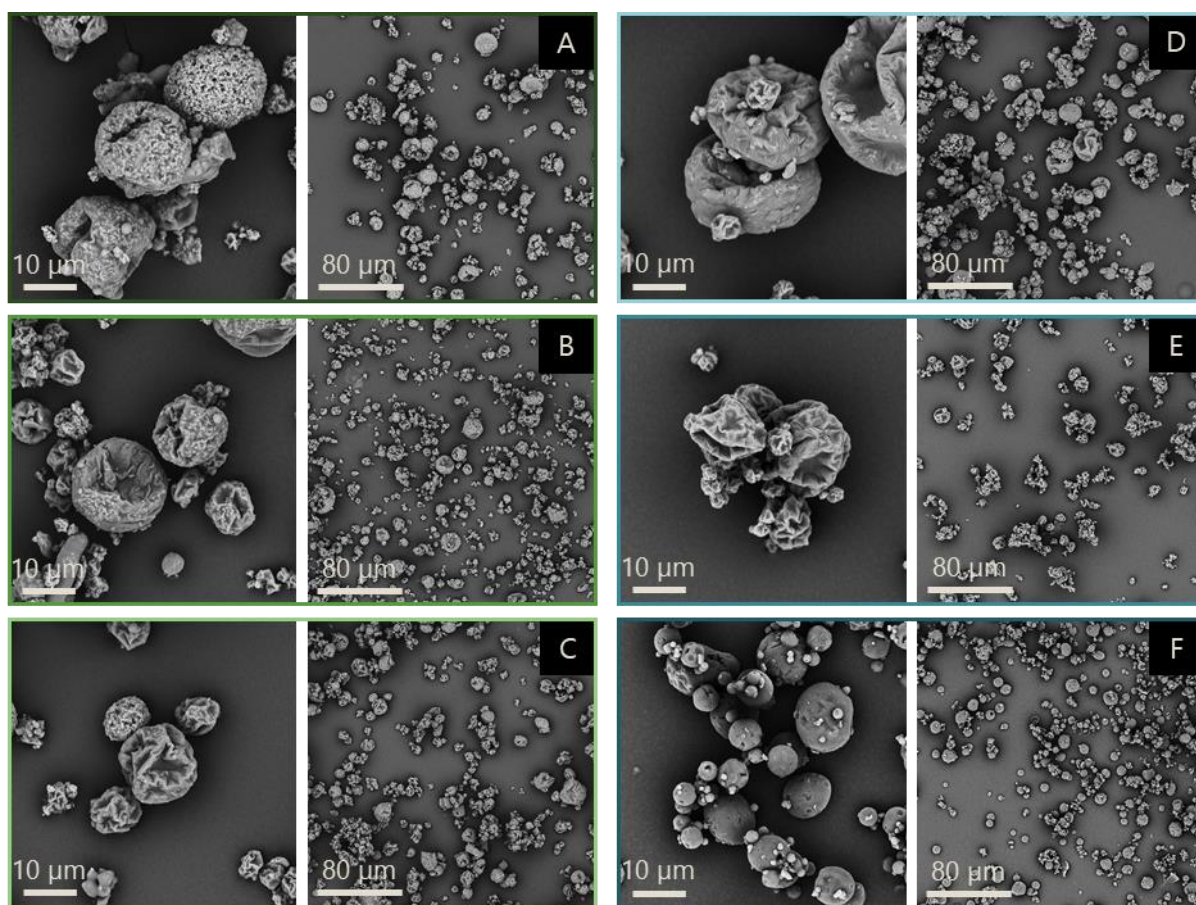


Figure 6.14. Representative scanning electron microscope images showing all spray dried powders with different amounts of zinc oxide (ZnO) and mannitol and additionally constant concentrations of ovalbumin (10 %) and hyaluronic acid (1 %). A) 100 % ZnO and 0 % mannitol; B) 80 % ZnO and 20 % mannitol; C) 60 % ZnO and 40 % mannitol; D) 40 % ZnO and 60 % mannitol; E) 20 % ZnO and 80 % mannitol; F) 0 % ZnO and 100 % mannitol.

To make sure that the different compositions of the spray dried particles were not just a visual impression but based on the actual composition of the formulation, an elemental analysis was performed. Energy dispersive X-ray spectroscopy was the method of choice for the detection of elements in the scanning electron microscope. An electron beam was used to excite the samples to emit X-rays. This enabled the detection of substance quantities of less than 0.1 pg [194].

In Figure 6.15 the atomic concentrations of the four most significant contained elements: zinc (Zn), oxygen (O), carbon (C) and nitrogen (N) are plotted against the individual formulations. Hydrogen (atomic number too low) and sulfur (concentration too low) were not considered because the detection is too unspecific. Table 6.5 contains the corresponding numerical values. As can be seen very clearly in the diagram (Figure 6.15), there are differences in the composition of the formulations. While the atomic zinc concentration decreases with increasing number of formulation (F1 = 35.34 % \pm 2.89 %, F2 = 28.87 % \pm 2.26 %, F3 = 20.34 % \pm 1.88 %, F4 = 21.33 % \pm 1.71 %, F5 = 16.41 % \pm 6.65 %, F6 = 0.03 % \pm 0.03 %), the atomic carbon concentration increases (F1 = 4.72 % \pm 1.17 %, F2 = 7.12 % \pm 1.63 %, F3 = 15.84 % \pm 3.05 %, F4 = 20.62 % \pm 2.18 %, F5 = 28.57 % \pm 1.91 %, F6 = 48.92 % \pm 0.97 %). This can be explained by the different amounts of the starting materials and their atomic composition. The matrix of formulation 1 consists of 100 % zinc oxide, which contains the atomic elements zinc and oxygen, and the matrix of formulation 6 consists of 100 % mannitol, which contains the atomic elements carbon and oxygen. From formulation 1 to formulation 6 the zinc oxide concentration and thus also the atomic zinc concentration decreases. In formulation 1, a not inconsiderable amount of carbon (F1 = 4.72 % \pm 1.17 %) can be seen, even if no mannitol is present. This can be explained by the other components, ovalbumin and hyaluronic acid, because they also contain the element carbon. Additionally, they have the elements oxygen and nitrogen. Since oxygen is present in all starting materials, the atomic concentration of oxygen is similar in all formulations (F1 = 59.64 % \pm 3.70 %, F2 = 63.64 % \pm 1.83 %, F3 = 62.72 % \pm 1.03 %, F4 = 56.55 % \pm 4.34 %, F5 = 52.77 % \pm 4.36 %, F6 = 46.27 % \pm 0.78 %).

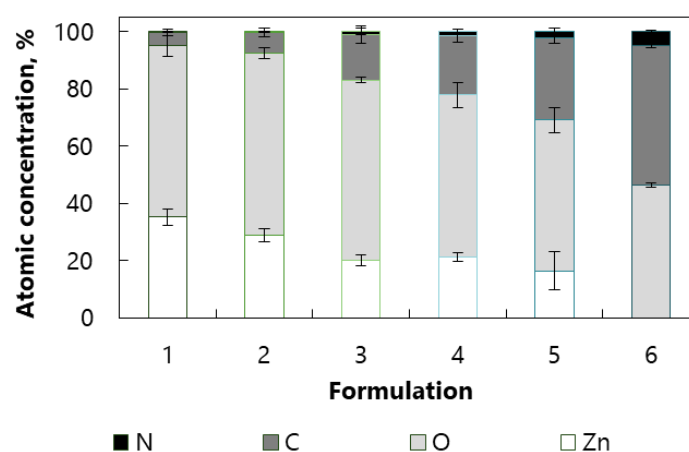


Figure 6.15. Elemental identification of all formulations with energy-dispersive X-ray spectroscopy. 1) 100 % ZnO and 0 % mannitol; 2) 80 % ZnO and 20 % mannitol; 3) 60 % ZnO and 40 % mannitol; 4) 40 % ZnO and 60 % mannitol; 5) 20 % ZnO and 80 % mannitol; 6) 0 % ZnO and 100 % mannitol. $n = 3$, error bars = standard deviation.

The concentrations of ovalbumin and hyaluronic acid, the two ingredients that contain nitrogen, are identical in all formulations. Nonetheless, the concentration of nitrogen in the particles increases with increasing amount of mannitol and decreasing amount of zinc oxide, which is remarkable. When

evaluating the results, it should be considered that a quantitative analysis of elements with low atomic numbers is problematic and only possible with an atomic number higher than four [226]. Carbon has an atomic number of six, nitrogen of seven, oxygen of eight and zinc of 30. The quantitative elemental analysis of zinc is therefore more precise due to the higher atomic number. Thus, a higher concentration of zinc oxide in the formulation interferes with the detection of the other elements, especially if they are present in low atomic concentration. The increasing amount of nitrogen with increasing formulation number could be the result of a measurement problem in the method. Further variations of the measurements could be caused by the measuring principle. For optimal detection the surface should be smooth. Since the formulations were wrinkled spheres, elemental analysis using EDS should only be used to get a first idea of the composition. An absolute statement was not possible.

Table 6.5. Atomic concentration in % of all formulations using energy dispersive X-ray spectroscopy. F1) 100 % ZnO and 0 % mannitol; F2) 80 % ZnO and 20 % mannitol; F3) 60 % ZnO and 40 % mannitol; F4) 40 % ZnO and 60 % mannitol; F5) 20 % ZnO and 80 % mannitol; F6) 0 % ZnO and 100 % mannitol. n = 3, ± = standard deviation.

	N, %	C, %	O, %	Zn, %
F1	0.30 ± 0.17	4.72 ± 1.17	59.64 ± 3.70	35.34 ± 2.89
F2	0.38 ± 0.14	7.12 ± 1.63	63.64 ± 1.83	28.87 ± 2.26
F3	1.10 ± 1.09	15.84 ± 3.05	62.72 ± 1.03	20.34 ± 1.88
F4	1.50 ± 0.79	20.62 ± 2.18	56.55 ± 4.34	21.33 ± 1.71
F5	2.25 ± 1.11	28.57 ± 1.91	52.77 ± 4.36	16.41 ± 6.65
F6	4.77 ± 0.31	48.92 ± 0.97	46.27 ± 0.78	0.03 ± 0.03

As already mentioned, particle size or particle size distribution plays an important role in nasal application. For nasal spray products, the FDA requires a particle size larger than 10 µm (aerodynamic diameter) for most of the particles. For nasal dry powders, Hickey [58,102] recommends a particle size of 50 µm (aerodynamic diameter) to ensure deposition in the nose. The particle size distribution of all formulations was determined by laser diffraction (volume-based diameter).

In Figure 6.16 and Table 6.6, the x50 and the span values from the measurements with the RODOS module of all formulations are shown. With an x50 of 8.75 µm ± 0.13 µm (F1), 7.85 µm ± 0.57 µm (F2), 8.67 µm ± 0.29 µm (F5) and 7.13 µm ± 0.34 µm (F6), 50 % of the particles of formulations 1, 2, 5 and 6 are smaller than 10 µm. With 10.56 µm ± 0.15 µm (F3) and 12.59 µm (F4) the x50 of formulations 3 and 4 is higher than 10 µm.

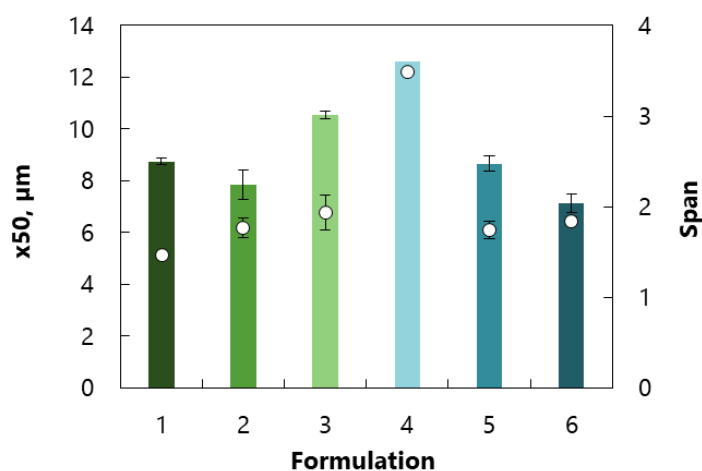


Figure 6.16. Particle size distribution using laser diffraction (HELOS) in combination with the RODOS module, x_{50} (primary axis) and span (secondary axis) of all formulations; 1) 100 % ZnO and 0 % mannitol; 2) 80 % ZnO and 20 % mannitol; 3) 60 % ZnO and 40 % mannitol; 4) 40 % ZnO and 60 % mannitol; 5) 20 % ZnO and 80 % mannitol; 6) 0 % ZnO and 100 % mannitol. $n = 3$, error bars = standard deviation; F3 RODOS: $n = 2$, error bars = min/max; F4 RODOS: $n = 1$.

The span value describes the distribution width and is especially useful, when the distribution is not normally distributed. Spray drying is a fast process with a resulting logarithmic normally particle size distribution. In the logarithmic graph (x-axis), the curves of formulations 1, 2, 5 and 6 showed a monomodal distribution with a small shoulder in the direction of the smaller particle sizes. Formulations 3 and 4 had a bimodal distribution with a second smaller peak at larger particle sizes, which could be generated from potential agglomerations. This is also reflected in the span values of formulation 3 with 1.94 ± 0.20 and especially of formulation 4 with 3.49. As it was not possible to measure formulations 3 and 4 three times, no statistical analysis of the data was performed.

Table 6.6. x_{10} , x_{50} , x_{90} and span of all formulations using the HELOS in combination with the RODOS module. F1) 100 % ZnO and 0 % mannitol; F2) 80 % ZnO and 20 % mannitol; F3) 60 % ZnO and 40 % mannitol; F4) 40 % ZnO and 60 % mannitol; F5) 20 % ZnO and 80 % mannitol; F6) 0 % ZnO and 100 % mannitol. $n = 3$, \pm = standard deviation; F3: $n = 2$, \pm = min/max; F4: $n = 1$.

	x_{10} , μm	x_{50} , μm	x_{90} , μm	Span
F1	3.23 ± 0.08	8.75 ± 0.13	16.02 ± 0.23	1.46 ± 0.01
F2	2.09 ± 0.22	7.85 ± 0.57	15.90 ± 0.40	1.76 ± 0.11
F3	3.77 ± 0.02	10.56 ± 0.15	24.27 ± 2.38	1.94 ± 0.20
F4	3.49	12.59	47.42	3.49
F5	2.84 ± 0.12	8.67 ± 0.29	17.95 ± 0.88	1.74 ± 0.10
F6	1.58 ± 0.08	7.13 ± 0.34	14.71 ± 0.41	1.84 ± 2.25

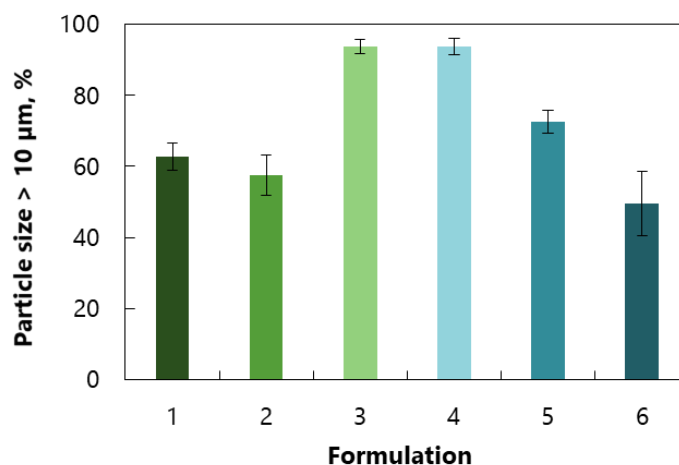


Figure 6.17. Particle size distribution using laser diffraction (HELOS) in combination with the SPRAYER module (> 10 µm) and the UDS powder device, cumulative distribution of all formulations; 1) 100 % ZnO and 0 % mannitol; 2) 80 % ZnO and 20 % mannitol; 3) 60 % ZnO and 40 % mannitol; 4) 40 % ZnO and 60 % mannitol; 5) 20 % ZnO and 80 % mannitol; 6) 0 % ZnO and 100 % mannitol. $n = 3$, error bars = standard deviation.

In Figure 6.17 and Table 6.7, the results of the measurements with the SPRAYER module in combination with the UDS powder device are shown. Since only the device contributed to the dispersion, the HELOS with the SPRAYER module rather provided data about the realistic particle size distribution than the HELOS with the RODOS module. Nevertheless, a similar trend can be seen. Illustrated is the cumulative distribution of particles larger than 10 µm (volume-based diameter). Formulations 3 and 4 also show the highest values with 93.65 % ± 1.94 % and 93.59 % ± 2.31 % of particles larger than 10 µm. For Formulations 1, 2 and 5 more than 50 % (F1 = 62.77 % ± 3.83 %, F2 = 57.42 % ± 5.60 %, F5 = 72.43 % ± 3.20 %) of the particles are larger than 10 µm and for formulation 6 almost 50 % (F6 = 49.49 % ± 9.11 %). The amount of particles larger than 10 µm in formulation 3 is very significantly different to formulation 6 (p-value = 0.0012) and highly significantly different to formulations 1 (p-value = 0.0002), 2 (p-value = 0.0005) and 5 (p-value = 0.0006). Formulation 4 has a very significantly different percentage of particles above 10 µm than formulation 6 (p-value = 0.0012) and a highly significantly different percentage than formulations 1 (p-value = 0.0003), 2 (p-value = 0.0005) and 5 (p-value = 0.007). Formulation 5 shows a significant difference to formulations 1 (p-value = 0.0284), 2 (p-value = 0.0157) and 6 (p-value = 0.0147).

Table 6.7. Cumulative distribution (> 10 µm) of all formulations using the HELOS in combination with the SPAYER module and the UDS powder device. F1) 100 % ZnO and 0 % mannitol; F2) 80 % ZnO and 20 % mannitol; F3) 60 % ZnO and 40 % mannitol; F4) 40 % ZnO and 60 % mannitol; F5) 20 % ZnO and 80 % mannitol; F6) 0 % ZnO and 100 % mannitol. $n = 3$, ± = standard deviation.

	F1	F2	F3	F4	F5	F6
Particle size > 10 µm, %	62.77 ± 3.83	57.42 ± 5.60	93.65 ± 1.94	93.59 ± 2.31	72.43 ± 3.20	49.49 ± 9.11

6.2.1.2 Aerodynamic assessment using the NGI

The deposition in the nose of a spray dried powder for nasal application could not be assessed by using laser diffraction and a geometric diameter. Aerodynamic performance with the help of an NGI took different parameters of the formulation into account, e.g., density and morphology and can measure the aerodynamic diameter.

In Figure 6.18 and Table 6.8, deposition profiles of all formulations using the NGI in combination with the NEC and the UDS powder device are shown. A similar trend to the laser diffraction measurements is obtained. Formulations 3, 4 and 5 have the highest deposition in the NEC (F3 = 84.82 % \pm 6.43 %, F4 = 87.54 % \pm 2.24 %, F5 = 81.64 % \pm 2.21 %). Formulations 1, 2 and 6 have a nasal fraction below 80 % (F1 = 73.00 % \pm 4.13 %, F2 = 73.36 % \pm 8.98 %, F6 = 75.56 % \pm 7.55 %). There is a very significant difference between formulation 1 and formulation 4 (p-value = 0.0058) and a significant difference between formulation 1 and formulation 5 (p-value = 0.0330). There is also a significant difference between formulation 4 and formulation 5 (p-value = 0.0315) with regard to the deposition in the NEC.

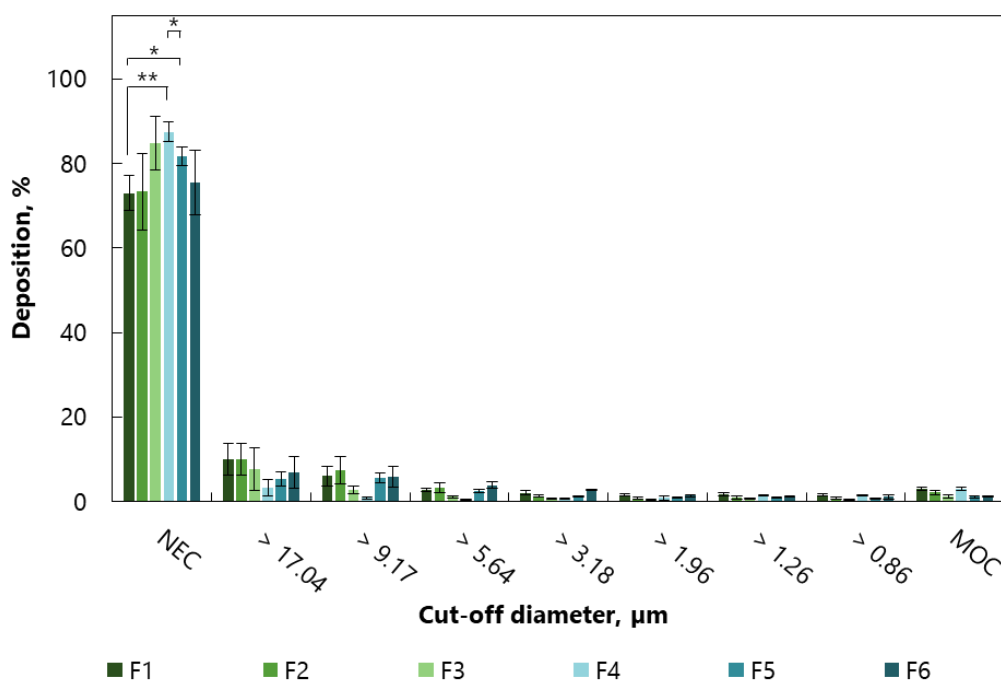


Figure 6.18. Deposition profiles of all formulations using the NGI at 15 L/min in combination with the NEC and the UDS powder device. F1) 100 % ZnO and 0 % mannitol; F2) 80 % ZnO and 20 % mannitol; F3) 60 % ZnO and 40 % mannitol; F4) 40 % ZnO and 60 % mannitol; F5) 20 % ZnO and 80 % mannitol; F6) 0 % ZnO and 100 % mannitol. $n = 3$, error bars = standard deviation, p-value < 0.05 = significant difference (*), p-value < 0.01 = very significant difference (**).

Table 6.8. Deposition data of all formulations using the NGI at 15 L/min in combination with the NEC and the UDS powder device. F1) 100 % ZnO and 0 % mannitol; F2) 80 % ZnO and 20 % mannitol; F3) 60 % ZnO and 40 % mannitol; F4) 40 % ZnO and 60 % mannitol; F5) 20 % ZnO and 80 % mannitol; F6) 0 % ZnO and 100 % mannitol. $n = 3$, \pm = standard deviation.

	NEC, %	> 17.04 μm , %	> 9.17 μm , %	> 5.64 μm , %	> 3.18 μm , %	> 1.96 μm , %	> 1.26 μm , %	> 0.86 μm , %	MOC, %
F1	73.00 \pm 4.13	10.02 \pm 3.88	6.02 \pm 2.39	2.81 \pm 0.44	2.11 \pm 0.53	1.58 \pm 0.18	1.69 \pm 0.41	1.57 \pm 0.18	2.97 \pm 0.42
F2	73.36 \pm 8.98	10.04 \pm 3.70	7.44 \pm 3.32	3.20 \pm 1.16	1.29 \pm 0.32	0.75 \pm 0.28	0.97 \pm 0.43	0.73 \pm 0.24	2.21 \pm 0.48
F3	84.82 \pm 6.43	7.67 \pm 5.07	2.80 \pm 0.85	1.10 \pm 0.20	0.70 \pm 0.18	0.61 \pm 0.08	0.63 \pm 0.18	0.41 \pm 0.05	1.26 \pm 0.47
F4	87.54 \pm 2.24	3.28 \pm 1.84	0.86 \pm 0.17	0.65 \pm 0.03	0.78 \pm 0.12	0.92 \pm 0.51	1.48 \pm 0.10	1.53 \pm 0.08	2.96 \pm 0.34
F5	81.64 \pm 2.21	5.32 \pm 1.77	5.54 \pm 1.20	2.60 \pm 0.36	1.25 \pm 0.15	0.93 \pm 0.09	0.85 \pm 0.14	0.73 \pm 0.15	1.13 \pm 0.21
F6	75.56 \pm 7.55	6.90 \pm 3.65	5.90 \pm 2.36	3.87 \pm 0.80	2.80 \pm 0.14	1.35 \pm 0.35	1.20 \pm 0.14	1.14 \pm 0.46	1.27 \pm 0.16

As already mentioned, the impaction tests with the NGI were also performed to determine the percentage of fine particles in a formulation. According to Ph. Eur. 2.9.18 "Preparation for inhalation: aerodynamic assessment of fine particles" [153], the FPF was calculated. The corresponding values can be found in Table 6.9. Formulation 3 shows a significant difference to formulation 5 (p -value = 0.0303), a very significant difference to formulations 1 (p value= 0.0035), 4 (p -value = 0.0036) and 6 (p -value = 0.0068). The FPF of formulation 5 is significantly different to formulations 4 (p -value = 0.0118) and 6 (p -value = 0.0245) and very significantly different to formulation 1 (p -value = 0.0080).

Table 6.9. FPF of all formulations using the NGI at 15 L/min in combination with the NEC and the UDS powder device. F1) 100 % ZnO and 0 % mannitol; F2) 80 % ZnO and 20 % mannitol; F3) 60 % ZnO and 40 % mannitol; F4) 40 % ZnO and 60 % mannitol; F5) 20 % ZnO and 80 % mannitol; F6) 0 % ZnO and 100 % mannitol. $n = 3$, $\pm =$ standard deviation.

	F1	F2	F3	F4	F5	F6
Fine particle fraction, %	8.91 \pm 1.48	5.61 \pm 1.65	3.43 \pm 0.42	7.46 \pm 1.06	4.57 \pm 0.43	7.03 \pm 1.14

Overall, the NGI measurements and the HELOS measurements gave a similar impression. Formulations 3, 4 and 5 provided the highest nasal fraction with almost 85 % (F3), 88 % (F4) and 82 % (F5) deposited in the NEC, respectively. Looking at the total mucosal deposition in the nose and the lungs, i.e., NEC and FPF, the difference of formulations 1, 2, 5 and 6 to formulation 3 is slightly smaller. Formulation 4 stands out with almost 95 % of nasal and pulmonary deposition.

6.2.1.3 pH and solubility

While particle size and morphology play an important role in the characterisation of nasal formulations with respect to nasal deposition, the pH value and solubility of nasal powders for mucosal vaccination are also of interest. In order to induce an immune response in the respiratory tract, the antigen has to be taken up in a particulate form by antigen presenting cells [35]. A 24-h-solubility study was conducted to investigate the amount of soluble zinc oxide, which serves as a protein adsorbent and adjuvant in the formulation. In addition, pH changes in different solutions after adding the formulations were measured to show the influence of zinc oxide (dissolved or undissolved) on the pH value. Zinc oxide as raw material was used as reference. As mentioned above in chapter 5.2.6, different solutions were used: sodium chloride solution adjusted to six different pH levels that mimic relevant pH conditions in the human body, was the simplest solution. pH levels to mimic relevant pH conditions in the human body. Since buffer systems often exist in the body, additional phosphate buffers with different pH values were used. Finally simulated nasal fluid (SNF) was used, which took account of the salt and pH conditions in the nose.

In Figure 6.19 and Table 11.1 the results of the 24-h-solubility study of zinc oxide as raw material and in formulation 1 are shown. With a solubility between 1 mg/mL and 10 mg/mL, both zinc oxide and formulation 1 are slightly soluble at pH 1.2 according to Ph. Eur. classification. The exact values are shown in Table 11.1. At pH 2.5, zinc oxide and formulation 1 are very slightly soluble in both the phosphate buffer and the sodium chloride solution with a solubility between 0.1 mg/mL and 1 mg/mL. Zinc oxide is practically insoluble in all tested pH values above pH 2.5 with a solubility of less than 0.1 mg/mL. While formulation 1 is practically insoluble in the phosphate buffer at all tested pH values above pH 2.5, it is very slightly soluble in the corresponding sodium chloride solutions. It is noticeable

that at all pH values of the sodium chloride solution and in the SNF, the differences in solubility between zinc oxide as raw material and formulation 1 is similar. This leads to the assumption that a different zinc compound was formed in the formulation during spray drying.

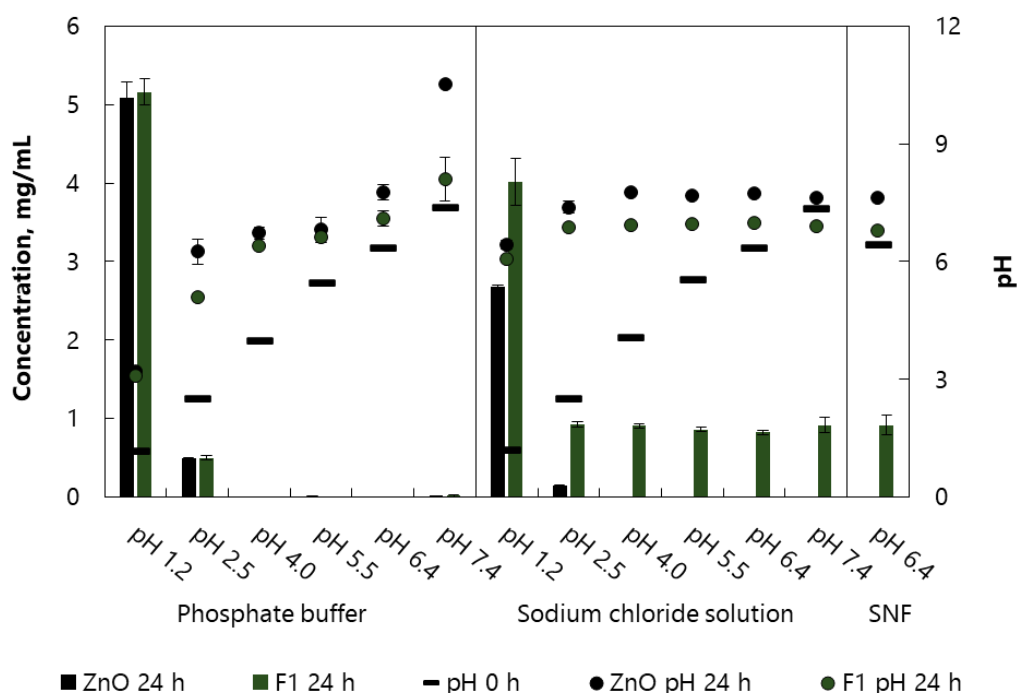


Figure 6.19. 24-h-pH- and solubility study showing starting pH (pH 0 h, black bars) and pH change of different solutions/suspensions after 24 h with zinc oxide as raw material (ZnO 24 h, black dots) in comparison to formulation 1 (F1 24 h, green dots). Saturation solubility after 24 h is shown for zinc oxide (ZnO 24 h, black bars) in comparison to formulation 1 (F1 24 h, green bars). F1) 100 % ZnO and 0 % mannitol. $n = 3$, error bars = standard deviation.

In order to exclude the possibility that the differences in solubility of zinc oxide as raw material and formulation 1 is merely a phenomenon of formulation 1, the experiment was repeated with all formulations and zinc oxide as raw material in SNF at pH 6.4. The results are presented in Figure 6.20. For zinc oxide as raw material and formulation 6, as shown in Table 6.10, no dissolved zinc was detectable, hence the values are not shown in the diagram.

Since formulation 6 did not contain zinc oxide and zinc oxide as raw material is practically insoluble at pH 6.4 these results are not surprising. However, formulations 1 to 5 show a constant amount of dissolved zinc ions, shown in Table 6.10. Even if the values of formulation 1 from the two experiments differ slightly, the difference is not significant. In order to explain the phenomenon of differences in solubility, the preparation of the formulations is examined in detail. As the very first step in preparing the suspension for spray drying, zinc oxide and mannitol were suspended in acetic acid 2 %. It would therefore only be obvious if zinc acetate was formed during spray drying. But why was dissolved zinc from zinc acetate only detectable in sodium chloride solution?

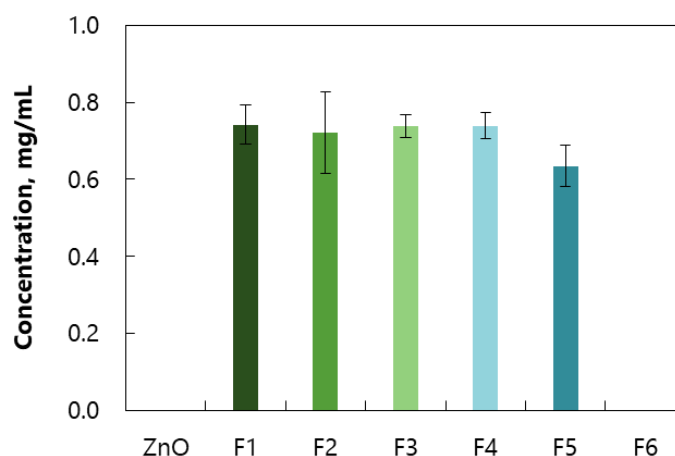


Figure 6.20. 24 h-solubility study showing saturation solubility of zinc oxide as raw material (ZnO) in comparison to all formulations in simulated nasal fluid pH 6.4 (SNF) after 24 h. F1) 100 % ZnO and 0 % mannitol; F2) 80 % ZnO and 20 % mannitol; F3) 60 % ZnO and 40 % mannitol; F4) 40 % ZnO and 60 % mannitol; F5) 20 % ZnO and 80 % mannitol; F6) 0 % ZnO and 100 % mannitol. $n = 3$, error bars = standard deviation.

Table 6.10. 24 h-solubility study showing saturation solubility of zinc oxide as raw material (ZnO) in comparison to all formulations in simulated nasal fluid pH 6.4 (SNF) after 24 h. F1) 100 % ZnO and 0 % mannitol; F2) 80 % ZnO and 20 % mannitol; F3) 60 % ZnO and 40 % mannitol; F4) 40 % ZnO and 60 % mannitol; F5) 20 % ZnO and 80 % mannitol; F6) 0 % ZnO and 100 % mannitol. $n = 3$, \pm = standard deviation.

	ZnO	F1	F2	F3	F4	F5	F6
Concentration, mg/mL	0.00 ± 0.00	0.74 ± 0.05	0.72 ± 0.11	0.74 ± 0.03	0.74 ± 0.03	0.63 ± 0.05	0.00 ± 0.00

To clarify the question whether it is really zinc acetate, measurements of formulation 1 were carried out with differential scanning calorimetry (DSC). Formulation 1 was chosen because its matrix consisted of only zinc oxide. All other formulations contained mannitol, which might interfere with the measurements. Zinc oxide and zinc acetate (dihydrate) were chosen as reference substances. The results are shown in Figure 6.21 and Table 6.11.

For zinc oxide as raw material, no event is detectable during DSC measurements in the observed temperature range as zinc oxide melts at 1975 °C. For zinc acetate, two endothermic events are detectable: a double peak at 105.20 °C and a peak at 259.41 °C [227]. Hydrate water is an example of strongly bound water and since zinc acetate is a dihydrate, a double peak between 80 and 140 °C is an indication of the elimination of the dihydrate, the dehydration. The melting point for zinc acetate dihydrate is reported to be at 237 °C [228] and for zinc acetate anhydrous at 200 °C [229]. The peak at 259.41 °C could therefore be explained by the melting of zinc acetate dihydrate. For formulation 1 three peaks are visible: a broad peak at 103.8 °C, a peak at 240.54 °C and a peak at 298.03 °C. The first two peaks are endothermic events and the latter is an exothermic one. Comparing the values of formulation 1 with the values of zinc acetate dihydrate, it is noticeable that the curves and values differ only minimally

and formulation 1 therefore contains a certain amount of zinc acetate. The small exothermic peak is probably an artefact, because no process could be found in literature at this temperature in the context with zinc acetate or other components in formulation 1.

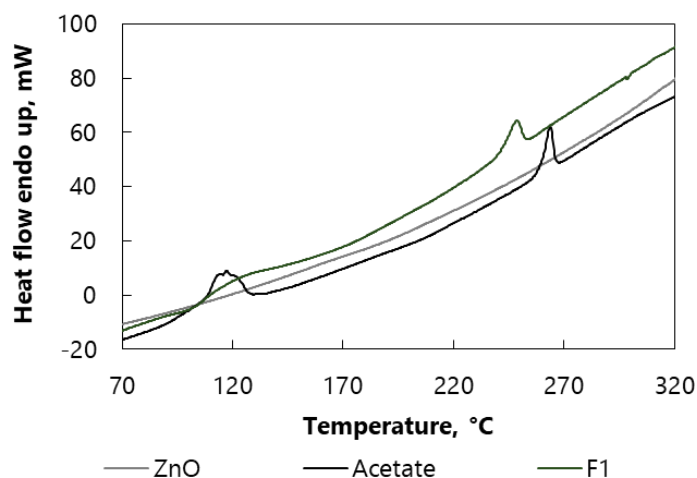


Figure 6.21. Representative chromatograms showing differential scanning calorimetry to answer the question of composition of formulation 1 after the spray drying process. In the diagram zinc oxide as raw material (ZnO), zinc acetate as raw material (Acetate) and formulation 1 (F1) is visible. F1) 100 % ZnO and 0 % mannitol. $n = 1$.

Table 6.11. Data table of the differential scanning calorimetry showing peaks of zinc oxide (ZnO), zinc acetate (Acetate) and formulation 1 (F1). F1) 100 % ZnO and 0 % mannitol.

	Weight, mg	Onset, °C	Peak, °C	Area, mJ	Delta H, J/g
ZnO	2.50	-	-	-	-
Acetate	2.37	105.20	117.28	759.65	320.53
		259.41	263.91	227.13	95.83
F1	11.00	103.08	124.27	380.47	37.59
		240.54	248.34	224.78	20.43
		298.03	298.73	-4.16	-0.38

The question remains, why is dissolved zinc from the zinc acetate formed in formulation 1 only detectable in sodium chloride solution? This could be explained by the solubility of the individual salts. With 430 g/L, zinc acetate is freely soluble in water. Zinc chloride, which could theoretically be formed in sodium chloride, is very soluble in water with 4,300 g/L [230] and is therefore not a problem. In the phosphate buffer, zinc phosphate could theoretically be formed from the dissolved zinc acetate, which is practically insoluble in water and would therefore precipitate.

In order to investigate further influences on solubility in addition to the formation of zinc acetate, the following section examines whether all formulations have a similar crystalline state. Zinc oxide as raw material serves as a reference (Figure 6.22).

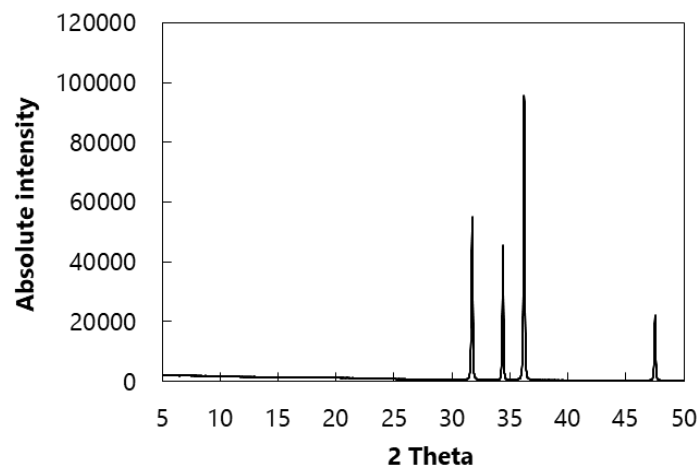


Figure 6.22. Representative diffractogram of X-ray powder diffraction showing the degree of crystallinity of zinc oxide as raw material. $n = 1$.

In Figure 6.23 representative diffractograms of the formulations are shown. The flat baseline and sharp diffraction patterns indicate that the formulations contain crystalline substances. In comparison to the reference in Figure 6.22, it can be seen that the diffraction patterns are primarily zinc oxide, which can be recognised by the four sharp peaks.

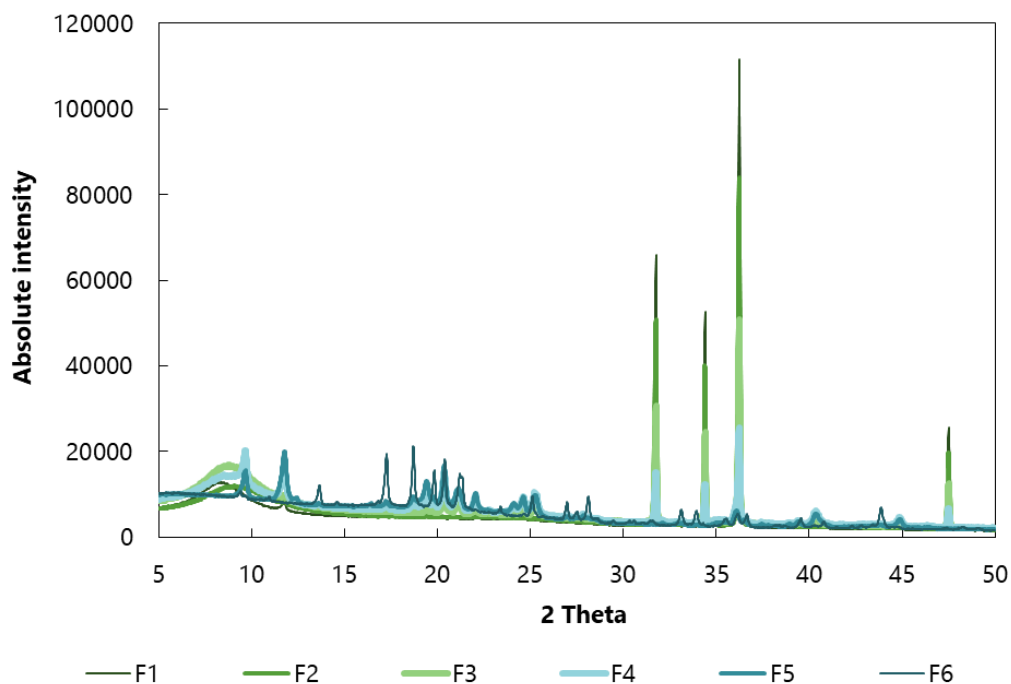


Figure 6.23. Representative diffractograms of X-ray powder diffraction showing the degree of crystallinity of all formulations. F1) 100 % ZnO and 0 % mannitol; F2) 80 % ZnO and 20 % mannitol; F3) 60 % ZnO and 40 % mannitol; F4) 40 % ZnO and 60 % mannitol; F5) 20 % ZnO and 80 % mannitol; F6) 0 % ZnO and 100 % mannitol. $n = 1$.

The decrease in absolute intensity of the peaks from formulations 1 to 4 shows the decreasing amount of zinc oxide in the formulations. The broad peak at the beginning of the diffractograms indicates a certain amount of amorphous product. As this is particularly noticeable in formulations with a higher zinc oxide content, formulations 1 to 4, this indicates the formation of amorphous components from zinc oxide. In combination with representative diffractograms of zinc acetate [231], it could be assumed that there is again a correlation with the suspension agent used in spray drying and therefore with the zinc acetate produced. In formulation 5, the concentration of zinc oxide is too low and formulation 6 does not contain zinc oxide. Therefore, they do not show any of the corresponding peaks.

In addition to the characteristic peaks of zinc oxide, further peaks can be identified, especially in the formulations with decreasing amount of zinc oxide. Mannitol was not measured as a reference because sufficient data on the polymorphism of mannitol is already available. A comparison with the diagrams of the different forms of mannitol in the study of Fronczek and coworkers [232] and the increase in the absolute intensity of the peaks with increasing amount of mannitol clearly indicates that these peaks are caused by mannitol. A closer look at the diffractograms revealed that the spray dried mannitol was the β -modification which is the thermodynamically most stable one.

Coming back to the 24-h-solubility study, not only the solubility but also the change of the pH value of the solutions after adding the formulations was investigated. The pH value is plotted on the right-hand y-axis of Figure 6.19. The black bars are plotted as the pH value before the start of the experiment, and the black (ZnO) and dark green (F1) dots for the pH values after 24 h. The corresponding pH values are listed in Table 11.2.

In the phosphate buffers zinc oxide and formulation 1 lead to similar pH values. The shift of the pH value after 24 h shows an increase with different gradients, depending on the initial pH value. In the sodium chloride solutions, both zinc oxide and formulation 1 reach a plateau of the pH value after 24 h. For zinc oxide, this plateau is approximately pH 7.6, independent of the initial value, and for formulation 1 it is pH 6.9. Only at a pH value of pH 1.2 a lower pH value (ZnO = 6.43 ± 0.11 , F1 = 6.08 ± 0.09) was measured after 24 h. In order to analyse the influence of the different amounts of zinc oxide in the formulations on the pH, the pH values after 24 h of formulations 2 to 6 were also tested. In Figure 6.24 pH values are shown as a function of the solutions with different pH values. The starting pH is shown in black bars and the individual formulations in dots. Again, a similar behaviour of all formulations in SNF and the sodium chloride solutions can be seen.

For the phosphate buffers, the pH value increases in relation to the initial pH value. After combining the individual dots of the respective formulation, a higher gradient of the lower pH values (pH 1.2 and pH 2.5) and the higher pH values (pH 5.5, pH 6.4 and pH 7.4) is visible. For the pH values in the middle pH 2.5, pH 4.0 and pH 5.5 the gradient is rather flat. However, the gradient is similar for all formulations.

It can be seen that the zinc oxide content has an influence on the pH change. The higher the zinc oxide percentage, the stronger the pH shift. The strongest pH increase shows zinc oxide as raw material, followed by formulations 1 and 2. Formulation 3 also leads to an increase of the pH value in the lower pH ranges up to pH 4.0. For pH values above pH 5.5 the pH values after 24 h are almost identical to the original pH values. For formulations 4 and 5, i.e., the formulations with a higher mannitol amount, a pH increase can also be seen for the three lower pH values. For the three higher pH values, however, the pH value decreases after 24 h. In formulation 6, after 24 h no difference can be seen from the initial pH value.

For the sodium chloride solutions, a clearly different picture is obtained. Regardless of the starting pH except for pH 1.2, the pH value after 24 h of formulations 1 to 5 form a plateau of approximately pH 7 and of zinc oxide of approximately pH 7.5. As already mentioned, pH 1.2 is an exception, where a dependence of the zinc oxide concentration can be seen. While zinc oxide and formulation 1 with a matrix of 100 % zinc oxide have a strong increase in pH, the pH of the other formulations does not increase as much. The increase gets smaller with lower zinc oxide percentage. After 24 h formulations 5 and 6 have a similar pH to the starting pH. Formulation 6 shows a special characteristic. While the pH values pH 2.5 and pH 4.0 show an increase in pH parallel to the starting pH, a plateau below the starting pH of the three higher pH values is reached of approximately pH 4.5.

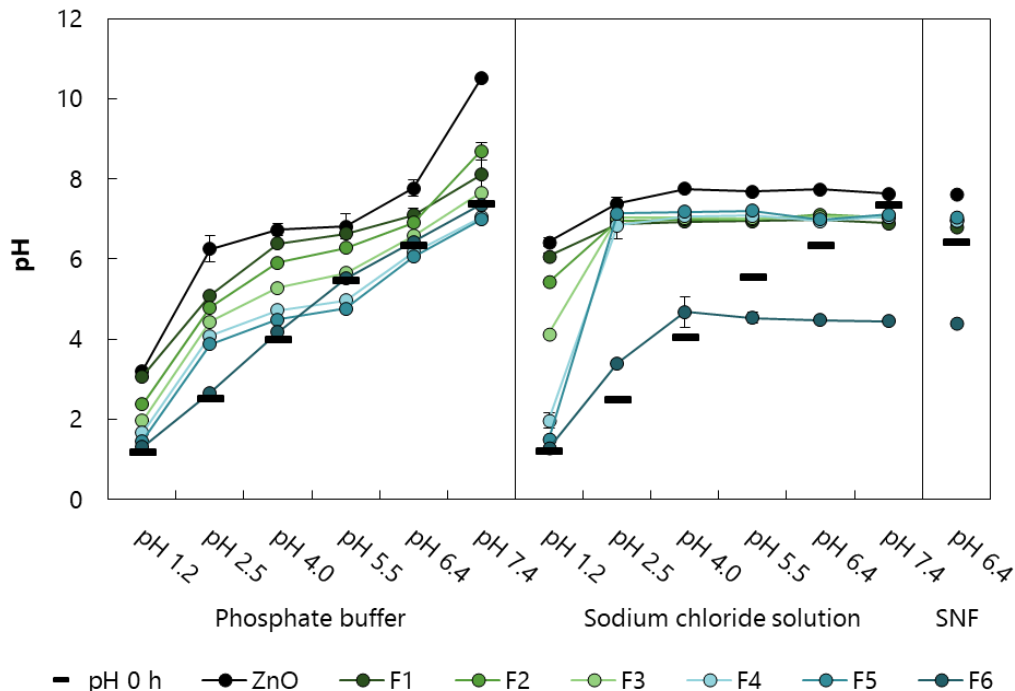


Figure 6.24. 24 h-pH study showing starting pH (pH 0 h, black bars) and pH change of different solutions/suspensions after 24 h with zinc oxide as raw material (ZnO) in comparison to all formulations (coloured dots and lines). F1) 100 % ZnO and 0 % mannitol; F2) 80 % ZnO and 20 % mannitol; F3) 60 % ZnO and 40 % mannitol; F4) 40 % ZnO and 60 % mannitol; F5) 20 % ZnO and 80 % mannitol; F6) 0 % ZnO and 100 % mannitol. $n = 3$, error bars = standard deviation.

The behaviour of the formulations in SNF is similar to the behaviour in the sodium chloride solution at the corresponding pH value.

A connection with the production and composition of the formulation is evident. The starting materials were dissolved or suspended in acetic acid 2 %. After spray drying, the ions of the acetic acid are still present in the formulation. Zinc oxide in the formulation contributes to an increase of the pH value independent of the starting pH of the sodium chloride solution. Formulation 6 does not contain zinc oxide. This allows the ions of acetic acid to set a corresponding pH value close to the pK_a value of acetic acid ($pK_a = 4.76$).

Even if the pH change in the phosphate buffer is somewhat attenuated or buffered, the increase by zinc oxide as well as the change by the ions of acetic acid is evident.

6.2.1.4 Mucus rheology

Not only the characteristics of the formulation, but also the properties of the nose and their effect on nasal formulations must be considered when developing nasal formulations. An essential aspect is the mucosal clearance. The ciliary beating ensures the replacement of the nasal mucus on average every 30 min [233]. To increase the retention time, mucoadhesive or viscosity increasing substances can be used. Due to the longer time of the formulation in the nose, the interaction time of the formulation with the mucosa is increased and thus fosters the possibility of the antigens being absorbed by the nasal mucosa.

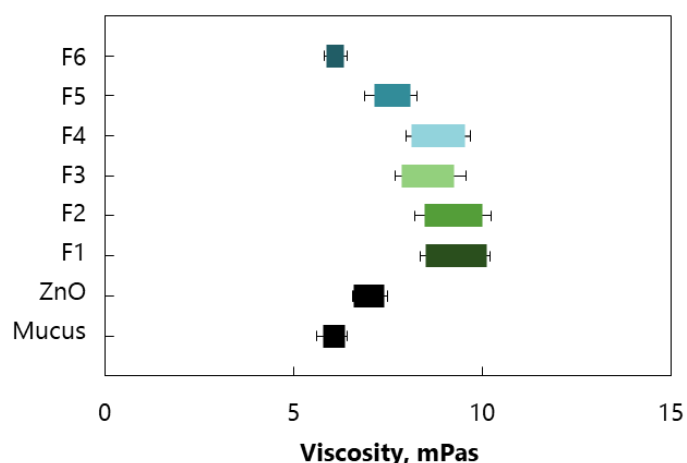


Figure 6.25. Rheology studies of simulated nasal mucus without (Mucus, black bar) and with added zinc oxide as raw material (ZnO, black bar) or one formulation (F1 – F6, coloured bars). Viscosity ranges at shear rates from $60 - 100 \text{ s}^{-1}$ are shown. F1) 100 % ZnO and 0 % mannitol; F2) 80 % ZnO and 20 % mannitol; F3) 60 % ZnO and 40 % mannitol; F4) 40 % ZnO and 60 % mannitol; F5) 20 % ZnO and 80 % mannitol; F6) 0 % ZnO and 100 % mannitol. $n = 3$, error bars = standard deviation.

Simulated nasal mucus was used as a model in these experiments. To investigate the influence of the different formulations and therefore, e.g., the influence of the different zinc oxide concentrations on rheology, first the viscosity of the pure artificial mucus at 32 °C was determined. Afterwards, the mucus

was mixed with the formulations and after 30 s resting time, the viscosity at 32 °C was measured again. The results of the measurements are given in Figure 6.25 and Table 6.12.

The viscosity of pure mucus at shear rates from 60 s⁻¹ to 100 s⁻¹ ranges from 5.78 mPas ± 0.17 mPas to 6.36 mPas ± 0.05 mPas. Formulation 6 without zinc oxide shows a similar viscosity from 5.87 mPas ± 0.07 mPas to 6.32 mPas ± 0.09 mPas. Zinc oxide as a raw material increases the viscosity of the mucus to 6.58 mPas ± 0.01 mPas (min) and 7.40 mPas ± 0.09 mPas (max).

The viscosity of the mucus in combination with formulations 1 to 5 is higher than the viscosity of pure mucus and mucus in combination with formulation 6 and zinc oxide as raw material. There is no significant difference between formulations 1 to 5. While formulation 5 shows a slightly lower viscosity increase, there is almost no difference between formulations 1 to 4. There is no direct correlation between the increase of the viscosity and the different concentrations of the components of the formulations, e.g., the different zinc oxide concentrations. In a further study (shown in chapter 6.2.2.4) to investigate pulmonary formulations, different starting materials were examined for their viscosity increasing properties. Water with a viscosity at shear rates from 60 s⁻¹ to 100 s⁻¹ of 1.29 mPas ± 0.11 mPas to 1.51 mPas ± 0.07 mPas was used as reference material and suspending agent. Mannitol (1.32 mPas ± 0.03 mPas to 1.50 mPas ± 0.04 mPas) and ovalbumin (1.32 mPas ± 0.08 mPas to 1.49 mPas ± 0.04 mPas), in the corresponding concentration in the formulation, showed no increase in viscosity, and the addition of zinc oxide slightly increased the viscosity (1.75 mPas ± 0.16 mPas to 2.02 mPas ± 0.16 mPas). The addition of hyaluronic acid caused an increase in viscosity to a range of 9.75 mPas ± 0.29 mPas to 12.23 mPas ± 0.35 mPas.

Table 6.12. Rheology studies of simulated nasal mucus without and with added zinc oxide as raw material or one formulation (F1 – F6, coloured bars). Viscosity ranges at shear rates from 60 – 100 s⁻¹ are shown. F1) 100 % ZnO and 0 % mannitol; F2) 80 % ZnO and 20 % mannitol; F3) 60 % ZnO and 40 % mannitol; F4) 40 % ZnO and 60 % mannitol; F5) 20 % ZnO and 80 % mannitol; F6) 0 % ZnO and 100 % mannitol. n = 3, ± = standard deviation.

	Mucus	ZnO	F1	F2	F3	F4	F5	F6
Viscosity (min), mPas	5.78 ± 0.17	6.58 ± 0.01	8.50 ± 0.14	8.48 ± 0.28	7.88 ± 0.18	8.13 ± 0.15	7.14 ± 0.25	5.87 ± 0.07
Viscosity (max), mPas	6.36 ± 0.05	7.40 ± 0.09	10.11 ± 0.11	10.01 ± 0.24	9.26 ± 0.30	9.54 ± 0.15	8.08 ± 0.20	6.32 ± 0.09

A similar picture can be observed in measurements with simulated nasal mucus. Even if the addition of zinc oxide contributes to an increase in the viscosity of the mucus, the increase in viscosity of mucus in combination with the formulations can be explained mainly by hyaluronic acid. Hyaluronic acid is biodegradable and biocompatible, has a high molecular mass and special viscoelastic properties. It is

used in numerous areas of medicine and pharmacy, e.g., in the treatment of arthritis, ophthalmic surgery, drug delivery and tissue engineering [234]. In formulation development within this work, it is mainly used as an adhesive between individual nanoparticles to produce a microparticle. Furthermore, it serves as mucoadhesive excipient and penetration enhancer. The influence of the formulations on rheological properties are of great interest in all formulations for nasal application. Since different pH values exist in the human body, the pH dependent viscosity change of hyaluronic acid has already been investigated in many ways. Maleki and coworkers [234] investigated among other things the effect of the pH value on the rheological properties of hyaluronic acid in different diluted aqueous solutions. It was found that the effect of the pH value on the viscosity is related to intramolecular rupture of the polymer chain at low and high pH values. That means at a very low or very high pH value, irreversible degradation of the polymer takes place, which leads to a reduction of viscosity. If the pH value measurements of the 24-h-solubility study are taken into account, it is noticeable that after 24 h in simulated nasal fluid, a constant pH value of $\text{pH } 4.40 \pm 0.03$ was reached with formulation 6. As mentioned before, hyaluronic acid is known to undergo acid hydrolysis in acidic media, this would explain the lack of viscosity increase of formulation 6 [235]. Formulation 6 consists mainly of mannitol, which is also discussed in many papers connected with hyaluronic acid. Mannitol has a long-established safety profile and is among other things used as an antioxidant and free radical scavenger. With these properties, it protects hyaluronic acid against degradation by free radicals. However, even the addition of high concentrations of mannitol does not protect hyaluronic acid against the low pH resulting by adding the formulations to the simulated nasal fluid. Thus, hyaluronic acid does not increase the viscosity of mucus when adding formulation 6 [236].

6.2.1.5 Cytotoxicity

While mannitol did not affect the rheology in-vitro, it can irritate the mucosa in-vivo. Generally, water-soluble components start dissolving in the nasal mucus. This may result in a concentrated solution of high osmolarity and can also cause irritancy and a running nose because of increased water ingress to dilute the substance. The influence of the formulations and zinc oxide on nasal cells was evaluated in in-vitro cell experiments. Specifically, the toxicity on nasal epithelial cells (RPMI2650) after contact with the formulations was studied.

In Figure 6.26 and Table 6.13, the LD50 of the formulations are shown. The LD50 provides information about the toxicity of substances and indicates the dose, where 50 % of the cells die after incubation. It should be mentioned that after incubation of the cells with the formulations, the higher concentrated formulations could not be completely removed from the cells because zinc oxide had very adhesive properties. For this reason, the absorption, and thus apparently the viability, increased again with increasing concentrations. This would imply that the viability increased with increasing concentrations.

However, visual inspection of the cells after they came into contact with the formulations showed a significant decrease in viability. For this reason, the higher concentrations are not shown in Figure 6.27.

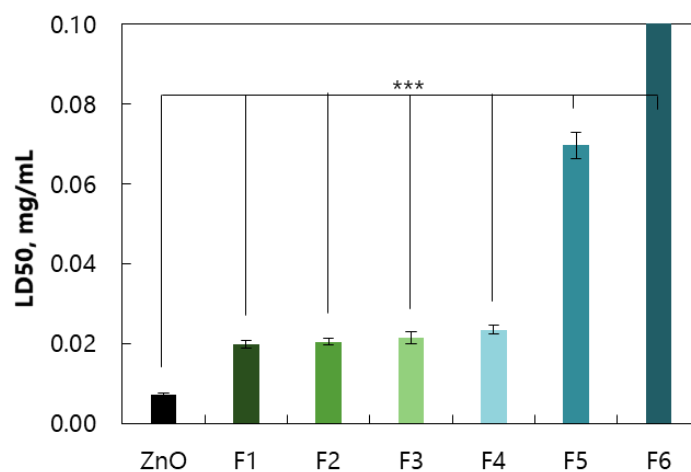


Figure 6.26. LD50 of zinc oxide as raw material (ZnO) in comparison to all formulations in a RPMI2650 model. F1) 100 % ZnO and 0 % mannitol; F2) 80 % ZnO and 20 % mannitol; F3) 60 % ZnO and 40 % mannitol; F4) 40 % ZnO and 60 % mannitol; F5) 20 % ZnO and 80 % mannitol; F6) 0 % ZnO and 100 % mannitol. $n = 3$, error bars = standard deviation, p -value < 0.001 = highly significant difference (***).

With an LD50 of 0.007 mg/mL \pm 0.000 mg/mL, zinc oxide as raw material shows the highest toxicity in Figure 6.26. With a p -value < 0.0001 , the toxicity of formulations 1 (0.020 mg/mL \pm 0.001 mg/mL), 2 (0.021 mg/mL \pm 0.001 mg/mL), 3 (0.021 mg/mL \pm 0.001 mg/mL) and 4 (0.023 mg/mL \pm 0.001 mg/mL) is highly significantly lower than the toxicity of zinc oxide. Formulations 5 (0.070 mg/mL \pm 0.003 mg/mL) with a p -value of 0.0004 and 6 (3.200 mg/mL \pm 0.178 mg/mL) with a p -value of 0.0005 are also highly significantly less toxic than zinc oxide.

Table 6.13. LD50 of zinc oxide as raw material (ZnO) in comparison to all formulations in a RPMI2650 model. F1) 100 % ZnO and 0 % mannitol; F2) 80 % ZnO and 20 % mannitol; F3) 60 % ZnO and 40 % mannitol; F4) 40 % ZnO and 60 % mannitol; F5) 20 % ZnO and 80 % mannitol; F6) 0 % ZnO and 100 % mannitol. $n = 3$, \pm = standard deviation.

	ZnO	F1	F2	F3	F4	F5	F6
LD50, mg/mL	0.007 \pm 0.000	0.020 \pm 0.001	0.021 \pm 0.001	0.021 \pm 0.001	0.023 \pm 0.001	0.070 \pm 0.003	3.200 \pm 0.178

The LD50 increases from formulation 1 to 6 which means that the toxicity decreases. It is hence reasonable to assume that there is a correlation between toxicity and zinc oxide concentration.

For this reason, in Figure 6.27 the viability of all formulations is considered as a function of the zinc oxide concentration. If the toxicity depends on the zinc oxide concentration, the resulting curves would overlap and be almost identical. As formulation 6 does not contain zinc oxide, it is not considered in Figure 6.27 and Table 11.3. All curves show a similar trend. While the viability at a zinc oxide concentration of less

than 0.005 mg/mL is almost 100 %, it decreases in the range of 0.005 mg/mL to 0.05 mg/mL to finally almost 0 % viability at concentrations higher than 0.05 mg/mL. Although the range of the LD50 value, i.e., 50 % viability, is between 0.005 mg/mL and 0.05 mg/mL for all formulations, the curves are not identical. However, as in-vitro cell experiments are living systems, variability can easily occur.

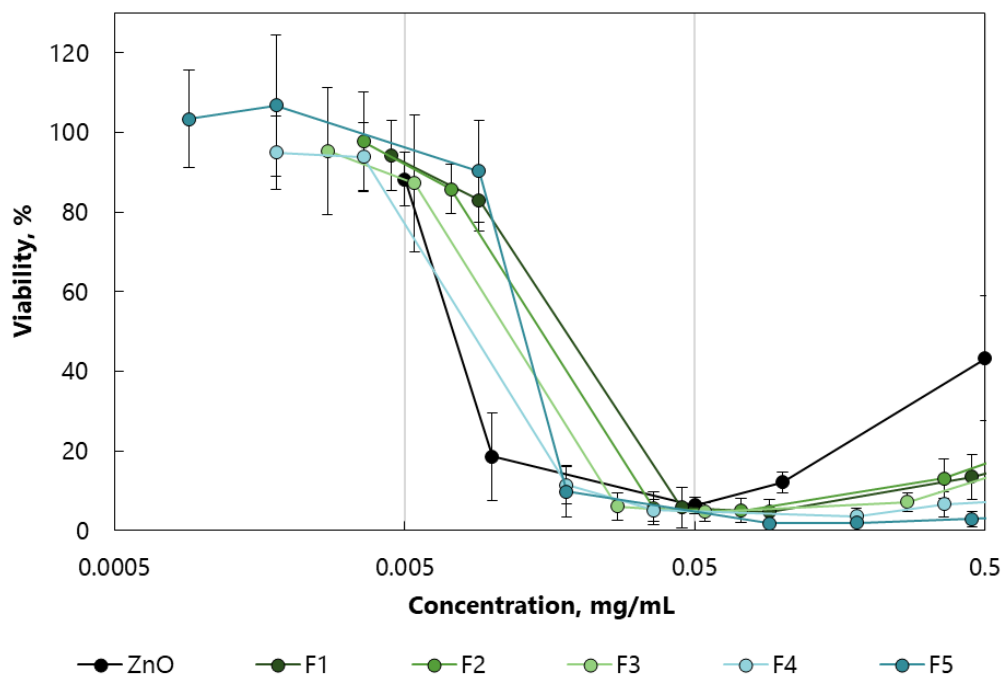


Figure 6.27. Viability as a function of the zinc oxide concentration in all formulations, to identify whether toxicity is dependent on zinc oxide concentrations in the formulation. Zinc oxide as raw material (ZnO) is used as a reference. F1) 100 % ZnO and 0 % mannitol; F2) 80 % ZnO and 20 % mannitol; F3) 60 % ZnO and 40 % mannitol; F4) 40 % ZnO and 60 % mannitol; F5) 20 % ZnO and 80 % mannitol. $n = 3$, error bars = standard deviation.

6.2.1.6 Loading

The main mission of a formulation for vaccination is the effective delivery of the antigen along with the adjuvant. In the current work, proteins are considered as safe and effective antigens. For that reason, protein loading plays a crucial role. The loading was determined after spray drying via UV spectroscopy at 205 nm.

Protein loading in spray dried particles was dictated by the amount of protein in the feed solution of the process, but might further be influenced by the process parameters and reactions via the spray drying process. Figure 6.28 shows the found concentration of ovalbumin in all formulations after the spray drying process compared to the added concentration of ovalbumin. 0.1 mg ovalbumin per mg formulation was added to all formulations, but only 50 % of the used ovalbumin is recovered after spray drying (Table 6.14).

There is no significant difference between individual formulations. The detection of the ovalbumin was based on the absorption of the peptide bond at 205 nm. Since numerous interference factors at this wavelength could falsify the result, a blank was previously determined with the buffer and the calibration

curve was established with the buffer. To ensure that the ovalbumin had not already been lost before spray drying, the suspension for spray drying was also assessed. The measured concentrations match the added concentrations.

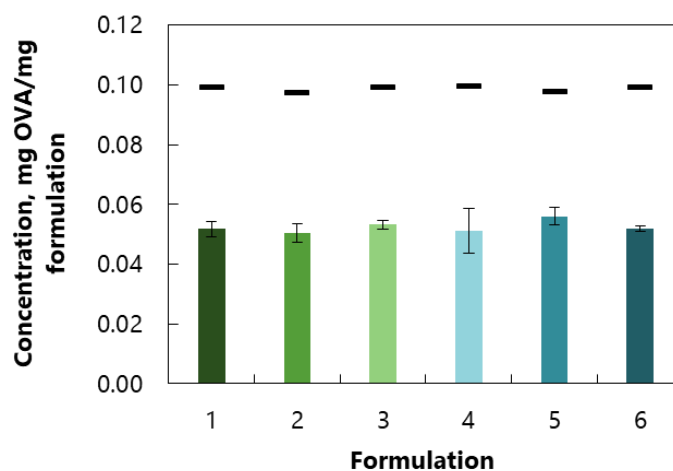


Figure 6.28. Concentration of ovalbumin (coloured bars) in all formulations after the spray drying process in comparison to the used amount of ovalbumin (black bars). 1) 100 % ZnO and 0 % mannitol; 2) 80 % ZnO and 20 % mannitol; 3) 60 % ZnO and 40 % mannitol; 4) 40 % ZnO and 60 % mannitol; 5) 20 % ZnO and 80 % mannitol; 6) 0 % ZnO and 100 % mannitol. $n = 3$, error bars = standard deviation.

Table 6.14. Concentration of ovalbumin in all formulations after the spray drying process in comparison to the starting concentration of ovalbumin. F1) 100 % ZnO and 0 % mannitol; F2) 80 % ZnO and 20 % mannitol; F3) 60 % ZnO and 40 % mannitol; F4) 40 % ZnO and 60 % mannitol; F5) 20 % ZnO and 80 % mannitol; F6) 0 % ZnO and 100 % mannitol. $n = 3$, \pm = standard deviation.

	F1	F2	F3	F4	F5	F6
Starting concentration, mg OVA/mg formulation	0.099	0.097	0.099	0.100	0.098	0.099
Concentration, mg OVA/mg formulation	0.052 ± 0.002	0.050 ± 0.003	0.053 ± 0.002	0.051 ± 0.007	0.056 ± 0.003	0.052 ± 0.001

A phosphate buffer instead of water was used to dissolve or suspend the samples to guarantee that no zinc oxide or zinc acetate is in solution, since zinc acetate and zinc oxide did not dissolve in phosphate buffers with higher pH values ($\text{pH} > 2.5$) as shown in the 24-h-solubility studies in chapter 6.2.1.3, and therefore did not disturb the measurements. In principle, interference of the measurements by zinc oxide or mannitol can be excluded, since there is no significant difference depending on the different concentrations in the formulations. Nevertheless, the question remains why 50 % of the ovalbumin has been lost. Too high temperatures, acids or alkalis can denature proteins. When a protein is denatured,

its tertiary structure changes, and sometimes the secondary structure is also affected. However, the primary structure is usually retained, i.e., the sequence of amino acids and thus also the peptide bonds are retained and can be measured at 205 nm. During the spray drying process water was evaporating, acetic acid was getting more concentrated and remained in the formulation as acetate and proton. As mentioned before, ovalbumin concentrations in the suspension prior to the spray drying corresponded the added concentration. It could thus be possible, that denatured material became insoluble and thus was removed together with the other undissolved components during sample preparation prior to the measurements.

In Figure 6.29, representative chromatograms of size exclusion chromatography (graphs) and representative pictures of SDS-PAGE of ovalbumin as raw material in comparison to formulations 1 and 6 (left) are shown. The horizontal dotted lines above the peaks show the individual molar mass of the molecules that contribute to the formation of the peak. The flatter the slope of this line, the more homogeneous is the distribution of the molar masses. Ovalbumin as a raw material was used as a reference substance in the SEC measurements and in the SDS-PAGE to see if there is a difference between the starting material and the ovalbumin in the formulation. As reference for the analysis of the SDS-PAGE a marker with the given molecular weights was used additionally (left, white font).

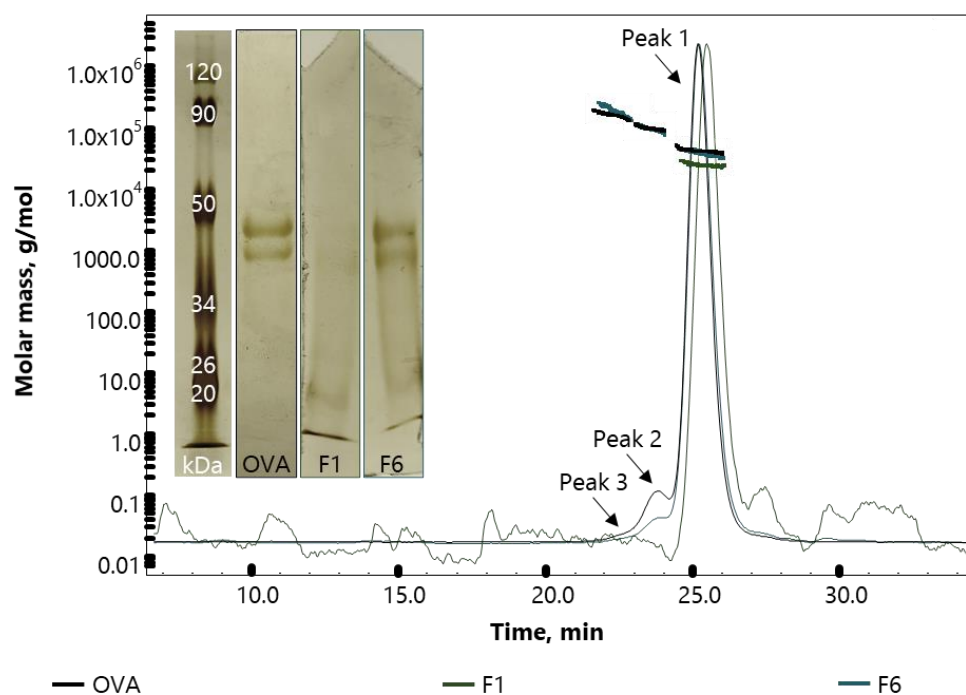


Figure 6.29. Representative chromatograms of size exclusion chromatography and representative pictures of SDS-PAGE of ovalbumin (OVA) as raw material in comparison to formulation 1 (F1) and formulation 6 (F6). F1) 100 % ZnO and 0 % mannitol; F6) 0 % ZnO and 100 % mannitol. $n = 1$.

In Table 6.15 the individual peaks of the SEC are analysed from right to left, with peak 1 representing the monomer, peak 2 the dimer and peak 3 the trimer. All peaks were used to calculate the total molecular weight.

In Figure 6.29, there is a large peak (peak 1) for ovalbumin (black), a smaller peak (peak 2) in front of it and a shoulder (peak 3) in front of peak 2. The ovalbumin used as starting material consists of monomers, dimers and trimers, whereas the distribution of the molar masses is homogeneous. With a mass recovery of 67.9 %, the monomer (39.8 kDa) makes up the largest part, followed by the dimer (83.1 kDa) with 5.8 % and finally the trimer (127.5 kDa) with 1.0 %. With a total molecular weight of 44.4 kDa 74.8 % of the used amount could be detected with SEC. This brings up the question why only about 75 % of the ovalbumin used could be recovered? For this purpose, the ovalbumin as well as the settings on the instrument and the experiment must be considered. Ovalbumin with a purity of at least 98 % was used for the experiments. As described in the SDS-PAGE results below, the used ovalbumin batch contained two different glycosylated forms of ovalbumin. For the determination of the molecular mass, the refractive index, among others, was needed. The refractive index is strongly discussed in the literature, as it can be influenced by various factors [237]. Besides the glycosylation and folding of a protein, pH value and matrix composition are also of interest. All these factors lead to changes in the refractive index and thus to inaccuracies in the results. Furthermore, the samples were first weighed, then the formulations were suspended and ovalbumin was dissolved, filtered and finally injected with a syringe. Since all these steps were performed manually, inaccuracies could have occurred both in the equipment and in the procedure. The combination of all these factors could explain the recovery of about 75 % of the ovalbumin used.

Formulation 1 with the highest zinc oxide concentration and no mannitol and formulation 6 with the highest mannitol concentration and no zinc oxide were used as representative samples.

Formulation 6 (blue) shows a similar curve to ovalbumin, i.e., a large peak (peak 1), a larger shoulder (peak 2) and a smaller shoulder (peak 3) and thus consists of monomers, dimers and trimers. The slope of the dotted line of peak 3 is higher compared to the dotted line of peak 3 of ovalbumin. The distribution is therefore somewhat more inhomogeneous in the direction of higher molar masses. This indicates the formation of multimers. For peak 1 and peak 2 there is no visible difference to ovalbumin. With a mass recovery of 73.1 %, the monomer (36.3 kDa) makes up the largest part, followed by the dimer (78.3 kDa) with 2.8 % and finally the trimer (138.9 kDa) with 0.9 %. With a total molecular weight of 39.1 kDa 76.8 % of the used amount could be detected. Since the loading of the formulations with 50 % of the used ovalbumin was already taken into account when weighing the formulation, the same amount is detected in relation to ovalbumin as raw material.

The measurement of formulation 1 was very difficult. The formulations were suspended, filtered and then injected into the system. While this was not a problem with ovalbumin and formulation 6, formulation 1 precipitated at the start of the stationary phase. Therefore, the ovalbumin in formulation 1 was no longer dissolved and could not be measured. This can also be seen in Figure 6.29 and Table 6.15. Peak 1, which is the largest peak, is shifted towards higher retention times and the dotted line is also

shifted towards lower molar masses. The baseline shows a strong noise. With a molecular weight of 23.2 kDa and a mass recovery of 8.5 % for peak 1, and since it is the only peak for all peaks, formulation 1 has only one-ninth of the recovery and half of the molecular weight of ovalbumin as raw material.

Table 6.15. Representative data of size exclusion chromatography of ovalbumin (OVA) as raw material in comparison to formulation 1 (F1) and formulation 6 (F6). F1) 100 % ZnO and 0 % mannitol; F6) 0 % ZnO and 100 % mannitol. n = 1.

	Peak 1		Peak 2		Peak 3		All peaks	
	Molecular weight, kDa	Mass recovery, %	Molecular weight, kDa	Mass recovery, %	Molecular weight, kDa	Mass recovery, %	Molecular weight, kDa	Mass recovery, %
OVA	39.8	67.9	83.1	5.8	127.5	1.0	44.4	74.8
F1	23.2	8.5	n/a	n/a	n/a	n/a	23.2	8.5
F6	36.3	73.1	78.2	2.8	138.9	0.9	39.1	76.8

Similar difficulties with formulation 1 can be observed in SDS-PAGE. A doublet of ovalbumin as raw material is detected between 34 kDa and 50 kDa [238]. Two different glycosylated forms of ovalbumin within the purified protein preparation might cause the presence of a doublet. Formulation 6 also shows a doublet between 34 kDa and 50 kDa and a weaker band at about 20 kDa. In addition, a veil extends from the stronger bands to the weaker band. This could be sign of a disturbing matrix. Formulation 1 shows a weak band at about 20 kDa, similar to the measurements of formulation 1 with the SEC, and an even weaker doublet between 34 kDa and 50 kDa. Ovalbumin might already be denatured before the measurement. By centrifugation, the denatured ovalbumin would be separated. With the small amounts of ovalbumin in the samples for SDS-PAGE, a pellet of this size would not have been noticed at all.

If the data from SEC and SDS-PAGE are combined, it could be assumed that ovalbumin was denatured due to the acetic acid 2 % and gradually loses its functionality. However, as this was included in both formulation 1 and formulation 6, there must be another factor affecting the stability of ovalbumin. In this case the composition of the matrix must be considered. While the matrix in formulation 1 consists of 100 % zinc oxide, the matrix in formulation 6 consists of 100 % mannitol. Even if the addition of zinc oxide led to an increase in pH value and thus to a less acidic environment, the stabilising effect of mannitol on proteins during spray drying was probably more pronounced. The ovalbumin in formulation 6 was thus stabilised and remained largely intact, while the ovalbumin in formulation 1 is denatured by the combination of acetic acid and spray drying.

6.2.1.7 Summary and conclusion

The zinc oxide used showed a needle-shaped morphology with particles in the nanometre range, resulting in a large surface area and a tendency to form undefined agglomerates.

The project aimed to use zinc oxide as an alternative adjuvant. By spray drying, it was possible to produce particles with a defined particle size $> 10 \mu\text{m}$, which is usually the particle size required for nasal application. Zinc oxide was spray dried together with hyaluronic acid, ovalbumin and mannitol in acetic acid (2 %). Six different formulations were prepared with different concentrations of zinc oxide and mannitol. The matrix of formulation 1 consisted of 100 % zinc oxide and the matrix of formulation 6 of 100 % mannitol. The concentrations of hyaluronic acid and ovalbumin remained constant.

All formulations resulted in a white powder after spray drying, with differences in morphology. Formulations 1 and 6 had the typical uniform spherical shape, with formulation 1 being slightly indented and formulation 6 having a smooth surface. Formulations 2 to 5 were all clearly wrinkled particles. The difference in composition was not only visible by the decreasing proportion of zinc oxide particles present from formulation 1 (100 % zinc oxide) to formulation 6 (0 % zinc oxide), but also measurable using EDS. The produced white dry powders had almost no visible differences in particle size. Measurements of the particle size distribution with the RODOS module showed an x50 smaller than $10 \mu\text{m}$ for formulations 1, 2, 5 and 6 and an x50 higher than $10 \mu\text{m}$ for formulations 3 and 4. When measuring the particle size distribution with the SPRAYER module in combination with the UDS powder device, formulation 6 had almost 50 % of particles larger than $10 \mu\text{m}$, formulations 1, 2 and 5 had over 50 % of particles larger than $10 \mu\text{m}$ and formulations 3 and 4 had over 90 % of particles larger than $10 \mu\text{m}$.

An NGI was used in combination with the nasal expansion chamber and the UDS powder device for aerodynamic characterisation. With more than 80 %, formulations 3, 4 and 5 showed the highest deposition percentage in the nasal expansion chamber. For formulations 1, 2 and 6, less than 80 % of the delivered dose was deposited in the nasal expansion chamber.

To stimulate an immune response in the respiratory tract, an antigen has to be taken up in a particulate form by antigen presenting cells. For this reason, the amount of dissolved zinc oxide in different media was investigated. Sodium chloride solutions and phosphate buffers with different pH levels were prepared to mimic relevant pH conditions in the human body. In addition, simulated nasal fluid was tested, which took account of the salt and pH conditions in the nose. In addition to the solubility, the influence of zinc oxide (dissolved or undissolved) on the pH values after 24 h was also investigated. Formulation 1, as representative sample, was slightly soluble in pH 1.2 and very slightly soluble in pH 2.5, both in sodium chloride solution and in phosphate buffer. At pH values above pH 2.5, formulation 1 was practically insoluble in phosphate buffer, but very slightly soluble in sodium chloride. In simulated nasal

fluid, formulations 1 to 5 were very slightly soluble. The difference in solubility in phosphate buffers compared to sodium chloride solutions and simulated nasal fluid was due to the formation of zinc acetate during spray drying. The pH value after 24 h also showed a difference between phosphate buffer and both the sodium chloride solutions and the simulated nasal fluid. After 24 h, the pH value increased in relation to the initial pH value in the phosphate buffer, while the zinc oxide content had an influence on the pH change: the higher the zinc oxide percentage, the stronger the pH shift. In both the sodium chloride solutions and simulated nasal fluid, the pH value reached a plateau of approximately pH 7 after 24 h for the formulations 1 to 5 and of approximately pH 4.5 for formulation 6.

Looking at the physiology of the nose, mucosal clearance plays an important role. The ciliary beating ensures the replacement of the nasal mucus every 30 min. The retention time increases with increasing viscosity of the mucus. Simulated nasal mucus was used for the tests. Formulations 1 to 5 led to an increase in the viscosity of the mucus compared to pure mucus, whereby the increase in viscosity was mainly due to the hyaluronic acid. At low and high pH values, as for example in formulation 6, there was an intramolecular rupture of the polymer chains and thus a loss of the viscosity increasing effect. While no dependence on the zinc oxide concentration could be seen in the viscosity experiments, the concentration played an important role in the toxicity tests of the formulations. After 24 h incubation of RPMI2650 with the formulations, the LD50 increased from formulation 1 to formulation 6, i.e., the toxicity decreased from formulation 1 to formulation 6.

The goal of the spray dried formulation was to increase the protein loading. The loading of the particles after spray drying was investigated. Only 50 % of the used ovalbumin was recovered after spray drying. SEC and SDS-PAGE were used to investigate the stability of the ovalbumin. Ovalbumin was denatured due to acetic acid (2 %) and gradually loses functionality. While in formulation 6 the high mannitol concentrations had a stabilising effect on the ovalbumin and thus it remained largely intact, the ovalbumin in formulation 1 was mostly denatured. The combination of acetic acid (2 %) and spray drying caused denaturation of ovalbumin.

In conclusion, the increase in protein loading (from 0.013 mg ovalbumin/mg zinc oxide as raw material to about 0.05 mg ovalbumin/mg spray dried zinc oxide for nasal application) with ovalbumin was generally successful. However, only 50 % of the ovalbumin used was recovered after spray drying and the use of acetic acid (2 %) as a medium for dissolving or suspending all materials prior to the spray drying caused repeated difficulties during characterisation. To overcome these problems and to achieve a higher loading of the particles, for further investigations the formulations were spray dried using water as medium. Using the same concentrations as for the production of the nasal particles would lead to clogging of the two-fluid nozzle during spray drying of an aqueous suspension. By using lower concentrations, pulmonary formulations were prepared, which had the great advantage that they could subsequently be used in in-vivo experiments to investigate pulmonary immunisation in mice.

6.2.2 Spray dried zinc oxide for pulmonary application

By spray drying, it is not only possible to produce particles for nasal application, but also for pulmonary administration with a defined particle size < 5 µm. Zinc oxide as an alternative adjuvant was spray dried together with hyaluronic acid, ovalbumin and mannitol. The composition of the six pulmonary formulations was the same as the composition of the six nasal formulations, but with water as a liquid medium for spray drying instead of acetic acid (2 %) as mentioned in chapter 5.1. However, to obtain smaller particles, a lower concentration of the components in the suspension to be dried was used, since in spray drying, among other things, the concentration of the feed liquid influences the particle size [189].

The six spray dried formulations are all dry white powders independent of their composition. They were physiochemically characterised, i.e., morphology, particle size distribution, aerodynamic behaviour, 24-h-solubility and dissolution. Moreover, various protein characterisation methods were evaluated and the behaviour of the formulations in in-vitro cell experiments were assessed.

6.2.2.1 Morphology and particle size distribution

Six formulations with different concentrations of zinc oxide and mannitol as matrix were spray dried. The amounts of ovalbumin and hyaluronic acid remained constant. The formulations were visualised with scanning electron microscopy.

Figure 6.30 shows representative pictures of the six formulations in two different magnifications. Image A depicts formulation 1 with the highest amount of zinc oxide (100 %) and image F formulation 6 without zinc oxide (0 %). From formulation 1 to formulation 6, the zinc oxide concentration decreases and the mannitol concentration increases. Both the particle size, better visible in the smaller magnification (left), and the particle size distribution, better visible in the higher magnification (right), are similar for all formulations. With geometric diameters of approximately 10 µm, the particles seem to be too large for pulmonary application, since, as already mentioned, an aerodynamic diameter smaller than 5 µm is required. However, geometric and aerodynamic diameters cannot be compared directly. The aerodynamic diameter also considers the morphology and density of a particle, i.e., aerodynamic diameter assumes a sphere with a density of 1 g/cm³. Therefore, a porous particle with low density with a geometric diameter above 5 µm may still have an aerodynamic diameter below 5 µm. This is the reason why both the geometric and the aerodynamic diameter were determined.

Similar to the spray dried nasal formulations, there was almost no difference in particle size visible between the six formulations but there is a difference in morphology. Formulation 6 (Figure 6.30, image F), formulation 1 (Figure 6.30, image A) and formulation 2 (Figure 6.30, image B) show the typical uniform spherical shape of a spray dried powder [191]. Particles of formulation 6 show a smooth surface. Particles of formulation 1 and formulation 2 show an irregular surface. In formulation 1, individual zinc

oxide particles are visible which do not contribute to the formation of the spray dried particle. All other formulations have wrinkled particles mixed with spherical particles (Figure 6.30, images C to E). The different compositions are clearly visible in the SEM images. Small particles and areas in a lighter grey represent zinc oxide particles and areas in a darker grey represent mannitol. The different morphology can be explained by the particle forming process.

Mannitol (formulation 6) was, similar to the nasal formulations, dissolved in the drop produced by the two-fluid nozzle. During the spray drying process, mannitol precipitated on the surface of the drop and a shell was formed. The particle no longer changed its size. Due to the low glass transition point and the low outlet temperature, a crystalline, uniform and smooth particle was formed.

While zinc oxide in the nasal formulations was initially partially dissolved in acetic acid (2%), the zinc oxide in the pulmonary formulations (formulation 1) was suspended in the drop produced by the two-fluid nozzle. By drying the solvent off, a layer of individual zinc oxide particles at the surface of the drop was formed. As they would not form stable particles by themselves, hyaluronic acid was added as an adhesive between those single zinc oxide particles [169]. In contrast, the spray dried nasal formulations formed a shell of precipitated zinc acetate in combination with single zinc oxide particles. A crystalline, uniform, almost spherical particle was formed whose matrix consists of individual zinc oxide particles. Using 1 % hyaluronic acid was not sufficient to form stable spherical particles in formulation 1, where the matrix consisted of 100 % zinc oxide. However, if the matrix consisted of 80 % zinc oxide and 20 % mannitol (formulation 2), stable particles could be formed and almost no individual zinc oxide particles were visible.

If mannitol and zinc oxide are processed together as a matrix, mannitol was dissolved and zinc oxide was suspended. The drying of water led to a higher concentration of mannitol and zinc oxide on the surface of the drop. Crystalline and spherical particles with single zinc oxide particles embedded in the continuous mannitol matrix were formed. As this was a suspension, the particle was formed more quickly than in a solution. The solvent vapour inside the particles, which was now exposed to higher temperatures, created higher pressure. As a consequence, when the solvent vapour condenses, decreasing volume created a vacuum and the shell collapsed.

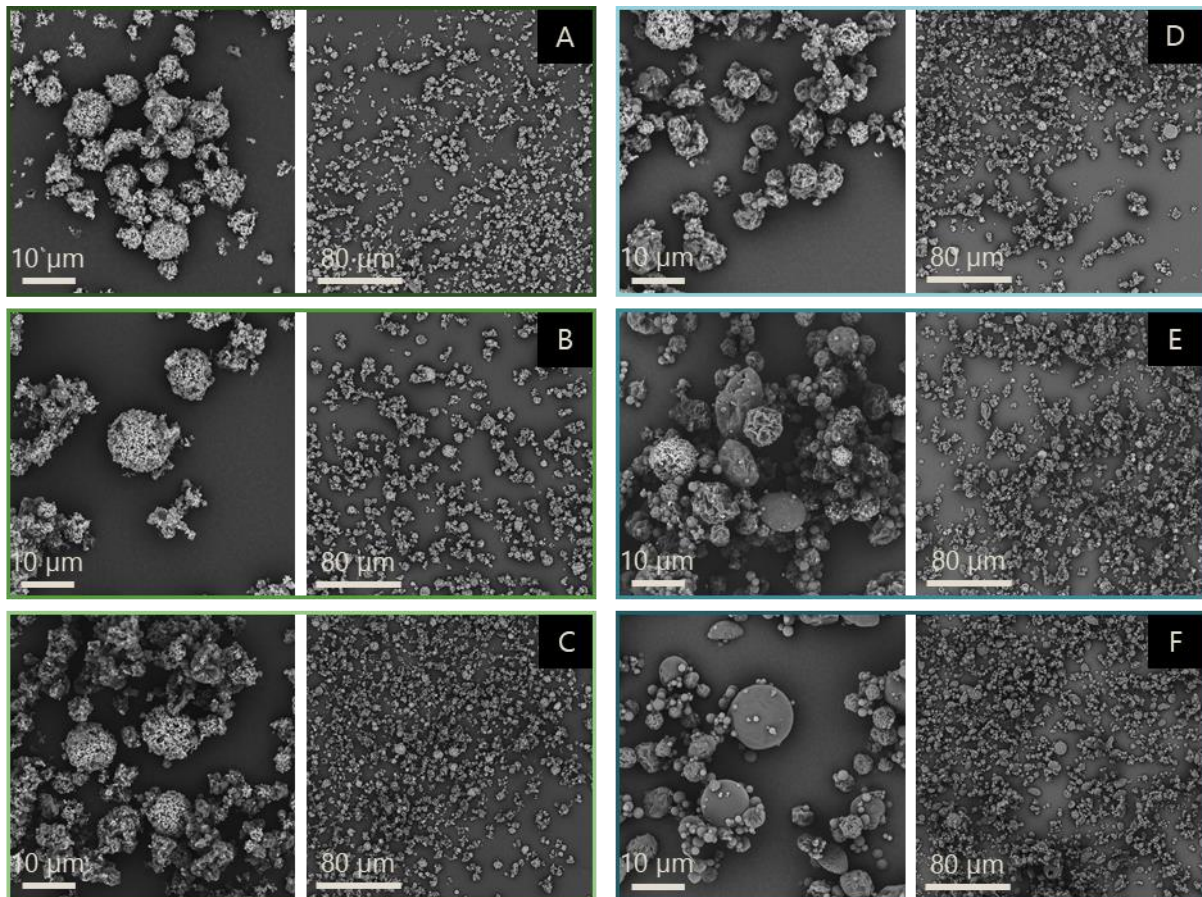


Figure 6.30. Representative scanning electron microscope images showing all spray dried powders with different amounts of zinc oxide (ZnO) and mannitol and additionally constant concentrations of ovalbumin (10 %) and hyaluronic acid (1 %). A) 100 % ZnO and 0 % mannitol; B) 80 % ZnO and 20 % mannitol; C) 60 % ZnO and 40 % mannitol; D) 40 % ZnO and 60 % mannitol; E) 20 % ZnO and 80 % mannitol; F) 0 % ZnO and 100 % mannitol.

The particle size distribution of all formulations was determined by laser diffraction (volume-based diameter). In Figure 6.31, the x50 and the span of the measurements with the RODOS module of all formulations are shown. The corresponding values can be found in Table 6.16. With an x50 of $1.32 \mu\text{m} \pm 0.07 \mu\text{m}$ (F1), $3.20 \mu\text{m} \pm 0.08 \mu\text{m}$ (F2), $3.64 \mu\text{m} \pm 0.25 \mu\text{m}$ (F3), $3.63 \mu\text{m} \pm 0.04 \mu\text{m}$ (F4), $3.98 \mu\text{m} \pm 0.06 \mu\text{m}$ (F5) and $4.00 \mu\text{m} \pm 0.14 \mu\text{m}$ (F6) 50 % of the particles of formulations 1 to 6 are smaller than 5 μm . Formulation 1 shows with $1.32 \mu\text{m} \pm 0.07 \mu\text{m}$ a highly significantly smaller particle size than formulations 2, 3, 4, 5 and 6 (p-value < 0.0001). Formulation 2 is significantly smaller than formulation 3 (p-value = 0.0224) and highly significantly smaller than formulations 4 (p-value = 0.0005), 5 (p-value < 0.0001) and 6 (p-value = 0.0005). Formulation 3 is significantly smaller than formulations 5 (p-value = 0.0440) and 6 (p-value = 0.0491). Formulation 4 is highly significantly smaller than formulation 5 (p-value = 0.0006) and very significantly smaller than formulation 6 (p-value = 0.0057).

As mentioned above, zinc oxide particles alone could not form a shell. Hyaluronic acid as an adhesive between the individual zinc oxide particles was not sufficient and individual zinc oxide particles were not involved in the forming of the spherical particles. If the zinc oxide concentration per particle was decreased the particles became smaller. If mannitol was added as a continuous matrix, the spray dried

particles became larger, because all zinc oxide particles were included in the formation of the particle. In addition, the individual zinc oxide particles not involved in the formation of a stable particle formed separate agglomerates and as such contributed to the particle size distribution. As a result, the particle size distribution was shifted towards smaller particle sizes. This is also reflected in the increased span value of 3.47 ± 0.06 for formulation 1. The span value describes the distribution width. Spray drying is a fast process usually resulting in a lognormal particle size distribution.

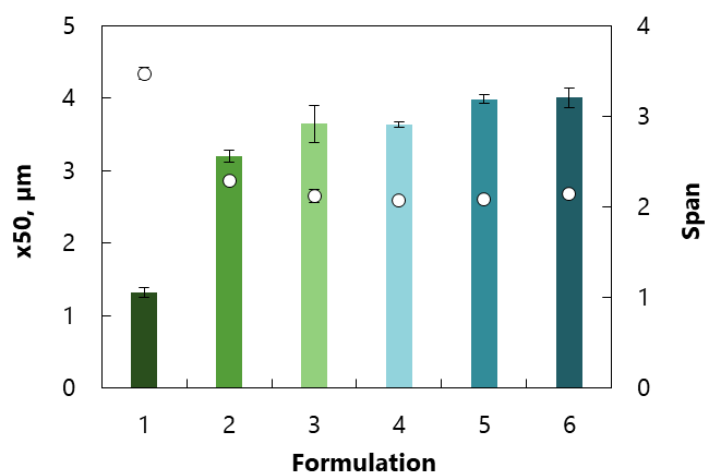


Figure 6.31. Particle size distribution using laser diffraction (HELOS) in combination with the RODOS module, x50 (primary axis) and span (secondary axis) of all formulations; 1) 100 % ZnO and 0 % mannitol; 2) 80 % ZnO and 20 % mannitol; 3) 60 % ZnO and 40 % mannitol; 4) 40 % ZnO and 60 % mannitol; 5) 20 % ZnO and 80 % mannitol; 6) 0 % ZnO and 100 % mannitol. $n = 3$, error bars = standard deviation.

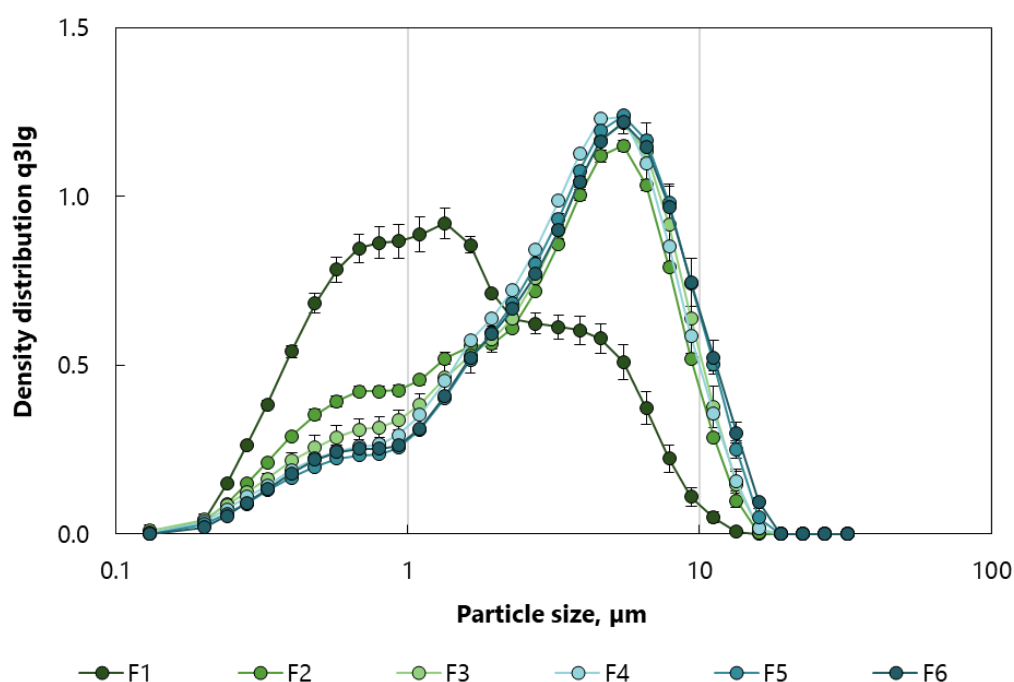


Figure 6.32. Density distribution using laser diffraction (HELOS) in combination with the RODOS module; F1) 100 % ZnO and 0 % mannitol; F2) 80 % ZnO and 20 % mannitol; F3) 60 % ZnO and 40 % mannitol; F4) 40 % ZnO and 60 % mannitol; F5) 20 % ZnO and 80 % mannitol; F6) 0 % ZnO and 100 % mannitol. $n = 3$, error bars = standard deviation.

Curves of all formulations show a bimodal distribution as shown in Figure 6.32. Formulation 1, as the x50 already suggests, shows a higher maximum at smaller particle sizes. All other formulations show a higher maximum at larger particle sizes, with formulations 3 to 6 showing almost identical curves. The higher span value of formulation 1 indicates a broader particle size distribution due to the individual zinc oxide particles.

Table 6.16. x_{10} , x_{50} , x_{90} and span of all formulations using the HELOS in combination with the RODOS module. F1) 100 % ZnO and 0 % mannitol; F2) 80 % ZnO and 20 % mannitol; F3) 60 % ZnO and 40 % mannitol; F4) 40 % ZnO and 60 % mannitol; F5) 20 % ZnO and 80 % mannitol; F6) 0 % ZnO and 100 % mannitol. $n = 3$, \pm = standard deviation.

	x_{10} , μm	x_{50} , μm	x_{90} , μm	Span
F1	0.43 ± 0.01	1.32 ± 0.07	5.01 ± 0.32	3.47 ± 0.06
F2	0.56 ± 0.01	3.20 ± 0.08	7.88 ± 0.07	2.29 ± 0.04
F3	0.66 ± 0.02	3.64 ± 0.25	8.38 ± 0.34	2.12 ± 0.07
F4	0.75 ± 0.02	3.63 ± 0.04	8.28 ± 0.12	2.07 ± 0.01
F5	0.84 ± 0.01	3.98 ± 0.06	9.11 ± 0.19	2.08 ± 0.01
F6	0.80 ± 0.02	4.00 ± 0.14	9.35 ± 0.29	2.14 ± 0.003

In Figure 6.33 and Table 6.17, the results of the measurements with the INHALER module in combination with the Cyclohaler are shown.

The use of an inhaler and the corresponding settings (simulated inspiration instead of pressurised air and a 90° glass pipe bend for the simulation of the throat) led to more meaningful particle size distributions related to the lung deposition than the HELOS with the RODOS module. In Figure 6.33 the cumulative distribution of particles smaller than 5 μm (volume-based diameter) is illustrated. The trend of the measurements with the RODOS module that formulation 1 was highly significantly smaller than all the other formulations and therefore had a higher number of particles smaller than 5 μm is not visible. For the Cyclohaler, a pressure drop of 4 kPa is recommended, i.e., 0.04 bar. This corresponds to a flow rate of 100 L/min. The highest value that could be set for the flow rate in the combination of HELOS and INHALER module however was 82.7 L/min. Either way, the pressure responsible for powder dispersion is not comparable between the RODOS module and the INHALER module as the principle of these two modules differ as mentioned in chapter 5.2.2. With 65.31 % \pm 4.76 % (< 5 μm) formulation 6 shows the highest percentage of particles smaller than 5 μm . It thus has a significantly higher (p-value = 0.0152) percentage of smaller particles than formulation 2 (< 5 μm = 47.49 % \pm 8.11 %) and a very significantly higher percentage of smaller particles than formulation 1 (p-value = 0.0036,

< 5 μm = 35.20 % \pm 9.13 %), formulation 3 (p-value = 0.0020, < 5 μm = 45.49 % \pm 4.29 %), formulation 4 (p-value = 0.0024, < 5 μm = 42.04 % \pm 5.25 %) and formulation 5 (p-value = 0.0037, < 5 μm = 41.57 % \pm 2.48 %). All other formulations do not show significant differences.

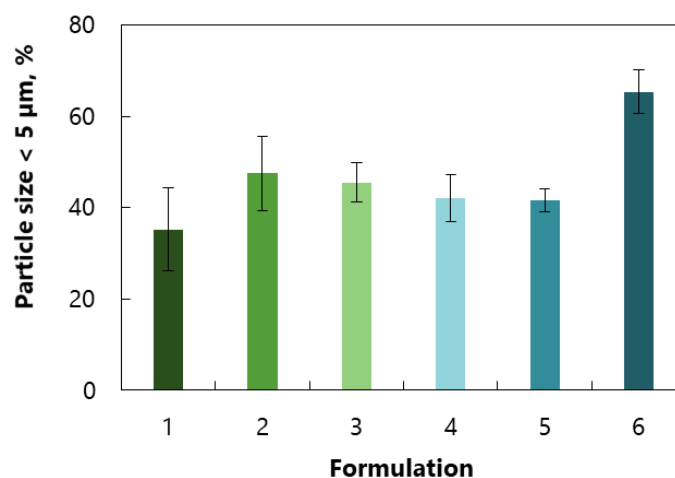


Figure 6.33. Particle size distribution using laser diffraction (HELOS) in combination with the INHALER module (< 5 μm) and the Cyclohaler, cumulative distribution of all formulations; 1) 100 % ZnO and 0 % mannitol; 2) 80 % ZnO and 20 % mannitol; 3) 60 % ZnO and 40 % mannitol; 4) 40 % ZnO and 60 % mannitol; 5) 20 % ZnO and 80 % mannitol; 6) 0 % ZnO and 100 % mannitol. $n = 3$, error bars = standard deviation.

Table 6.17. Particle size distribution using laser diffraction (HELOS) in combination with the INHALER module (< 5 μm) and the Cyclohaler. F1) 100 % ZnO and 0 % mannitol; F2) 80 % ZnO and 20 % mannitol; F3) 60 % ZnO and 40 % mannitol; F4) 40 % ZnO and 60 % mannitol; F5) 20 % ZnO and 80 % mannitol; F6) 0 % ZnO and 100 % mannitol. $n = 3$, \pm = standard deviation.

	F1	F2	F3	F4	F5	F6
Particle size < 5 μm , %	35.20 \pm 9.13	47.49 \pm 8.11	45.49 \pm 4.29	42.04 \pm 5.25	41.57 \pm 2.48	65.31 \pm 4.76

6.2.2.2 Aerodynamic assessment using the NGI

In addition to the volume-based diameter via laser diffraction, the aerodynamic particle size distribution was assessed. The aerodynamic diameter is an equivalent diameter, i.e., the measured diameter corresponds to that of a sphere with a density of 1 g/cm³ having the same settling velocity as the particle under consideration. It also considers the morphology and density of a particle. Therefore, a porous particle with low density with a geometric diameter above 5 μm may still have an aerodynamic diameter below 5 μm .

Figure 6.34 and Table 6.18 show deposition profiles of all formulation using the NGI in combination with the Cyclohaler, the mouthpiece, the throat and the preseparator.

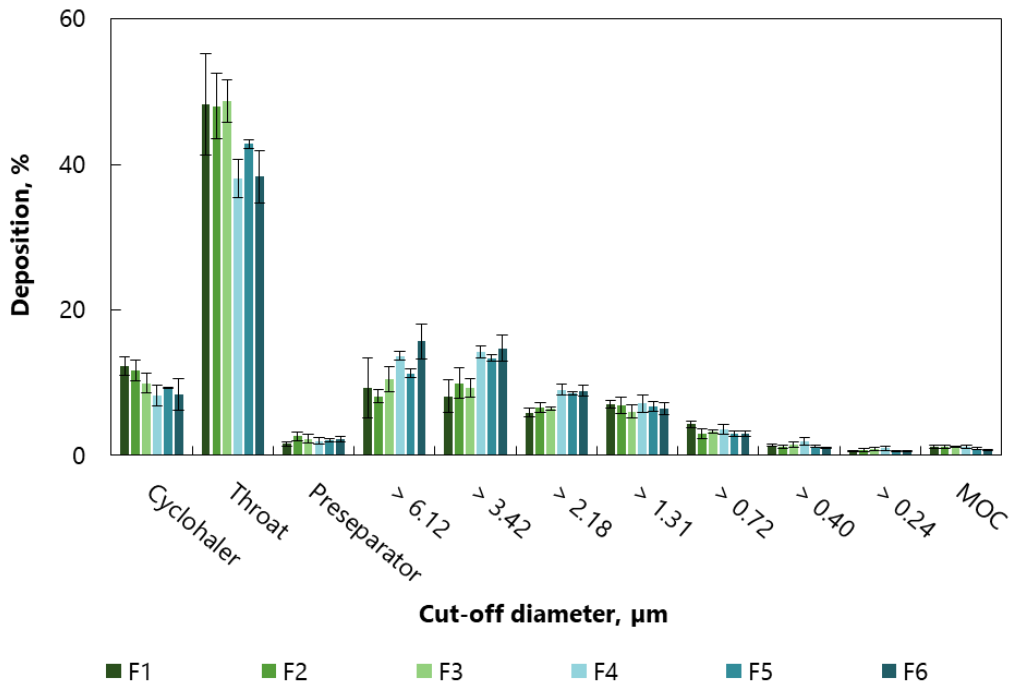


Figure 6.34. Deposition profiles of all formulations using the NGI in combination with the mouthpiece, the throat, the preseparator and the Cyclohaler. F1) 100 % ZnO and 0 % mannitol; F2) 80 % ZnO and 20 % mannitol; F3) 60 % ZnO and 40 % mannitol; F4) 40 % ZnO and 60 % mannitol; F5) 20 % ZnO and 80 % mannitol; F6) 0 % ZnO and 100 % mannitol. $n = 3$, error bars = standard deviation.

All formulations show a similar trend. Formulations with a higher zinc oxide content, formulations 1 to 3, and those with a higher mannitol content, formulations 4 to 6, can be grouped together. The emitted dose of all formulations is about 90 % (formulation 1 = 87.70 % \pm 1.26 %, formulation 2 = 88.31 % \pm 1.47 %, formulation 3 = 90.06 % \pm 1.39 %, formulation 4 = 91.7 % \pm 1.39 %, formulation 5 = 90.72 % \pm 0.12 %, formulation 6 = 91.63 % \pm 2.21 %). While approximately 50 % of the formulations with the higher zinc oxide content are found in the throat, only 40 % of the formulations with the higher mannitol content were found in the throat. This difference could be explained by the adhesive properties of zinc oxide, which could be observed in almost all experiments. The high amount of the formulations in the throat was due to impaction. The emitted particles could no longer follow the air flow at the 90° angle of the throat and impacted at the surface. The higher the speed of the flow and the weightier the particle, the higher was the probability of impaction.

The structure of the lungs is similar to that of a tree. The trachea is the trunk that branches 23 times down to the alveoli. The diameter decreases from 12 mm (upper airways) to 410 μ m (lower airways), while the number of branches increases. The total diameter of all branches of one generation from the trachea to the lobe bronchi initially remains constant in comparison to the previous generation but increases rapidly from the lobe bronchi onwards. Accordingly, the breathing air speed decreases more and more from the upper to the lower airways. The separation of the particles in the lungs is based on five different mechanisms: Impaction, sedimentation, diffusion, interception and electrostatic

precipitation. Interception and electrostatic precipitation play a secondary role. The impaction described above takes place mainly in the upper respiratory tract and depends not only on the speed of the air, but also on the diameter, density and shape of the particles. In the lower respiratory tract, sedimentation and diffusion are the driving forces for particle separation. Sedimentation follows Stokes' law of sedimentation and depends mainly on the diameter and density of the particle as well as on the viscosity of the dispersion medium. Particles smaller than 1 μm are exposed to the Brownian molecular movement of the surrounding gas molecules and are separated by diffusion. The diffusion rate also depends on the size of the particles. While sedimentation and impaction increase with increasing particle size, diffusion decreases. Various physiological factors can also further influence particle deposition, e.g., the geometry of the respiratory tract and the inhalation technique. The target size for pulmonary application is an aerodynamic diameter of 1 μm to 5 μm , as small particles, typically smaller than 1 μm , are exhaled again [239].

Table 6.18. Deposition data of all formulations using the NGI in combination with the mouthpiece, the throat, the preseparator and the Cyclohaler. F1) 100 % ZnO and 0 % mannitol; F2) 80 % ZnO and 20 % mannitol; F3) 60 % ZnO and 40 % mannitol; F4) 40 % ZnO and 60 % mannitol; F5) 20 % ZnO and 80 % mannitol; F6) 0 % ZnO and 100 % mannitol. $n = 3$, $\pm =$ standard deviation.

	Cyclohaler, %	Throat, %	Preseparator, %	> 6.12 μm , %	> 3.42 μm , %	> 2.18 μm , %	> 1.31 μm , %	> 0.72 μm , %	> 0.40 μm , %	> 0.24 μm , %	MOC, %
F1	12.30 ± 1.26	48.25 ± 6.94	1.57 ± 0.24	9.28 ± 4.14	8.15 ± 2.25	5.91 ± 0.59	7.06 ± 0.52	4.27 ± 0.45	1.39 ± 0.11	0.62 ± 1.21	1.21 ± 0.24
F2	11.69 ± 1.47	48.02 ± 4.48	2.63 ± 0.55	8.15 ± 0.86	9.92 ± 2.09	6.55 ± 0.64	6.89 ± 1.19	3.03 ± 0.65	1.20 ± 0.19	0.74 ± 0.23	1.19 ± 0.25
F3	9.94 ± 1.39	48.68 ± 2.95	2.29 ± 0.57	10.43 ± 1.72	9.23 ± 1.28	6.49 ± 0.23	6.05 ± 0.92	3.28 ± 0.26	1.53 ± 0.40	0.91 ± 0.19	1.17 ± 0.11
F4	8.28 ± 1.39	38.07 ± 2.60	2.01 ± 0.41	13.66 ± 0.57	14.20 ± 0.81	9.04 ± 0.71	7.15 ± 1.21	3.59 ± 0.66	1.90 ± 0.50	0.98 ± 0.24	1.15 ± 0.20
F5	9.28 ± 0.12	42.82 ± 0.60	2.05 ± 0.25	11.27 ± 0.57	13.40 ± 0.44	8.53 ± 0.24	6.76 ± 0.66	3.03 ± 0.38	1.25 ± 0.14	0.66 ± 0.06	0.97 ± 0.19
F6	8.37 ± 2.21	38.29 ± 3.60	2.17 ± 0.38	15.72 ± 2.39	14.74 ± 1.75	8.87 ± 0.74	6.40 ± 0.82	2.94 ± 0.37	1.07 ± 0.08	0.63 ± 0.06	0.82 ± 0.05

As already mentioned, the target particle size for pulmonary application is an aerodynamic diameter of 1 μm to 5 μm . According to Ph. Eur. 2.9.18 "Preparation for inhalation: aerodynamic assessment of fine particles" [153], the FPF of the emitted dose of all formulations was calculated (Table 6.19). With 35.03 % \pm 2.65 % formulation 4 is significantly different to formulations 2 with 28.76 % \pm 2.39 % (p-value = 0.0382), 3 with 27.57 % \pm 1.83 % (p-value = 0.0160) and 6 with 30.34 % \pm 1.13 % (p-value = 0.0378). Formulation 5 with 32.00 % \pm 0.87 % is significantly different to formulation 3 (p-value = 0.0194). Formulation 1 with 28.75 % \pm 3.17 % has no significant difference to the other formulations.

Table 6.19. Particles with an aerodynamic diameter < 5 μm , < 3 μm and < 1 μm of all formulations using the NGI in combination with the mouthpiece, the throat, the preseparator and the Cyclohaler F1) 100 % ZnO and 0 % mannitol; F2) 80 % ZnO and 20 % mannitol; F3) 60 % ZnO and 40 % mannitol; F4) 40 % ZnO and 60 % mannitol; F5) 20 % ZnO and 80 % mannitol; F6) 0 % ZnO and 100 % mannitol. n = 3, \pm = standard deviation.

	Particles with an aerodynamic diameter < x, %		
	5 μm (FPF)	3 μm	1 μm
F1	28.75 \pm 3.17	21.87 \pm 1.36	14.99 \pm 0.76
F2	28.76 \pm 2.39	20.43 \pm 1.36	12.09 \pm 2.16
F3	27.57 \pm 1.83	19.99 \pm 1.23	12.40 \pm 1.19
F4	35.03 \pm 2.65	23.55 \pm 2.61	12.06 \pm 2.81
F5	32.00 \pm 0.87	21.05 \pm 1.01	10.11 \pm 1.23
F6	30.34 \pm 1.13	18.43 \pm 2.24	6.51 \pm 3.42

A grouping can be seen for formulations with a higher amount of zinc oxide and a higher amount of mannitol. While the deposition of formulations with a higher amount of zinc oxide is higher in the throat, the fine particle fraction of the formulations with a higher amount of mannitol is higher. If the particles with an aerodynamic diameter below 5 μm are considered, it is noticeable that the formulations with a higher mannitol amount are more represented at higher cut-off diameters (> 2.18 μm) than the formulations with a higher zinc oxide amount.

As the target size for pulmonary application is < 5 μm and particles smaller than 1 μm are exhaled again, the percentage of particles < 1 μm was calculated. Dendritic cells as immunocompetent cells form a bridge between the innate and the adaptive immune system and are specialised in taking up a broad spectrum of pathogens to present their antigens on the cell surface [171]. Dendritic cells are also located in the lungs, i.e., in the epithelial linings of the conducting airways and in the submucosa and the surface

of the alveoli [28]. For targeted uptake of the particles by dendritic cells in the respiratory tract, the particle size should be lower than 3 μm [45]. That is why the percentage of the particles < 3 μm was also calculated. The calculation of the deposition of particles with an aerodynamic diameter < 3 μm and < 1 μm were carried out analogously to the calculation of the fine particle fraction according to Ph. Eur. 2.9.18 "Preparation for inhalation: aerodynamic assessment of fine particles" [153].

Considering the deposition of particles with an aerodynamic diameter < 1 μm , formulations with a higher amount of zinc oxide have a higher percentage of smaller particles. When subtracting the percentage of particles with an aerodynamic diameter < 1 μm from the fine particle fraction, the above-mentioned observation that particles with a higher mannitol amount were more represented at higher cut-off diameters below 5 μm is confirmed. Formulation 6 with the highest amount of mannitol shows about 24 % of the formulation deposited in the lung. Formulation 1, on the other hand, shows only about 14 % of the formulation deposited in the lung.

As for targeted uptake of particles by dendritic cells in the respiratory tract a particle size below 3 μm is recommended, the percentage of particles with an aerodynamic diameter < 3 μm was calculated. With no significant differences, all formulations show about 21 % of the formulation with an aerodynamic diameter < 3 μm and thus an equal amount of particles that could theoretically be taken up by dendritic cells. However, a prediction of in-vivo deposition was not possible using the NGI, as essential factors of in-vivo conditions are not considered in the Ph. Eur. method.

6.2.2.3 pH and solubility

A 24-h-solubility study as already described in chapter 6.2.1.3 was conducted to investigate the amount of soluble zinc oxide. In addition, the pH change after adding the formulations to different environments was measured to show the influence of zinc oxide on their pH value. While phosphate buffers and sodium chloride solutions with six different pH conditions were used for both the nasal and the pulmonary formulations, simulated lung fluid (SLF, pH 7.4) was used for the pulmonary formulations instead of simulated nasal fluid used for the nasal formulations. SLF took account of the salt and pH conditions in the lungs.

In Figure 6.35 and Table 11.4, the results of the 24-h-solubility study of zinc oxide as raw material and formulation 1 are shown. Zinc oxide and formulation 1 show similar results for the concentration of dissolved zinc and pH value in the 24-h-solubility study.

With a solubility between 1 mg/mL and 10 mg/mL, both zinc oxide and formulation 1 are slightly soluble at pH 1.2 according to Ph. Eur. classification. At a pH value of pH 2.5, zinc oxide and formulation 1 are very slightly soluble in both the phosphate buffer and the sodium chloride solution with a solubility between 0.1 mg/mL and 1 mg/mL. Zinc oxide and formulation 1 are practically insoluble in all tested pH

values, including SLF, above pH 2.5 with a solubility of less than 0.1 mg/mL. The exact values are shown in Table 11.4.

Besides the results of the dissolved zinc concentrations, the pH values before and after adding zinc oxide and formulation 1 are also shown in Table 11.4. Zinc oxide and formulation 1 result in similar pH values.

In the phosphate buffers the pH values have increased after 24 h. The extent of the increase is dependent on the starting pH value. The lower the starting pH, the higher the increase. An exception to this is phosphate buffer at pH 4.0. The pH increase is more distinct than for phosphate buffer at pH 2.5.

In the sodium chloride solutions, the pH value reaches a plateau at approximately pH 7.5 independent of the starting pH (beginning at pH 4).

In SLF the shift of the pH value after 24 h shows an increase to approximately pH 8.2 for both zinc oxide and formulation 1.

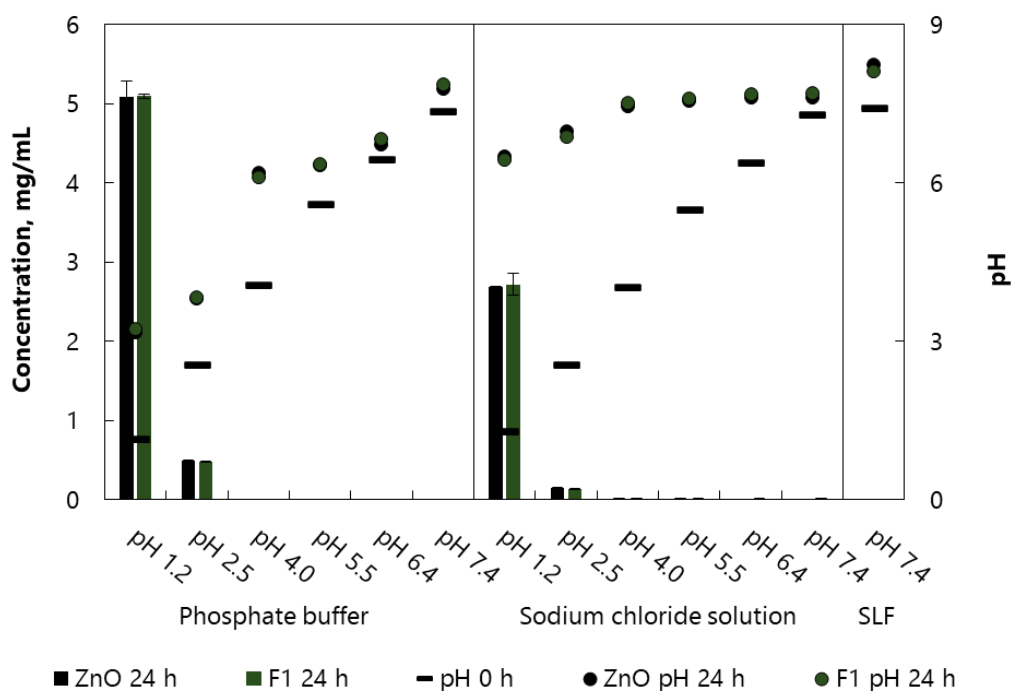


Figure 6.35. 24-h-pH- and solubility study showing starting pH (pH 0 h, black bars) and pH after 24 h with zinc oxide as raw material (ZnO 24 h, black dots) in comparison to formulation 1 (F1 24 h, green dots). Saturation solubility after 24 h is shown for zinc oxide (ZnO 24 h, black bars) in comparison to formulation 1 (F1 24 h, green bars). F1) 100 % ZnO and 0 % mannitol. $n = 3$, error bars = standard deviation.

In order to analyse the influence of different zinc oxide amounts in the formulations on the pH, the pH values after 24 h of formulations 2 to 6 were also tested. In Figure 6.36, pH values are shown as a function of the solutions with different pH values. The starting pH is shown as black bars and the formulations as coloured dots. The exact values are shown in Table 11.5.

In phosphate buffers, as seen for formulation 1 before, the pH increases after 24 h for all formulations containing zinc oxide. After combining the individual dots of the respective formulation, it can be seen

that the zinc oxide content has an influence on the extent of the pH change. While zinc oxide and formulations 1 and 2 show almost identical trends, the change in pH value decreases with decreasing zinc oxide content. Formulation 6 containing no zinc oxide shows an almost similar curve with the starting pH. The trend observed for formulation 1 can also be observed for all other formulations. The extent of the increase is dependent on the starting pH value. The lower the starting pH, the higher the increase. An exception to this is phosphate buffer at pH 4. The pH increase is more distinct than for phosphate buffer at pH 2.5.

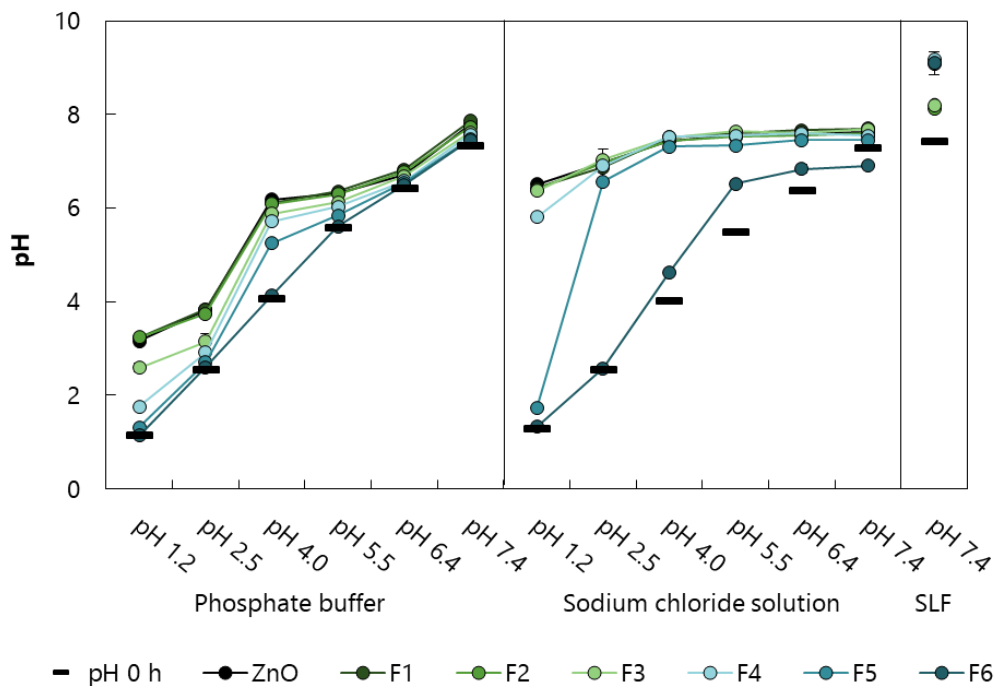


Figure 6.36. 24 h-pH study showing starting pH (pH 0 h, black bars) and pH change of different solutions/suspensions after 24 h with zinc oxide as raw material (ZnO) in comparison to all formulations (coloured dots and lines). F1) 100 % ZnO and 0 % mannitol; F2) 80 % ZnO and 20 % mannitol; F3) 60 % ZnO and 40 % mannitol; F4) 40 % ZnO and 60 % mannitol; F5) 20 % ZnO and 80 % mannitol; F6) 0 % ZnO and 100 % mannitol. $n = 3$, error bars = standard deviation.

For the sodium chloride solution, a different picture is obtained. Zinc oxide and all formulations reach a plateau of the pH value after 24 h. Zinc oxide and all formulations with a higher zinc oxide amount, formulations 1 to 3, show almost identical graphs. Formulations 4 to 6 however behave differently. At pH 1.2 the difference to the starting pH depends on the zinc oxide content in the formulation. Formulation 6, without zinc oxide, shows a pH value similar to that of the starting solution, formulation 5, including 20 % zinc oxide, increases the pH value to $\text{pH } 1.72 \pm 0.01$ and formulation 4, 40 % zinc oxide, to $\text{pH } 5.81 \pm 0.36$. At pH 2.5 all formulations except formulations 5 ($\text{pH } 6.57 \pm 0.07$) and 6 ($\text{pH } 2.58 \pm 0.02$) show an almost identical pH value of about pH 6.9. From the starting pH of 4.0, formulations 1 to 5 reach a plateau of approximately pH 7.5. From pH 5.5 onwards, formulation 6 shows only a slight change in the difference of pH value after 24 h to starting pH from pH 6.5 to pH 6.9 (starting pH 7.4).

In SLF zinc oxide and the formulations with a higher zinc oxide amount, formulations 1 to 3, increase the initial pH to about pH 8.3. The formulations with a lower zinc oxide content, formulations 4 to 6, increase the pH value even more to approximately pH 9.1.

A correlation of the pH value with the composition of the formulation is obvious. The starting materials were dissolved or suspended in water. Zinc oxide as raw material and zinc oxide in the formulations contributed to an increase of the pH value after spray drying in the phosphate buffers, which was dependent on the initial pH value and in the sodium chloride solutions, which was independent of the initial pH value in higher pH values. The pH increase of the zinc oxide in the buffer solutions (phosphate buffer) was not as pronounced as in the simple salt solutions (sodium chloride solution). This reflected the ability of the buffer to attenuate slight pH changes. Formulation 6 contained no zinc oxide and therefore showed almost no change compared to the initial pH and all other formulations.

In order to investigate further influences on solubility, representative diffractograms of X-ray powder diffraction of all formulations are shown in Figure 6.37. The diffractogram of zinc oxide as reference was shown in Figure 6.22. The flat baseline and sharp diffraction patterns indicate that the formulations contain crystalline substances. By comparison with the reference, it is clear that the diffraction patterns can be primarily assigned to zinc oxide, which can be recognised by the four sharp peaks. In addition to the characteristic peaks of zinc oxide, further peaks can be identified, especially in the formulations with decreasing amount of zinc oxide. As already mentioned in chapter 6.2.1.3, mannitol was not measured as a reference because sufficient data on the polymorphism of mannitol is already available.

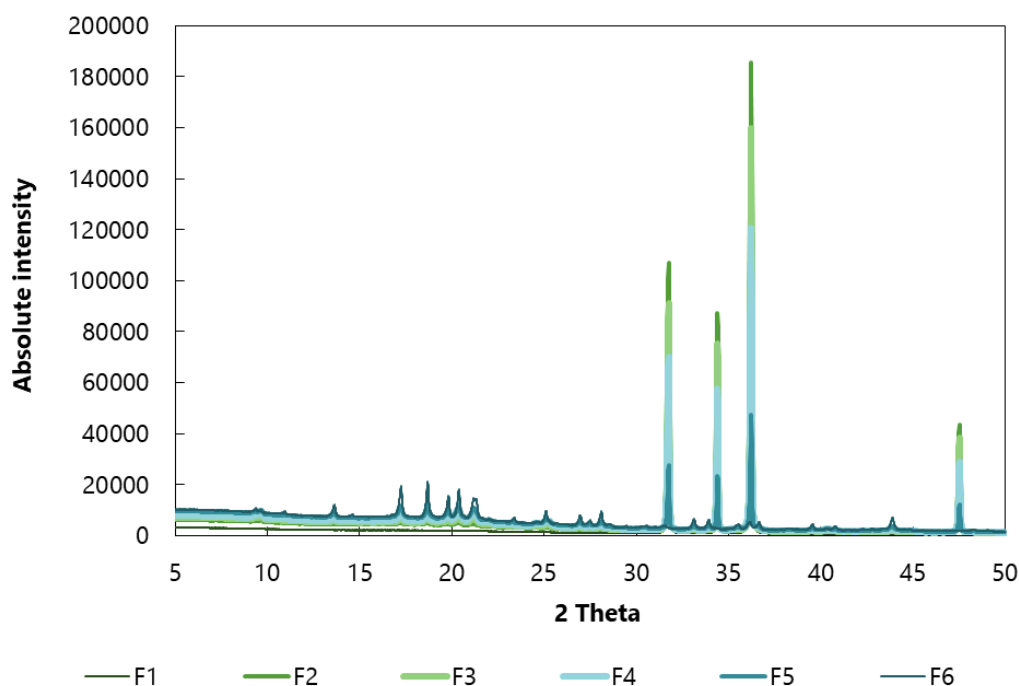


Figure 6.37. Representative diffractograms of X-ray powder diffraction showing the degree of crystallinity of all formulations. F1) 100 % ZnO and 0 % mannitol; F2) 80 % ZnO and 20 % mannitol; F3) 60 % ZnO and 40 % mannitol; F4) 40 % ZnO and 60 % mannitol; F5) 20 % ZnO and 80 % mannitol; F6) 0 % ZnO and 100 % mannitol. $n = 1$.

6.2.2.4 Release study

The release of the model antigen ovalbumin from the spray dried pulmonary formulations was evaluated using ThinCert cell culture inserts. The dry formulations and pure ovalbumin as reference were placed on the ThinCert and the released ovalbumin content in the medium was analysed. As the amount of ovalbumin in the solution at the end of the dissolution or the release study with maximum 1 mg/mL does not exceed 10 % of the saturation concentration of the used ovalbumin in water (saturation concentration = 40 mg/mL [176]), it could be assumed that perfect sink conditions exist. In Figure 6.38 and Table 6.20, the released ovalbumin quantities are plotted in % against time.

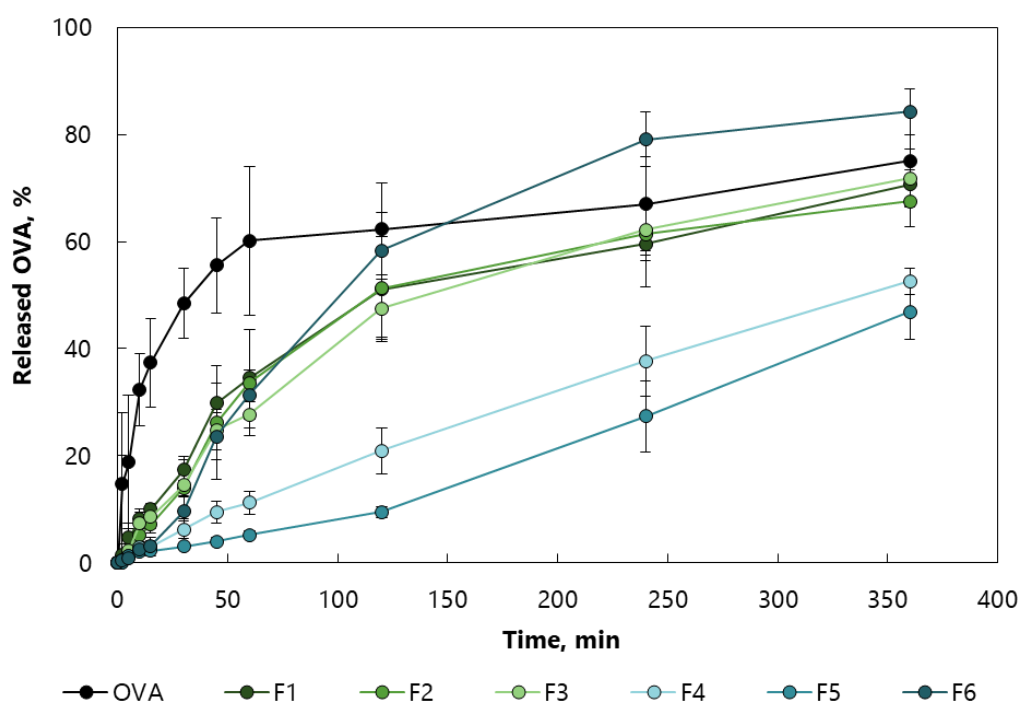


Figure 6.38. Release curves of the formulations and ovalbumin as reference. F1) 100 % ZnO and 0 % mannitol; F2) 80 % ZnO and 20 % mannitol; F3) 60 % ZnO and 40 % mannitol; F4) 40 % ZnO and 60 % mannitol; F5) 20 % ZnO and 80 % mannitol; F6) 0 % ZnO and 100 % mannitol. $n = 3$, error bars = standard deviation.

The black curve shows the dissolution of pure ovalbumin as a reference. It shows a steep increase at first and reaches a plateau after 60 min showing only a weak increase afterwards. The initially undissolved ovalbumin was located on the ThinCert and could not pass the membrane with a pore size of 1 μm . If the insert was now placed in the 12-well plate with the release medium water, the ovalbumin dissolved and could freely diffuse through the membrane. In order to match the amount of pure ovalbumin to the amount of ovalbumin in the formulations, only 1 mg was used in the test. The amount released at a certain time was related to the total amount recovered at the end of the experiment. After 6 h, 75.0 % \pm 8.5 % of the total amount of ovalbumin has been released, i.e., 25 % of the ovalbumin is not released into the release medium. Due to the structure of the ThinCert, some material might have stuck in the contact well of the membrane and the insert, which would only be detected at the end. Ovalbumin shows a first-order release kinetic, which is typical for an uncontrolled release, respectively, since

ovalbumin was present as single substance, this is correctly not a release, but rather a dissolution. Due to a high difference in concentration between the active pharmaceutical ingredient and the medium, the release starts quickly. The smaller this difference in concentration becomes, the slower the release takes place.

Equation 6.1 shows the corresponding mathematical function.

Equation 6.1. Mathematical function of a first-order release kinetic.

$$M_t = M_0 * (1 - e^{-k * t})$$

M_t stands for the released drug amount at time t , M_0 for the initial amount of the drug and k is the reaction rate constant of the release.

The coloured curves show the formulations with different release profiles. The different release profiles depend on the composition of the matrix of the formulations.

Formulations 1 to 3 with the higher zinc oxide content show the same release profile with a delayed start and more continuous release compared to ovalbumin. Subsequently, the release speed increases until approximately 120 min and slows down again with time. This release kinetic can best be described with the Higuchi release kinetic. The release is initially fast and then slows down. Although this law was first described for the release of suspended drugs from semi-solid preparations, it could also be used, for example, to describe the release of drugs from non-erodible matrix tablets. In the case of a non-erodible matrix tablet the drug substance has to move further and further over time. Within the experiment, it is not possible to say whether the particles remained intact or not. Since the dry formulation was placed on the ThinCert and only had contact with liquid on one side, the experiments were not directly similar to the common examples of the release kinetics, but had to be considered with a slightly different perspective.

Equation 6.2 shows the corresponding mathematical function.

Equation 6.2. Mathematical function of a Higuchi release kinetic.

$$\frac{M_t}{A} = \sqrt{2 * c_0 * D * c_s * t}$$

M_t stands for the released drug amount at time t , A for the effective diffusion surface, D is the diffusion coefficient, c_0 describes the initial concentration in the carrier matrix and c_s is the saturation concentration in the matrix material. The simplified form of the Higuchi release kinetics is shown in Equation 6.3 with k as reaction rate constant of the release.

Equation 6.3. Simplified mathematical function of a Higuchi release kinetic.

$$M_t = k * \sqrt{t}$$

Linearisation can be achieved by using the square root of time as x-value instead of time.

With a coefficient of determination of $R^2 = 0.9702$ (F1), $R^2 = 0.9575$ (F2) and $R^2 = 0.9836$ (F3), formulations 1 to 3 closely follow a Higuchi release kinetic. The formulations consisted mainly of zinc oxide, which is practically insoluble in water. First the ovalbumin located on the surface of the particle at the bottom of the ThinCert was dissolved. The water penetrates further and further into the particle and the dry formulation on the ThinCert and dissolved the ovalbumin, which had to travel an increasingly longer way to pass through the membrane of the insert, as the zinc oxide matrix did not dissolve. The increasing amount of mannitol from formulation 1 to formulation 3 did not seem to influence the release kinetics as long as the zinc oxide content is predominant.

If the formulations with the lower proportion of zinc oxide and the higher proportion of mannitol (formulations 4 and 5) are considered, a clear difference to formulations 1 to 3 can be seen. The formulations with a higher mannitol content show an almost uniform release, which can best be described with the zero-order release kinetic (Equation 6.4). As long as undissolved ovalbumin was in the formulations, the same amount of ovalbumin was dissolved and released in each time interval, i.e., the rate is constant. Equation 6.4 can be used to describe the drug release from an erodible matrix. In this model, the drug substance always has to overcome the same distance to be released. The matrix is continuously degraded, while the release medium, which is responsible for dissolving the drug, penetrates further and further into the inner part of the particle.

Equation 6.4. Mathematical function of a zero-order release kinetic.

$$M_t = k * t$$

M_t stands for the released drug amount at time t and k is the reaction rate constant of the release.

If the amount of the drug released in formulations 4 and 5 is plotted against time, a straight line can be seen. With a coefficient of determination of $R^2 = 0.9945$ (F4) and $R^2 = 0.9799$ (F5), formulations 4 and 5 closely follow a zero-order release kinetic. The formulations consisted mainly of mannitol, which is easily soluble in water. Both formulations also contained zinc oxide, which is practically insoluble in water. The mannitol was thus dissolved during the experiment, but the zinc oxide was not, i.e., the matrix and the amount of dry formulation on the ThinCert decreased further and further up to a certain point and the ovalbumin was released steadily. It should be noted that at the end of the experiment, approximately 100 μL of a viscous suspension was formed on the insert of formulation 4 and 250 μL on the insert of formulation 5. The higher volume of the viscous suspension and therefore the lower volume of release medium would explain why formulation 5 shows a slower release than formulation 4. The viscous suspension led to a longer diffusion path for the ovalbumin in formulation 5 than in formulation 4, i.e., the release was slower.

If formulation 6 with a matrix of 100 % mannitol is considered, it is noticeable that the release after 1 h is more similar to the formulations with the higher zinc oxide content, but then exceeds the plateau of

the reference ovalbumin. Finally, after 6 h, $84.2 \% \pm 4.2 \%$ of the total ovalbumin is released. With a coefficient of determination of $R^2 = 0.9926$ this release corresponds to a first-order kinetic (Equation 6.1). The difference of almost 10 % to ovalbumin could be explained by the fact that the weighed amount of ovalbumin was only 10 % of formulation 6, i.e., the amount of ovalbumin sticking in the contact weld of the membrane and the insert was much more relevant for ovalbumin as single material than for formulation 6 as formulation 6 consisted of mannitol, ovalbumin and hyaluronic acid.

Table 6.20. Release study of the formulations and ovalbumin (OVA) as reference with the released amount of ovalbumin in %. F1) 100 % ZnO and 0 % mannitol; F2) 80 % ZnO and 20 % mannitol; F3) 60 % ZnO and 40 % mannitol; F4) 40 % ZnO and 60 % mannitol; F5) 20 % ZnO and 80 % mannitol; F6) 0 % ZnO and 100 % mannitol. n = 3, \pm = standard deviation.

	OVA	F1	F2	F3	F4	F5	F6
2 min	14.8 \pm 13.2	1.5 \pm 1.9	0.5 \pm 0.4	-0.1 \pm 1.0	0.0 \pm 0.7	0.0 \pm 0.5	0.4 \pm 0.3
5 min	18.8 \pm 12.5	4.7 \pm 2.7	1.9 \pm 0.3	2.4 \pm 1.1	1.4 \pm 1.1	1.2 \pm 1.3	0.9 \pm 0.6
10 min	32.3 \pm 6.8	8.2 \pm 1.9	5.2 \pm 0.7	7.4 \pm 2.1	2.9 \pm 0.9	2.2 \pm 0.8	2.4 \pm 1.1
15 min	37.4 \pm 8.3	10.0 \pm 1.0	7.1 \pm 1.5	8.6 \pm 2.3	2.9 \pm 1.7	2.2 \pm 0.6	3.2 \pm 1.0
30 min	48.4 \pm 6.6	17.4 \pm 2.0	14.0 \pm 5.9	14.5 \pm 2.0	6.2 \pm 1.7	3.1 \pm 0.5	9.6 \pm 2.8
45 min	55.6 \pm 8.9	29.9 \pm 3.7	26.2 \pm 10.6	24.9 \pm 3.8	9.5 \pm 2.0	4.0 \pm 0.7	23.6 \pm 4.5
60 min	60.2 \pm 13.9	34.5 \pm 1.4	33.6 \pm 9.9	27.7 \pm 2.4	11.2 \pm 2.2	5.2 \pm 0.7	31.4 \pm 4.6
120 min	62.4 \pm 8.6	51.1 \pm 9.8	51.3 \pm 9.6	47.5 \pm 5.4	20.9 \pm 4.3	9.5 \pm 1.0	58.3 \pm 7.1
240 min	67.0 \pm 8.8	59.5 \pm 8.0	61.4 \pm 5.1	62.2 \pm 4.7	37.7 \pm 6.5	27.3 \pm 6.7	79.1 \pm 5.1
360 min	75.0 \pm 8.5	70.7 \pm 2.6	67.5 \pm 4.7	71.9 \pm 5.4	52.6 \pm 2.5	46.9 \pm 5.1	84.2 \pm 4.2

The question of why a viscous suspension has formed on the inserts in formulations 4 and 5 needs to be clarified. In addition to the hygroscopicity and osmolality of the formulations, the viscosity of the formulations was also considered.

DVS was used to determine the hygroscopicity of all formulations and thus the ability to absorb water from the environment. In Figure 6.39 the change in mass is plotted for both cycles against the formulations. The corresponding values can be found in Table 6.21. All formulations show an almost identical characteristic curve in cycle 1 and cycle 2, i.e., the mass increases gradually as relative humidity increases and decreases gradually as relative humidity decreases. In both, cycle 1 and cycle 2, no specific events during water sorption and desorption can be seen. With over 2 % mass change at 80 % relative

humidity, all formulations are hygroscopic according to Ph. Eur. classification. In cycle 2 the change in mass for formulations 2 to 5 is smaller than in cycle 1. For formulation 1, change in mass increases minimally from 2.14 % to 2.16 %. Amorphous hydrophilic materials can adsorb water on their surface and absorb water inside. Crystalline materials, on the other hand, adsorb water only on their surface. Therefore, the recrystallisation of a material is accompanied by water loss in the sample and leads to a smaller mass change [240–242]. Since the water loss was usually fast and relatively strong, it could only be a recrystallisation of small percentages in the respective formulations. The diffractograms of X-ray powder diffraction (Figure 6.37) of all formulations were examined again and it is noticeable that only very small amorphous proportions can be involved.

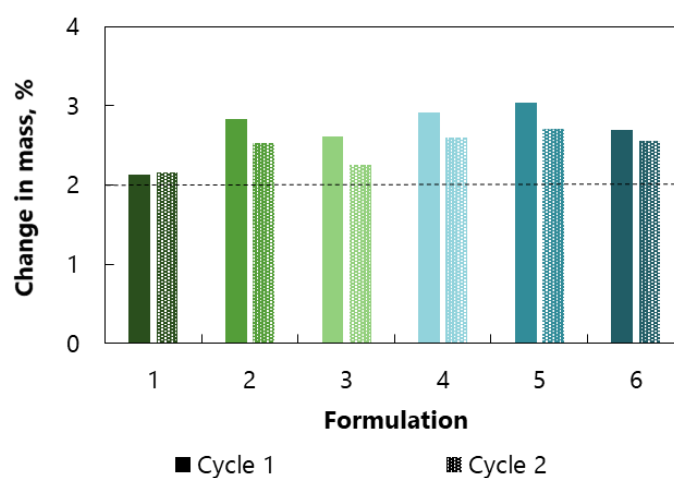


Figure 6.39. Hygroscopicity of all formulations at 80 % relative humidity with two bars showing the change in mass for cycles 1 and cycle 2 of the DVS double tree method. F1) 100 % ZnO and 0 % mannitol; F2) 80 % ZnO and 20 % mannitol; F3) 60 % ZnO and 40 % mannitol; F4) 40 % ZnO and 60 % mannitol; F5) 20 % ZnO and 80 % mannitol; F6) 0 % ZnO and 100 % mannitol. $n = 1$.

Table 6.21. Hygroscopicity of all formulations at 80 % relative humidity showing the change in mass for cycle 1 and cycle 2 using the DVS double tree method. F1) 100 % ZnO and 0 % mannitol; F2) 80 % ZnO and 20 % mannitol; F3) 60 % ZnO and 40 % mannitol; F4) 40 % ZnO and 60 % mannitol; F5) 20 % ZnO and 80 % mannitol; F6) 0 % ZnO and 100 % mannitol. $n = 1$.

	F1	F2	F3	F4	F5	F6
Change in mass (Cycle 1), %	2.14	2.83	2.61	2.92	3.04	2.69
Change in mass (Cycle 2), %	2.16	2.53	2.25	2.59	2.71	2.55

The hygroscopicity probably only had a minor influence on the formation of the viscous suspension in the case of formulations 4 and 5 because the hygroscopic behaviour was very similar in all formulations. The formulations differed slightly in their change in mass during the absorption of water.

Osmolality of all formulations and thus the possibility to pull water through the membrane of the insert was evaluated. With very significant (F3: p-value = 0.0012, F4: p-value = 0.0039, F5: p-value = 0.0063) or highly significant (F2: p-value < 0.0001, F6: p-value = 0.0009) differences in osmolality, all formulations show an increase in osmolality compared to the previous formulation, e.g., formulation 2 is highly significantly different from formulation 1.

The osmolality depends on the number of osmotically active particles in a certain mass of solvent. Zinc oxide as a component of the matrix of the formulations is practically insoluble in water. Mannitol as a component of the matrix of the formulations is dissolved in water and is therefore osmotically active. Ovalbumin and hyaluronic acid were present in all formulations in the same quantity and therefore have only a negligible effect on the different osmolalities of the various formulations. The observation of increasing osmolality can be seen in Figure 6.40 and Table 6.22, the higher the mannitol concentration, the higher the osmotic activity.

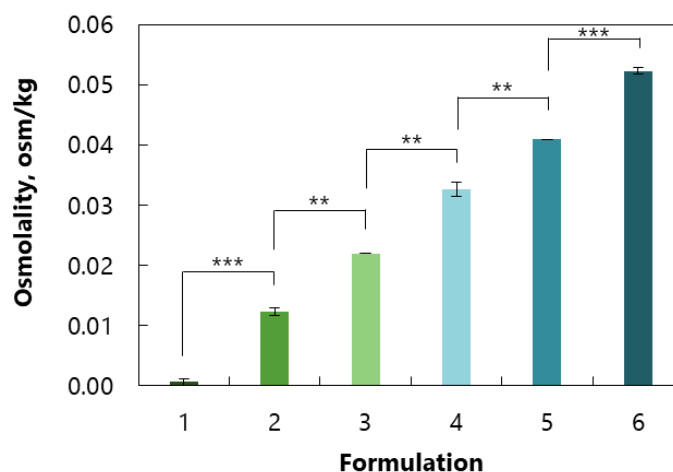


Figure 6.40. Osmolality of all formulations. F1) 100 % ZnO and 0 % mannitol; F2) 80 % ZnO and 20 % mannitol; F3) 60 % ZnO and 40 % mannitol; F4) 40 % ZnO and 60 % mannitol; F5) 20 % ZnO and 80 % mannitol; F6) 0 % ZnO and 100 % mannitol. $n = 3$, error bars = standard deviation, p-value < 0.01 = very significant difference (**), p-value < 0.001 = highly significant difference (***).

These differences in osmolality might explain the viscous residues found during the release experiment for formulations 4 and 5. At the beginning of the experiment, the particles were undissolved and there was no osmotic activity. With progressing time, the mannitol components of the matrix dissolved and the osmolality increased. In the formulations 1 to 3, the zinc oxide portion, which is practically insoluble in water, predominated. In formulations 4 to 6, water soluble mannitol predominated and the osmotic activity increased with increasing mannitol content. In formulation 6 the osmolality was the highest. And, as no insoluble material was present, the dissolved mannitol could diffuse through the membrane and no residue was formed on the insert. In formulations 4 and 5, zinc oxide was present in the matrix. This means that the dissolved mannitol did not immediately diffuse through the membrane, as undissolved zinc oxide blocked the membrane and a viscous suspension could form on the insert. Formulation 4

contained 40 % zinc oxide and 60 % mannitol in the matrix, the osmotic activity was less and the insoluble amount higher than for formulation 5 with 20 % zinc oxide and 80 % mannitol. As a result, there were finally approximately 100 μL on the insert of formulation 4 and 250 μL on the insert of formulation 5.

Table 6.22. Osmolality of all formulations. F1) 100 % ZnO and 0 % mannitol; F2) 80 % ZnO and 20 % mannitol; F3) 60 % ZnO and 40 % mannitol; F4) 40 % ZnO and 60 % mannitol; F5) 20 % ZnO and 80 % mannitol; F6) 0 % ZnO and 100 % mannitol. $n = 3$, \pm = standard deviation.

	F1	F2	F3	F4	F5	F6
Osmolality, osm/kg	0.0007 \pm 0.0006	0.0123 \pm 0.0006	0.0220 \pm 0.0000	0.0327 \pm 0.0012	0.0410 \pm 0.0000	0.0523 \pm 0.0006

To check whether viscosity also influences the release, the viscosity of all formulations and the starting materials, in the maximum concentrations present in the formulations, dissolved or suspended in water were tested. The results of the rheology studies of all formulations in water are shown in Figure 6.41 and Table 6.23. All samples show a pseudoplastic flow behaviour, i.e., the viscosity decreases with increasing shear rate. The initially disordered molecules align themselves with increasing shear rate, which reduces the internal resistance, i.e., a decreased viscosity. Once the orientation process is complete, the viscosity remains constant and a plateau is formed. In order to be able to compare the formulations, the viscosity at the plateau was used for evaluation.

While mannitol and ovalbumin do not lead to an increase in viscosity, and zinc oxide only leads to a minimal increase in viscosity, hyaluronic acid has a strong influence on viscosity. With regard to viscosity, the formulations with higher mannitol content (formulations 4 to 6) have a slightly higher viscosity compared to the formulations with higher zinc oxide content (formulations 1 to 3). However, there is neither a trend in terms of concentrations nor is the difference significant. As observed in the previous experiment with the pure starting materials, there was no correlation between increasing viscosity and differences in the concentrations of mannitol and zinc oxide in the matrix. Hyaluronic acid led to strong increases in viscosity compared to the other starting materials.

Since different pH values exist in the human body, the pH value dependent viscosity change of hyaluronic acid has already been investigated in many ways. As already mentioned in chapter 6.2.1.4, Maleki and coworkers investigated the effect of the pH value on the hyaluronic acid behaviour in different diluted aqueous solutions [234]. If the pH value measurements of the 24-h-solubility study are taken into account, it was noticeable that after 24 h in a sodium chloride solution a constant pH value almost independent of the starting pH was reached with approximately pH 7.6 for the formulations 1 to 5. Formulation 6 showed no plateau, but a slight increase from pH 6.5 to pH 6.9. These

pH values were rather in the neutral than in the low or high pH range. Therefore, the different viscosity of the formulations due to the pH dependent viscosity of hyaluronic acid could not only be explained by the pH value of the solutions.

Burger und coworkers investigated the formation of a zinc (II) complex of hyaluronic acid [243]. Among other things, the viscosity of an aqueous solution of sodium hyaluronate and the corresponding zinc complex was investigated. They found that sodium hyaluronate has a six times higher viscosity than the zinc complex of hyaluronic acid. Zinc (II) ions in the aqueous solution bound to the oxygen-containing donor groups of hyaluronic acid in the pH range between pH 6.0 and pH 6.5. As a result, the random coil structure that led to the formation of a gel could no longer be formed and the viscosity decreased. At pH values starting from pH 4.0 the solubility of zinc oxide in the 24-h solubility study was only 0.01 mg/mL. Nonetheless, this small amount of dissolved zinc might already led to a change in the structure, but had to be investigated further to be confirmed. Furthermore, formulation 6 did not contain zinc oxide, but showed a viscosity similar to all the other formulations.

It can be assumed that both the composition of the formulations and the pH value had the effect that hyaluronic acid could not form its complete random coil structure. Therefore, hyaluronic acid in the formulations did not lead to the same viscosity increase as the pure hyaluronic acid. The formulations have a lower viscosity increase. However, it is less a question of the type and quantity of the different components than of the presence of other substances in much higher concentrations than the hyaluronic acid itself.

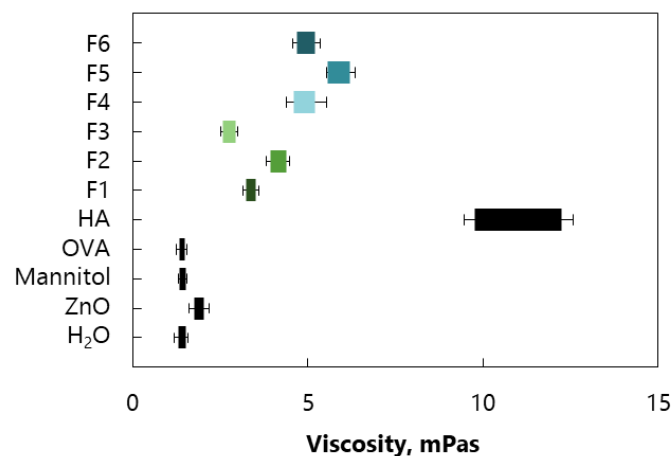


Figure 6.41. Rheology studies of all formulations in water. H₂O, ZnO, Mannitol, OVA and HA are used as references. Viscosity ranges at shear rates from 60 s⁻¹ – 100 s⁻¹ are shown. F1) 100 % ZnO and 0 % mannitol; F2) 80 % ZnO and 20 % mannitol; F3) 60 % ZnO and 40 % mannitol; F4) 40 % ZnO and 60 % mannitol; F5) 20 % ZnO and 80 % mannitol; F6) 0 % ZnO and 100 % mannitol. n = 3, error bars = standard deviation.

Formulations 4 and 5 have, as all the other formulations, a higher viscosity than water. The difference in viscosity between formulation 4 and 5 was only small and not significant. If the detected volume was taken into account, the higher volume of formulation 5 (250 µL) resulted in a lower viscosity compared

to formulation 4 (100 μL), because the amount of hyaluronic acid was the same, but the higher volume reduced the concentration. The small differences in viscosity and concentration would probably compensate each other and there would be no significant difference in the viscosity of the suspension on the insert between formulations 4 and 5.

Table 6.23. Rheology studies of all formulations in water. H₂O, ZnO, Mannitol, OVA and HA are used as references. Viscosity ranges at shear rates from 60 – 100 s⁻¹ are shown. F1) 100 % ZnO and 0 % mannitol; F2) 80 % ZnO and 20 % mannitol; F3) 60 % ZnO and 40 % mannitol; F4) 40 % ZnO and 60 % mannitol; F5) 20 % ZnO and 80 % mannitol; F6) 0 % ZnO and 100 % mannitol. n = 3, \pm = standard deviation.

	H ₂ O	ZnO	Mannitol	HA	OVA	F1	F2	F3	F4	F5	F6
Viscosity (min), mPas	1.29 \pm 0.11	1.75 \pm 0.16	1.32 \pm 0.03	9.75 \pm 0.29	1.32 \pm 0.08	3.23 \pm 0.08	3.93 \pm 0.12	2.55 \pm 0.04	4.78 \pm 0.19	5.57 \pm 0.04	4.70 \pm 0.15
Viscosity (max), mPas	1.51 \pm 0.07	2.02 \pm 0.16	1.50 \pm 0.04	12.23 \pm 0.35	1.49 \pm 0.04	3.50 \pm 0.09	4.38 \pm 0.10	2.92 \pm 0.07	5.21 \pm 0.30	6.19 \pm 0.17	5.21 \pm 0.15

6.2.2.5 Cytotoxicity

The influence of the formulations and zinc oxide on pulmonary cells was evaluated in an in-vitro cell experiment. Specifically, the toxicity on pulmonary epithelial cells (Calu-3) after contact with the formulations was studied. Calu-3 were incubated for 24 h with the formulations as suspensions in different concentrations. In Figure 6.42 and Table 6.24, the LD50 of the formulations are shown. It should be mentioned that after incubation of the cells with the formulations, the formulations in the higher concentrations could not be completely removed from the cells because zinc oxide had very adhesive properties. For this reason, the higher concentrations are not shown and considered for the evaluation of LD50.

With an LD50 of 0.018 mg/mL \pm 0.006 mg/mL (zinc oxide), 0.013 mg/mL \pm 0.005 mg/mL (F1) and 0.010 mg/mL \pm 0.000 mg/mL (F2), zinc oxide as raw material, formulations 1 and 2 show the highest toxicity with no significant difference. With a p-value of 0.0236 (F3) and a p-value of 0.0102 (F4), the toxicity of formulation 3 with 0.031 mg/mL \pm 0.005 mg/mL and of formulation 4 with 0.037 mg/mL \pm 0.006 mg/mL are significantly lower than the toxicity of zinc oxide. Formulation 5 (0.049 mg/mL \pm 0.025 mg/mL) shows no significant differences in toxicity to zinc oxide as raw material. Formulation 6 (4.720 mg/mL \pm 0.570 mg/mL) is very significantly less toxic than zinc oxide with a p-value of 0.0024.

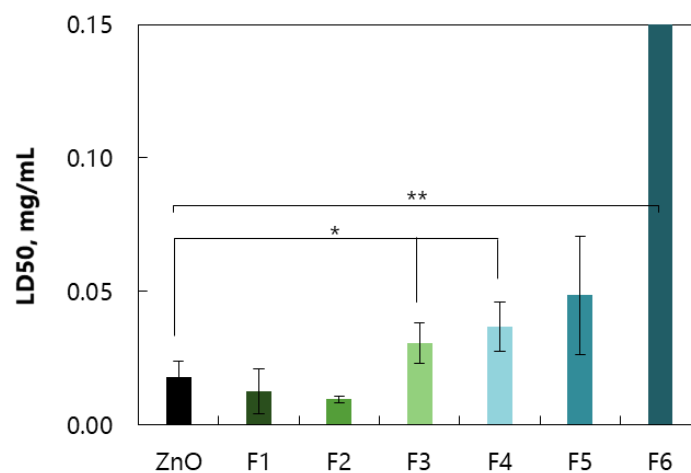


Figure 6.42. LD50 of zinc oxide as raw material (ZnO) in comparison to all formulation in a Calu-3 model. F1) 100 % ZnO and 0 % mannitol; F2) 80 % ZnO and 20 % mannitol; F3) 60 % ZnO and 40 % mannitol; F4) 40 % ZnO and 60 % mannitol; F5) 20 % ZnO and 80 % mannitol; F6) 0 % ZnO and 100 % mannitol. $n = 3$, error bars = standard deviation, p -value < 0.05 = significant difference (*), p -value < 0.01 = very significant difference (**).

Table 6.24. LD50 of zinc oxide as raw material (ZnO) in comparison to all formulation in a Calu-3 model. F1) 100 % ZnO and 0 % mannitol; F2) 80 % ZnO and 20 % mannitol; F3) 60 % ZnO and 40 % mannitol; F4) 40 % ZnO and 60 % mannitol; F5) 20 % ZnO and 80 % mannitol; F6) 0 % ZnO and 100 % mannitol. $n = 3$, \pm = standard deviation.

	ZnO	F1	F2	F3	F4	F5	F6
LD50, mg/mL	0.018 ± 0.006	0.013 ± 0.005	0.010 ± 0.000	0.031 ± 0.005	0.037 ± 0.006	0.049 ± 0.025	4.720 ± 0.570

The LD50 values of zinc oxide and formulations 1 and 2 are not significantly different and increases from formulation 2 to 6, which means that the toxicity decreases. Therefore, the following section will examine whether there is a correlation between toxicity and zinc oxide concentration in the formulations.

For this reason, in Figure 6.43 and Table 11.6 the viability of formulations is considered as a function of the zinc oxide concentration. If the toxicity depends on the zinc oxide concentration, the resulting curves would be similar. As formulation 6 did not contain zinc oxide, it is not included in the graph. All curves show similar graphs. While the viability at a zinc oxide concentration of less than 0.005 mg/mL is almost 100 %, it decreases in the range of 0.005 mg/mL to 0.05 mg/mL to finally almost 30 % viability at concentrations of approximately 0.05 mg/mL. The toxicity is thus mainly dependent on the zinc oxide concentration. However, as in-vitro-cell experiments are living systems, variability can easily occur.

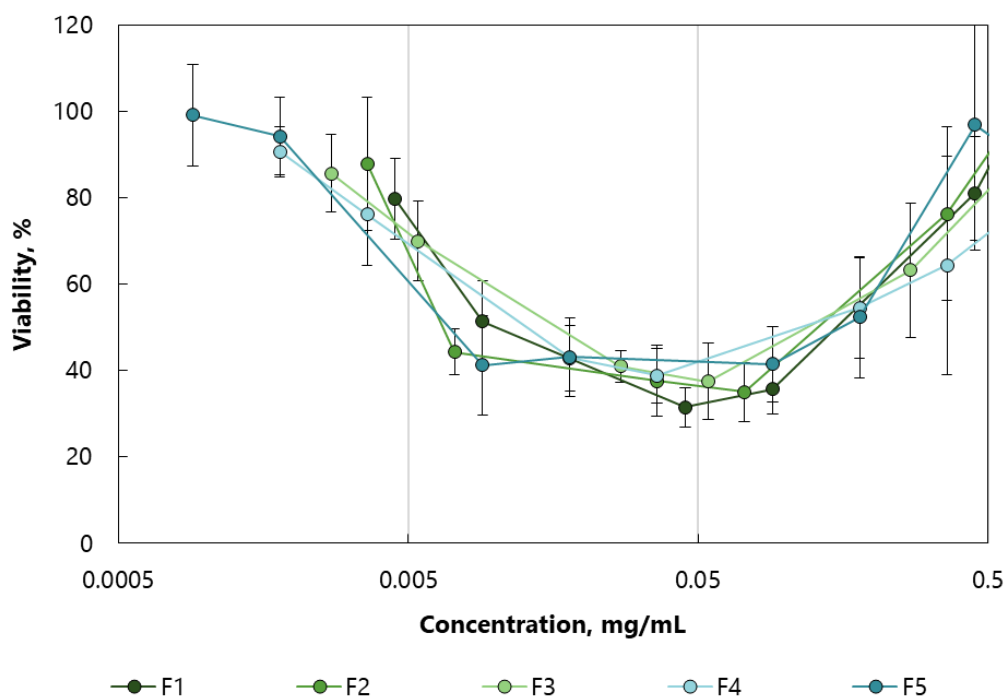


Figure 6.43. Viability as a function of the zinc oxide concentration in all formulations, to identify whether toxicity is dependent on zinc oxide concentrations in the formulation. Zinc oxide as raw material (ZnO) is used as a reference. F1) 100 % ZnO and 0 % mannitol; F2) 80 % ZnO and 20 % mannitol; F3) 60 % ZnO and 40 % mannitol; F4) 40 % ZnO and 60 % mannitol; F5) 20 % ZnO and 80 % mannitol. $n = 3$, error bars = standard deviation.

6.2.2.6 pH – cell culture

After determining the LD50 of each formulation and of zinc oxide, these concentrations of 50 % viability should be used to test the reaction, resulting pH values, of the cells in the air-liquid interface. As shown in the 24-h-solubility study, the zinc oxide concentration had a partial influence on the pH value of a solution or buffer. In order to see whether the formulations and thus the zinc oxide concentration also have an influence on the cells and thus on the resulting pH and whether the reaction of the cells influences the resulting pH, the pH value in in-vitro cell experiments was examined. To ensure that a Calu-3 monolayer had been formed, the TEER was determined at the beginning of the experiments. Measurement of TEER provides a value for the formation of tight junctions and is often used as a marker of disruption [244]. A Calu-3 monolayer usually show a plateau of a TEER value of $300 \Omega/\text{cm}^2$ between day 10 and day 13 in an air-liquid interface [244–246]. After 10 days of growing the Calu-3 monolayer was used. They showed a TEER value of $140.9 \Omega/\text{cm}^2 \pm 89.9 \Omega/\text{cm}^2$, which was a little lower than usually shown. The formulations (formulations 1 to 3) with higher zinc oxide amount and zinc oxide as raw material are shown in Figure 6.44. The formulations with lower zinc oxide content (formulations 4 to 6) and cells without formulation are shown in Figure 6.45. The exact values can be found in Table 6.25.

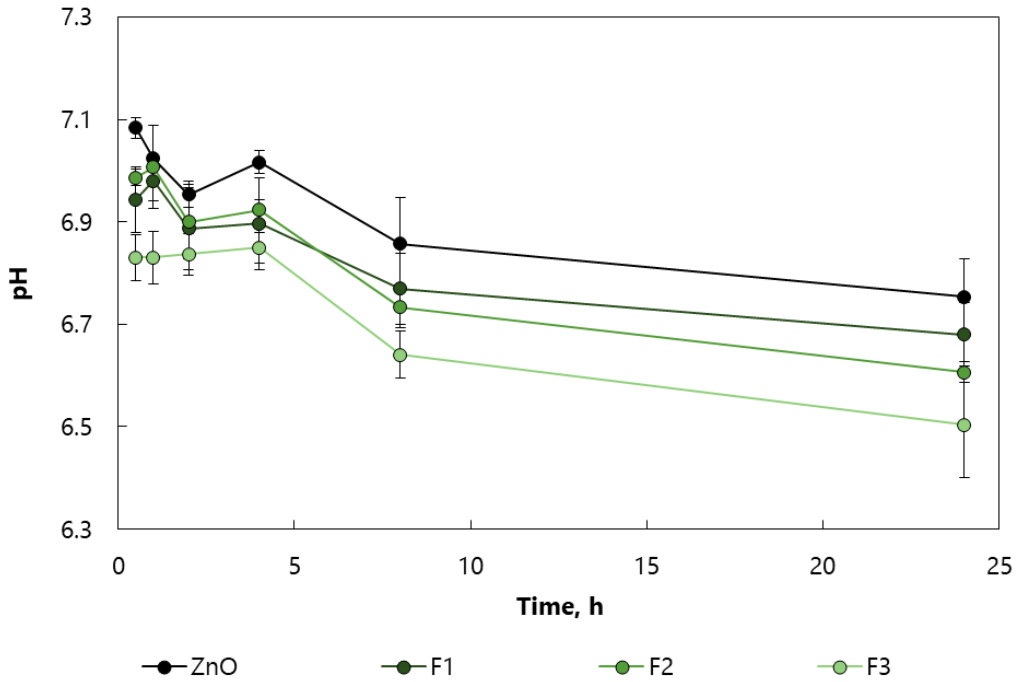


Figure 6.44. The influence of formulations 1, 2 and 3 on pH values in a Calu-3 model. Zinc oxide as raw material is used as reference. F1) 100 % ZnO and 0 % mannitol; F2) 80 % ZnO and 20 % mannitol; F3) 60 % ZnO and 40 % mannitol. $n = 3$, error bars = standard deviation.

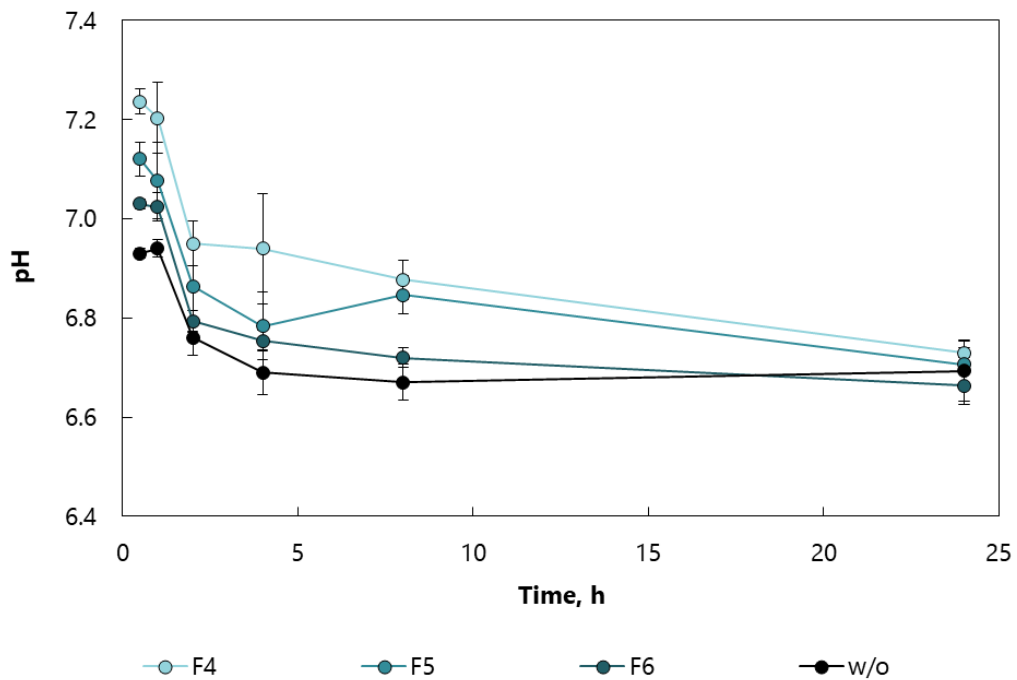


Figure 6.45. The influence of formulations 4, 5 and 6 on pH values in a Calu-3 model. Calu-3 cells without a formulation are used as reference. F4) 40 % ZnO and 60 % mannitol; F5) 20 % ZnO and 80 % mannitol; F6) 0 % ZnO and 100 % mannitol. $n = 3$, error bars = standard deviation.

The formulations with a higher amount of zinc oxide show a plateau at the beginning of the measurement until 4 h, while zinc oxide as raw material creates the highest pH value. The starting pH decreases with decreasing zinc oxide amount. The pH value decreases from 4 h to 24 h for all

formulations. Even after 24 h the pH value is dependent on the zinc oxide concentration, i.e., formulation 3 has the lowest pH value with $\text{pH } 6.50 \pm 0.10$. Formulations 2 with $\text{pH } 6.61 \pm 0.02$ and 1 with $\text{pH } 6.68 \pm 0.06$ follow. The highest pH value is shown by Calu-3 cells with zinc oxide as raw material ($\text{pH } 6.75 \pm 0.08$).

The formulations with a lower content of zinc oxide and the cells without a formulation show a totally different behaviour from formulations with higher zinc oxide content as well as pure zinc oxide. While the pH value is decreasing at the beginning, a plateau is reached after 4 h. Again, the pH value is dependent on the zinc oxide concentration. Formulation 4 has the highest pH value at the beginning ($\text{pH } 7.24 \pm 0.03$) and after 24 h ($\text{pH } 6.73 \pm 0.01$). Formulation 5 show a lower pH value at the beginning ($\text{pH } 7.12 \pm 0.03$) and after 24 h ($\text{pH } 6.71 \pm 0.05$). The lowest pH value at the beginning ($\text{pH } 7.03 \pm 0.01$) and after 24 h ($\text{pH } 6.66 \pm 0.04$) is shown by formulation 6.

Table 6.25. The influence of formulations 1 to 6 on pH values in a Calu-3 model. Calu-3 with zinc oxide as raw material as well as Calu-3 without formulation are used as references. F1) 100 % ZnO and 0 % mannitol; F2) 80 % ZnO and 20 % mannitol; F3) 60 % ZnO and 40 % mannitol; F4) 40 % ZnO and 60 % mannitol; F5) 20 % ZnO and 80 % mannitol; F6) 0 % ZnO and 100 % mannitol. $n = 3$, \pm = standard deviation.

	ZnO	F1	F2	F3	F4	F5	F6	w/o
0.5 h	7.08 ± 0.02	6.94 ± 0.06	6.99 ± 0.02	6.83 ± 0.05	7.24 ± 0.03	7.12 ± 0.03	7.03 ± 0.01	6.93 ± 0.01
1 h	7.02 ± 0.01	6.98 ± 0.04	7.01 ± 0.08	6.83 ± 0.05	7.20 ± 0.07	7.08 ± 0.08	7.02 ± 0.03	6.94 ± 0.02
2 h	6.95 ± 0.03	6.89 ± 0.08	6.90 ± 0.07	6.84 ± 0.04	6.95 ± 0.05	6.86 ± 0.09	6.79 ± 0.02	6.76 ± 0.04
4 h	7.02 ± 0.02	6.90 ± 0.07	6.92 ± 0.02	6.85 ± 0.03	6.94 ± 0.11	6.78 ± 0.07	6.75 ± 0.02	6.69 ± 0.05
8 h	6.86 ± 0.09	6.77 ± 0.07	6.73 ± 0.04	6.64 ± 0.05	6.88 ± 0.04	6.85 ± 0.04	6.72 ± 0.02	6.67 ± 0.04
24 h	6.75 ± 0.08	6.68 ± 0.06	6.61 ± 0.02	6.50 ± 0.10	6.73 ± 0.01	6.71 ± 0.05	6.66 ± 0.04	6.69 ± 0.06

To make sure that these changes in pH were not due to the toxicity of the formulations, the viability was determined visually and the disruption of the monolayer by measuring the TEER. As mentioned before, the Calu-3 monolayer showed a start TEER value of $140.9 \Omega \cdot \text{cm}^2 \pm 89.9 \Omega \cdot \text{cm}^2$. To avoid including the TEER of the insert in the TEER of the cells, the value of the inserts without the cells

($290.0 \Omega \cdot \text{cm}^2 \pm 10.0 \Omega \cdot \text{cm}^2$) was also determined at the beginning and had already been included in the calculations.

A trend in the TEER measurements after 24 h could be assumed and is shown in Figure 6.46 and Table 6.26. While zinc oxide as raw material and formulations 1 to 3 with a higher zinc oxide amount increase the TEER values compared to the starting TEER, the formulations with a higher mannitol amount and the Calu-3 monolayer without a formulation decrease the TEER values compared to the starting TEER. There are also significant differences of the TEER values of the Calu-3 monolayer after 24 h with or without the formulations and with zinc oxide as raw material to the starting TEER.

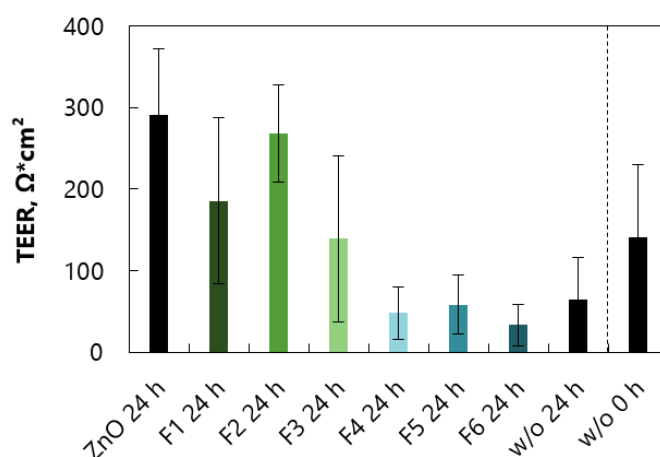


Figure 6.46. Confluency of Calu-3 cell monolayer, measured as TEER value. Calu-3 with zinc oxide as raw material as well as Calu-3 without formulation after 24 h as well as inserts without cells and Calu-3 without formulation at the beginning of the experiment are used as references F1) 100 % ZnO and 0 % mannitol; F2) 80 % ZnO and 20 % mannitol; F3) 60 % ZnO and 40 % mannitol; F4) 40 % ZnO and 60 % mannitol; F5) 20 % ZnO and 80 % mannitol; F6) 0 % ZnO and 100 % mannitol. $n = 3$, error bars = standard deviation.

After 24 h without a formulation, the Calu-3 monolayer shows a significantly different TEER with $64.6 \Omega \cdot \text{cm}^2 \pm 51.6 \Omega \cdot \text{cm}^2$ and a p-value of 0.0465 compared to the starting TEER. Also, formulations 4 with $48.3 \Omega \cdot \text{cm}^2 \pm 32.0 \Omega \cdot \text{cm}^2$ (p-value = 0.0177) and 5 with $58.4 \Omega \cdot \text{cm}^2 \pm 36.1 \Omega \cdot \text{cm}^2$ (p-value = 0.0196) show a significant difference. Formulation 6 with $33.3 \Omega \cdot \text{cm}^2 \pm 25.4 \Omega \cdot \text{cm}^2$ (p-value = 0.0068) and zinc oxide as raw material with $290.6 \Omega \cdot \text{cm}^2 \pm 81.5 \Omega \cdot \text{cm}^2$ (p-value = 0.0021) show a very significantly different TEER to the starting TEER. Formulation 2 with $268.4 \Omega \cdot \text{cm}^2 \pm 59.3 \Omega \cdot \text{cm}^2$ (p-value = 0.0008) and the starting TEER are highly significantly different. Formulations 1 with $185.7 \Omega \cdot \text{cm}^2 \pm 102.2 \Omega \cdot \text{cm}^2$ and 3 with $139.4 \Omega \cdot \text{cm}^2 \pm 101.9 \Omega \cdot \text{cm}^2$ show no significant difference.

Table 6.26. Confluency of Calu-3 cell monolayer, measured as TEER value. Calu-3 with zinc oxide as raw material as well as Calu-3 without formulation after 24 h as well as inserts without cells and Calu-3 without formulation at the beginning of the experiment are used as references F1) 100 % ZnO and 0 % mannitol; F2) 80 % ZnO and 20 % mannitol; F3) 60 % ZnO and 40 % mannitol; F4) 40 % ZnO and 60 % mannitol; F5) 20 % ZnO and 80 % mannitol; F6) 0 % ZnO and 100 % mannitol. $n = 3$, \pm = standard deviation.

	ZnO 24 h	F1 24 h	F2 24 h	F3 24 h	F4 24 h	F5 24 h	F6 24 h	w/o 24 h	w/o 0 h
TEER, $\Omega \cdot \text{cm}^2$	290.6 ± 81.5	185.7 ± 102.2	268.4 ± 59.3	139.4 ± 101.9	48.3 ± 32.0	58.4 ± 36.1	33.3 ± 25.4	64.6 ± 51.6	140.9 ± 89.9

Even if a trend in the data was visible, the visual observation and also the toxicity measurements in chapter 6.2.2.5 would not indicate a toxic effect. The statistical differences in the TEER values after 24 h compared to the TEER values at the beginning indicated rather a disruption of the Calu-3 monolayer when incubating the cells with the formulations with a higher mannitol amount (formulation 4 to 6) and without formulation. It should be mentioned that the start TEER value was relatively low with $140.9 \Omega \cdot \text{cm}^2 \pm 89.9 \Omega \cdot \text{cm}^2$. The TEER values after 24 h of the Calu-3 monolayer incubated with the formulation with a higher zinc oxide amount (formulations 1 to 3) and with zinc oxide would indicate a further formation of the Calu-3 monolayer as the TEER values increased and the cells with zinc oxide reached the TEER value of $300 \Omega \cdot \text{cm}^2$ described for the Calu-3 monolayer.

Calu-3 as an epithelial cell model produces in-vivo characteristics similar to native airways epithelium in terms of differentiation, morphology, polarisation and TEER. The Calu-3 model is investigated in numerous experiments, e.g., to study toxicological effects or transport mechanisms. Ong et al. [247] investigated the effect of mannitol on the transport of ciprofloxacin across respiratory epithelia. They also studied the change in pH on the surface of the Calu-3 monolayer 1 h after adding mannitol. It was shown that the deposition of mannitol increased osmolarity. This in turn increased the transepithelial water flow and lowers the pH value. Furthermore, the stress caused by the increased osmolarity was mentioned as an influencing variable of the ion response of the epithelial cells.

When comparing these results with the pH changes of pulmonary formulations with a higher mannitol content (formulations 4 to 6), certain similarities could be seen. Formulation 6 had the highest mannitol content and showed the lowest pH after 1 h with a pH value of $\text{pH } 7.02 \pm 0.03$. Formulation 4, with a mannitol content of 60 %, had the lowest mannitol content of the three tested formulations, but the highest pH value of $\text{pH } 7.20 \pm 0.07$. An explanation could be found in the increasing osmolality by higher mannitol content. However, the cells without formulation in the same diagram (Figure 6.45) showed an even lower pH value ($\text{pH } 6.94 \pm 0.02$) in comparison to cells incubated with formulation 6. Regardless of the formulation used, all Calu-3 monolayers showed a pH value of about pH 6.7 after 24 h incubation.

In a review of Fischer et al. [248] different mechanism of acid and base secretion by the airway epithelium are summarised. Among other things, it was found that both acid and carbonates are permanently secreted in considerable quantities in the airways. Investigations of different acid transporters were carried out using different molecular and functional approaches. However, a more detailed understanding of the individual acid transporters for the regulation of acidification of the air-liquid interface is still missing.

Looking at the pH changes of the Calu-3 monolayer of the formulations with a higher mannitol amount and without a formulation, a decrease in pH due to acidic metabolic products can nevertheless not be ruled out.

But what causes the differences in cells incubated with the pulmonary formulations? A possible explanation could again be the different amounts of zinc oxide. If the Calu-3 monolayer was alkalisied to a higher pH value by zinc oxide, the cells tried to equalise the pH value again and acidify. In the 24-h-solubility tests, the formulations increased the pH value almost independently of the initial pH value and, depending on the system used, almost independently of the zinc oxide concentration, if zinc oxide was present in the formulation. The Calu-3 air-liquid interface is a living model and not a static experiment in the laboratory. The amount of zinc oxide exposed to the Calu-3 cells affects both the cells and the pH value. The formulations with the higher zinc oxide amount (formulations 1 to 3) led to longer maintenance of the alkaline pH value, because the acidification of the cell did not initially compensate the alkaline effect of the zinc oxide. Again, a connection with the zinc oxide concentration could be seen. While zinc oxide as raw material and formulation 1 with 100 % zinc oxide as matrix show a similar pH value with pH 7.02 ± 0.01 (ZnO) and pH 6.98 ± 0.04 (formulation 1), the pH value of formulation 3 drops to pH 6.83 ± 0.05 . As the experiment progressed, the acidification progresses and hence the cells and consequently also the medium was acidified to a pH value suitable for the cells. Even if a pH value of pH 7.4 is assumed in the lung, the literature reports a repeatable and consistent pH value of about pH 6.6 for the air-liquid interface [248]. Even with small deviations in the experiments, the pH value of approximately pH 6.6 could be recognised as the pH value after 24 h.

6.2.2.7 Loading

The main mission of vaccination is to deliver a certain concentration of the antigen. In order to verify the exact loading of the particles with the antigen, the loading was determined after spray drying via UV/Vis spectroscopy at 205 nm.

Figure 6.47 shows the found concentration of ovalbumin in all formulations after the spray drying process compared to the added concentration of ovalbumin. 0.1 mg ovalbumin per mg formulation was added to all formulations as starting concentration and almost 100 % of the used ovalbumin is recovered after spray drying (Table 6.27). There is no significant difference between individual formulations.

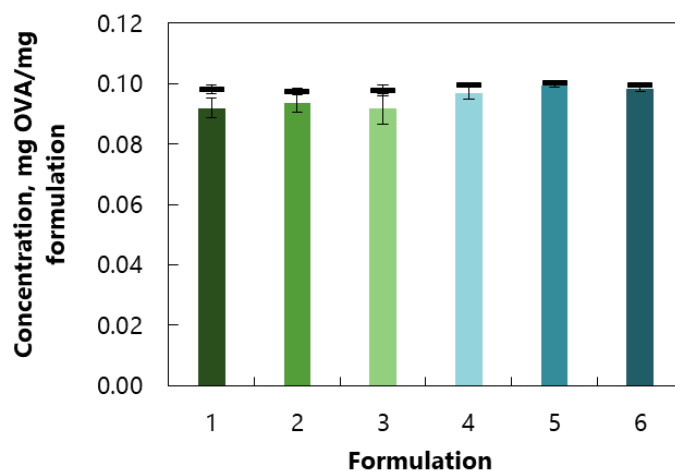


Figure 6.47. Concentration of ovalbumin (coloured bars) in all formulations after the spray drying process in comparison to the used amount of ovalbumin (black bars). 1) 100 % ZnO and 0 % mannitol; 2) 80 % ZnO and 20 % mannitol; 3) 60 % ZnO and 40 % mannitol; 4) 40 % ZnO and 60 % mannitol; 5) 20 % ZnO and 80 % mannitol; 6) 0 % ZnO and 100 % mannitol. $n = 3$, error bars = standard deviation.

Table 6.27. Concentration of ovalbumin in all formulations after the spray drying process in comparison to the used amount of ovalbumin. 1) 100 % ZnO and 0 % mannitol; 2) 80 % ZnO and 20 % mannitol; 3) 60 % ZnO and 40 % mannitol; 4) 40 % ZnO and 60 % mannitol; 5) 20 % ZnO and 80 % mannitol; 6) 0 % ZnO and 100 % mannitol. $n = 3$, \pm = standard deviation.

	F1	F2	F3	F4	F5	F6
Starting concentration, mg OVA/mg formulation	0.098 ± 0.002	0.097 ± 0.001	0.098 ± 0.002	0.100 ± 0.000	0.100 ± 0.001	0.100 ± 0.000
Concentration, mg OVA/mg formulation	0.092 ± 0.003	0.094 ± 0.003	0.092 ± 0.005	0.097 ± 0.002	0.099 ± 0.000	0.098 ± 0.001

Besides loading, the stability of the protein after spray drying is also of interest. In Figure 6.48, representative chromatograms of size exclusion chromatography (graphs) and representative pictures of SDS-PAGE of pure ovalbumin in comparison to all formulations are shown.

The horizontal dotted lines above the peaks show the individual molar mass of the molecules that contributes to the formation of the peak. Pure ovalbumin was used as a reference substance in the SEC measurements and in the SDS-PAGE to see if there is a difference between the starting material and the ovalbumin in the formulation. As reference for the analysis of the SDS-PAGE a marker with the given molecular weights was used additionally (left, white font).

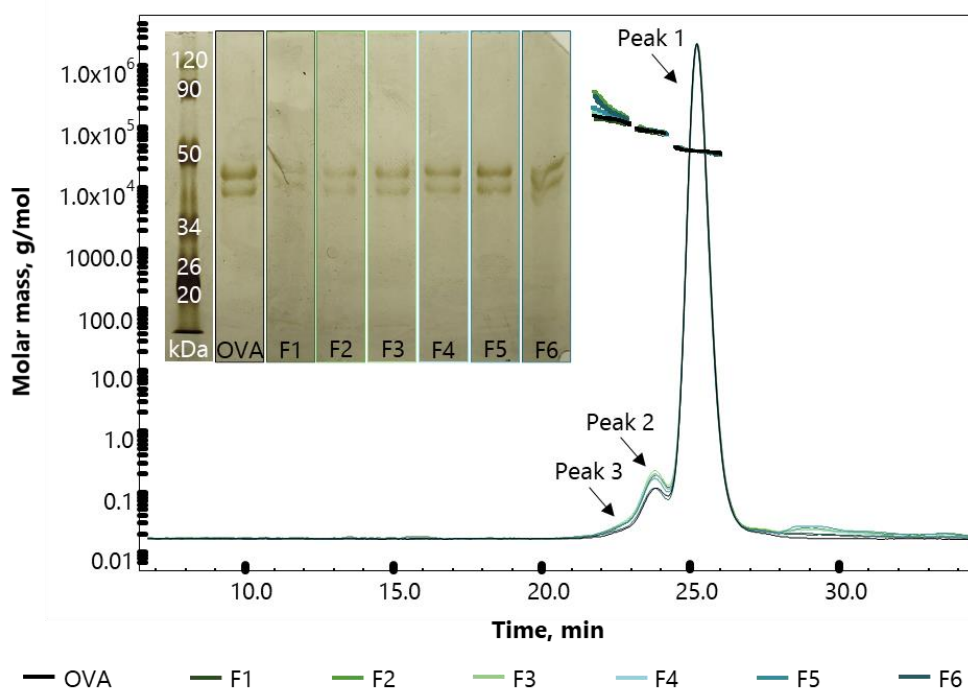


Figure 6.48. Representative chromatograms of size exclusion chromatography and representative pictures of SDS-PAGE of ovalbumin (OVA) as raw material in comparison to all formulations. F1) 100 % ZnO and 0 % mannitol; F2) 80 % ZnO and 20 % mannitol; F3) 60 % ZnO and 40 % mannitol; F4) 40 % ZnO and 60 % mannitol; F5) 20 % ZnO and 80 % mannitol; F6) 0 % ZnO and 100 % mannitol. $n = 1$.

In Table 6.28 the individual peaks of the SEC are analysed from right to left, with peak 1 representing the monomer, peak 2 the dimer and peak 3 the trimer. All peaks are used to calculate the total molecular weight. In Figure 6.48, there is a large peak (peak 1) for ovalbumin (black), a smaller peak (peak 2) in front of it and a shoulder (peak 3) in front of peak 2. The ovalbumin used as starting material consists of monomers, dimers and trimers, whereas the distribution of the molar masses is homogeneous as there is almost no slope visible in the dotted black lines. With a mass recovery of 67.9 %, the monomer (39.8 kDa) makes up the largest part, followed by the dimer (83.1 kDa) with 5.8 % and finally the trimer (127.5 kDa) with 1.0 %. With a total molecular weight of 44.4 kDa 74.8 % of the used amount could be detected with SEC. The question why only 75 % of the ovalbumin could be recovered is already discussed in chapter 6.2.1.6.

All formulations show a curve similar to ovalbumin, i.e., a large peak (peak 1), a smaller peak with a slightly different height (peak 2) and a small shoulder (peak 3) and thus consist of monomers, dimers and trimers. The dotted lines of peak 1 and peak 2 of all formulations are similar to the dotted lines of ovalbumin. The slope of the dotted line of peak 3 of the formulations is higher compared to the dotted line of peak 3 of ovalbumin and varies within the formulations depending on the composition of the formulation. The slope becomes steeper the higher the zinc oxide concentration in the formulation, i.e., the slope is highest for formulation 1 and becomes flatter and flatter until finally the dotted line of

formulation 6 is almost identical to the dotted line of ovalbumin. The distribution is therefore fairly more inhomogeneous in the direction of higher molar masses. This indicates the formation of multimers.

Table 6.28. Representative data of size exclusion chromatography of ovalbumin (OVA) as raw material in comparison to all formulations. F1) 100 % ZnO and 0 % mannitol; F2) 80 % ZnO and 20 % mannitol; F3) 60 % ZnO and 40 % mannitol; F4) 40 % ZnO and 60 % mannitol; F5) 20 % ZnO and 80 % mannitol; F6) 0 % ZnO and 100 % mannitol. n = 1.

	Peak 1		Peak 2		Peak 3		All peaks	
	Molecular weight, kDa	Mass recovery, %	Molecular weight, kDa	Mass recovery, %	Molecular weight, kDa	Mass recovery, %	Molecular weight, kDa	Mass recovery, %
OVA	39.8	67.9	83.1	5.8	127.5	1.0	44.4	74.8
F1	38.4	44.0	79.7	4.8	118.0	1.1	44.2	50.0
F2	39.2	45.6	82.1	5.5	132.1	1.5	46.4	52.8
F3	39.7	44.0	87.4	4.7	189.5	0.9	47.0	49.6
F4	39.2	49.6	83.9	5.9	146.5	1.2	46.2	56.9
F5	39.4	59.2	84.7	6.5	153.4	1.5	46.4	67.3
F6	39.1	50.9	85.8	4.5	175.5	0.8	44.9	56.4

For all formulations, with a mass recovery of 44.0 % to 59.2 %, the monomer (38.4 kDa to 39.7 kDa) makes up the largest part, followed by the dimer (79.7 kDa to 87.4 kDa) with 4.5 % to 6.5 % and finally the trimer (118.0 kDa to 189.5 kDa) with 0.8 % to 1.5 %. With a total molecular weight of 44.2 kDa to 47.0 kDa 49.6 % to 67.3 % of the used amount could be detected. However, a trend in the molecular weights and the mass recovery of the formulations depending on the composition cannot be seen, but all formulations show less mass recovery than pure ovalbumin.

In addition to the SEC graphs, representative pictures from the SDS-PAGE can also be seen in Figure 6.48. Pure ovalbumin shows a doublet between 34 kDa and 50 kDa [238]. All formulations show a similar doublet between 34 kDa and 50 kDa with varying intensities depending on the composition of the matrix. The irregular shape of the doublet of formulation 6 is due to the position in the gel of SDS-PAGE. While the doublet is palest in formulation 1 with the highest content of zinc oxide and without mannitol, the intensity continues to increase until formulation 6 with the highest amount of mannitol and without zinc oxide. Ovalbumin might already be denatured before the measurements. By centrifugation, the denatured ovalbumin would have been separated and can hence not be detected by SDS-PAGE.

If the data from SEC and SDS-PAGE are combined, it became obvious that the composition of the matrix had an influence on the denaturation of the ovalbumin in the formulations. As the amount of mannitol increased, the stabilising effect on ovalbumin during spray drying also increased. The ovalbumin in formulation 6 was thus stabilised and remained largely intact, while the ovalbumin in formulation 1 was denatured.

6.2.2.8 Aerodynamic assessment using the Precise Inhale

To identify the best formulation of the six spray dried formulations for pulmonary application for the finally planned in-vivo studies, the yield, the maximum aerosol concentration and the inhaled aerosol dose was assessed using the Precise Inhale.

Figure 6.49 shows the yield, which is the amount of formulation found on the filter in the in-vitro exposure block after the experiment in relation to the weighed quantity. Figure 6.50 shows the maximum aerosol concentration shown as coloured bars as well as the inhaled aerosol dose shown as dots of all formulations using the Precise Inhale in combination with an impactor nozzle. The same trend can be seen in both diagrams.

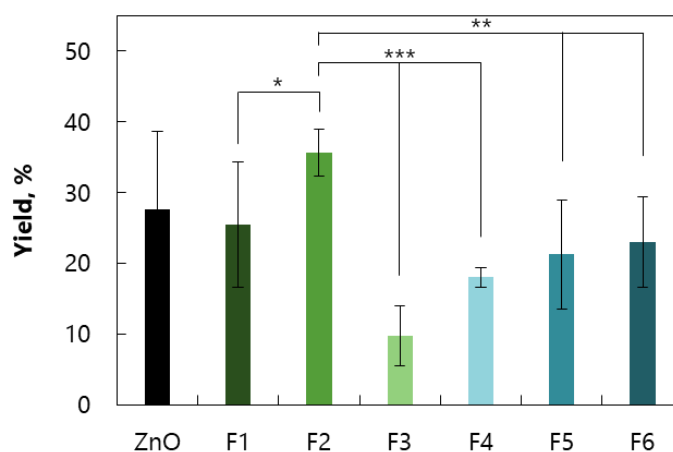


Figure 6.49. Yield of the aerodynamic assessment using the Precise Inhale of zinc oxide as raw material in comparison to all formulations. F1) 100 % ZnO and 0 % mannitol; F2) 80 % ZnO and 20 % mannitol; F3) 60 % ZnO and 40 % mannitol; F4) 40 % ZnO and 60 % mannitol; F5) 20 % ZnO and 80 % mannitol; F6) 0 % ZnO and 100 % mannitol. $n = 5$, error bars = standard deviation, p -value < 0.05 = significant difference (*), p -value < 0.01 = very significant difference (**), p -value < 0.001 = highly significant difference (***)

Formulation 2 shows the highest yield (35.6 % \pm 3.3 %) as well as the highest maximum aerosol concentration (1.87 mg/L \pm 0.26 mg/L) and inhaled aerosol dose (0.488 mg \pm 0.063 mg). Formulation 2 has no significantly higher yield compared to zinc oxide as raw material, a significantly higher yield compared to formulation 1 (p -value = 0.0218), a highly significantly higher yield compared to formulations 3 (p -value < 0.0001) and 4 (p -value < 0.0001) and a very significantly higher yield compared to formulations 5 (p -value = 0.0025) and 6 (p -value = 0.0023).

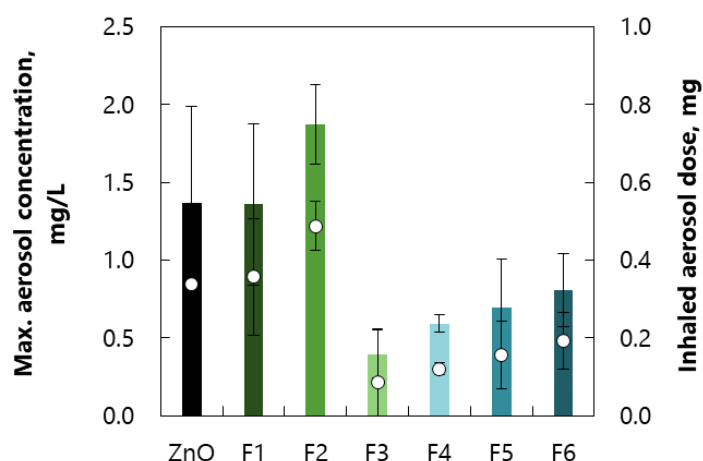


Figure 6.50. Max. aerosol concentration (primary axis) and inhaled aerosol dose (secondary axis) of the aerodynamic assessment using the Precise Inhale of zinc oxide as raw material in comparison to all formulations. F1) 100 % ZnO and 0 % mannitol; F2) 80 % ZnO and 20 % mannitol; F3) 60 % ZnO and 40 % mannitol; F4) 40 % ZnO and 60 % mannitol; F5) 20 % ZnO and 80 % mannitol; F6) 0 % ZnO and 100 % mannitol. $n = 5$, error bars = standard deviation.

Formulation 2 shows no significantly higher maximum aerosol concentration compared to zinc oxide as raw material, but a significantly higher maximum aerosol concentration than formulation 1 (p -value = 0.0409) and highly significant higher values compared to formulations 3 (p -value < 0.0001), 4 (p -value = 0.0001), 5 (p -value < 0.0001) and 6 (p -value < 0.0001). A similar picture is visible for the inhaled aerosol dose. Formulation 2 also has no significantly higher amount compared to zinc oxide as raw material and formulation 1, but highly significantly higher values compared to formulations 3 (p -value = 0.0002), 4 (p -value < 0.0001), 5 (p -value < 0.0001) and 6 (p -value < 0.0001).

Table 6.29. Yield, max. aerosol concentration and inhaled aerosol dose of the aerodynamic assessment using the Precise Inhale of zinc oxide as raw material in comparison to all formulations. F1) 100 % ZnO and 0 % mannitol; F2) 80 % ZnO and 20 % mannitol; F3) 60 % ZnO and 40 % mannitol; F4) 40 % ZnO and 60 % mannitol; F5) 20 % ZnO and 80 % mannitol; F6) 0 % ZnO and 100 % mannitol. $n = 5$, \pm = standard deviation.

	Yield, %	Max. aerosol concentration, mg/L	Inhaled aerosol dose, mg
ZnO	27.7 ± 10.9	1.37 ± 0.34	0.337 ± 0.168
F1	25.5 ± 8.8	1.36 ± 0.52	0.357 ± 0.149
F2	35.6 ± 3.3	1.87 ± 0.26	0.488 ± 0.063
F3	9.7 ± 4.2	0.40 ± 0.16	0.085 ± 0.137
F4	18.0 ± 1.4	0.59 ± 0.06	0.120 ± 0.015
F5	21.2 ± 7.7	0.70 ± 0.31	0.155 ± 0.087
F6	23.1 ± 6.4	0.81 ± 0.23	0.192 ± 0.073

Since the yield as well as the maximum aerosol concentration and the inhaled aerosol dose should be as high as possible for the final in-vivo experiments, formulation 2 was further investigated in the following immunological in-vitro cell experiments. A maximum yield of approximately 35 % for formulation 2 was not really a high yield, which could lead to problems, i.e., too low concentrations of the formulation deposited in the lungs or too many experiments for the right dose in in-vivo experiments. This would not only lead to insufficient immunisation but also to an unacceptable stress for the animals. A production of smaller spray dried particles for pulmonary application increased the yield for formulation 2 from 35.6 % \pm 3.3 % to 51.4 % \pm 15.5 %, again showing the best performance. However, since the formulations had to be suspended anyway for the immunological in-vitro cell experiments and the composition of the particles is the same regardless of the particle size, formulation 2 could be used in the following cell activation experiments in the particle size of the results shown.

6.2.2.9 Cell activation experiment

Since formulation 2 showed the highest yield as well as the maximum aerosol concentration and the inhaled aerosol dose, the cell activation experiments were performed with formulation 2. BMDC obtained from female CF57BL/6N mice were evaluated after incubation with a negative control (RPMI), a positive control (10 ng LPS), the antigen (5 μ g ovalbumin) and formulation 2. Formulation 2 was tested in three different concentrations: 50 μ g, 25 μ g and 10 μ g per well. 50 μ g per well was chosen as the highest concentration, as this amount contains 4.5 μ g ovalbumin and thus approximately corresponded to the concentration of ovalbumin used as pure antigen control. The up-regulation of four different markers (CD40, CD80, CD86 and MHC-II) and thus the stimulation of the dendritic cells was examined after staining with fluorescent dyes using flow cytometry.

CD40 is known as a marker for B cell activation, CD86 for early DC maturation and CD80 for late DC maturation. In general, dendritic cells only have the ability to take up antigens in tissues. Once they have migrated into the lymphatic system, they lose this property and begin to mature and activate T cells. CD80 and CD86 are two important costimulatory molecules in this process. They are induced in response to contact with pathogens. They interact with receptors on the T cells, e.g., the best known costimulatory receptor CD28. To be activated, a naive T cell has to recognise both the antigen and a costimulatory ligand on the same antigen presenting cell. The signals from CD28 then support antigen dependent activation of T cells primarily by promoting T cell proliferation, cytokine production and cell survival. While CD28 is the primary costimulatory receptor for naive T cells, CD40 is the primary receptor for naive B cells. CD40 activates both the NF κ B and PI-3 kinase pathways after receptor stimulation. NF κ B activation enhances cell survival and PI-3 kinase shows a wide range of effects on B cell physiology. Generally speaking, the function of CD28 for the T cells corresponds to the function of CD40 on the B cells [171].

While CD80 and CD86 are expressed during DC maturation, the number of MHC molecules on the cell surface is increased. MHC-I molecules and MHC-II molecules are found on different cell types, but both are found on dendritic cells in lymphoid tissue. While MHC-I molecules present peptides from pathogens to the cytotoxic CD8 T cells and therefore all cells with these peptides are killed, CD4 T cells recognise the peptides presented by MHC-II molecules and thereby activate other effector cells of the immune system [171]. The stimulated CD4 T cells induce the development of IgA bound B cells in the lymphoid follicle. After maturation, these B cells migrate from the MALT to the regional cervical lymph nodes. Finally, antigen-specific CD4 T cells and IgA-positive B cells migrate to the effector sites [26].

Figure 6.51 and Table 6.30 show the results of the cell activation experiments. Based on the negative and positive control, it can be seen that the experiments are valid for all markers, since the negative control is lower than the positive control.

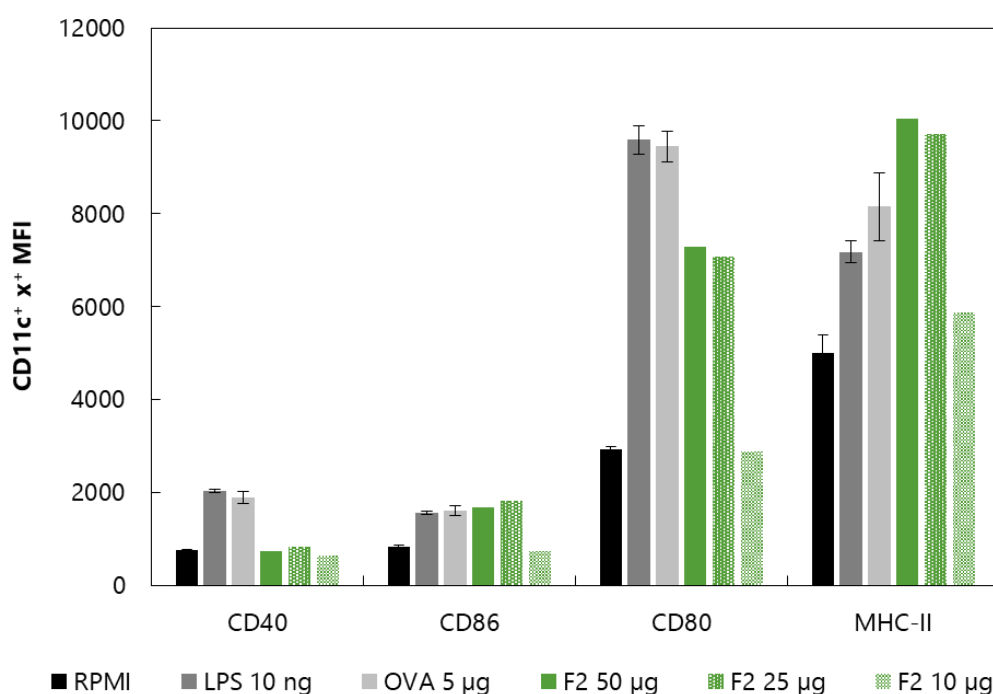


Figure 6.51. Immunological in-vitro cell experiments of formulation 2 in a BMDC model; F2) 80 % ZnO and 20 % mannitol. RPMI, LPS, OVA: $n = 2$, error bars = min/max; F2: $n = 1$.

Ovalbumin as antigen shows values comparable to the positive control, although the concentration used is many times higher. The different immunological markers give different values for the negative control, the positive control and the antigen. The fluorescent markers used for the immunological markers were excited at the same wavelength, but showed different fluorescence strengths, which explained the different MFI values of the controls. If formulation 2 is now examined in different concentrations with the different markers, differences can be seen. The different concentrations of formulation 2 do not show any increase in CD40 compared to the negative control. For CD86, formulation 2 at 25 µg and 50 µg shows similarly high values as the positive controls and the antigen and at 10 µg comparable values with

the negative control. Also, for CD80, the lowest concentration of formulation 2 shows comparable values with the negative control and the two higher concentrations of 25 µg and 50 µg show higher values than the negative control but lower values than the positive control and the antigen. For MHC-II, formulation 2 at the lowest concentration of 10 µg shows slightly higher values than the negative control and the two higher concentrations of 25 µg and 50 µg show higher values than the positive control and the antigen. It is important to note that the measured values of formulation 2 are only a single determination and therefore only a tendency could be identified from the data and not an absolute statement.

Table 6.30. Immunological in-vitro cell experiments of formulation 2 in a BMDC model; F2) 80 % ZnO and 20 % mannitol. RPMI, LPS, OVA: n = 2, ± = min/max; F2: n = 1.

	CD11c ⁺ x ⁺ MFI			
	CD40	CD86	CD80	MHC-II
RPMI	763.5 ± 3.5	826.0 ± 43.0	2,930.5 ± 63.5	5,005.5 ± 329.5
LPS 10 ng	2,041.0 ± 36.0	1,567.5 ± 33.5	9,589.0 ± 306.0	7,180.0 ± 245.0
OVA 5 µg	1,883.0 ± 127.0	1,605.0 ± 110.0	9,449.5 ± 324.5	8,150.0 ± 725.0
F2 50 µg	731.0	1,687.0	7,282.0	1,0056.0
F2 25 µg	826.0	1,812.0	7,071.0	9,717.0
F2 10 µg	637.0	728.0	2,881.0	5,863.0

As already mentioned, zinc oxide has many different applications. Roy and coworker investigated the immunomodulating effect of zinc oxide in their study [249]. The effect of zinc oxide was investigated in mice sensitised with ovalbumin. In addition to the increased proliferation of T cells compared to the control, a high expression of MHC-II molecules could also be observed. Transferring the results of the study to in-vitro cell experiments, the adjuvant effect of zinc oxide would be based on the increase of CD80 and CD86 and thus a theoretically increased proliferation of T cells and the high expression of MHC-II molecules. These expectations are reflected by the results of the in-vitro cell experiments. While MHC-II shows an increased expression compared to the antigen when using formulation 2, an increase is seen for CD80 and CD86 compared to the negative control. Thus, an activation of the dendritic cells can be observed for MHC-II as well as for CD80 and CD86. It is striking that there is almost no difference between 25 µg and 50 µg. For this purpose, the composition of formulation 2 had to be considered. The matrix consisted of 80 % zinc oxide and 20 % mannitol. Furthermore, it contained additional 10 % ovalbumin and 1 % hyaluronic acid. While 50 µg of formulation 2 per well contained approximately

36 µg zinc oxide and 4.5 µg ovalbumin, 25 µg of formulation 2 per well contained approximately 18 µg zinc oxide and 2.25 µg ovalbumin. On the one hand, the different concentrations of zinc oxide had different toxic effects on the dendritic cells and on the other hand, the basic level of activation of the dendritic cells by the antigen varied. While for 50 µg of formulation 2 5 µg ovalbumin could be considered as the reference concentration, for 25 µg of formulation 2 the reference concentration of the antigen has to be lower. In addition, as already shown in the toxicity studies, zinc oxide had a toxic effect at higher concentrations. Of course, the toxicity studies of the Calu-3 cells could not be applied one-to-one to the BMDC, but the trend was similar, i.e., toxicity increases or viability decreases with increasing concentration, i.e., 37.5 % viability for 50 µg and 45.8 % viability for 25 µg of formulation 2 per well. If the data are examined more closely, the adjuvant effect is probably higher at 25 µg per well than at 50 µg per well, since the toxic effect of the zinc oxide is higher at the higher concentration and thus the possibly higher immune response is masked by the higher toxicity. No adjuvant effect or activation of the BMDC is observed with CD40.

An adjuvant effect of the zinc oxide in formulation 2 can be assumed on the basis of the cell activation experiments through the expression of CD80, CD86 and MHC-II. However, a final statement is only possible when the formulations are tested in in-vivo studies. These studies had already been planned, but could not be carried out within the context of this thesis due to the COVID-19 pandemic. Nevertheless, the in-vitro experiments are a first indication for an adjuvant effect.

6.2.2.10 Summary and conclusion

By spray drying, it was not only possible to produce particles for nasal application, but also for pulmonary administration with a defined particle size < 5 µm. Zinc oxide was spray dried together with hyaluronic acid, ovalbumin and mannitol in water. A total of six different formulations was prepared with different concentrations of zinc oxide and mannitol. The matrix of formulation 1 consisted of 100 % zinc oxide and that of formulation 6 of 100 % mannitol. The concentrations of hyaluronic acid and ovalbumin remained constant.

All formulations formed dry white powder after spray drying with almost no visible differences in particle size and particle size distribution, but visible differences in morphology. Formulations 1, 2 and 6 showed the typical spherical shape of spray dried particles, with formulations 1 and 2 showing an irregular and formulation 6 a smooth surface. All other formulations had wrinkled particles in a mixture with spherical particles. The difference in composition was visible by the decreasing proportion of zinc oxide particles present from formulation 1 (100 % zinc oxide) to formulation 6 (0 % zinc oxide). Measurements of the particle size distribution with the RODOS module showed an x50 smaller than 5 µm for all formulations and an x90 of almost 5 µm for formulation 1. When measuring the particle size distribution with the INHALER module in combination with the Cyclohaler, formulation 6 had almost 65 % of the particles

smaller than 5 μm , formulations 2, 3, 4 and 5 had 40 % to 50 % of particles smaller than 10 μm and formulation 1 had almost 35 % of the particles smaller than 5 μm .

With more than 30 %, formulations 4, 5 and 6 showed higher fine particle fraction compared to formulations 1, 2 and 3 with less than 30 % of the delivered dose smaller than 5 μm (aerodynamic diameter). An NGI was used in combination with the mouthpiece, the throat, the preseparator and the Cyclohaler for aerodynamic characterisation.

To stimulate an immune response in the respiratory tract, an antigen has to be taken up in a particulate form by antigen presenting cells. For this reason, the amount of dissolved zinc oxide in different media was investigated. Sodium chloride solutions and phosphate buffers with different pH levels were prepared to mimic relevant pH conditions in the human body. In addition, simulated lung fluid was tested, which took account of the salt and pH conditions in the lungs. In addition to the solubility, the influence of zinc oxide (dissolved or undissolved) on the pH values after 24 h was also investigated. Formulation 1, as representative sample, was slightly soluble in pH 1.2, very slightly soluble in pH 2.5 and practically insoluble in pH values above pH 2.5, both in sodium chloride solution and in phosphate buffer. Similar to sodium chloride solution and phosphate buffer formulation 1 was also practically insoluble in simulated lung fluid. After 24 h, the pH value increased depending on the starting pH value in the phosphate buffer, while the zinc oxide content had an influence on the pH change: the higher the zinc oxide amount, the stronger the pH shift. In both the sodium chloride solution and simulated lung fluid, the pH value reached a plateau of approximately pH 7.5 after 24 h with the formulations for formulations 1 to 5 and of approximately pH 6.5 to pH 6.9 for formulation 6.

After the solubility of the individual formulations was investigated in relation to zinc oxide, the release of ovalbumin from the formulations was also examined. While ovalbumin as reference showed a first-order dissolution kinetic and formulation 6 showed a first-order release kinetic, formulations 4 and 5 followed a zero-order release kinetic and formulations 1, 2 and 3 a Higuchi release kinetic. The type of release therefore depended on the concentration of zinc oxide in the formulation, with a difference between formulations containing primarily zinc oxide as a matrix (formulations 1, 2 and 3), formulations containing less zinc oxide than mannitol as a matrix (formulations 4 and 5) and the formulation containing no zinc oxide as a matrix (formulation 6).

The concentration of zinc oxide played also an important role in the toxicity tests of the formulations. After 24 h incubation of Calu-3 with the formulations, the LD50 increased from formulation 1 to formulation 6, i.e., the toxicity decreased from formulation 1 to formulation 6 and is thus dependent on the zinc oxide concentration. The determined LD50 were used to test the resulting pH values of the cells in the air-liquid interface. All formulations showed a decreased pH value after 24 h. The formulations with a higher amount of zinc oxide (formulations 1, 2 and 3) had a pH value plateau at the beginning of

the measurement until 4 h with the highest pH value for formulation 1 with the highest zinc oxide amount. The formulations with a lower content of zinc oxide (formulations 4, 5 and 6) had a pH value plateau after 4 h. Again, the pH value was dependent on the zinc oxide concentration.

The goal of spray drying with water as solvent was to increase the recovery of the protein loading from 50 % to 100 % to use the pulmonary formulation, e.g., in in-vivo experiments to investigate pulmonary immunisation in mice. Almost 100 % of the used ovalbumin was recovered for all formulations after spray drying. SEC and SDS-PAGE were used to investigate the stability of the ovalbumin. The composition of the matrix had an influence on the denaturation of the ovalbumin in all formulations. As the amount of mannitol increased, the stabilising effect on ovalbumin during spray drying also increased.

In conclusion, the increase in recovery of the protein loading from 50 % to 100 % of the used ovalbumin was successful. The composition of the matrix and thus the zinc oxide concentration had an influence on almost all experiments. In order to identify the optimal formulation for in-vivo experiments to investigate pulmonary immunisation in mice, in-vitro cell experiments were first necessary. Here, different immunological cell markers were examined to give an indication of an immunological effect in-vivo. In the cell activation experiments, the higher expression of MHC-II and the expression of CD80 and CD86 indicated an activation of the used BMDC. The possibility of using zinc oxide as an alternative adjuvant for mucosal immunisation should finally be tested in an in-vivo mouse model.

7 Conclusion and outlook

Mucosal immunisation via the respiratory tract is one non-invasive chance to prevent infectious diseases, especially as it mimics the natural entry of antigens that usually have their first contact with the nasal or pulmonary mucosa when entering the human body. In order to obtain an immune response from an antigen that is not sufficiently immunogenic, it has to be combined with an adjuvant. In this thesis, zinc oxide in formulation for respiratory vaccination was investigated.

In the first part of the thesis, the adsorption properties of different zinc oxides were investigated. The adsorption of different proteins on zinc oxide tetrapods and zinc oxide in relation to their production method, their shape and their particle size was examined in more detail. It was found that the short milled zinc oxide tetrapods showed the best adsorption capacity, probably due to a combination of the production method, the shape and the particle size.

In the second part of the thesis, spray dried formulations with different concentrations of zinc oxide and mannitol and constant concentrations of ovalbumin and hyaluronic acid were prepared and characterised. Initially, nasal formulations with a target particle size $> 10 \mu\text{m}$ were prepared. Only 50 % of the ovalbumin used could be recovered in the spray dried formulations and the use of acetic acid (2 %) as a solvent or suspending agent in the spray drying process led to repeated difficulties in the characterisation. Acetic acid (2 %) was replaced by water and pulmonary formulations with a target particle size $< 5 \mu\text{m}$ were prepared and characterised in the same way. Both, the goal of increasing protein loading to a recovery of 100 % and the aim of eliminating the problems caused by acetic acid (2 %), were achieved. The matrix composition of different concentrations of zinc oxide and mannitol had an influence in almost all experiments. Formulation 2 was identified as the formulation best suited for in-vivo studies in terms of the aerodynamic performance. In in-vitro immunological cell studies with BMDC and formulation 2, the expression in CD80 and CD86 as well as the higher expression in MHC-II indicated DC maturation.

In summary, pulmonary formulation 2 had the most promising properties with regard to mucosal vaccination via the respiratory tract. However, since all the experiments had so far only been conducted in-vitro, it remained to be seen whether the promising properties will persist in-vivo.

In in-vivo mice experiments, it will be tested whether pulmonary formulation 2 also retains the most promising properties in-vivo and can be finally identified as the formulation with the "right" concentration of zinc oxide for the use as an alternative adjuvant for mucosal vaccination via the respiratory tract.

For the in-vivo studies, the immune response in mice vaccinated subcutaneously with formulations 2, 3 and 4 will be tested. For this purpose, 36 6-week-old, female, C57BL/6 mice will be necessary. These mice

will be divided into six groups of six mice each and vaccinated subcutaneously with 200 μ L each in week 0, 2 and 4. Group A will be again divided into two subgroups, whereby three mice will be vaccinated with 10 μ g ovalbumin and three mice with saline. They will be used as negative control. Group B vaccinated with 10 μ g ovalbumin and CAF01 (250 μ g DDA/ 50 μ g TDB) and group C with 10 μ g ovalbumin and Alhydrogel (500 μ g) will be used as positive control. Group D will be vaccinated with pulmonary formulation 2, group E with pulmonary formulation 3 and group F with pulmonary formulation 4, with the amount of powder adjusted to finally contain 10 μ g ovalbumin. Two weeks after the third immunisation, spleen, blood and lymph nodes will be collected and different antibodies, cytokines and markers will be analysed. The formulation performing best in the immunological in-vivo studies using subcutaneous vaccination should then be investigated in an immunological in-vivo study using pulmonary vaccination.

The next steps will certainly depend on the extent to which an immunological response can be induced in the in-vivo studies. If an immunological reaction can be observed, the model antigen ovalbumin should be replaced by other antigens in order to see which relevant properties an antigen must have in order to induce an immune response with zinc oxide as an adjuvant.

More or less independent from the in-vivo results is the exchange of the starting material. If the case occurs that no immune reaction can be observed, the exchange of zinc oxide could possibly lead to an immune reaction. However, if an immune response can be observed, replacement of zinc oxide could result in further understanding of the immune response. In this context it would be interesting to standardise the zinc oxide tetrapods and investigate them further as a potential adjuvant. Also, the influence of particle size of zinc oxide on the immunological response would also be another interesting point, as an adjuvant effect has already been described for nanoparticles [249].

In addition to the starting material, other formulation options could also be further investigated to obtain or increase the immune reaction. Although formulation development was the main focus of this thesis, the development of new inhalers for immunisation should also not be lost sight of. An interaction of the optimal formulation with an optimal inhaler would ultimately lead to an optimum immunisation via the respiratory tract.

8 Abstract

Active immunisation is the best option to prevent infectious diseases. Intramuscular application is the most commonly used administration route, because of systemic immune response and exact dosing possibilities. Due to its low cost and good effect, aluminium salts are the most frequently used adjuvants in adsorbate vaccines to enhance the immune response of an attenuated antigen or antigen components. While intramuscular administration requires the use of a needle and a sterile dosage form, mucosal immunisation is one opportunity of non-invasive administration. The respiratory tract comprises numerous immune competent cells as part of the MALT and thereby represents an excellent possibility to induce both local and systemic immune response. Since aluminium salts are ineffective as adjuvant on the mucosa, this work focussed on zinc oxide in formulations for respiratory vaccination.

Zinc oxide is well characterised in a number of clinical studies and has many different uses. An immunomodulating effect of zinc oxide based on an increasing proliferation of T cells and high expression of MHC-II molecules is described in a number of papers. A special form of zinc oxide are the zinc oxide tetrapods. They have a three-dimensional tetrapodial structure and the potential uses are manifold due to their properties. Worth mentioning is the potential application as a prophylactic, preventive and/or adjuvant formulation for viral infection as they have among other things the ability to bind antigens. Viruses bound to zinc oxide tetrapods can therefore be absorbed by antigen-presenting cells in the mucosa and then presented to activate the immune system.

In adsorption studies the adsorption capacity of zinc oxide, zinc oxide tetrapods, short milled and long milled zinc oxide tetrapods with five different proteins with varying isoelectric points and different molecular weights were investigated. While the zinc oxide tetrapods were able to adsorb mainly positively charged proteins due to their negatively charged surface, there was no discernible difference in the case of zinc oxide. All materials showed higher adsorption capacities towards the proteins with smaller molecular weights.

Formulations for the delivery to the respiratory tract with zinc oxide were spray dried for nasal and pulmonary administration. Six different formulations with various amounts of zinc oxide were produced for each application route. Mannitol and hyaluronic acid were used as additional excipient and ovalbumin served as model antigen. Since spray drying with acetic acid (2 %) for the nasal formulations led to numerous difficulties in characterisation and undesired properties, the pulmonary formulations were spray dried with water as suspension medium. After spray drying, all six formulations were white powders with an x50 smaller than 5 μm and almost 100 % of the ovalbumin used was recovered. The composition of the formulation and thus the zinc oxide concentration had an influence on almost all experiments. Finally, cell activation experiments were performed to investigate whether zinc oxide presented its adjuvant effect when formulated as dry powder. Since formulation 2 showed the best

aerodynamic properties for in-vivo studies, it was therefore used as example. The expression of CD80, CD86 and MHC-II indicated an activation of the used murine bone marrow-derived dendritic cells. The use of zinc oxide as an adjuvant thus appeared to be possible but needs to be further elucidated in in-vivo studies.

9 Zusammenfassung

Aktive Immunisierung ist die beste Möglichkeit Infektionskrankheiten zu verhindern. Neben der intramuskulären Gabe, die aufgrund der systemischen Immunantwort und der exakten Dosierungsmöglichkeit den beliebtesten Weg darstellt, gibt es zahlreiche nadelfreie Alternativen, die immer mehr an Interesse gewinnen. Die nicht-invasive Gabe und die dadurch entstehende Möglichkeit der Formulierung nicht steriler Darreichungsformen sind nur zwei Vorteile, die mit den alternativen kutanen und mukosalen Immunisierungswegen einhergehen. Der Respirationstrakt umfasst als Eintrittspforte der meisten Antigene und als Teil des Schleimhaut-assoziierten lymphatischen Gewebes zahlreiche immunkompetente Zellen und stellt damit eine hervorragende Chance dar, sowohl eine lokale als auch eine systemische Immunantwort zu induzieren. Die für die Immunisierung verwendeten abgeschwächten Antigenen oder Antigenkomponenten benötigen ein Adjuvans um die Immunantwort zu verstärken. Aluminiumsalze zählen hierbei zu den am häufigsten verwendeten Adjuvantien, u.a. aufgrund ihrer geringen Kosten und der guten Wirksamkeit. Die sogenannten Adsorbatimpfstoffe, die die abgeschwächten Antigene adsorbiert an Aluminiumsalzen enthalten, sind jedoch auf der Schleimhaut unwirksam. Im Rahmen dieser Arbeit wird Zinkoxid als Bestandteil von Formulierungen für die Immunisierung über den Respirationstrakt zunächst auf seine Adsorptionseigenschaften untersucht und anschließend als sprühgetrocknete Formulierungen charakterisiert und in in-vitro Zellexperimenten in Hinblick auf seine immunologische Aktivierung analysiert.

Zinkoxid ist in einer Reihe klinischer Studien gut charakterisiert und hat viele verschiedene Anwendungsmöglichkeiten. Eine immunmodulierende Wirkung von Zinkoxid, die auf einer erhöhten Proliferation von T-Zellen und einer hohen Expression von MHC-II-Molekülen beruht, wird in zahlreichen Arbeiten beschrieben. Eine spezielle Form des Zinkoxids sind die Zinkoxid Tetrapoden, die eine dreidimensionale Tetrapodenstruktur aufweisen und deren Einsatzmöglichkeiten aufgrund ihrer Eigenschaften vielfältig sind. Besonders interessant ist im Kontext der Arbeit die mögliche Anwendung als prophylaktische, präventive und/oder adjuvante Formulierung bei viralen Infektionen, da sie z.B. die Fähigkeit besitzen, Antigene zu binden. An Zinkoxid Tetrapoden gebundene Viren können dann von Antigen-präsentierenden Zellen in der Schleimhaut aufgenommen und zur Aktivierung des Immunsystems präsentiert werden.

In Adsorptionsstudien wurde zunächst die Adsorptionskapazität von Zinkoxid, den Zinkoxid Tetrapoden sowie kurz gemahlten und lang gemahlten Zinkoxid Tetrapoden mit fünf verschiedenen Proteinen mit unterschiedlichen isoelektrischen Punkten und Molekularmassen untersucht. Während die Zinkoxid Tetrapoden aufgrund ihrer negativ geladenen Oberfläche vor allem positiv geladene Proteine adsorbierten, gab es beim Zinkoxid keinen erkennbaren Unterschied in Hinblick auf die verschiedenen

isoelektrischen Punkte der Proteine. Alle Materialien zeigten höhere Adsorptionskapazitäten gegenüber den Proteinen mit kleineren Molekularmassen.

Mithilfe der Sprühtrocknung wurden sowohl nasale als auch pulmonale Pulvern hergestellt. Für jede Darreichungsform wurden sechs verschiedene Formulierungen mit unterschiedlichen Mengen an Zinkoxid produziert. Als zusätzliche Hilfsstoffe wurden Mannitol und Hyaluronsäure verwendet. Ovalbumin diente als Modellantigen. Da die Sprühtrocknung mit Essigsäure (2 %) für die Herstellung der nasalen Formulierungen zu zahlreichen Schwierigkeiten bei der Charakterisierung und zu für die Anwendung unerwünschten Eigenschaften führte, wurden die pulmonalen Formulierungen mit Wasser als Suspensionsmedium sprühgetrocknet. Sechs weiße Pulver mit unterschiedlichen Zinkoxidkonzentrationen, einem x50 kleiner als 5 µm und einer Beladung von 100 % des verwendeten Ovalbumins wurden hergestellt. Die verschiedenen Zinkoxidkonzentrationen der Formulierungen hatten bei fast allen Versuchen einen Einfluss. In immunologischen in-vitro Zellexperimenten zeigte Formulierung 2, die für die Versuche aufgrund der besten aerodynamischen Eigenschaften ausgewählt wurde, eine Expression von CD80, CD86 und MHC-II. Diese Ergebnisse deuteten auf eine Aktivierung der verwendeten dendritischen Zellen aus dem Knochenmark von Mäusen hin und geben so einen ersten Hinweis auf eine adjuvante Wirkung. Die Verwendung von Zinkoxid als Adjuvans scheint also möglich zu sein, sollte aber in in-vivo Studien weiter untersucht und aufgeklärt werden.

10 References

- [1] www.who.int/emergencies/diseases/novel-coronavirus-2019/interactive-timeline (last time accessed: 12.02.21).
- [2] www.covid19.who.int (last time accessed: 12.02.21).
- [3] www.rki.de/DE/Content/InfAZ/N/Neuartiges_Coronavirus/Steckbrief.html (last time accessed: 12.02.21).
- [4] www.rki.de/DE/Content/InfAZ/N/Neuartiges_Coronavirus/Virologische_Basisdaten.html (last time accessed: 12.02.21).
- [5] www.pharmazeutische-zeitung.de/impfen-mit-rna-oder-dna/ (last time accessed: 12.02.21).
- [6] www.pharmazeutische-zeitung.de/vektroviren-als-platform/ (last time accessed: 12.02.21).
- [7] www.pharmazeutische-zeitung.de/ganzvirus-impfstoffe-als-einfachste-form/ (last time accessed: 12.02.21).
- [8] www.pharmazeutische-zeitung.de/protein-basierte-impfstoffe-und-vlp/ (last time accessed: 12.02.21).
- [9] www.ema.europa.eu (last time accessed: 12.02.21).
- [10] www.nytimes.com/interactive/2020/science/coronavirus-vaccine-tracker.html (last time accessed: 12.02.21).
- [11] www.vaccination.info.eu/en/vaccine-facts/approval-vaccines-european-union (last time accessed: 12.02.21).
- [12] Hellfritzsch M., Scherließ R., Mucosal vaccination via the respiratory tract. *Pharmaceutics* (2019).
- [13] https://www.who.int/immunization/global_vaccine_action_plan/SAGE_GVAP_Assessment_Report_2018_EN.pdf?ua=1 (last time accessed: 15.01.19).
- [14] Orenstein W. A., Hinman A., Nkowane B., Olive J. M., Reingold A., Measles and rubella global strategic plan 2012-2020 midterm review. *Vaccine* (2018) A1-A34.
- [15] <https://www.healio.com/news/pediatrics/20190207/measles-cases-in-europe-tripled-in-2018-who-says> (last time accessed: 14.02.19).
- [16] Niewiesk S., Maternal antibodies- Clinical significance, mechanism of interference with immune responses, and possible vaccination strategies. *Frontiers in immunology* (2014) 446.

-
- [17] Mitragotri S., Immunization without needles. *Nature reviews. Immunology* (2005) 905–916.
- [18] Davis S. S., Nasal vaccines. *Advanced Drug Delivery Reviews* (2001) 21–42.
- [19] Pavot V., Rochereau N., Genin C., Verrier B., Paul S., New insights in mucosal vaccine development. *Vaccine* (2012) 142–154.
- [20] Cesta M. F., Normal structure, function, and histology of mucosa-associated lymphoid tissue. *Toxicologic pathology* (2006) 599–608.
- [21] Gebert A., Pabst R., M cells at locations outside the gut. *Seminars in immunology* (1999) 165–170.
- [22] Hathaway L. J., Kraehenbuhl J. P., The role of m cells in mucosal immunity. *Cellular and molecular life sciences : CMLS* (2000) 323–332.
- [23] Haneberg B., Holst J., Can nonliving nasal vaccines be made to work? *Expert review of vaccines* (2002) 227–232.
- [24] Neutra M. R., Kozlowski P. A., Mucosal vaccines- The promise and the challenge. *Nature reviews. Immunology* (2006) 148–158.
- [25] Park S.-K., Kim G.-Y., Lim J.-Y., Kwak J.-Y., Bae Y.-S., Lee J.-D., Oh Y.-H., Ahn S.-C., Park Y.-M., Acidic polysaccharides isolated from *phellinus linteus* induce phenotypic and functional maturation of murine dendritic cells. *Biochemical and biophysical research communications* (2003) 449–458.
- [26] Kiyono H., Fukuyama S., Nalt- versus peyer's-patch-mediated mucosal immunity. *Nature reviews. Immunology* (2004) 699–710.
- [27] Blank F., Wehrli M., Lehmann A., Baum O., Gehr P., von Garnier C., Rothen-Rutishauser B. M., Macrophages and dendritic cells express tight junction proteins and exchange particles in an in vitro model of the human airway wall. *Immunobiology* (2011) 86–95.
- [28] Lu D., Hickey A. J., Pulmonary vaccine delivery. *Expert review of vaccines* (2007) 213–226.
- [29] Vujanic A., Sutton P., Snibson K. J., Yen H.-H., Scheerlinck J.-P. Y., Mucosal vaccination- Lung versus nose. *Veterinary immunology and immunopathology* (2012) 172–177.
- [30] de Magistris M. T., Mucosal delivery of vaccine antigens and its advantages in pediatrics. *Advanced Drug Delivery Reviews* (2006) 52–67.
- [31] Illum L., Nasal drug delivery—possibilities, problems and solutions. *Journal of Controlled Release* (2003) 187–198.
-

-
- [32] Partidos C. D., Intranasal vaccines- Forthcoming challenges. *Pharmaceutical Science & Technology Today* (2000) 273–281.
- [33] Pilcer G., Amighi K., Formulation strategy and use of excipients in pulmonary drug delivery. *International journal of pharmaceutics* (2010) 1–19.
- [34] Türker S., Onur E., Ozer Y., Nasal route and drug delivery systems. *Pharmacy world & science : PWS* (2004) 137–142.
- [35] de Temmerman M.-L., Rejman J., Demeester J., Irvine D. J., Gander B., de Smedt S. C., Particulate vaccines- On the quest for optimal delivery and immune response. *Drug discovery today* (2011) 569–582.
- [36] Banchereau J., Steinman R. M., Dendritic cells and the control of immunity. *Nature* (1998) 245–252.
- [37] Li S., Wang L., Berman M., Kong Y.-Y., Dorf M. E., Mapping a dynamic innate immunity protein interaction network regulating type i interferon production. *Immunity* (2011) 647–648.
- [38] Rietscher R., Schröder M., Janke J., Czaplewska J., Gottschaldt M., Scherließ R., Hanefeld A., Schubert U. S., Schneider M., Knolle P. A., Lehr C.-M., Antigen delivery via hydrophilic peg-b-page-b-plga nanoparticles boosts vaccination induced t cell immunity. *European journal of pharmaceutics and biopharmaceutics : official journal of Arbeitsgemeinschaft fur Pharmazeutische Verfahrenstechnik e.V* (2016) 20–31.
- [39] Mann J. F. S., Shakir E., Carter K. C., Mullen A. B., Alexander J., Ferro V. A., Lipid vesicle size of an oral influenza vaccine delivery vehicle influences the th1/th2 bias in the immune response and protection against infection. *Vaccine* (2009) 3643–3649.
- [40] Slütter B., Hageaars N., Jiskoot W., Rational design of nasal vaccines. *Journal of drug targeting* (2008) 1–17.
- [41] Tafaghodi M., Abolghasem S. T. S., Jaafari M.-R., Zakavi S. R., Momen-Nejad M., Evaluation of the clearance characteristics of various microspheres in the human nose by gamma-scintigraphy. *International journal of pharmaceutics* (2004) 125–135.
- [42] Des Rieux A., Fievez V., Garinot M., Schneider Y.-J., Pr at V., Nanoparticles as potential oral delivery systems of proteins and vaccines- A mechanistic approach. *Journal of Controlled Release* (2006) 1–27.
-

-
- [43] Fifis T., Gamvrellis A., Crimeen-Irwin B., Pietersz G. A., Li J., Mottram P. L., McKenzie I. F. C., Plebanski M., Size-dependent immunogenicity- Therapeutic and protective properties of nano-vaccines against tumors. *Journal of immunology (Baltimore, Md. : 1950)* (2004) 3148–3154.
- [44] Singh M., Chakrapani A., O'Hagan D., Nanoparticles and microparticles as vaccine-delivery systems. *Expert review of vaccines* (2007) 797–808.
- [45] Ceresa B. (Ed.), *Molecular Regulation of Endocytosis*. InTech (2012).
- [46] Gratton S. E. A., Ropp P. A., Pohlhaus P. D., Luft J. C., Madden V. J., Napier M. E., DeSimone J. M., The effect of particle design on cellular internalization pathways. *Proceedings of the National Academy of Sciences of the United States of America* (2008) 11613–11618.
- [47] Champion J. A., Katare Y. K., Mitragotri S., Particle shape- A new design parameter for micro- and nanoscale drug delivery carriers. *Journal of controlled release : official journal of the Controlled Release Society* (2007) 3–9.
- [48] Champion J. A., Walker A., Mitragotri S., Role of particle size in phagocytosis of polymeric microspheres. *Pharmaceutical research* (2008) 1815–1821.
- [49] Sharma S., Mukkur T. K. S., Benson H. A. E., Chen Y., Pharmaceutical aspects of intranasal delivery of vaccines using particulate systems. *Journal of pharmaceutical sciences* (2009) 812–843.
- [50] Fröhlich E., The role of surface charge in cellular uptake and cytotoxicity of medical nanoparticles. *International journal of nanomedicine* (2012) 5577–5591.
- [51] Foged C., Brodin B., Frokjaer S., Sundblad A., Particle size and surface charge affect particle uptake by human dendritic cells in an in vitro model. *International journal of pharmaceutics* (2005) 315–322.
- [52] Slütter B., Bal S. M., Que I., Kaijzel E., Löwik C., Bouwstra J., Jiskoot W., Antigen-adjuvant nanoconjugates for nasal vaccination- An improvement over the use of nanoparticles? *Molecular pharmaceutics* (2010) 2207–2215.
- [53] Vyas S. P., Gupta P. N., Implication of nanoparticles/microparticles in mucosal vaccine delivery. *Expert review of vaccines* (2007) 401–418.
- [54] Illum L., Nanoparticulate systems for nasal delivery of drugs- A real improvement over simple systems? *Journal of pharmaceutical sciences* (2007) 473–483.
-

-
- [55] Cruz L. J., Tacke P. J., Fokkink R., Joosten B., Stuart M. C., Albericio F., Torensma R., Figdor C. G., Targeted plga nano- but not microparticles specifically deliver antigen to human dendritic cells via dc-sign in vitro. *Journal of controlled release : official journal of the Controlled Release Society* (2010) 118–126.
- [56] Chadwick S., Krieger C., Amiji M., Delivery strategies to enhance mucosal vaccination. *Expert opinion on biological therapy* (2009) 427–440.
- [57] Thiele L., Rothen-Rutishauser B., Jilek S., Wunderli-Allenspach H., Merkle H. P., Walter E., Evaluation of particle uptake in human blood monocyte-derived cells in vitro. Does phagocytosis activity of dendritic cells measure up with macrophages? *Journal of Controlled Release* (2001) 59–71.
- [58] Hickey A. J., Garmise R. J., Dry powder nasal vaccines as an alternative to needle-based delivery. *Critical reviews in therapeutic drug carrier systems* (2009) 1–27.
- [59] Roth Y., Chapnik J. S., Cole P., Feasibility of aerosol vaccination in humans. *The Annals of otology, rhinology, and laryngology* (2003) 264–270.
- [60] Bennett J. V., Fernandez de Castro, J., Valdespino-Gomez J. L., Garcia-Garcia M. de L., Islas-Romero R., Echaniz-Aviles G., Jimenez-Corona A., Sepulveda-Amor J., Aerosolized measles and measles-rubella vaccines induce better measles antibody booster responses than injected vaccines- Randomized trials in mexican schoolchildren. *Bulletin of the World Health Organization* (2002) 806–812.
- [61] Ausar S. F., Hasija M., Li L., Rahman N., Forced degradation studies- An essential tool for the formulation development of vaccines. *VDT* (2013) 11.
- [62] Brandau D. T., Jones L. S., Wiethoff C. M., Rexroad J., Middaugh C. R., Thermal stability of vaccines. *Journal of pharmaceutical sciences* (2003) 218–231.
- [63] Taneja S., Ahmad F., Increased thermal stability of proteins in the presence of amino acids. *The Biochemical journal* (1994) 147–153.
- [64] Rajapaksa T. E., Bennett K. M., Hamer M., Lytle C., Rodgers V. G. J., Lo D. D., Intranasal m cell uptake of nanoparticles is independently influenced by targeting ligands and buffer ionic strength. *The Journal of biological chemistry* (2010) 23739–23746.
- [65] Wang W., Lyophilization and development of solid protein pharmaceuticals. *International journal of pharmaceutics* (2000) 1–60.
-

-
- [66] Amorij J.-P., Huckriede A., Wilschut J., Frijlink H. W., Hinrichs W. L. J., Development of stable influenza vaccine powder formulations- Challenges and possibilities. *Pharmaceutical research* (2008) 1256–1273.
- [67] Amorij J.-P., Meulenaar J., Hinrichs W. L. J., Stegmann T., Huckriede A., Coenen F., Frijlink H. W., Rational design of an influenza subunit vaccine powder with sugar glass technology - Preventing conformational changes of haemagglutinin during freezing and freeze-drying. *Vaccine* (2007) 6447–6457.
- [68] Hansen L. J. J., Daoussi R., Vervaet C., Remon J.-P., de Beer T. R. M., Freeze-drying of live virus vaccines- A review. *Vaccine* (2015) 5507–5519.
- [69] Tonnis W. F., Amorij, J.-P., Vreeman M. A., Frijlink H. W., Kersten G. F., Hinrichs W. L. J., Improved storage stability and immunogenicity of hepatitis b vaccine after spray-freeze drying in presence of sugars. *European journal of pharmaceutical sciences : official journal of the European Federation for Pharmaceutical Sciences* (2014) 36–45.
- [70] Garmise R. J., Staats H. F., Hickey A. J., Novel dry powder preparations of whole inactivated influenza virus for nasal vaccination. *AAPS PharmSciTech* (2007) E81.
- [71] Saluja V., Amorij J.-P., Kapteyn J. C., de Boer A. H., Frijlink H. W., Hinrichs W. L. J., A comparison between spray drying and spray freeze drying to produce an influenza subunit vaccine powder for inhalation. *Journal of controlled release : official journal of the Controlled Release Society* (2010) 127–133.
- [72] Minne A., Boireau H., Horta M. J., Vanbever R., Optimization of the aerosolization properties of an inhalation dry powder based on selection of excipients. *European Journal of Pharmaceutics and Biopharmaceutics* (2008) 839–844.
- [73] Raula J., Thielmann F., Naderi M., Lehto V.-P., Kauppinen E. I., Investigations on particle surface characteristics vs. Dispersion behaviour of l-leucine coated carrier-free inhalable powders. *International journal of pharmaceutics* (2010) 79–85.
- [74] Weiler C., Egen M., Trunk M., Langguth P., Force control and powder dispersibility of spray dried particles for inhalation. *Journal of pharmaceutical sciences* (2010) 303–316.
- [75] Westmeier R., Steckel H., In-situ fine particle excipient as dispersion modifier for a dry powder inhalation product. *DDL 19, Aerosol Society* (2008).
- [76] Trows S., Scherließ R., Preparation and characterization of dry powder agarose nano-in-microparticles for nasal vaccination. *Respiratory Drug Delivery, Davies Healthcare International Publishing* (2012).
-

-
- [77] Azad N., Rojanasakul Y., Nanobiotechnology in drug delivery. *American Journal of Drug Delivery* (2006) 79–88.
- [78] Mestecky J., Russell M. W., Elson C. O., Perspectives on mucosal vaccines- Is mucosal tolerance a barrier? *Journal of immunology (Baltimore, Md. : 1950)* (2007) 5633–5638.
- [79] Chadwick S., Kriegel C., Amiji M., Nanotechnology solutions for mucosal immunization. *Advanced Drug Delivery Reviews* (2010) 394–407.
- [80] Zuercher A. W., Upper respiratory tract immunity. *Viral immunology* (2003) 279–289.
- [81] Yanagita M., Hiroi T., Kitagaki N., Hamada S., Ito H. O., Shimauchi H., Murakami S., Okada H., Kiyono H., Nasopharyngeal-associated lymphoreticular tissue (nalt) immunity- Fimbriae-specific th1 and th2 cell-regulated iga responses for the inhibition of bacterial attachment to epithelial cells and subsequent inflammatory cytokine production. *Journal of immunology (Baltimore, Md. : 1950)* (1999) 3559–3565.
- [82] Boukhvalova M. S., Prince G. A., Soroush L., Harrigan D. C., Vogel S. N., Blanco J. C. G., The tlr4 agonist, monophosphoryl lipid a, attenuates the cytokine storm associated with respiratory syncytial virus vaccine-enhanced disease. *Vaccine* (2006) 5027–5035.
- [83] Childers N. K., Miller K. L., Tong G., Llarena J. C., Greenway T., Ulrich J. T., Michalek S. M., Adjuvant activity of monophosphoryl lipid a for nasal and oral immunization with soluble or liposome-associated antigen. *Infection and immunity* (2000) 5509–5516.
- [84] Wang C., Muttill P., Lu D., Beltran-Torres A. A., Garcia-Contreras L., Hickey A. J., Screening for potential adjuvants administered by the pulmonary route for tuberculosis vaccines. *The AAPS journal* (2009) 139–147.
- [85] Shafique M., Meijerhof T., Wilschut J., de Haan A., Evaluation of an intranasal virosomal vaccine against respiratory syncytial virus in mice- Effect of tlr2 and nod2 ligands on induction of systemic and mucosal immune responses. *PLoS one* (2013) e61287.
- [86] Alignani D., Maletto B., Liscovsky M., Rópolo A., Morón G., Pistoiresi-Palencia M. C., Orally administered ova/cpg-odn induces specific mucosal and systemic immune response in young and aged mice. *Journal of leukocyte biology* (2005) 898–905.
- [87] Todoroff J., Ucakar B., Inglese M., Vandermarliere S., Fillee C., Renaud J.-C., Huygen K., Vanbever R., Targeting the deep lungs, poloxamer 407 and a cpg oligonucleotide optimize immune responses to mycobacterium tuberculosis antigen 85a following pulmonary delivery. *European journal of pharmaceuticals and biopharmaceutics : official journal of Arbeitsgemeinschaft fur Pharmazeutische Verfahrenstechnik e.V* (2013) 40–48.
-

-
- [88] Ogra P. L., Faden H., Welliver R. C., Vaccination strategies for mucosal immune responses. *Clinical microbiology reviews* (2001) 430–445.
- [89] Giri P. K., Khuller G. K., Is intranasal vaccination a feasible solution for tuberculosis? *Expert review of vaccines* (2008) 1341–1356.
- [90] Johnson A. G., Molecular adjuvants and immunomodulators- New approaches to immunization. *Clinical microbiology reviews* (1994) 277–289.
- [91] Wolvers D. A. W., Bakker J. M., Bagchus W. M., Kraal G., The steroid hormone dehydroepiandrosterone (dhea) breaks intranasally induced tolerance, when administered at time of systemic immunization. *Journal of Neuroimmunology* (1998) 19–25.
- [92] Boyaka P. N., McGhee J. R., Cytokines as adjuvants for the induction of mucosal immunity. *Advanced Drug Delivery Reviews* (2001) 71–79.
- [93] Bijker M. S., van den Eeden S. J. F., Franken K. L., Melief C. J. M., Offringa R., van der Burg S. H., Cd8+ ctl priming by exact peptide epitopes in incomplete freund's adjuvant induces a vanishing ctl response, whereas long peptides induce sustained ctl reactivity. *Journal of immunology (Baltimore, Md. : 1950)* (2007) 5033–5040.
- [94] Foged C., Hansen J., Agger E. M., Formulation requirements for optimal priming of cd8(+) ctl responses with particulate vaccine delivery systems. *European journal of pharmaceutical sciences : official journal of the European Federation for Pharmaceutical Sciences* (2012) 482–491.
- [95] Lycke N., Recent progress in mucosal vaccine development- Potential and limitations. *Nature reviews. Immunology* (2012) 592–605.
- [96] Jabbal-Gill I., Nasal vaccine innovation. *Journal of drug targeting* (2010) 771–786.
- [97] Melief C. J. M., van Hall T., Arens R., Ossendorp F., van der Burg S. H., Therapeutic cancer vaccines. *The Journal of clinical investigation* (2015) 3401–3412.
- [98] Pannemans K., Hellings N., Stinissen P., Therapeutic vaccines for autoimmune diseases. *Drug Discovery Today: Therapeutic Strategies* (2009) 39–44.
- [99] Chen D. S., Mellman I., Oncology meets immunology- The cancer-immunity cycle. *Immunity* (2013) 1–10.
- [100] Palucka K., Ueno H., Banchereau J., Recent developments in cancer vaccines. *Journal of immunology (Baltimore, Md. : 1950)* (2011) 1325–1331.
- [101] Rabinovich G. A., Gabrilovich D., Sotomayor E. M., Immunosuppressive strategies that are mediated by tumor cells. *Annual review of immunology* (2007) 267–296.
-

- [102] <https://www.fda.gov/media/70857/download> (last time accessed: 15.09.20).
- [103] Marple B., Roland P., Benninger M., Safety review of benzalkonium chloride used as a preservative in intranasal solutions- An overview of conflicting data and opinions. *Otolaryngology--head and neck surgery : official journal of American Academy of Otolaryngology-Head and Neck Surgery* (2004) 131–141.
- [104] Merkus P., Romeijn S. G., Verhoef J. C., Merkus F. W., Schouwenburg P. F., Classification of cilio-inhibiting effects of nasal drugs. *The Laryngoscope* (2001) 595–602.
- [105] Yuki Y., Nochi T., Harada N., Katakai Y., Shibata H., Mejima M., Kohda T., Tokuhara D., Kurokawa S., Takahashi Y., Ono F., Kozaki S., Terao K., Tsukada H., Kiyono H., In vivo molecular imaging analysis of a nasal vaccine that induces protective immunity against botulism in nonhuman primates. *Journal of immunology (Baltimore, Md. : 1950)* (2010) 5436–5443.
- [106] Perrie Y., Mohammed A. R., Kirby D. J., McNeil S. E., Bramwell V. W., Vaccine adjuvant systems- Enhancing the efficacy of sub-unit protein antigens. *International journal of pharmaceutics* (2008) 272–280.
- [107] Carter N. J., Curran M. P., Live attenuated influenza vaccine (flumist®; fluenz™)- A review of its use in the prevention of seasonal influenza in children and adults. *Drugs* (2011) 1591–1622.
- [108] Belshe R. B., Edwards K. M., Vesikari T., Black S. V., Walker R. E., Hultquist M., Kemble G., Connor E. M., Live attenuated versus inactivated influenza vaccine in infants and young children. *The New England journal of medicine* (2007) 685–696.
- [109] Bosquillon C., Lombry C., Pr at V., Vanbever R., Influence of formulation excipients and physical characteristics of inhalation dry powders on their aerosolization performance. *Journal of Controlled Release* (2001) 329–339.
- [110] Carvalho T. C., Peters J. I., Williams R. O., Influence of particle size on regional lung deposition--what evidence is there? *International journal of pharmaceutics* (2011) 1–10.
- [111] Steckel H., Bolzen N., Alternative sugars as potential carriers for dry powder inhalations. *International journal of pharmaceutics* (2004) 297–306.
- [112] Telko M. J., Hickey A. J., Dry powder inhaler formulation. *Respiratory care* (2005) 1209–1227.
- [113] Newman S. P., Busse W. W., Evolution of dry powder inhaler design, formulation, and performance. *Respiratory medicine* (2002) 293–304.

- [114] Baldrick P., Pharmaceutical excipient development- The need for preclinical guidance. *Regulatory toxicology and pharmacology : RTP* (2000) 210–218.
- [115] Steinberg M., Borzelleca J. F., Enters E. K., Kinoshita F. K., Loper A., Mitchell D. B., Tamulinas C. B., Weiner M. L., A new approach to the safety assessment of pharmaceutical excipients. The safety committee of the international pharmaceutical excipients council. *Regulatory toxicology and pharmacology : RTP* (1996) 149–154.
- [116] Vandevanter D. R., Geller D. E., Tobramycin administered by the tobi(®) podhaler(®) for persons with cystic fibrosis- A review. *Medical devices (Auckland, N.Z.)* (2011) 179–188.
- [117] Rice-Ficht A. C., Arenas-Gamboa A. M., Kahl-McDonagh M. M., Ficht T. A., Polymeric particles in vaccine delivery. *Current opinion in microbiology* (2010) 106–112.
- [118] Smith J. D., Morton L. D., Ulery B. D., Nanoparticles as synthetic vaccines. *Current opinion in biotechnology* (2015) 217–224.
- [119] Han J., Zhao D., Li D., Wang X., Jin Z., Zhao K., Polymer-based nanomaterials and applications for vaccines and drugs. *Polymers* (2018).
- [120] Jaganathan K. S., Vyas S. P., Strong systemic and mucosal immune responses to surface-modified plga microspheres containing recombinant hepatitis b antigen administered intranasally. *Vaccine* (2006) 4201–4211.
- [121] Pawar D., Mangal S., Goswami R., Jaganathan K. S., Development and characterization of surface modified plga nanoparticles for nasal vaccine delivery- Effect of mucoadhesive coating on antigen uptake and immune adjuvant activity. *European journal of pharmaceuticals and biopharmaceutics : official journal of Arbeitsgemeinschaft fur Pharmazeutische Verfahrenstechnik e.V* (2013) 550–559.
- [122] Illum L., Jabbal-Gill I., Hinchcliffe M., Fisher A. N., Davis S. S., Chitosan as a novel nasal delivery system for vaccines. *Advanced Drug Delivery Reviews* (2001) 81–96.
- [123] Heidland J., Scherließ R., Nim powders for nasal vaccination—insights into particle forming process. *10th World Meeting on Pharmaceutics, Biopharmaceutics and Pharmaceutical* (2016).
- [124] Smith A., Perelman M., Hinchcliffe M., Chitosan- A promising safe and immune-enhancing adjuvant for intranasal vaccines. *Human vaccines & immunotherapeutics* (2014) 797–807.
- [125] Heidland J., Scherließ R., Nano-in-microparticle powders for mucosal vaccination— understanding the particle forming process. *DDL 27, Aerosol Society* (2016).

-
- [126] Heidland J., Scherließ R., Nano-in-microparticles for dry powder vaccination—possible or nasal application? *DDL 2017, Aerosol Society* (2017).
- [127] Buske S. D. L., Chitosan as adjuvant and particle forming excipient in a nano-in-microparticulate dry powder for nasal and pulmonary vaccine delivery. *Ph.D. Thesis, Kiel University* (2014).
- [128] Diedrich A., Entwicklung einer nanopartikelären formulierung zur vakzinierung über den respirationstrakt. *Ph.D. Thesis, Kiel University* (2015).
- [129] Scherließ R., Diedrich A., Ebensen T., Guzmán C. A., Wolf M., Hanefeld A., Chitosan nanoparticulate formulation for pulmonary vaccination—formulation and in vivo proof of concept. *Respiratory Drug Delivery, Davies Healthcare International Publishing* (2015).
- [130] Trows S., Pulverformulierungen für die nasale Vakzinierung. *Ph.D. Thesis, Kiel University* (2013).
- [131] Scherließ R., Mönckedieck M., Young K., Trows S., Buske S., Hook S., First in vivo evaluation of particulate nasal dry powder vaccine formulations containing ovalbumin in mice. *International journal of pharmaceutics* (2015) 408–415.
- [132] Tonnis W. F., Kersten G. F., Frijlink H. W., Hinrichs W. L. J., de Boer A. H., Amorij J.-P., Pulmonary vaccine delivery- A realistic approach? *Journal of aerosol medicine and pulmonary drug delivery* (2012) 249–260.
- [133] Sou T., Meeusen E. N., de Veer M., Morton D. A. V., Kaminskas L. M., McIntosh M, P., New developments in dry powder pulmonary vaccine delivery. *Trends in biotechnology* (2011) 191–198.
- [134] Kisich K. O., Higgins M. P., Park I., Cape S. P., Lindsay L., Bennett D. J., Winston S., Searles J., Sievers R. E., Dry powder measles vaccine- Particle deposition, virus replication, and immune response in cotton rats following inhalation. *Vaccine* (2011) 905–912.
- [135] Lin W.-H., Griffin D. E., Rota P. A., Papania M., Cape S. P., Bennett D., Quinn B., Sievers R. E., Shermer C., Powell K., Adams R. J., Godin S., Winston S., Successful respiratory immunization with dry powder live-attenuated measles virus vaccine in rhesus macaques. *Proceedings of the National Academy of Sciences of the United States of America* (2011) 2987–2992.
- [136] Sievers R. E., Cape S. P., McAdams D. H., Manion J. R., Shah N. K., Chen D. J., Winston S. E., Optimizing the effectiveness of live-attenuated measles vaccine aerosols: Effects of different delivery modes. *Respiratory Drug Delivery, Davies Healthcare International Publishing* (2012).
-

-
- [137] Low N., Bavdekar A., Jeyaseelan L., Hirve S., Ramanathan K., Andrews N. J., Shaikh N., Jadi R. S., Rajagopal A., Brown K. E., Brown D., Fink J. B., John O., Scott P., Riveros-Balta A. X., Greco M., Dhere R., Kulkarni P. S., Henao Restrepo A. M., A randomized, controlled trial of an aerosolized vaccine against measles. *The New England journal of medicine* (2015) 1519–1529.
- [138] Dhere R., Yeolekar L., Kulkarni P., Menon R., Vaidya V., Ganguly M., Tyagi P., Barde P., Jadhav S., A pandemic influenza vaccine in india- From strain to sale within 12 months. *Vaccine* (2011) A16-21.
- [139] Audouy S. A. L., van der Schaaf G., Hinrichs W. L. J., Frijlink H. W., Wilschut J., Huckriede A., Development of a dried influenza whole inactivated virus vaccine for pulmonary immunization. *Vaccine* (2011) 4345–4352.
- [140] Källenius G., Pawlowski A., Brandtzaeg P., Svenson S., Should a new tuberculosis vaccine be administered intranasally? *Tuberculosis (Edinburgh, Scotland)* (2007) 257–266.
- [141] Fourie P. B., Germishuizen W. A., Wong Y.-L., Edwards D. A., Spray drying tb vaccines for pulmonary administration. *Expert opinion on biological therapy* (2008) 857–863.
- [142] Garcia-Contreras L., Wong Y.-L., Muttill P., Padilla D., Sadoff J., Derosse J., Germishuizen W. A., Goonesekera S., Elbert K., Bloom B. R., Miller R., Fourie P. B., Hickey A., Edwards D., Immunization by a bacterial aerosol. *Proceedings of the National Academy of Sciences of the United States of America* (2008) 4656–4660.
- [143] Muttill P., Prego C., Garcia-Contreras L., Pulliam B., Fallon J. K., Wang C., Hickey A. J., Edwards D., Immunization of guinea pigs with novel hepatitis b antigen as nanoparticle aggregate powders administered by the pulmonary route. *The AAPS journal* (2010) 330–337.
- [144] Djupesland P. G., Nasal drug delivery devices- Characteristics and performance in a clinical perspective-a review. *Drug delivery and translational research* (2013) 42–62.
- [145] Huang J., Garmise R. J., Crowder T. M., Mar K., Hwang C. R., Hickey A. J., Mikszta J. A., Sullivan V. J., A novel dry powder influenza vaccine and intranasal delivery technology - Induction of systemic and mucosal immune responses in rats. *Vaccine* (2004) 794–801.
- [146] Friebel C., Steckel H., Müller B. W., Rational design of a dry powder inhaler - Device design and optimisation. *The Journal of pharmacy and pharmacology* (2012) 1303–1315.
- [147] Friebel C., Steckel H., Single-use disposable dry powder inhalers for pulmonary drug delivery. *Expert opinion on drug delivery* (2010) 1359–1372.
-

- [148] de Boer A. H., Hagedoorn P., Westerman E. M., Le Brun P. P. H., Heijerman H. G. M., Frijlink H. W., Design and in vitro performance testing of multiple air classifier technology in a new disposable inhaler concept (twincer) for high powder doses. *European journal of pharmaceutical sciences : official journal of the European Federation for Pharmaceutical Sciences* (2006) 171–178.
- [149] Papavlassopoulos H., Mishra Y. K., Kaps S., Paulowicz I., Abdelaziz R., Elbahri M., Maser E., Adelung R., Röhl C., Toxicity of functional nano-micro zinc oxide tetrapods - impact of cell culture conditions, cellular age and material properties. *PLoS one* (2014) e84983.
- [150] Antoine T. E., Mishra Y. K., Trigilio J., Tiwari V., Adelung R., Shukla D., Prophylactic, therapeutic and neutralizing effects of zinc oxide tetrapod structures against herpes simplex virus type-2 infection. *Antiviral research* (2012) 363–375.
- [151] Antoine T. E., Hadigal S. R., Yakoub A. M., Mishra Y. K., Bhattacharya P., Haddad C., Valyi-Nagy T., Adelung R., Prabhakar B. S., Shukla D., Intravaginal zinc oxide tetrapod nanoparticles as novel immunoprotective agents against genital herpes. *Journal of immunology (Baltimore, Md. : 1950)* (2016) 4566–4575.
- [152] Mishra Y. K., Adelung R., ZnO tetrapod materials for functional applications. *Materials Today* (2018) 631–651.
- [153] Bundesinstitut für Arzneimittel und Medizinprodukte, Europäisches Arzneibuch 9.0 - 9.8: Amtliche deutsche Ausgabe. 8th ed., Deutscher Apotheker-Verlag (2019).
- [154] <https://nanopartikel.info/wissen/materialien/zinkoxid/> (last time accessed: 05.04.20).
- [155] <https://www.norkem.de/products/zinkoxid> (last time accessed: 06.04.20).
- [156] <https://gestis.dguv.de/data?name=002090> (last time accessed: 06.04.20).
- [157] <https://www.ptaheute.de/news/spezial/wissen-am-hv/zink/erkaeltung-im-griff-dank-hochdosiertem-zink/> (last time accessed: 06.04.20).
- [158] <https://www.spipharma.com/media/2418/vac-20-ghs-sds.pdf> (last time accessed: 07.04.20).
- [159] Baker B., Water content of pseudoboehmite- A new model for its structure. *Journal of Catalysis* (1974) 265–278.
- [160] <https://www.spipharma.com/media/3321/vac-adjutant-brochure-final-spread-091119.pdf> (last time accessed: 07.04.20).
- [161] Maughan C. N., Preston S. G., Williams G. R., Particulate inorganic adjuvants - Recent developments and future outlook. *The Journal of pharmacy and pharmacology* (2015) 426–449.

- [162] Al-Shakhshir R., Regnier F., White J. L., Hem S. L., Effect of protein adsorption on the surface charge characteristics of aluminium-containing adjuvants. *Vaccine* (1994) 472–474.
- [163] <https://www.invivogen.com/adju-phos> (last time accessed: 07.04.20).
- [164] Giese M., Introduction to Molecular Vaccinology. Springer-Verlag (2016).
- [165] Huang M., Wang W., Factors affecting alum-protein interactions. *International journal of pharmaceutics* (2014) 139–146.
- [166] https://www.bfarm.de/SharedDocs/Downloads/DE/Arzneimittel/Pharmakovigilanz/Bulletin/2015/3-2015.pdf;jsessionid=D3A8FE7EB66F2DC510540F7A7B11FC84.1_cid506?__blob=publicationFile&v=6 (last time accessed: 07.04.20).
- [167] https://www.roquette.com/-/media/roquette-sharepoint-libraries/sdol_product-specification-sheet/roquette_quality_specification-sheet_pearlitol-200-sd---mannitol_50_450320_en.pdf (last time accessed: 07.04.20).
- [168] Depreter F., Pilcer G., Amighi K., Inhaled proteins- Challenges and perspectives. *International journal of pharmaceutics* (2013) 251–280.
- [169] Gómez-Gaete C., Fattal E., Silva L., Besnard M., Tsapis N., Dexamethasone acetate encapsulation into trojan particles. *Journal of controlled release : official journal of the Controlled Release Society* (2008) 41–49.
- [170] Sandri G., Rossi S., Ferrari F., Bonferoni M. C., Zerrouk N., Caramella C., Mucoadhesive and penetration enhancement properties of three grades of hyaluronic acid using porcine buccal and vaginal tissue, caco-2 cell lines, and rat jejunum. *The Journal of pharmacy and pharmacology* (2004) 1083–1090.
- [171] Murphy K., Weaver C., Janeway Immunologie. 9th ed., Springer Berlin Heidelberg (2018).
- [172] Majorek K. A., Porebski P. J., Dayal A., Zimmerman M. D., Jablonska K., Stewart A. J., Chruszcz M., Minor W., Structural and immunologic characterization of bovine, horse, and rabbit serum albumins. *Molecular immunology* (2012) 174–182.
- [173] <https://www.carlroth.com/medias/Info-Brochure-Albumins-EN.pdf?context=bWFzdGVyfHRIY2huaWNhbERvY3VtZW50c3w0OTg1MjZ8YXBwbGljYXRpb24vcGRmfHRIY2huaWNhbERvY3VtZW50cy9oNTEvaDhhLzg5NzcyNzE1MjEzMTAucGRmfDZhoDU2MDc3ZDhiODgxMTM3OTZkMDBiMWJhMzYyZTAzOGM0Y2QyNzZiOTQ5Njg2NDFIMDNkZGY1NzgxNjQxMGI> (last time accessed: 18.11.20).
- [174] <https://www.sigmaldrich.com/catalog/product/sigma/a2153?lang=de®ion=DE> (last time accessed: 22.11.20).

-
- [175] Judge R. A., Johns M. R., White E. T., Protein purification by bulk crystallization- The recovery of ovalbumin. *Biotechnology and bioengineering* (1995) 316–323.
- [176] <https://www.sigmaaldrich.com/catalog/product/sigma/a5503?lang=de®ion=DE> (last time accessed: 08.04.20).
- [177] Fitzgerald D. K., Brodbeck U., Kiyosawa I., Mawal R., Colvin B., Ebner K. E., A -lactalbumin and the lactose synthetase reaction. *Journal of Biological Chemistry* (1970) 2103–2108.
- [178] Goodall S., Grandison A. S., Jauregi P. J., Price, J., Selective separation of the major whey proteins using ion exchange membranes. *Journal of dairy science* (2008) 1–10.
- [179] Gésan-Guiziou G., Separation, extraction and concentration processes in the food, beverage and nutraceutical industries. *Woodhead Publishing Series in Food Science, Technology and Nutrition* (2013) 341–380.
- [180] Shahmohammadi A., Lysozyme separation from chicken egg white- A review. *Eur Food Res Technol* (2018) 577–593.
- [181] https://www.lgcstandards-atcc.org/products/all/HTB-55.aspx?geo_country=de (last time accessed: 08.04.20).
- [182] Zhu Y., Chidekel A., Shaffer T. H., Cultured human airway epithelial cells (calu-3)- A model of human respiratory function, structure, and inflammatory responses. *Critical care research and practice* (2010).
- [183] https://www.lgcstandards-atcc.org/products/all/CCL-30.aspx?geo_country=de (last time accessed: 08.04.20).
- [184] Pozzoli M., Ong H. X., Morgan L., Sukkar M., Traini D., Young P. M., Sonvico F., Application of RPMI2650 nasal cell model to a 3d printed apparatus for the testing of drug deposition and permeation of nasal products. *European journal of pharmaceuticals and biopharmaceutics : official journal of Arbeitsgemeinschaft fur Pharmazeutische Verfahrenstechnik e.V* (2016) 223–233.
- [185] Wengst A., Reichl S., RPMI2650 epithelial model and three-dimensional reconstructed human nasal mucosa as in vitro models for nasal permeation studies. *European journal of pharmaceuticals and biopharmaceutics : official journal of Arbeitsgemeinschaft fur Pharmazeutische Verfahrenstechnik e.V* (2010) 290–297.
- [186] Roney K., Bone marrow-derived dendritic cells. *Methods in molecular biology (Clifton, N.J.)* (2019) 57–62.
- [187] <https://www.aptar.com/products/pharmaceutical/uds/> (last time accessed: 08.04.20).
-

-
- [188] Vehring R., Pharmaceutical particle engineering via spray drying. *Pharmaceutical research* (2008) 999–1022.
- [189] https://static1.buchi.com/sites/default/files/downloads/Set_3_Training_Papers_Spray_Drying_en_01.pdf?996b2db24007502bd69c913b675467cfc63880ba (last time accessed: 10.11.20).
- [190] <https://www.buchi.com/en/products/spray-drying-and-encapsulation/mini-spray-dryer-b-290> (last time accessed: 10.11.20).
- [191] Schiffler H. A., Sprühtrocknung - so schnell kann trocknen sein. *Deutsche Apotheker Zeitung* (2012) 78.
- [192] Voigt R., Fahr A., Pharmazeutische Technologie: Für Studium und Beruf ; mit 110 Tabellen. 11th ed., Deutscher Apotheker-Verlag (2010).
- [193] Kühl S., Kühle S., Ilsinger B., Lenz S., Thaler M. (Eds.), Grundlagen der Licht- und Elektronenmikroskopie. Verlag Eugen Ulmer (2018).
- [194] Eggert F., Standardfreie Elektronenstrahl-Mikroanalyse: Mit dem EDX im Rasterelektronenmikroskop ; ein Handbuch für die Praxis. Books on Demand (2005).
- [195] Fahr A., Voigt R., Voigt pharmazeutische Technologie: Für Studium und Beruf ; mit 113 Tabellen. 12th ed., Deutscher Apotheker-Verlag (2015).
- [196] Benninger M. S., Hadley J. A., Osguthorpe J. D., Marple B. F., Leopold D. A., Derebery M. J., Hannley M., Techniques of intranasal steroid use. *Otolaryngology--head and neck surgery : official journal of American Academy of Otolaryngology-Head and Neck Surgery* (2004) 5–24.
- [197] Walker J. M. (Ed.), The protein protocols handbook. 3rd ed., Humana Press (2009).
- [198] Thomas S., Thomas R., Zachariah A. K., Mishra R. K. (Ed.), Thermal and rheological measurement techniques for nanomaterials characterization. Elsevier (2017).
- [199] <https://www.agilent.com/cs/library/primers/public/5991-3651DEE.pdf> (last time accessed: 10.11.20).
- [200] Khago D., Bierma J. C., Roskamp K. W., Kozlyuk N., Martin R. W., Protein refractive index increment is determined by conformation as well as composition. *Journal of physics. Condensed matter : an Institute of Physics journal* (2018) 435101.

- [201] Marple V. A., Roberts D. L., Romay F. J., Miller N. C., Truman K. G., van Oort M., Olsson B., Holroyd M. J., Mitchell J. P., Hochrainer D., Next generation pharmaceutical impactor (a new impactor for pharmaceutical inhaler testing). Part i- Design. *Journal of aerosol medicine : the official journal of the International Society for Aerosols in Medicine* (2003) 283–299.
- [202] <https://inhalation.se/> (last time accessed: 05.02.21).
- [203] Huppelsberg J., Walter K., *Kurzlehrbuch Physiologie*. 4th ed., Thieme (2013).
- [204] Washington N., Steele R.J.C., Jackson S.J., Bush D., Mason J., Gill D.A., Pitt K., Rawlins D.A., Determination of baseline human nasal pH and the effect of intranasally administered buffers. *International journal of pharmaceutics* (2000) 139–146.
- [205] Callens C., Ceulemans J., Ludwig A., Foreman P., Remon J. P., Rheological study on mucoadhesivity of some nasal powder formulations. *European Journal of Pharmaceutics and Biopharmaceutics* (2003) 323–328.
- [206] Marques M. R. C., Loebenberg R., Almukainzi M., Simulated biological fluids with possible application in dissolution testing. *Dissolution Technol.* (2011) 15–28.
- [207] Pohling R., *Chemische Reaktionen in der Wasseranalyse*. Springer Spektrum (2015).
- [208] McCall J. T., Davis G. K., Stearns T. W., Spectrophotometric determination of copper and zinc in animal tissues. *Anal. Chem.* (1958) 1345–1347.
- [209] Säbel C. E., Neureuther J. M., Siemann S., A spectrophotometric method for the determination of zinc, copper, and cobalt ions in metalloproteins using zincon. *Analytical biochemistry* (2010) 218–226.
- [210] Duralliu A., Matejtschuk P., Williams D. R., Measuring the specific surface area (ssa) of freeze-dried biologics using inverse gas chromatography. *European journal of pharmaceutics and biopharmaceutics : official journal of Arbeitsgemeinschaft fur Pharmazeutische Verfahrenstechnik e.V* (2019) 216–221.
- [211] <https://www.hosokawa-alpine.de/mechanische-verfahrenstechnik/maschinen/luftstrahlsieb-und-laborgeraete/luftstrahlsieb-e200-ls/> (last time accessed: 27.03.20).
- [212] Keck T., Leiacker R., Riechelmann H., Rettinger G., Temperature profile in the nasal cavity. *The Laryngoscope* (2000) 651–654.
- [213] Castell J. V. (Ed.), *In vitro methods in pharmaceutical research*. Academic Press, San Diego, Calif. 1997.
- [214] <https://www.sinobiological.com/category/fcm-facs-facs> (last time accessed: 12.03.21).

-
- [215] <https://www.unimedizin-mainz.de/facs/durchflussszytometrie/prinzip-der-durchflussszytometrie.html> (last time accessed: 24.02.21).
- [216] Polarz S., Strunk J., Ischenko V., van den Berg M. W. E., Hinrichsen O., Muhler M., Driess M., On the role of oxygen defects in the catalytic performance of zinc oxide. *Angewandte Chemie (International ed. in English)* (2006) 2965–2969.
- [217] Wang J., Wang Z., Huang B., Ma Y., Liu Y., Qin X., Zhang X., Dai Y., Oxygen vacancy induced band-gap narrowing and enhanced visible light photocatalytic activity of zno. *ACS applied materials & interfaces* (2012) 4024–4030.
- [218] Bruch R. C., White H. B., Compositional and structural heterogeneity of avidin glycopeptides. *Biochemistry* (1982) 5334–5341.
- [219] Reimers A., Wet-chemical surface treatment of tetrapodal zinc oxide for functional applications. *Master Thesis, Kiel University* (2018).
- [220] Degen A., Kosec M., Effect of pH and impurities on the surface charge of zinc oxide in aqueous solution. *Journal of the European Ceramic Society* (2000) 667–673.
- [221] Choi S.-J., Choy J.-H., Biokinetics of zinc oxide nanoparticles- Toxicokinetics, biological fates, and protein interaction. *International journal of nanomedicine* (2014) 261–269.
- [222] Mortimer C. E., Müller U., Chemie: Das Basiswissen der Chemie ; 128 Tabellen. 10th ed., Thieme (2010).
- [223] Jiang L., Lai L., Ch...O hydrogen bonds at protein-protein interfaces. *The Journal of biological chemistry* (2002) 37732–37740.
- [224] Fritsching U. (Ed.), Process-Spray: Functional Particles Produced in Spray Processes. Springer International Publishing (2016).
- [225] Yu L., Mishra D. S., Rigsbee D. R., Determination of the glass properties of d-mannitol using sorbitol as an impurity. *Journal of pharmaceutical sciences* (1998) 774–777.
- [226] Abd M. M., Rahman M. A., Othman M. H. D., Ismail A. F., Jaafar J., Membrane Characterization. Elsevier (2017).
- [227] <https://prozesstechnik.industrie.de/chemie/thermoanalyse-praktisch/> (last time accessed: 30.09.20).
- [228] https://www.caelo.de/apotheken_rezeptursubstanzen.html?start=560 (last time accessed: 30.09.20).
- [229] www.alfa.com/de/catalog/035792 (last time accessed: 13.03.21).
-

- [230] <https://gestis.dguv.de/data?name=001330> (last time accessed: 08.10.20).
- [231] Arii T., Kishi A., The effect of humidity on thermal process of zinc acetate. *Thermochimica Acta* (2003) 175–185.
- [232] Fronczek F. R., Kamel H. N., Slattery M., Three polymorphs (α , β , and δ) of d-mannitol at 100 k. *ChemInform* (2004) o567.
- [233] Rutland J., Morgan L., de longh R. (Ed.), Respiratory Ciliary Dysfunction. 2nd ed., Pediatric Respiratory Medicine (2008).
- [234] Maleki A., Kjøniksen A.-L., Nyström B., Effect of pH on the behavior of hyaluronic acid in dilute and semidilute aqueous solutions. *Macromol. Symp.* (2008) 131–140.
- [235] Uspenskii S. A., Kil'deeva N. R., Maslova M. V., Demina T. S., Vikhoreva G. A., A study of the viscosity of hyaluronic acid solutions for the preparation of polyelectrolyte complexes with chitosan. *Russ Chem Bull* (2016) 273–276.
- [236] André P. V. F., Free radical scavenging properties of mannitol and its role as a constituent of hyaluronic acid fillers- A literature review. *International journal of cosmetic science* (2017) 355–360.
- [237] Zhao H., Brown P. H., Schuck P., On the distribution of protein refractive index increments. *Biophysical journal* (2011) 2309–2317.
- [238] <https://www.thermofisher.com/antibody/product/Ovalbumin-Antibody-Polyclonal/PA1-196-HRP> (last time accessed: 26.09.20).
- [239] <https://www.pharmazeutische-zeitung.de/ausgabe-402006/physikalische-einfluesse-steuern-die-pulmonale-deposition/> (last time accessed: 23.11.20).
- [240] Hancock B. C., Zografi G., Characteristics and significance of the amorphous state in pharmaceutical systems. *Journal of pharmaceutical sciences* (1997) 1–12.
- [241] Guo Y., Shalaev E., Smith S., Physical stability of pharmaceutical formulations- Solid-state characterization of amorphous dispersions. *TrAC Trends in Analytical Chemistry* (2013) 137–144.
- [242] Müller T., Schiewe J., Smal R., Weiler C., Wolkenhauer M., Steckel H., Measurement of low amounts of amorphous content in hydrophobic active pharmaceutical ingredients with dynamic organic vapor sorption. *European journal of pharmaceutics and biopharmaceutics: official journal of Arbeitsgemeinschaft fur Pharmazeutische Verfahrenstechnik e.V* (2015) 102–111.

- [243] Burger K., Illés J., Gyurcsik B., Gazdag M., Forrai E., Dékány I., Mihályfi K., Metal ion coordination of macromolecular bioligands- Formation of zinc(ii) complex of hyaluronic acid. *Carbohydrate Research* (2001) 197–207.
- [244] Stewart C. E., Torr E. E., Nur H. M. J., Bosquillon C., Sayers I., Evaluation of differentiated human bronchial epithelial cell culture systems for asthma research. *Journal of allergy* (2012) 943982.
- [245] Grainger C. I., Greenwell L. L., Lockley D. J., Martin G. P., Forbes B., Culture of calu-3 cells at the air interface provides a representative model of the airway epithelial barrier. *Pharmaceutical research* (2006) 1482–1490.
- [246] Foster K. A., Avery M. L., Yazdanian M., Kenneth A. L., Characterization of the calu-3 cell line as a tool to screen pulmonary drug delivery. *International journal of pharmaceuticals* (2000) 1–11.
- [247] Ong H. X., Traini D., Salama R., Anderson S. D., Daviskas E., Young P. M., The effects of mannitol on the transport of ciprofloxacin across respiratory epithelia. *Molecular pharmaceuticals* (2013) 2915–2924.
- [248] Fischer H., Widdicombe J. H., Mechanisms of acid and base secretion by the airway epithelium. *The Journal of membrane biology* (2006) 139–150.
- [249] Roy R., Kumar S., Verma A. K., Sharma A., Chaudhari B. P., Tripathi A., Das M., Dwivedi P. D., Zinc oxide nanoparticles provide an adjuvant effect to ovalbumin via a th2 response in balb/c mice. *International immunology* (2014) 159–172.

11 Appendix

11.1 Tables

Table 11.1. 24-h-pH- and solubility study showing saturation solubility, starting pH and pH change of different solutions/suspensions after 24 h for zinc oxide in comparison to formulation 1. F1) 100 % ZnO and 0 % mannitol. $n = 3$, \pm = standard deviation.

		ZnO 24 h, mg/mL	F1 24 h, mg/mL	pH 0 h	ZnO pH 24 h	F1 pH 24 h
Phosphate buffer	pH 1.2	5.09 \pm 0.20	5.16 \pm 0.17	1.18	3.21 \pm 0.03	3.08 \pm 0.03
	pH 2.5	0.49 \pm 0.01	0.47 \pm 0.05	2.53	6.25 \pm 0.33	5.09 \pm 0.09
	pH 4.0	0.01 \pm 0.00	0.01 \pm 0.002	4.00	6.73 \pm 0.16	6.39 \pm 0.02
	pH 5.5	0.01 \pm 0.004	0.01 \pm 0.003	5.48	6.81 \pm 0.32	6.63 \pm 0.07
	pH 6.4	0.01 \pm 0.001	0.01 \pm 0.00	6.36	7.76 \pm 0.20	7.10 \pm 0.18
	pH 7.4	0.01 \pm 0.00	0.004 \pm 0.002	7.39	10.51 \pm 0.06	8.10 \pm 0.55
Sodium chloride solution	pH 1.2	2.68 \pm 0.01	4.01 \pm 0.30	1.21	6.43 \pm 0.11	6.08 \pm 0.09
	pH 2.5	0.15 \pm 0.001	0.92 \pm 0.04	2.50	7.38 \pm 0.15	6.88 \pm 0.02
	pH 4.0	0.02 \pm 0.001	0.91 \pm 0.03	4.07	7.76 \pm 0.01	6.93 \pm 0.001
	pH 5.5	0.01 \pm 0.002	0.86 \pm 0.02	5.55	7.68 \pm 0.05	6.95 \pm 0.01
	pH 6.4	0.01 \pm 0.001	0.82 \pm 0.03	6.35	7.74 \pm 0.03	6.98 \pm 0.02
	pH 7.4	0.01 \pm 0.001	0.92 \pm 0.09	7.36	7.63 \pm 0.004	6.89 \pm 0.08
SNF	pH 6.4	0.00 \pm 0.001	0.91 \pm 0.13	6.43	7.63 \pm 0.02	6.79 \pm 0.06

Appendix

Table 11.2. 24 h-pH study showing starting pH and pH change of different solutions/suspensions after 24 h with zinc oxide as raw material (ZnO) in comparison to all formulations. F1) 100 % ZnO and 0 % mannitol; F2) 80 % ZnO and 20 % mannitol; F3) 60 % ZnO and 40 % mannitol; F4) 40 % ZnO and 60 % mannitol; F5) 20 % ZnO and 80 % mannitol; F6) 0 % ZnO and 100 % mannitol. n = 3, ± = standard deviation.

		pH 0 h	ZnO	F1	F2	F3	F4	F5	F6
Phosphate buffer	pH 1.2	1.18	3.21 ± 0.03	3.08 ± 0.03	2.37 ± 0.02	1.96 ± 0.00	1.66 ± 0.01	1.45 ± 0.02	1.30 ± 0.00
	pH 2.5	2.53	6.25 ± 0.33	5.09 ± 0.09	4.80 ± 0.03	4.44 ± 0.01	4.08 ± 0.01	3.88 ± 0.02	2.66 ± 0.01
	pH 4.0	4.00	6.73 ± 0.16	6.39 ± 0.02	5.91 ± 0.04	5.28 ± 0.01	4.72 ± 0.00	3.48 ± 0.00	4.18 ± 0.00
	pH 5.5	5.48	6.81 ± 0.32	6.63 ± 0.07	6.28 ± 0.01	5.65 ± 0.04	4.97 ± 0.01	4.77 ± 0.00	5.51 ± 0.00
	pH 6.4	6.36	7.76 ± 0.20	7.10 ± 0.18	6.90 ± 0.10	6.58 ± 0.05	6.17 ± 0.01	6.05 ± 0.00	6.42 ± 0.00
	pH 7.4	7.39	10.51 ± 0.06	8.10 ± 0.55	8.69 ± 0.23	7.66 ± 0.01	7.05 ± 0.00	6.99 ± 0.01	7.35 ± 0.01
Sodium chloride solution	pH 1.2	1.21	6.43 ± 0.11	6.08 ± 0.09	5.43 ± 0.04	4.14 ± 0.02	1.98 ± 0.19	1.50 ± 0.02	1.28 ± 0.01
	pH 2.5	2.50	7.38 ± 0.15	6.88 ± 0.02	6.97 ± 0.02	7.03 ± 0.01	6.84 ± 0.34	7.13 ± 0.02	3.40 ± 0.06
	pH 4.0	4.07	7.76 ± 0.01	6.93 ± 0.00	6.99 ± 0.01	7.03 ± 0.03	7.08 ± 0.02	7.19 ± 0.02	4.68 ± 0.39
	pH 5.5	5.55	7.68 ± 0.05	6.95 ± 0.01	6.98 ± 0.00	7.01 ± 0.01	7.08 ± 0.01	7.20 ± 0.02	4.54 ± 0.13
	pH 6.4	6.35	7.74 ± 0.03	6.98 ± 0.02	7.11 ± 0.02	7.06 ± 0.02	6.94 ± 0.01	6.99 ± 0.05	4.47 ± 0.01
	pH 7.4	7.36	7.64 ± 0.00	6.89 ± 0.08	7.04 ± 0.02	7.06 ± 0.00	7.06 ± 0.01	7.11 ± 0.01	4.45 ± 0.01
SNF	pH 6.4	6.43	7.63 ± 0.02	6.79 ± 0.06	6.98 ± 0.01	6.99 ± 0.01	6.98 ± 0.01	7.05 ± 0.03	4.40 ± 0.03

Appendix

Table 11.3. Viability as a function of the zinc oxide concentration in all formulations, to identify whether toxicity is dependent on zinc oxide concentrations in the formulation. Zinc oxide as raw material (ZnO) is used as a reference. F1) 100 % ZnO and 0 % mannitol; F2) 80 % ZnO and 20 % mannitol; F3) 60 % ZnO and 40 % mannitol; F4) 40 % ZnO and 60 % mannitol; F5) 20 % ZnO and 80 % mannitol. $n = 3$, \pm = standard deviation.

	ZnO	F1	F2	F3	F4	F5
Formulation concentration: 0.005 mg/mL						
ZnO Concentration, mg/mL	0.005	0.005	0.004	0.003	0.002	0.001
Viability, %	88.27 \pm 6.66	94.17 \pm 8.85	97.75 \pm 12.35	95.33 \pm 15.90	94.91 \pm 9.23	103.37 \pm 12.22
Formulation concentration: 0.010 mg/mL						
ZnO Concentration, mg/mL	0.010	0.009	0.007	0.005	0.004	0.002
Viability, %	18.59 \pm 11.06	83.03 \pm 7.88	85.70 \pm 6.19	87.31 \pm 17.21	93.84 \pm 8.61	106.79 \pm 17.70
Formulation concentration: 0.050 mg/mL						
ZnO Concentration, mg/mL	0.050	0.045	0.036	0.027	0.018	0.009
Viability, %	6.28 \pm 2.16	5.73 \pm 5.12	5.54 \pm 4.21	6.05 \pm 3.47	11.40 \pm 4.79	90.23 \pm 12.76
Formulation concentration: 0.100 mg/mL						
ZnO Concentration, mg/mL	0.100	0.090	0.072	0.054	0.036	0.018
Viability, %	12.08 \pm 2.60	4.68 \pm 3.06	5.00 \pm 3.07	4.68 \pm 2.33	5.11 \pm 2.70	9.71 \pm 6.27
Formulation concentration: 0.500 mg/mL						
ZnO Concentration, mg/mL	0.500	0.450	0.360	0.270	0.180	0.090
Viability, %	43.24 \pm 15.68	13.44 \pm 5.58	13.02 \pm 4.87	7.09 \pm 2.42	3.63 \pm 1.84	1.77 \pm 2.15

Appendix

	ZnO	F1	F2	F3	F4	F5
Formulation concentration: 1.000 mg/mL						
ZnO Concentration, mg/mL	n/a	n/a	n/a	n/a	0.360	0.180
Viability, %	n/a	n/a	n/a	n/a	6.64 ± 3.18	1.93 ± 1.74
Formulation concentration: 2.500 mg/mL						
ZnO Concentration, mg/mL	n/a	n/a	n/a	n/a	n/a	0.450
Viability, %	n/a	n/a	n/a	n/a	n/a	2.83 ± 1.96

Table 11.4. 24-h-pH- and solubility study showing saturation solubility, starting pH and pH change of different solutions/suspensions after 24 h for zinc oxide in comparison to formulation 1. F1) 100 % ZnO and 0 % mannitol. $n = 3$, \pm = standard deviation.

		ZnO 24 h, mg/mL	F1 24 h, mg/mL	pH 0 h	ZnO pH 24 h	F1 pH 24 h
Phosphate buffer	pH 1.2	5.09 \pm 0.20	5.09 \pm 0.02	1.15	3.16 \pm 0.03	3.24 \pm 0.02
	pH 2.5	0.49 \pm 0.01	0.48 \pm 0.01	2.56	3.82 \pm 0.04	3.83 \pm 0.04
	pH 4.0	0.01 \pm 0.00	0.01 \pm 0.001	4.08	6.19 \pm 0.01	6.11 \pm 0.05
	pH 5.5	0.01 \pm 0.004	0.01 \pm 0.00	5.60	6.33 \pm 0.01	6.36 \pm 0.04
	pH 6.4	0.01 \pm 0.001	0.01 \pm 0.001	6.44	6.72 \pm 0.00	6.82 \pm 0.01
	pH 7.4	0.01 \pm 0.00	0.004 \pm 0.001	7.35	7.79 \pm 0.04	7.86 \pm 0.04
Sodium chloride solution	pH 1.2	2.68 \pm 0.01	2.72 \pm 0.14	1.29	6.51 \pm 0.02	6.43 \pm 0.02
	pH 2.5	0.15 \pm 0.001	0.13 \pm 0.01	2.55	6.98 \pm 0.02	6.88 \pm 0.06
	pH 4.0	0.02 \pm 0.001	0.01 \pm 0.002	4.02	7.45 \pm 0.01	7.51 \pm 0.07
	pH 5.5	0.01 \pm 0.002	0.01 \pm 0.001	5.49	7.56 \pm 0.03	7.59 \pm 0.02
	pH 6.4	0.01 \pm 0.001	0.01 \pm 0.002	6.38	7.61 \pm 0.06	7.67 \pm 0.03
	pH 7.4	0.01 \pm 0.001	0.01 \pm 0.002	7.30	7.62 \pm 0.04	7.70 \pm 0.04
SLF	pH 7.4	0.004 \pm 0.00	0.01 \pm 0.001	7.43	8.24 \pm 0.00	8.11 \pm 0.02

Appendix

Table 11.5. 24 h-pH study showing starting pH and pH change of different solutions/suspensions after 24 h with zinc oxide as raw material (ZnO) in comparison to all formulations. F1) 100 % ZnO and 0 % mannitol; F2) 80 % ZnO and 20 % mannitol; F3) 60 % ZnO and 40 % mannitol; F4) 40 % ZnO and 60 % mannitol; F5) 20 % ZnO and 80 % mannitol; F6) 0 % ZnO and 100 % mannitol. n = 3, ± = standard deviation.

		pH 0 h	ZnO	F1	F2	F3	F4	F5	F6
Phosphate buffer	pH 1.2	1.15	3.16 ± 0.03	3.24 ± 0.02	3.25 ± 0.02	2.59 ± 0.10	1.76 ± 0.01	1.32 ± 0.01	1.14 ± 0.03
	pH 2.5	2.56	3.82 ± 0.04	3.83 ± 0.04	3.75 ± 0.01	3.15 ± 0.16	2.92 ± 0.03	2.71 ± 0.01	2.60 ± 0.01
	pH 4.0	4.08	6.19 ± 0.01	6.11 ± 0.05	6.09 ± 0.01	5.88 ± 0.04	5.72 ± 0.06	5.25 ± 0.01	4.13 ± 0.01
	pH 5.5	5.60	6.33 ± 0.01	6.36 ± 0.04	6.30 ± 0.01	6.13 ± 0.02	6.04 ± 0.01	5.85 ± 0.02	5.62 ± 0.02
	pH 6.4	6.44	6.72 ± 0.00	6.82 ± 0.01	6.78 ± 0.01	6.68 ± 0.00	6.58 ± 0.04	6.54 ± 0.01	6.50 ± 0.01
	pH 7.4	7.35	7.79 ± 0.04	7.86 ± 0.04	7.74 ± 0.05	7.62 ± 0.02	7.57 ± 0.03	7.48 ± 0.01	7.46 ± 0.00
Sodium chloride solution	pH 1.2	1.29	6.51 ± 0.02	6.43 ± 0.02	6.41 ± 0.04	6.38 ± 0.01	5.81 ± 0.36	1.72 ± 0.01	1.33 ± 0.00
	pH 2.5	2.55	6.98 ± 0.02	6.88 ± 0.06	6.96 ± 0.01	7.04 ± 0.03	6.91 ± 0.03	6.57 ± 0.07	2.58 ± 0.02
	pH 4.0	4.02	7.45 ± 0.01	7.51 ± 0.07	7.44 ± 0.03	7.50 ± 0.02	7.53 ± 0.05	7.31 ± 0.06	4.61 ± 0.01
	pH 5.5	5.49	7.56 ± 0.03	7.59 ± 0.02	7.53 ± 0.01	7.64 ± 0.04	7.55 ± 0.01	7.33 ± 0.08	6.53 ± 0.06
	pH 6.4	6.38	7.61 ± 0.06	7.67 ± 0.03	7.56 ± 0.04	7.61 ± 0.04	7.60 ± 0.06	7.45 ± 0.05	6.84 ± 0.1
	pH 7.4	7.30	7.62 ± 0.04	7.70 ± 0.04	7.60 ± 0.02	7.68 ± 0.06	7.55 ± 0.04	7.46 ± 0.04	6.91 ± 0.04
SLF	pH 7.4	7.43	8.24 ± 0.00	8.11 ± 0.02	8.13 ± 0.01	8.20 ± 0.00	9.18 ± 0.04	9.09 ± 0.24	9.10 ± 0.24

Appendix

Table 11.6. Viability as a function of the zinc oxide concentration in all formulations, to identify whether toxicity is dependent on zinc oxide concentrations in the formulation. Zinc oxide as raw material (ZnO) is used as a reference. F1) 100 % ZnO and 0 % mannitol; F2) 80 % ZnO and 20 % mannitol; F3) 60 % ZnO and 40 % mannitol; F4) 40 % ZnO and 60 % mannitol; F5) 20 % ZnO and 80 % mannitol. $n = 3$, \pm = standard deviation.

	F1	F2	F3	F4	F5
Formulation concentration: 0.005 mg/mL					
ZnO Concentration, mg/mL	0.005	0.004	0.003	0.002	0.001
Viability, %	79.69 \pm 9.33	87.85 \pm 15.50	85.61 \pm 8.98	90.72 \pm 8.53	99.10 \pm 11.81
Formulation concentration: 0.010 mg/mL					
ZnO Concentration, mg/mL	0.009	0.007	0.005	0.004	0.002
Viability, %	51.28 \pm 9.52	44.20 \pm 5.32	69.98 \pm 9.20	76.18 \pm 11.78	94.26 \pm 8.87
Formulation concentration: 0.050 mg/mL					
ZnO Concentration, mg/mL	0.045	0.036	0.027	0.018	0.009
Viability, %	31.46 \pm 4.48	37.59 \pm 8.16	40.95 \pm 3.61	42.90 \pm 7.58	41.21 \pm 11.52
Formulation concentration: 0.100 mg/mL					
ZnO Concentration, mg/mL	0.090	0.072	0.054	0.036	0.018
Viability, %	35.64 \pm 5.73	34.97 \pm 6.88	37.44 \pm 8.90	38.75 \pm 6.25	43.07 \pm 9.06
Formulation concentration: 0.500 mg/mL					
ZnO Concentration, mg/mL	0.450	0.360	0.270	0.180	0.090
Viability, %	81.01 \pm 13.06	76.25 \pm 20.06	63.22 \pm 15.59	54.44 \pm 11.73	41.45 \pm 8.73

Appendix

	F1	F2	F3	F4	F5
Formulation concentration: 1.000 mg/mL					
ZnO Concentration, mg/mL	n/a	n/a	n/a	0.360	0.180
Viability, %	n/a	n/a	n/a	64.38 ± 25.30	52.30 ± 14.02
Formulation concentration: 2.500 mg/mL					
ZnO Concentration, mg/mL	n/a	n/a	n/a	n/a	0.450
Viability, %	n/a	n/a	n/a	n/a	96.89 ± 26.84

11.2 Abbreviations

APC	Antigen-presenting cells
ATCC	American Type Culture Collection
BALT	Bronchus-associated lymphoid tissue
BCG	Bacillus Calmette-Guerin
BET	Brunauer, Emmet, Teller
BMDC	Bone marrow-derived dendritic cells
BSA	Bovine serum albumin
cAMP	Cyclic adenosine monophosphate
CD	Cluster of differentiation
CMC	Carboxymethyl cellulose
CNS	Central nervous system
COPD	Chronic obstructive pulmonary disease
CpG	Oligonucleotides
CT	Cholera enterotoxin
CTL	Cytotoxic T lymphocytes
DC	Dendritic cell
DHEA	Dehydroepiandrosterone
DNA	Deoxyribonucleic acid
DOC	Sodium deoxycholate
DPI	Dry powder inhaler
DPPC	Dipalmitoyl phosphatidylcholine
DSC	Differential scanning calorimetry
DVS	Dynamic vapor sorption
EDS	Energy dispersive X-ray spectroscopy
EMA	European Medicine Agency
EU	European Union

F*	Formulation (followed by the number of the formulation)
FACS	Fluorescence activated cell sorting
FBS	Fetal bovine serum
FDA	Food and drug administration
FPF	Fine particle fraction
FTS	Flame transport synthesis
GM-CSF	Granulocyte-macrophage colony-stimulating factor
HA	Hyaluronic acid
HEPES	4-(2-hydroxyethyl)-1-piperazineethanesulfonic acid
HES	Hydroxyethyl starch
HIV	Human immunodeficiency virus
HSV	Herpes simplex virus
IEP	Isoelectric point
iGC-SEA	Inverse gas chromatography surface energy analyser
IL	Interleukin
ISCOM	Immunostimulating complex
LALT	Larynx-associated lymphoid tissue
LD	Lethal dose
LPS	Lipopolysaccharide
LT	Heat-labile enterotoxine
MALS	Multi angle light scattering
MALT	Mucosa-associated lymphoid tissue
MDP	Muramyl dipeptide
MHC	Major histocompatibility complex
MMAD	Mass median aerodynamic diameter
MOC	Micro-orifice collector
MPL	Monophosphoryl lipid A
m-RNA	Messenger ribonucleic acid

MTT	3-(4,5-dimethylthiazol-2-yl)-2,5-diphenyltetrazolium bromide
NALT	Nose-associated lymphoid tissue
NEC	Nasal expansion chamber
NFκB	Nuclear factor kappa-light-chain-enhancer of activated B cells
NGI	Next generation pharmaceutical impactor
NiM	Nano-in-Microparticle
OTC	Over the counter
OVA	Ovalbumin
PAMP	Pathogen-associated molecular pattern
PBS	Phosphate buffer solution
PCL	Polycaprolactone
PEG	Polyethylene glycol
PEI	Polyethyleneimine
PET	Polyethylene terephthalate
PGA	Polyglutamic acid
PI-3	Phosphatidylinositol-3
PLA	Poly lactide
PLGA	Poly lactide-co-glycolic acid
pMDI	Pressurised metered dose inhaler
PMMA	Polymethyl methacrylate
PVB	Polyvinyl butyral
RNA	Ribonucleic acid
SARS-CoV-2	Severe acute respiratory syndrome coronavirus type 2
SDS-PAGE	Sodium dodecyl sulphonate polyacrylamide gel electrophoresis
SEC	Size exclusion chromatography
SEM	Scanning electron microscopy
TEER	Transepithelial electrical resistance
TLR 4	Toll-like Receptor 4

UDS	Unit dose powder system
UK	United Kingdom of Great Britain and Northern Ireland
USA	United states of America
UV/Vis	Ultraviolet-visible spectroscopy
WHO	World Health Organisation
Zn	Zinc
ZnO	Zinc oxide
ZnOT	Zinc oxide tetrapods

11.3 Reagents

Reagents	Company
1,2-propanediol	Merck KGaA, Germany
Acetic acid glacial $\geq 99\%$	J. T. Baker Corporate, USA
Acrylamide/bisacrylamide stock solution	Carl Roth GmbH & Co. KG, Germany
Alpha-Lactalbumin (from bovine milk)	Merck KGaA, Germany
Aluminium phosphate (Adju-Phos)	Brenntag Biosector, Denmark
Aluminium hydroxide (VAC20)	SPI Pharma, USA
Ammonium persulphate	Carl Roth GmbH & Co. KG, Germany
anti-CD11c-BUV737, HL3	BD Biosciences, Denmark
anti-CD40-PE, 3.23	BD Biosciences, Denmark
anti-CD80-APC, 16-10A1	BD Biosciences, Denmark
anti-CD86-FITC, GL1	BD Biosciences, Denmark
anti-MHC-II-eF450, M5/114.15.2	eBioscience, Thermo Fisher Scientific Inc., USA
Avidin	Merck KGaA, Germany
Bovine serum albumin	Merck KGaA, Germany
Bromophenol blue	Carl Roth GmbH & Co. KG, Germany
Calcium chloride dihydrate	Merck KGaA, Germany
Coomassie brilliant blue	Carl Roth GmbH & Co. KG, Germany
Dimethylformamide	Merck KGaA, Germany
Di-sodium hydrogen phosphate	Merck KGaA, Germany
Di-sodium hydrogen phosphate dihydrate	Merck KGaA, Germany
Di-sodium tetraborate decahydrate	Merck KGaA, Germany

Appendix

Reagents	Company
Dulbecco's Modified Eagle's Medium – high glucose, w 4.5 g/L glucose, w L-glutamine, w sodium carbonate, w/o sodium pyruvate	Merck KGaA, Germany
Dulbecco's Phosphate Buffered Saline, w/o Ca ²⁺ , w/o Mg ²⁺	Merck KGaA, Germany
Ethanol	Merck KGaA, Germany
Fetal bovine serum	Merck KGaA, Germany
Gibco RPMI 1640 Medium, GlutaMAX Supplement, w GlutaMAX, w/o sodium pyruvate	Thermo Fisher Scientific Inc., USA
Glycerol 99 %	AppliChem GmbH, Germany
Glycine	Carl Roth GmbH & Co. KG, Germany
GM-CSF	PeptoTech Inc., USA
Hanks' salt solution – w 0.35 g/L NaHCO ₃ , w Ca ²⁺ , w Mg ²⁺ , w/o Phenol red	Merck KGaA, Germany
Hyaluronic acid (sodium salt)	Caesar & Loretz GmbH, Germany
Hydrochloric acid 37 %	AppliChem GmbH, Germany
Isopropanol	AppliChem GmbH, Germany
Lysozyme	Merck KGaA, Germany
Magnesium chloride	Merck KGaA, Germany
Mannitol (Pearlitol 200 SD)	Roquette Frères, France
MTT (3-(4,5-dimethylthiazol-2-yl)-2,5-diphenyltetrazolium bromide)	Merck KGaA, Germany
Mucin of porcine stomach type II	Merck KGaA, Germany
Non-essential amino acid	Merck KGaA, Germany
Ovalbumin	Merck KGaA, Germany

Appendix

Reagents	Company
Penicillin-streptomycin	Merck KGaA, Germany
Penicillin-streptomycin (100 x)	Invitrogen, Thermo Fisher Scientific Inc., USA
peqGOLD Protein Marker III	VWR Internationl GmbH
Potassium chloride	Carl Roth GmbH & Co. KG, Germany
Potassium dihydrogen phosphate	Carl Roth GmbH & Co. KG, Germany
RBC Lysis Buffer (10 x)	BioLegend Inc., USA
Silver staining kit	GE Healthcare GmbH, Germany
Sodium acetate	Merck KGaA, Germany
Sodium chloride	Carl Roth GmbH & Co. KG, Germany
Sodium citrate dihydrate	AppliChem GmbH, Germany
Sodium dihydrogen phosphate monohydrate	Merck KGaA, Germany
Sodium dodecyl sulphonate	Carl Roth GmbH & Co. KG, Germany
Sodium hydrogen carbonate	Merck KGaA, Germany
Sodium hydroxide	Carl Roth GmbH & Co. KG, Germany
Sodium pyruvate	Merck KGaA, Germany
Sodium sulphate	Merck KGaA, Germany
Tetramethyl ethylenediamine	Carl Roth GmbH & Co. KG, Germany
Tris-base	Merck KGaA, Germany
Triton-X	Merck KGaA, Germany
Trypan blue 0.5 % (w/w) in physiological saline	Merck KGaA, Germany
Zinc oxide (for external use)	Caesar & Loretz GmbH, Germany
Zinc oxide tetrapods	Working group "Functional Nanomaterials" headed by Prof. Rainer Adelung, Institute of Material Science, Faculty of Engineering, Kiel University, Germany

Reagents	Company
Zincon	Carl Roth GmbH & Co. KG, Germany
β -Mercaptoethanol	Carl Roth GmbH & Co. KG, Germany

11.4 Cells

Cells	Company
BMDC from CF57BL/6N mice	Vaccine Design and Delivery Group of Prof Camilla Foged, University of Copenhagen, Denmark
Calu-3	American Type Culture Collection, USA
RPMI2650	Working Group of Prof Ben Forbes, Kings College London, UK

11.5 Materials

Materials	Company
96-well plates: Lumox 96 multiwell Microplate 96 well F TC-plate 96 well, Standard, F	Sarstedt AG & Co. KG, Germany
BD syringe (1 mL)	BD (Becton, Dickinson and Company) Corporation, USA
Carbon tabs (12 mm)	Micro to Nano, The Netherlands
Cellstar 12-well-plates	Greiner Bio One International GmbH, Austria
Cellstar 24-well plates	Greiner Bio One International GmbH, Austria
Chromafil Xtra PET 45/25	Macherey-Nagel GmbH & Co. KG, Germany
Corning cell strainer, 40 μ m blue	Merck KGaA, Germany
Cyclohaler	Jenapharm GmbH & Co. KG, Germany
DSC pans (40 μ L) and covers	PerkinElmer Inc., USA
DURAN funnel (80 mm)	DWK Life Science GmbH, Germany

Materials	Company
DURAN laboratory bottle (250 mL)	DWK Life Science GmbH, Germany
DURAN measuring cylinder (10 mL)	DWK Life Science GmbH, Germany
DURAN volumetric flask (500 mL)	DWK Life Science GmbH, Germany
Filter paper circles (125 mm)	Whatman, Inc., UK
Magnetic stir bar	Brand GmbH & Co. KG, Germany
Petri dishes, polystyrene (100 x 50 mm)	Merck KGaA, Germany
Pipette tips (10 mL, 5 mL, 1 mL, 100 µL)	Sarstedt AG & Co. KG, Germany
Reaction tubes (2 mL, 1.5 mL, 100 µL)	Sarstedt AG & Co. KG, Germany
SEC glass column (C-MF-144, C-MF-145, C-MF-146)	Surface Measurement System Ltd., UK
SEM pin stub (12.7 mm)	Micro to Nano, The Netherlands
Semi micro quartz cuvette	Hellma GmbH & Co. KG, Germany
TC flask T25, Stand., Vent. Cap	Sarstedt AG & Co. KG, Germany
TC flask T75, Stand., Vent. Cap	Sarstedt AG & Co. KG, Germany
TC flask T175, Stand., Vent. Cap	Sarstedt AG & Co. KG, Germany
ThinCerts (12 well)	Greiner Bio One International GmbH, Austria
Tubes (15 mL, 50 mL)	Sarstedt AG & Co. KG, Germany
Unit dose system powder device	Aptar Pharma, France
VCaps Plus HPMC capsules	Lonza Group, Switzerland

11.6 Instruments

Instruments	Company
Air jet sieve	Alpine Air Jet Sieve e200 LS Hosokawa Alpine AG, Germany

Instruments		Company
Centrifuge	Centrifuge 5430 R	Eppendorf AG, Germany
	Heraeus Biofuge pico	Thermo Fisher Scientific Inc., USA
	Heraeus Biofuge 28 RS	Thermo Fisher Scientific Inc., USA
Differential scanning calorimetry	Diamond DSC	PerkinElmer Inc., USA
Drying oven	Heraeus	Thermo Fisher Scientific Inc., USA
Dynamic vapour sorption	DVS 1	Surface Measurement System Ltd., UK
Flow cytometer	BD LSRFortessa	BD (Becton, Dickinson and Company) Corporation, USA
Flow meter	DFM 2000 flow meter	Copley Scientific, UK
Friabilator	Erweka	Erweka GmbH, Germany
Impactor	Next Generation Pharmaceutical Impactor in combination with nasal expansion chamber, mouthpiece, throat, preseparator	Copley Scientific, UK
Incubator	HERAcell 150	Thermo Fisher Scientific Inc., USA
Inverse gas chromatography surface energy analyser	iGC-SEA	Surface Measurement System Ltd., UK
Lab Balances	Sartorius A200S	Sartorius AG, Germany
	Sartorius MC1	Sartorius AG, Germany
	Sartorius MC5	Sartorius AG, Germany
Laser diffractometer	HELOS in combination with RODOS module, INHALER module, SPRAYER module	Sympatec GmbH, Germany
Magnetic stirrer	IKA IKAMAG RET-GS	IKA-Werke GmbH & Co. KG, Germany

Appendix

Instruments		Company
Microscope	Olympus IMT-2	Olympus Deutschland GmbH, Germany
Multi angle light scattering detector	DAWN 8+	Wyatt Technology Corporation, Germany
Orbital shaker	Universalschüttler SM	Edmund Bühler GmbH, Germany
	GFL Schüttelapparatur 3005	GFL Gesellschaft für Labortechnik GmbH, Germany
Osmometer	Osmomat 030	Gonotec GmbH, Germany
pH-meter in combination with pH-electrode	WTW Inolab pH 730 with SentTix 81	Xylem Analytics Germany ales GmbH & Co. KG, Germany
	Mettler Toledo SevenCompact Benchtop Meter with InLab Ultra-Micro-ISM	Mettler Toledo GmbH, Germany
Pipettes	Accu jet pro	Brand GmbH & Co. KG, Germany
	Eppendorf Reference 10 – 100 µL	Eppendorf AG, Germany
	Eppendorf Reference 100 – 1000 µL	Eppendorf AG, Germany
	Eppendorf Research Pro 1000 – 5000 µL	Eppendorf AG, Germany
	Eppendorf Multipette	Eppendorf AG, Germany
	Tranferpipette-8 10 – 100 µL	Brand GmbH & Co. KG, Germany
Plate reader	FluoStar Omega	BMG Labtech GmbH, Germany
Pumps	HCP4	Copley Scientific, UK
	HCP5	Copley Scientific, UK
Pycnometer	AccuPyk	POROTEC GmbH, Germany
Refraction index detector	Optilab T-rex	Wyatt Technology Corporation, Germany
Rheometer	Bohlin CVO 120 High Resolution	Bohlin Instruments, Germany

Appendix

Instruments		Company
Scanning electron microscope	Phenom World XL	Thermo Fisher Scientific Inc., USA
SDS-PAGE	Mini-Protean Tetra Cell	Bio-Rad Laboratories Inc., USA
Sieve	Diameter 20 cm with different mesh sizes (45 µm, 75 µm)	Retsch GmbH, Germany
Size exclusion chromatograph	Äkta Pure 25	GE Healthcare, Germany
Size exclusion chromatography column	Superose™ 6 Increase 10/300 GL	GE Healthcare Bio-Sciences AB, Sweden
Software	FACSDiva software	BD (Becton, Dickinson and Company) Corporation, USA
	FlowJo software v 10	Tree Star, USA
Sonicator	SONOPLUS ultrasonic homogeniser HD 4100 in combination with sonotrode TS 103	BANDELIN electronic GmbH & Co. KG, Germany
	Bandelin SONOREX SUPER RK 514 BH ultrasonic water bath	BANDELIN electronic GmbH & Co. KG, Germany
Spectrometer	Shimadzu UV-1280	Shimadzu Corporation, Japan
Spray Dryer	Mini Spray Dryer B-290	Büchi Labortechnik AG, Switzerland
Sputter coater	BAL-Tec SCP 050 Sputter Coater	Leica Microsystems, UK
Transepithelial electrical resistance	EVOM	World Precision Instruments, USA
Vortex	IKA Vortex 4 basic	IKA-Werke GmbH & Co. KG, Germany
X-ray powder diffractometer	STOE STADI P in combination with a DECTRIS MYTHEN 1K detector	STOE & Cie GmbH, Germany

Danksagung

Während meiner Promotion haben mich viele Menschen begleitet, unterstützt und inspiriert. Ich möchte hier nun die Gelegenheit nutzen, um Danke zu sagen.

Ein großes Dankeschön geht an Prof. Dr. Regina Scherließ. Vielen Dank, dass du mir 2017 die Möglichkeit gegeben hast, dieses herausfordernde Thema zu bearbeiten. Dank deiner Ermutigung, deines Vertrauens und deiner Unterstützung hatte ich in den letzten Jahren stets die Möglichkeit und Freiheit meine eigenen Ideen und Vorhaben zu verwirklichen und mich sowohl beruflich als auch persönlich weiterzuentwickeln. Danke.

Danke an Prof. Dr. Ben Forbes (Kings College London) und Prof. Dr. Camilla Foged (University of Copenhagen) für die Möglichkeit ein kleines Teilprojekt meines Promotionsthemas in Kooperation mit der jeweiligen Arbeitsgruppe durchführen zu können. Danke für die herzliche Aufnahme in euren Arbeitskreis und den etwas anderen Blickwinkel auf mein Thema. Ein besonderer Dank geht dabei an Dr. Aneesh Thakur (University of Copenhagen). Danke, dass wir auch nach meinem Aufenthalt in Kopenhagen und trotz Corona weiter zusammengearbeitet haben und du durch deinen unermüdlichen Einsatz für die erfolgreiche Durchführung der in-vivo Studien gesorgt hast. In diesem Zusammenhang möchte ich zudem NordicPOP und der Aerosol Society für die Finanzierung der jeweiligen Projekte in London und Kopenhagen danken.

Danke an Prof. Dr. Rainer Adelung, Dr. Martina Baum und Leonard Siebert für die materialwissenschaftliche Unterstützung während meiner Promotion.

Ein herzliches Dankeschön an Prof. Dr. Thomas Gutschmann und Dr. Susanne Homolka für die vielen gemeinsamen Messtage und die stetige Erinnerung daran, wie viel Spaß gemeinsames Forschen machen kann.

Ein großes Dankeschön an all meine Wegbegleiter am pharmazeutischen Institut.

Danke an den „alten“ Arbeitskreis, dass ihr mich 2017 so herzlich aufgenommen habt und ihr ein wichtiger Teil meiner Promotionszeit gewesen seid.

Danke an den „neuen“ Arbeitskreis für die vielen wichtigen fachlichen und privaten Gespräche bei einem Feierabendbier oder einem gemeinsamen Mittagessen.

Danke an meine Jungs aus dem Büro 106, dass wir alle Höhen und Tiefen miteinander geteilt haben, der ein oder andere Gedanke zur Entwicklung der Arbeit beigetragen hat und wir nun alle ein paar Lachfalten mehr haben.

Danke an meine Masterandin, meine Wahlpflichtfachstudenten /-studentinnen und alle Studierende, die ich im Laufe meiner Promotionszeit betreuen durfte, für die Möglichkeit euch beim fachlichen Wachsen zu begleiten und zu unterstützen.

Danke an alle Festangestellten der Technologie und des pharmazeutischen Institutes für die guten Gespräche bei einem Kaffee, den kreativen Input und die schnelle Hilfe, wenn die Technowelt einmal drohte unterzugehen.

Vielen Dank an alle für die tolle gemeinsame Zeit.

Vielen lieben Dank an die helfenden Hände und schlauen Köpfe für die unermüdliche, genaue, fachliche und kreative Unterstützung bei der Korrektur der Doktorarbeit und der Erstellung der Verteidigung. Danke.

Ein herzliches Dankeschön an meine Kieler Familie. Dankeschön, dass ihr mich auf dem kompletten Weg, vom ersten Tag des Studiums bis zum Abschluss der Promotion, begleitet und unterstützt habt. Ihr habt die Kieler Zeit zu etwas ganz Besonderem gemacht.

Mein größter Dank geht an meine Familie. Danke Mama und Papa, dass ihr uns euren Weitblick, euren Optimismus, eure Zielstrebigkeit und euer gutes Herz weitergegeben habt. Danke Mama mit Heiko und Hans mit Gina, dass ihr mich bei all meinen Entscheidungen unterstützt und ich in jeder Lebenslage auf euch zählen kann. Dankeschön Oma Elfriede, Opa Hermann, Oma Jutta und Opa Lothar, dass ihr mich ermutigt habt, die Welt mit einem offenen Herzen zu erkunden und für die Dinge, die einem wichtig sind, zu kämpfen.

Dankeschön.

Erklärung nach § 9 der Promotionsordnung

Hiermit erkläre ich gemäß § 9 der Promotionsordnung der Mathematisch-Naturwissenschaftlichen Fakultät der Christian-Albrechts-Universität zu Kiel, dass ich die vorliegende Arbeit, abgesehen von der Beratung durch meinen Betreuer, selbstständig und ohne fremde Hilfe verfasst habe. Weiterhin habe ich keine anderen als die angegebenen Quellen oder Hilfsmittel benutzt und die den benutzten Werken wörtlich oder inhaltlich entnommenen Stellen als solche kenntlich gemacht. Die vorliegende Arbeit ist unter Einhaltung der Regeln guter wissenschaftlicher Praxis entstanden und wurde bei keiner anderen Universität zur Begutachtung eingereicht. Es wurde mir kein akademischer Grad entzogen.

Teile dieser Arbeit sind in der folgenden Publikation veröffentlicht oder wurden wie folgt präsentiert:

Publikation:

Hellfritzsch, M. and Scherließ, R. Mucosal Vaccination via the Respiratory Tract. *Pharmaceutics* 11 (2019)

Konferenzbeiträge:

Hellfritzsch, M. and Scherließ, R. Spray Dried Zinc Oxide as an Alternative to Aluminium Salts in Mucosal Vaccination. *Präsentation*, Kiel Life Science Studierendentagung. Kiel (2018)

Hellfritzsch, M. and Scherließ, R. Spray Dried Formulations containing Zinc Oxide for Nasal Immunisation – A Story from Manufacture to Target. *Posterpräsentation*, Drug Delivery to the Lungs 2019. Edinburgh (2019)

Hellfritzsch, M. and Scherließ, R. Characterisation of Zinc Oxide as an Alternative to Aluminium Hydroxide in Nasal Vaccination. *Posterpräsentation*, Drug Delivery to the Lungs 2018. Edinburgh (2018)

Hellfritzsch, M. and Scherließ, R. Characterisation of Zinc Oxide Particles as Protein Carrier System. *Posterpräsentation*, 11th World Meeting on Pharmaceutics, Biopharmaceutics and Pharmaceutical Technology. Granada (2018)

Kiel 2021

Marie Gerda Hellfritzsch